Tracking the history of Baltic Sea hypoxia with bivalve shells

Dissertation
zur Erlangung des Grades
”Doktor der Naturwissenschaften”
im Promotionsfach
Geowissenschaften/Paläontologie

Am Fachbereich 09 für Chemie, Pharmazie und Geowissenschaften der Johannes Gutenberg-Universität Mainz

von
Xizhi Huang
geb. in Zhejiang, China

Mainz, 2024

1. Berichterstatter: Removed for reasons of data protection

2. Berichterstatter: Removed for reasons of data protection

Tag der mündlichen Prüfung: Removed for reasons of data protection

Hiermit erkläre ich, dass ich die vorliegende Arbeit selbstständig verfasst und keine anderen als die angegebenen Quellen und Hilfsmittel benutzt habe.

_____

Xizhi Huang

Abstract

Deoxygenation is a growing issue in global open oceans, coastal waters and semi-enclosed seas including one of largest oxygen-deficient settings, The Baltic Sea. Most organisms suffer or die once levels of dissolved oxygen (DO) dropped below approx. 72 µmol/L (=2.3 mg/L or 1.6 mL/L), the threshold where hypoxia begins. As a model region, understanding the past occurrence of Baltic Sea hypoxia is crucial for informing present-day coastal perturbations and developing future mitigation strategies. To date, reconstructing the history of hypoxia in the Baltic Sea is almost exclusively based on proxies archived in sediment cores, which have low temporal resolution and poor dating control, limiting the ability to provide detail information on DO variability and hypoxic events. To reliably predict the DO development in the Baltic Sea, it is of paramount importance to identify the causes leading to oxygen depletion. This can be achieved by understanding historical trends of DO. Hence, developing temporally well-constrained and highly resolved DO proxy archives that can overcome the limitations of sedimentary records is imperative. The shells of bivalve mollusks may fulfill this task as they can function as precisely dated and seasonally to interannually resolved archives of environmental changes. Specifically, a redox-sensitive element such as Mn has the potential to be used as a surrogate for DO. However, it remains a challenge to quantify environmental signatures from elemental impurities in bivalve shells. Before shell Mn/Ca values can be used to quantify DO concentrations, this proxy needs to be calibrated. The present study was based on shell materials of long-lived bivalve specimens and sclerochronological techniques (Chapter 2). The results of this project comprise four manuscripts published in international, peer-reviewed scientific journals.

In Chapter 3, the ocean quahog *Arctica islandica*, an extremely long-lived and low-oxygen adapted bivalve species commonly used for paleoclimate reconstructions, was studied. All specimens of *A. islandica* were collected alive at the same time from the Mecklenburg Bight, SW Baltic Sea. The results showed that Mn/Ca_{shell} values were statistically significantly negative correlated with DO levels in the water column ($r = - 0.68$; $R^2 = 0.46$, $p < 0.0001$). This relationship reflects that the Mn in shells is mainly derived from the dissolved Mn in the surrounding waters. These findings demonstrated the great potential of bivalve shells *A. islandica* as archives for tracking the history of hypoxia in the Baltic Sea.

In Chapter 4, it was investigated whether shells of *Astarte borealis* and *Astarte elliptice* can record DO in a similar way as those in *A. islandica* and thus serve as alternative DO archives. In specimens of all three species living on the seafloor in the same region of the Fehmarn Belt

in the SW Baltic Sea, the Mn/Ca_{shell} data were statistically significantly linked to DO concentrations (r = - 0.66 to – 0.75, R^2 = 0.43 to 0.5, $p < 0.0001$). These relationships can be used to infer DO data, with *A. elliptica* providing a slightly higher precision (± 1.5 mL/L) of DO data than *A. islandica* or *A. borealis* (± 1.6 mL/L), suggesting that DO reconstructions can be conducted with all three species.

Besides chemical analyses, Chapter 5 explored if the shell ultrastructure (microstructure), specifically disturbance lines, can be used as an alternative proxy to track the frequency and severity of past deoxygenation events. As demonstrated, oxygen depletion < 45 µmol/L leads to the formation of (Mn-rich) disturbance lines that become increasingly more prominent as DO declines. Disturbance lines consist of fine-complex crossed-lamellar ultrastructure with small and elongated biomineral units (BMUs) that can easily be distinguished from annual growth lines where irregular simple/spherulitic prismatic ultrastructures with large blocky BMUs prevail. Although the relationship between DO and BMU size was statistically significant ($p < 0.05$), the explained variability was too small to quantify past DO. Yet, in conjunction with Mn/Ca_{shell} data, disturbance lines are still useful to reconstruct the frequency of past low-oxygen events.

In Chapter 6, long-term and high-resolution Mn/Ca_{shell} chronologies were constructed from shells of *A. islandica* that covered the second half of the 19th century as well as the late 20th century to study if DO in the past was significantly different from modern conditions. All specimens were live-collected at water depths of 23.5 to 25 m in the Mecklenburg Bight, SW Baltic Sea. Data indicated that seasonal deoxygenation had already occurred in the SW Baltic Sea in the mid-19th century, however, it was less frequent than in the late 20th century. In addition, with the help of other environmental proxies in the shell (i.e., Ba/Ca_{shell} values and annual increment width), the causes of oxygen depletion in the SW Baltic Sea were inferred. Strong anthropogenic nutrient input was probably the main cause of oxygen depletion shortly after the onset of the Industrial Revolution (ca. 1850), whereas the present low DO level in bottom waters seems to be the result of a combined effect of eutrophication and Major Baltic Inflows (MBIs).

In summary, with Mn/Cs_{shell} a robust DO indicator was developed, calibrated and applied to infer the DO history in the SW Baltic Sea during nearly two centuries with unprecedented temporal resolution. Future research should broaden the spatial and temporal scales for retrospective monitoring of the Baltic Sea deoxygenation.

Zusammenfassung

Sauerstoffmangel ist ein zunehmendes Problem im offenen Ozean, Küstengewässern und halb geschlossenen Meeres, incl. der Ostsee, eine der größten sauerstoffarmen Regionen. Die meisten Lebewesen leiden massiv oder sterben, wenn der Gehalt an gelöstem Sauerstoff (DO) unter ca. 72 µmol/L (=2.3 mg/L oder 1.6 mL/L) fällt, der Grenze, unter der Hypoxie beginnt. Das Verständnis über frühere Hypoxie-Ereignisse der Modellregion Ostsee ist von entscheidender Bedeutung, um Informationen über ökologische Veränderungen in Küstenregionen zu gewinnen und um Strategien zur Verbesserung der ökologischen Situation zu entwickeln. Bislang wurde die Geschichte der Hypoxie in der Ostsee fast ausschließlich anhand von den in Sedimentkernen archivierten Proxys rekonstruiert, die allerdings eine vergleichsweise geringe zeitliche Auflösung bieten und nicht präzise datierbar sind, so daß kaum detaillierte Information zur DO-Variabilität auf kurzen Zeitskalen und zur Häufigkeit saisonaler hypoxischer Ereignisse ermittelt werden können. Um die Entwicklung des Sauerstoffgehalts in der Ostsee zuverlässig vorhersagen zu können, ist es von großer Bedeutung, die Ursachen für die Sauerstoffverarmung auf der Grundlage eines genauen Verständnisses der historischen DO-Trends zu ermitteln. Daher ist die Erforschung von zeitlich gut bekannten und hoch aufgelösten DO-Proxy-Archiven, ohne die Einschränkungen der Sedimentbohrkerne, zwingend erforderlich. Die Schalen von Muscheln bieten sich als geeignetes Archiv an, weil sie Umweltveränderungen zeitlich hoch aufgelöst (saisonal und jährlich) in Form geochemischer Proxys aufzeichnen. Insbesondere das redoxempfindliche Element Mn hat das Potenzial, als Anzeiger für den Sauerstoffgehalt des Wassers verwendet zu werden. Es bleibt jedoch eine Herausforderung, elementchemische Daten der Muschelschalen in Umweltdaten zu übersetzen. Dies erfordert eine genaue Kalibrierung der in Muschelschalen gemessenen Mn/Ca-Verhältnisse. Die vorliegende Studie basiert auf Schalenmaterial langlebiger Muscheln, die mit sclerochronologischen Methoden untersucht wurden (Kapitel 2). Die Ergebnisse dieses Projekts sind in vier Publikationen geflossen, die in internationalen, begutachteten Fachzeitschriften erschienen sind.

In Kapitel 3 wurde die extrem langlebige und an niedrigen Sauerstoffgehalt angepaßte Muschelart, *Arctica islandica*, untersucht. Diese Art wird häufig für Paläoklima-Rekonstruktionen verwendet. Alle Exemplare von *A. islandica* wurden zur gleichen Zeit lebend aus der Mecklenburger Bucht im Südwesten der Ostsee gesammelt. Die Ergebnisse zeigten, dass die Mn/Ca_{shell}-Werte statistisch signifikant negativ mit den DO-Werten der Wassersäule korrelierten ($r = -0{,}68$; $R^2 = 0{,}46$, $p < 0{,}0001$). Diese Beziehung weist darauf hin, daß das Mn

in den Muschelschalen hauptsächlich aus dem gelösten Mn im umgebenden Wasser stammt und demonstriert das große Potenzial von *A. islandica* als geochemisches Archiv für die Rekonstruktion der Hypoxie-Geschichte in der Ostsee.

In Kapitel 4 wurde untersucht, ob die Schalen von *Astarte borealis* und *Astarte elliptica* den DO-Gehalt des Wassers in ähnlicher Weise aufzeichnen können wie *A. islandica* und somit als alternative DO-Archive dienen. Bei Exemplaren aller drei Arten, die in derselben Region des Fehmarnbelts in der südwestlichen Ostsee lebten, korrelierten die Mn/Ca-Daten der Schalen statistisch signifikant mit den DO-Konzentrationen (r = - 0,66 bis - 0,75, R^2 = 0,43 bis 0,5, p < 0,0001). Alle drei Muschelarten können deshalb genutzt werden, um auf die DO-Gehalte des Wassers rückschließen zu können, wobei *A. elliptica* eine etwas höhere Genauigkeit (± 1,5 mL/L) liefert als *A. islandica* oder *A. borealis* (± 1,6 mL/L).

Neben chemischen Analysen wurde in Kapitel 5 untersucht, ob die Ultrastruktur (Mikrostruktur) der Schale, insbesondere die Störungslinien, als alternativer Indikator für die Häufigkeit und Schwere vergangener Deoxygenierungs-Ereignisse verwendet werden kann. Die Ergebnisse zeigten, daß DO-Gehalte < 45 µmol/L zur Bildung von (Mn-reichen) Störungslinien führte, deren Prominenz mit sinkendem DO-Wert zunahm. Störungslinien bestehen aus fein-komplexer kreuzlamellarer Ultrastruktur mit kleinen, langgestreckten Biomineraleinheiten (BMUs) und können damit nicht mit Jahreslinien verwechselt werden; denn dort kommt irregulär einfache/spherulitisch-prisnatische Ultrastruktur mit großen, blockigen BMUs vor. Trotz der statistisch signifikanten (p < 0,05) Korrelation zwischen DO und BMU-Größe, war die erklärte Variabilität zu gering, um DO-Gehalte zu rekonstruieren. Dennoch eignen sich Störungslinien, in Verbindung mit Mn/Ca_{shell}-Daten, um die Häufigkeit vergangener Deoxygenierungs-Ereignisse zu ermitteln.

Die Zuverlässigkeit von DO-Rekonstruktionen auf der Grundlage von Mn/Ca-Werten in Muschelschalen wurde durch einen umfangreichen Datensatz über Zeit, Raum und Muschelarten bestätigt (Kapitel 3 und 4). Daher wurden in Kapitel 6 langfristige und hochauflösende Mn/Ca_{shell}-Chronologien aus Muscheln von *A. islandica* erstellt, welche die zweite Hälfte des 19. und das späte 20. Jahrhundert abdeckten. Alle Exemplare wurden lebend, in Wassertiefen von 23,5 bis 25 m in der Mecklenburger Bucht (südwestliche Ostsee), gesammelt. Laut der Daten, war die südwestliche Ostsee bereits Mitte des 19. Jahrhunderts von saisonaler Sauerstoffverarmung betroffen, allerdings weniger häufig als im späten 20. Jahrhundert. Darüber hinaus wurde versucht, mit Hilfe anderer Umweltindikatoren in der Muschel (d. h. Ba/Ca_{shell}-Werten und jährliche Zuwachsbreiten) die Ursachen der Sauerstoffverarmung in der südwestlichen Ostsee zu ermitteln. Starker anthropogener

Nährstoffeintrag war wahrscheinlich die Hauptursache für die Sauerstoffverarmung kurz nach Beginn der industriellen Revolution (ca. 1850), während der derzeitige geringe DO-Gehalt im Bodenwasser das Ergebnis einer Kombination von Eutrophierung und großen Einstromereignissen aus der Nordsee (MBI) zu sein scheint.

Mit dem Mn/Ca-Verhältnis der Muschelschalen wurde in der vorliegenden Doktorarbeit ein zuverlässiger DO-Indikator entwickelt, kalibriert und angewendet, um die DO-Geschichte der südwestlichen Ostsee in den vergangenen Jahrhunderten mit einer bisher unerreichten zeitlichen Auflösung zu dokumentieren. Zukünftige Forschungen sollten die räumlichen und zeitlichen Skalen für die retrospektive Überwachung der Sauerstoffarmut der Ostsee erweitern.

Acknowledgements

Removed for reasons of data protection

List of abbreviations

DO	dissolved oxygen
HTM	Holocene Thermal Maximum
MWP	Medieval Warm Period
Mn	manganese
Ba	barium
Mn/Ca	manganese-to-calcium
Ba/Ca	barium-to-calcium
LA-ICP-MS	laser ablation – inductively coupled plasma – mass spectrometry
MBIs	Major Baltic Inflows
MPIC	Max Planck Institute for Chemistry
JGU	Johannes Gutenberg University of Mainz
QCMs	quality control materials
$\delta^{18}O_{shell}$	shell oxygen isotope
$\delta^{18}O_{shell\ predicted}$	predicted shell oxygen isotope curve
SGI	standardized shell growth increment width
BMU	biomineral units
SEM	scanning electron microscopy
HOM	homogeneous microstructures
FCCL	fine complex crossed-lamellar
CA	crossed-acicular
ISP	irregular simple prismatic
Chl *a*	chlorophyll a
OSL	outer shell layer

ISL	inner shell layer
oOSL	outer portion of the outer shell layer
iOSL	inner portion of the outer shell layer
AMV	Atlantic Multidecadal Variability
SST	sea surface temperature

List of Figures

List of Tables

Table of Contents

1 Introduction

1.1 Ocean deoxygenation

Hypoxia, defined as dissolved oxygen (DO) content less than approx. 2.3 mg/L (Vaquer-Sunyer and Duarte, 2008, ≙ 1.7 mL/L or 72 μmol/L), is a growing environmental problem affecting coastal waters, semi-enclosed seas and the open ocean (Breitburg et al., 2018; Limburg et al., 2020). Oxygen is critical for all aerobic organisms, and its variation in the ocean can also induce changes to the biogeochemical cycling of carbon, nitrogen, phosphorus and other key elements (Giomi et al., 2023). According to IPCC, the oceans will lose about 5% of their oxygen inventory over the next century (Keeling et al., 2010; Bopp et al., 2013; Stocker et al., 2014). Such future ocean deoxygenation is expected to alter productivity, biodiversity and biogeochemical cycles, which add to the pressure impacting the functioning of marine ecosystems and the services they provide to the society (Altieri and Witman, 2006; Breitburg et al., 2009; Diaz and Rosenberg, 2011). Following a recent study by Sampaio et al. (2021), the negative effects of future oxygen depletion on marine organism will surpass those of acidification and warming. Although hypoxic waters occur naturally in the oceans (e.g., Zillén et al., 2008; Conley et al., 2009), human activities have led to a dramatic expansion of the area and duration of hypoxia, specifically since the mid-20th century (Diaz and Rosenberg, 1995; Diaz and Rosenberg, 2008; Vaquer-Sunyer and Duarte, 2008; Rabalais et al., 2010; Breitburg et al., 2018). Today, there are more than 700 coastal sites that reportedly face new or worsening hypoxic conditions (Limburg et al., 2020), of which ca. 20 % are located in the Baltic Sea (Conley et al., 2011). The hypoxic area of the Baltic Sea has varied between 50,000 and 80,000 km^2 over the past 20 years (Kõuts et al., 2021). As the largest hypoxic zone in the world (Diaz and Rosenberg, 2008), the Baltic Sea can serve as a model region for studying the mechanisms and consequences of hypoxia and potential mitigation of future coastal hypoxia (Reusch et al., 2018).

The Baltic Sea is permanently stratified and its deep water thus been naturally prone to hypoxia. A strong halocline prevents downward-mixing of oxygenated surface water (Schinke and Matthaus, 1998). Physical processes controlling stratification place important constraints on the formation and maintenance of hypoxia. Especially, climate-controlled inflow of saltwater is a critical determinant governing the spatial distribution and duration of hypoxia (Conley, 2002). For example, although a dense saltwater inflow brings more oxygenated waters to the bottom, it enhances the expansion of stratification making more bottom areas hypoxic. Since

the 1950s, large increases in nutrient inputs from land and atmosphere have greatly stimulated phytoplankton overpopulation and the subsequent decomposition of organic matter, causing a high oxygen demand (Savchuk et al., 2008). Superimposed on physical processes, anthropogenic eutrophication is the primary driver of significant deoxygenation in the Baltic deep water (Conley et al., 2011), although high temperature during the last few decades has contributed to worsening oxygen conditions due to enhanced respiration processes (Carstensen et al., 2014a). The persistence of hypoxia in the Baltic Sea due to the interplay of physical forcing, anthropogenic eutrophication and climate change has resulted in altered biogeochemical cycling of nutrients, increasing the release of phosphorus and nitrogen from the sediment into the overlying water, which in turn sustains nutrient-driven eutrophication and provides positive feedbacks for the development of hypoxia (Österblom et al., 2007).

It is widely accepted that the predominant cause of coastal hypoxia is anthropogenic eutrophication (e.g., Conley et al., 2007), hence, significant efforts have been made since the 1980s to reduce nutrient loading and mitigate associated environmental damage (Gustafsson et al., 2012). Despite enormous efforts and investment, oxygen availability in the Baltic Sea has not substantially improved to date (Kuliński et al., 2022). Given the interactions among different driving factors are complex, it remains a grand challenge to understand problems and develop an effective mitigation solution as reveled in a recently released State of the Ocean Report (IOC-UNESCO, 2022). Gaining a long-term perspective of hypoxia and related environmental problems beyond the time scale of oceanographic observation is invaluable for assessing and guiding management actives (Breitburg et al., 2018; Reusch et al., 2018). This is because that extending the occurrence of Baltic hypoxia back in time (i.e., centennial and millennial) can provide key information on (1) elucidating the driving processes involved in the development of hypoxia and estimating the anthropogenic contribution to the expansion of hypoxia (Sohlenius et al., 2001; Zillén et al., 2008); (2) establishing natural (pre-anthropogenic) baselines and quantifying relevant scales of natural variability (Sohlenius et al., 2001; Zillén et al., 2008), and (3) developing remediation strategies and setting restoration targets (Carstensen et al., 2014b; Caballero-Alfonso et al., 2015).

1.2 Past development of hypoxia in the Baltic Sea

1.2.1 Sedimentary evidence for hypoxia

The use of marine sediments to study hypoxia began in the 1980s (e.g., Brush, 1984; Tyson and Pearson, 1991), and since then, it has developed as an important tool for reconstructing the past

oxygen status in the water column (Zillén et al., 2003; Gooday et al., 2009). The occurrence of hypoxic events can be captured by a variety of sedimentary indicators, including laminations, the remains of benthic organisms mainly the foraminifera and ostracods (Nordberg et al., 2000; Filipsson and Nordberg, 2004), and geochemical properties (Jilbert and Slomp, 2013a). Its application is concentrated in areas such as the Louisiana Shelf, the Chesapeake Bay, the Norwegian Fjords, and the Baltic Sea (Gooday et al., 2009).

First, the laminated sediment is a widespread and independent proxy for low oxygenation and thus compensates for the lack of long instrumental records. The presence of laminated sediment fabric requires that the uppermost layers are not completely disrupted by bioturbation, physical disturbance, or the benthic burrowing activity (Kemp, 1996; Zillén et al., 2003). Hypoxic conditions can lead to the elimination of the macroinfauna, resulting in the formation of laminated sediments in deeper areas. The records of hypoxia in the Baltic Sea have been extended back to the early Holocene based on laminated sediment records (Zillén et al., 2008).

In addition to laminations, the preserved remains of benthic organisms, notably foraminifera can serve as indicators of the responses of benthic communities to environmental changes including hypoxia (Nordberg et al., 2000; Filipsson and Nordberg, 2004; Murray, 2006). The development of hypoxia in bottom waters can be inferred from characteristics of foraminifera, such as a decrease in species richness and diversity, coupled with a dominance of hypoxia-tolerant species (Phleger and Soutar, 1973; Gooday et al., 2000; Schmiedl et al., 2003; Asteman and Nordberg, 2013). In the Øresund of the Baltic Sea, benthic foraminiferal assemblages have been used to reconstruct historical environmental changes over the past two centuries, particularly with regards to DO concentration, salinity and organic matter content (Charrieau et al., 2019).

The elemental composition of the sediments can also provide valuable information about past and present oxidation-reduction (redox) conditions in the environment. A number of studies have demonstrated that trace element concentrations are generally elevated under low-oxygen conditions (Sohlenius and Westman, 1998; Sohlenius et al., 2001; van Helmond et al., 2018). In the Baltic Sea, the laminated sediments of the hypoxic interval are characterized by enrichment in molybdenum (Mo) and Uranium (U) which are correlated with high organic carbon content (Sternbeck et al., 2000; Jilbert and Slomp, 2013b; Hardisty et al., 2016; Papadomanolaki et al., 2018; van Helmond et al., 2018). The presence of pyrite in sediments is also thought to reflect reducing depositional conditions (Snowball, 1993). Besides, Lenz et al. (2015) suggested that sediment Mn enrichments can be used as a redox proxy in the deep basins of the Baltic Sea.

1.2.2 The occurrences of Baltic Sea hypoxia revealed by sediment cores

Based on laminated sediment records, the historical record of hypoxia in the Baltic Sea dates back to the early Holocene (Zillén et al., 2008). In the past ca. 8000 years, the Baltic Sea has experienced three defined intervals of extensive bottom water hypoxia, occurring during the Holocene Thermal Maximum (HTM), the Medieval Warm Period (MWP) and in recent decades (Zillén et al., 2008).

The first hypoxic event was dated to around ca. 8000–4000 cal. yr BP, following the transition from a freshwater *Ancylus* Lake to the brackish Littorina Sea (Björck, 1995). The expansion of hypoxia in this interval corresponded to an increase in the flux of saltwater, resulting in strong stratification that restricted the ventilation of bottom waters (Emeis et al., 2003; Zillén et al., 2008; Conley et al., 2009). Hypoxia disappeared following the stabilization of the *Littorina* Sea around 4000 cal. yr BP. This was due to the reduction in the depth of the Denmark Strait and decreased salinity, which led to increased vertical mixing and a replenishment of oxygen in deep basins (Gustafsson and Westman, 2002).

Widespread hypoxia was observed again in the Baltic proper between ca. 2000–800 cal. yr BP associated with the MWP, when the temperature of sea surface was ca. 1 °C higher than today (Keigwin, 1996). Climate warming decreases oxygen solubility and increases benthic respiration activity driving the occurrence of hypoxia (BACC Author Team, 2008). In addition, the increases of agricultural nutrients associated with population growth, together with climate warming during the MWP may have contributed to increased primary production (Zillén et al., 2008; Zillén and Conley, 2010), leading to accelerated oxygen consumption that further exacerbated hypoxia. The termination of this hypoxic period was likely associated with the cooling of the climate during the Little Ice Age (ca. 1300–1850 CE) (Clarke and Rendell, 2009; Kabel et al., 2012) and the depopulation caused by the Black Death and famine that hit Europe in the late 14th century and early 15th century (Andersson Palm, 2001; Zillén et al., 2008).

Since ca. 1900 CE, the Baltic Sea was hypoxic again with the hypoxic area more than ten-fold larger than ever before (Savchuk et al., 2008), coinciding with the beginning of the modern warming as well as with the start of the profound impact of human activities (especially the development and expansion of agriculture and forest industry) on the Baltic Sea (Zillén et al., 2008). The latter has been regarded as the primary driving factor generating widespread hypoxic events in the ocean (e.g., Conley et al., 2007). In particular, the central Baltic deep water has been depleted of oxygen since then and up to present time. Once the Baltic Sea became extensively hypoxic, processes such as enhanced phosphorus fluxes and reduced denitrification acted to sustain and continue hypoxic conditions.

Long sediment records have greatly improved our understanding about the timing and mechanisms of hypoxia in the Baltic Sea on millennial time scales. Furthermore, the significance of environmental changes in the semi-enclosed Baltic Sea and its catchment triggered by climate variability and/or human impact for the development of past hypoxia in different intervals has been realized. Yet, more research is needed to determine the relative importance of the main driving forces, i.e., climate change, human impact and internal feedback mechanisms. It would also be useful to qualitatively reproduce the spatial and temporal evolution of oxygen contents in the Baltic Sea in order to propose realistic measures to improve the environment of the Baltic Sea.

However, these objectives appear to be extremely difficult to achieve solely based on sediment proxy records as they suffer from several drawbacks. First of all, sediment cores have poor temporal resolution and dating control, thereby constraining the ability to resolve seasonal to inter-annual hypoxic events (e.g., Jilbert and Slomp, 2013b), which in turn, would reduce the reliability of reconstructing the DO history in the Baltic Sea and constrain the identification of the mechanisms driving the occurrence of oxygen depletion. Secondly, it is difficult to distinguish between the effects of hypoxia and eutrophication in sediment records. For instance, foraminifera are not only indicators of oxygen depletion, but are also associated with organic enrichment in the absence of hypoxia (Jorissen et al., 2007; Charrieau et al., 2019). Thirdly, given the qualitative nature of proxies derived from sediment cores (at least hitherto studied so far; Gooday et al., 2009), past hypoxia cannot be quantified. Thus, developing precisely dated and high-resolution proxy archives that overcome many of the limitations of sediment cores is a crucial research need. Shells of long-lived bivalves may be one of the promising high-resolution, temporally well-constrained archives for oxygen depletion and hypoxia that have virtually remained untapped. Using shell growth patterns as a time gauge, proxy records can be placed in a precise temporal content. In addition, bivalves are widely distributed and particularly abundant in the Baltic Sea, and there are numerous museum collections with fossil and recent shell materials.

1.3 Reconstruction of Baltic Sea hypoxia using bivalve shell

1.3.1 Bivalve sclerochronology

Sclerochronology includes studies of the physical and chemical properties in hard tissues that were deposited periodically during life such as mollusk shells, corals and fish otoliths (e.g., Clark, 1968; Buddemeier et al., 1974; Panfili et al., 2002; Oschmann, 2009). It is a powerful

tool for precise, temporally aligned and high-resolution and multi-proxy reconstruction of paleoenvironmental variations (e.g., Schöne et al., 2005; Gröcke and Gillikin, 2008; Oschmann, 2009; Wanamaker et al., 2011; Schöne and Gillikin, 2013; Butler and Schöne, 2017; Prendergast et al., 2017; Gillikin et al., 2019). In particular, bivalve sclerochronology has gained considerable momentum during the past decades (e.g., see review in Peharda et al., 2021).

Mollusks, specifically marine bivalves are an important taxon for the research of sclerochronology. First of all, bivalve mollusks have occupied a broad range of different aquatic habitats ranging from shallow waters to the deep sea, from the tropics to the poles and from freshwater and brackish to fully marine and hypersaline environments (Fedonkin and Waggoner, 1997; Peterson and Butterfield, 2005; Kocot et al., 2011), whereas other biogenic archives (e.g., corals, which live mainly in shallow, warm and clear water; Goreau et al., 1979) are more geographically restricted. Due to their largely sedentary lifestyle bivalves keep long-term environmental records from only one locality, rather than higher spatial variability provided by mobile organisms such as fish. Most importantly, bivalves build their shells periodically (i.e., daily, fortnightly or annually) as displayed in distinct growth lines and increments (reflecting periods of slow and fast growth, respectively), which can serve as a calendar to place the records of physicochemical proxies in an accurate temporal context and determine the ontogenetic age of each specimen (e.g., Schöne, 2013; Moss et al., 2021). The growth patterns of bivalve shells are highly synchronous within populations from the same locality (Butler et al., 2013; Marali and Schöne, 2015). Based on similar growth patterns, annual growth increment chronologies of specimens with overlapping lifespan can be crossdated to form a stacked or master chronology, which can extend decades, centuries or even longer into the past (Witbaard et al., 1997; Marchitto et al., 2000; Butler et al., 2009; Holland et al., 2014; Reynolds et al., 2016). Lastly, given that the occurrence of bivalves can be dated back to the Cambrian era (Sepkoski, 1981; Fraiser and Bottjer, 2007) and that their fossils are sometimes well-preserved in sedimentary deposits (Harper, 1998; Casella et al., 2017; Vendrasco et al., 2019), providing a valuable resource for paleoenvironmental studies on large time-scales. As demonstrated above, bivalve shells hold great promise as temporally well- constrained, ultra-high-resolution paleoclimate archives.

1.3.2 Bivalve species

In the Baltic Sea, bivalves play a significant role in the benthic macrofaunal community (e.g., Kube et al., 1996). As most adult bivalves are largely sessile once larvae settled, they can potentially provide a record of the surrounding environment through time, making them ideal

environmental monitors. The implementation of long-term monitoring depends on the availability of long-lived animals (Steinhardt et al., 2016). The selected bivalve species in this study are particularly suitable as they all live for decades to centuries.

The ocean quahog, *Arctica islandica*, is among the most suitable species for sclerochronological studies. This species is widely distributed in the northern Atlantic Ocean, including the North Sea and the Western Baltic Sea (Jagnow and Gosselck 1987). *A. islandica* is a shallow infaunal deposit-feeder (Morton, 2011), and has a very short siphon for filtering food particles from the bottom water and sediment-water interface. It prefers to live in muddy, sandy and gravely sediments (Lutz et al., 1981) and generally tolerates temperature and salinity ranges of 1° to 16 °C (Golikov and Scarlato, 1973; Mann, 1989; Witbaard et al., 1997) and 22 to 35 (Winter, 1969; Oeschger and Storey, 1993), respectively. *A. islandica* belongs to the slowest-growing and longest-lived bivalves, with a lifespan of over 500 years (Wanamaker et al., 2008; Butler et al., 2013). Owing to its wide geographical occurrence at extremely diverse environmental conditions combined with its extreme longevity, *A. islandica* has been used as an environmental sentinel (Goldberg, 1975) and its shell serves as an archive of climate change (Schöne and Gillikin, 2013).

In the Baltic Sea, *A. islandica* reaches its eastern limit of distribution in the Arkona Basin (von Oertzen and Schulz, 1973) and the largest populations reside in Kiel Bay and Mecklenburg Bight (Zettler et al., 2001; Darr et al., 2014). The Baltic populations of *A. islandica* are highly resistant to pollutants, acidification, eutrophication and specifically severe oxygen depletion (Theede et al., 1969; Taylor, 1976; Oeschger, 1990; Oeschger and Storey, 1993; Diaz and Rosenberg, 1995; Strahl et al., 2011). The longevity of *A. islandica* from the Baltic Sea tends to be shorter than specimens from the North Sea but still can attain several decades (e.g., the shell length of *A. islandica* from the Mecklenburg Bight measured 64 mm with an estimate age of 70 years, Zettler et al., 2001), which is sufficient to construct long, uninterrupted, and highly resolved time-series reflecting the ambient environment.

The other two bivalve species, *Astarte borealis* (Schumacher 1817) and *Astarte elliptica* (Brown 1827) are common in the Arctic and North Atlantic Ocean and adjacent waters, ranging from Greenland to Massachusetts (Abbott and Morris, 1995; Zettler, 2001; Zettler, 2002). *Astarte* spp. is a moderately long-lived genus characterized by low metabolic rates and slow growth. For example, the lifespan of *A. boreali*s and *A. elliptica* collected from the Baltic Sea has been reported to be up to 43 (Moss et al., 2018) and 20 years (Trutschler and Samtleben, 1988), respectively. These two species are infaunal suspension feeders which usually live buried in muddy sand with gravel (Kiihlmorgen-Hille 1963; Saniewski et al., 2022), and are usually

found in several meters of water depth (Trutschler and Samtleben, 1988; Zettler, 2001; Zettler, 2002; Saniewski et al., 2022). In the Baltic Sea, *Astarte* spp. is more widely distributed than *A. islandica* as the eastern distribution limit of the former is in the Bornholm Basin (von Oertzen and Schulz, 1973; Arntz et al., 1976; Darr et al., 2014; Saniewski et al., 2022). According to laboratory experiments, *Astarte* spp. is also slightly more tolerant against low DO than *A. islandica* (Theede, 1973; Dries and Theede, 1974). Therefore, it would be extremely useful if different bivalve species could be used interchangeably or alternatively to reconstruct the spatial and temporal environmental conditions in the Baltic Sea.

1.3.3 Shell geochemical proxies for low oxygenation

Manganese (Mn) is a redox-sensitive element that exists in dissolved form under reducing conditions and precipitates as particles in the presence of oxygen (e.g., Hem, 1963; Balzer, 1982; Rue et al., 1997). The relationship between Mn incorporation into biogenic carbonate and bottom water oxygenation is based on the combination of Mn bioavailability and redox chemistry. Generally, as the oxygen concentration in pore waters declines with depth, and Mn oxides and/or hydroxides are reduced to Mn^{2+} (Middelburg et al., 1987). Subsequently, Mn^{2+} diffuses across the sediment-water interface into the water column (Tebo, 1991; Pakhomova et al., 2007), resulting in elevated Mn^{2+} levels in low-oxygen waters (Groeneveld et al., 2018). Mn^{2+}, the biologically most available form of manganese (Langlet et al., 2006), can be rapidly incorporated into the carbonate skeleton of calcifying organisms living under oxygen-deficient conditions, e.g., into bivalve shells in less than one day (Langlet et al., 2006). In turn, many bivalve species, especially *Astarte* spp. and *A. islandica* used in this study, are extremely tolerant toward low DO levels and can survive the temporary lack of oxygen (anoxia) and presence of hydrogen sulfide (euxinia) (Theede et al., 1969; Taylor, 1976; Oeschger, 1990; Oeschger and Storey, 1993; Strahl et al., 2011). Thus, shell Mn/Ca ratios hold greater promise as a proxy for DO.

Prior to this research project, only a single qualitative study employed shell manganese-to-calcium (Mn/Ca) values from freshwater mussel *Hyriopsis cumingii* as a proxy for pore water DO content in a shallow eutrophic lake (Zhao et al., 2017). Yet, further efforts are needed to rigorously calibrate and refine Mn/Ca_{shell} values as a hypoxia proxy to quantitatively estimate past DO concentrations in the water column, especially given soil erosion and river discharge (e.g., Lazareth et al., 2003; Barats et al., 2008; Risk et al., 2010), or extreme weather events (e.g., tsunami, Murakami-Sugihara et al., 2019) that may interfere with Mn/Ca_{shell} shell records.

In order to elucidate the processes leading to hypoxia and disentangle the relative

importance of natural and anthropogenic causes, additional proxies recording eutrophication are required. Shell barium-to-calcium (Ba/Ca) ratios have been highlighted as a promising proxy for primary production and phytoplankton dynamics in marine settings (Stecher III et al., 1996; Vander Putten et al., 2000; Lazareth et al., 2003; Hatch et al., 2013; Marali et al., 2017a, b; Fröhlich et al., 2022a, b). In addition, annual growth increment widths can be used to gain information on primary productivity (Ballesta-Artero et al., 2018; Bonitz et al., 2018) as shell growth rate increases when phytoplankton availability increases.

1.4 Motivation and aim of the research

As highlighted in the previous sections, hypoxia has become a growing concern in the Baltic Sea due to its striking increasing spatial distribution, intensity, and duration over the last century (Carstensen et al., 2014a; Reusch et al., 2018). Extensive oxygen depletion in bottom waters can have serious consequences for living resources and ecosystem functioning (Diaz and Rosenberg, 2008; Breitburg et al., 2018). Thus, it is imperative to broaden our understanding of the long-term development of hypoxic events, specifically prior to the instrumental area. The reconstruction of the history of Baltic hypoxia has so for relied almost exclusively on sedimentary records (e.g., Emeis et al., 2003). Although sediment cores can provide information on millennial-scale variations in oxygenation (Zillén et al., 2008), poor temporal resolution and dating control do not allow to infer seasonal to inter-annual DO changes, which greatly limits a detailed understanding of the DO history. The accurate compilation of information on historical trends of hypoxia is of paramount important for elucidating the mechanisms driving the occurrence of oxygen depletion and thus reliably predicting the DO development in the Baltic Sea. Therefore, development of precisely dated and high-resolution proxy archives of hypoxia such as bivalve shells is a crucial research need. No attempt has yet been made to quantify DO levels in the ocean water column based on bivalve shell Mn/Ca values and also no long-term monitoring datasets are available. This thesis studies aim to evaluate the potential use of Mn/Ca_{shell} values as DO proxy with different bivalve shells and apply a multiproxy approach to quantifiably reconstruct the high-resolution DO history in the Baltic Sea since the mid-19th century.

Thus, geochemical data from three long-lived bivalve species (*A. islandica, A. borealis,* and *A. elliptica*) shells were analyzed by laser ablation – inductively coupled plasma – mass spectrometry (LA-ICP-MS), complemented by growth pattern and stable oxygen isotope analyses for precise temporal alignment. If relationships between target geochemical properties

and associated environmental variables can be established and refined quantitatively in modern shells, the final goal, i.e., to reconstruct the environmental changes from the elemental chemistry of historical shells, can be reached. The results of this thesis were published as four manuscripts in international, peer-reviewed journals, each of which tackling different research objectives:

Chapter 3 investigates the potential of shell Mn/Ca values of *A. islandica* as a hypoxia proxy in shallow ocean waters. The relationship between the high-resolution and temporally well-constrained Mn/Ca_{shell} data and the available instrumental records including DO was studied. As demonstrated, Mn/Ca_{shell} data can be used to quantify DO levels in the water column which opens the possibility of reconstructing low-oxygen and hypoxic event at an unprecedented resolution.

In Chapter 4, the Mn/Ca data in the shells of three bivalve species (*A. islandica, A. borealis,* and *A. elliptica*) were studied to evaluate if the different species can be used interchangeably as proxy DO archives. Specimens of all three species were live-collected from the same region in the Fehmarn Belt, Baltic Sea. As *Astarte* spp. is slightly more tolerant against low DO than *A. islandica* (Theede, 1973; Dries and Theede, 1974) and more wildly distributed in the Baltic Sea (Darr et al., 2014), results of this study are of great relevance to reconstruct multiregional and long-term DO trends in the Baltic Sea.

In Chapter 5, the ultrastructures of *A. islandica* from the western Baltic Sea were explored in the attempt to identify an alternative or complementary means to Mn/Ca_{shell} to track the frequency and severity of past low-DO events. In addition to a qualitative assessment of ultrastructural changes, the morphology of individual biomineral units (BMUs) was quantitatively determined by artificial intelligence-assisted image analysis to derive models for DO reconstruction.

Chapter 6 reconstructed the DO history in the Baltic Sea since the mid-19th century from high-resolution Mn/Ca_{shell} time-series extracted from *A. islandica* specimens living the Mecklenburg Bight, SW Baltic Sea at the water depths of 23.5 to 25 m during the second half of the 19^{th} and the late 20^{th} century. It was also assessed how bottom water oxygenation developed over the most recent history (19^{th} century onward) by comparing the Mn/Ca_{shell} values of modern shells with those of historical shells. In addition to Mn/Ca_{shell} ratios, Ba/Ca_{shell} values and annual shell growth rate were analyzed to identify the possible causes of oxygen depletion in the Baltic Sea during different time intervals.

References

Abbott, R.T., Percy, A.M. 1995. A field guide to shells: Atlantic and Gulf Coasts and the West Indies, 4th Edition. Houghton Mifflin Company, Boston, 350 pp.

Altieri, A.H., Witman, J.D., 2006. Local extinction of a foundation species in a hypoxic estuary: integrating individuals to ecosystem. Ecology 87, 717–730.

Arntz, W.E., Brunswig, D., Sarnthein, M., 1976. Zonierung von Mollusken und Schill im Rinnensystem der Kieler Bucht (Westliche Ostsee). Senckenbergiana maritima 8, 189-269.

Asteman, I.P., Nordberg, K., 2013. Foraminiferal fauna from a deep basin in Gullmar Fjord: The influence of seasonal hypoxia and North Atlantic Oscillation. J. Sea Res. 79, 40–49.

Andersson Palm, L., 2001. Livet, kärleken och döden. Livet, kärleken och döden. L Palm. Historiska institutionen, Gothenburg, Sweden, 203 pp.

BACC Author Team. 2008. Assessment of climate change for the Baltic Sea basin. Regional climate studies. Springer-Verlag, Berlin, 474 pp.

Ballesta-Artero, I., Zhao, L., Milano, S., Mertz-Kraus, R., Schöne, B.R., van der Meer, J., Witbaard, R., 2018. Environmental and biological factors influencing trace elemental and microstructural properties of *Arctica islandica* shells. Sci. Total Environ. 645, 913–923.

Balzer, W., 1982. On the distribution of iron and manganese at the sediment/water interface: thermodynamic versus kinetic control. Geochim. Cosmochim. Acta 46, 1153–1161.

Barats, A., Amouroux, D., Pecheyran, C., Chauvaud, L., Donard, O.F., 2008. High-frequency archives of manganese inputs to coastal waters (Bay of Seine, France) resolved by the LA-ICP-MS analysis of calcitic growth layers along scallop shells (*Pecten maximus*). Environ. Sci. Technol. 42, 86–92.

Björck, S., 1995. A review of the history of the Baltic Sea, 13.0-8.0 ka BP. Quat. Int. 27, 19–40.

Bonitz, F.G.W., Andersson, C., Trofimova, T., Hátún, H., 2018. Links between phytoplankton dynamics and shell growth of *Arctica islandica* on the Faroe Shelf. J. Mar. Syst. 179, 72–87.

Bopp, L., Resplandy, L., Orr, J.C., Doney, S.C., Dunne, J.P., Gehlen, M., Halloran, P., Heinze, C., Ilyina, T., Séférian, R., Tjiputra, J., Vichi, M., 2013. Multiple stressors of ocean ecosystems in the 21st century: projections with CMIP5 models. Biogeosciences 10, 6225–6245.

Breitburg, D., Levin, L.A., Oschlies, A., Gregoire, M., Chavez, F.P., Conley, D.J., Garcon, V., Gilbert, D., Gutierrez, D., Isensee, K., Jacinto, G.S., Limburg, K.E., Montes, I., Naqvi, S.W.A., Pitcher, G.C., Rabalais, N.N., Roman, M.R., Rose, K.A., Seibel, B.A., Telszewski, M., Yasuhara, M., Zhang, J., 2018. Declining oxygen in the global ocean and coastal waters. Science 359, eaam7240.

Breitburg, D.L., Hondorp, D.W., Davias, L.A., Diaz, R.J., 2009. Hypoxia, nitrogen, and fisheries: integrating effects across local and global landscapes. Ann. Rev. Mar. Sci. 1, 329–49.

Brush, G.S., 1984. Patterns of recent sediment accumulation in Chesapeake Bay (Virginia—Maryland, U.S.A.) tributaries. Chem. Geol. 44, 227–242.

Buddemeier, R.W., Maragos, J.E., Knutson, D.W., 1974. Radiographic studies of reef coral exoskeletons – rates and patterns of coral growth. J. Exp. Mar. Bio. Ecol. 14, 179–200.

Butler, P.G., Freitas, P.S., Burchell, M., Chauvaud, L., 2009. Archaeology and sclerochronology of marine bivalves. Goods and Services of Marine Bivalves, Springer, Cham, 413–444 pp.

Butler, P.G., Schöne, B.R., 2017. New research in the methods and applications of sclerochronology. Palaeogeogr. Palaeoclimatol. Palaeoecol. 465, 295–299.

Butler, P.G., Wanamaker, A.D., Scourse, J.D., Richardson, C.A., Reynolds, D.J., 2013. Variability of marine climate on the North Icelandic Shelf in a 1357-year proxy archive based on growth increments in the bivalve *Arctica islandica*. Palaeogeogr. Palaeoclimatol. Palaeoecol. 373, 141–151.

Caballero-Alfonso, A.M., Carstensen, J., Conley, D.J., 2015. Biogeochemical and environmental drivers of coastal hypoxia. J. Mar. Syst. 141, 190–199.

Carstensen, J., Andersen, J.H., Gustafsson, B.G., Conley, D.J., 2014a. Deoxygenation of the Baltic Sea during the last century. Proc. Natl. Acad. Sci. U.S.A. 111, 5628–5633.

Carstensen, J., Conley, D.J., Bonsdorff, E., Gustafsson, B.G., Hietanen, S., Janas, U., Jilbert, T., Maximov, A., Norkko, A., Norkko, J., Reed, D.C., Slomp, C.P., Timmermann, K., Voss, M., 2014b. Hypoxia in the Baltic Sea: biogeochemical cycles, benthic fauna, and management. Ambio 43, 26–36.

Casella, L.A., Griesshaber, E., Yin, X., Ziegler, A., Mavromatis, V., Müller, D., Ritter, A.-C., Hippler, D., Harper, E.M., Dietzel, M., Immenhauser, A., Schöne, B.R., Angiolini, L., Schmahl, W.W., 2017. Experimental diagenesis: insights into aragonite to calcite transformation of *Arctica islandica* shells by hydrothermal treatment. Biogeosciences 14, 1461–1492.

Charrieau, L.M., Ljung, K., Schenk, F., Daewel, U., Kritzberg, E., Filipsson, H.L., 2019. Rapid environmental responses to climate-induced hydrographic changes in the Baltic Sea entrance. Biogeosciences 16, 3835–3852.

Clark, G.R., 1968. Mollusk shell: daily growth lines. Science 161, 800–802.

Clarke, M.L., Rendell, H.M., 2009. The impact of North Atlantic storminess on western European coasts: A review. Quat. Int.195, 31–41.

Conley, D.J., 2002. Terrestrial ecosystems and the global biogeochemical silica cycle. Global Biogeochem. Cycles 16, 68–1–68–8.

Conley, D.J., Bjorck, S., Bonsdorff, E., Carstensen, J., Destouni, G., Gustafsson, B.G., Hietanen, S., Kortekaas, M., Kuosa, H., Meier, H.E., Muller-Karulis, B., Nordberg, K., Norkko, A., Nurnberg, G., Pitkanen, H., Rabalais, N.N., Rosenberg, R., Savchuk, O.P., Slomp, C.P., Voss, M., Wulff, F., Zillen, L., 2009. Hypoxia-related processes in the Baltic Sea. Environ. Sci. Technol. 43, 3412–3420.

Conley, D.J., Carstensen, J., Ærtebjerg, G., Christensen, P.B., Dalsgaard, T., Hansen, J.L.S., Josefson, A.B., 2007. Long-term changes and impacts of hypoxia in Danish coastal waters. Ecol. Appl. 17, S165–S184.

Conley, D.J., Carstensen, J., Aigars, J., Axe, P., Bonsdorff, E., Eremina, T., Haahti, B.M., Humborg, C., Jonsson, P., Kotta, J., Lannegren, C., Larsson, U., Maximov, A., Medina, M.R., Lysiak-Pastuszak, E., Remeikaite-Nikiene, N., Walve, J., Wilhelms, S., Zillen, L., 2011. Hypoxia is increasing in the coastal zone of the Baltic Sea. Environ. Sci. Technol. 45, 6777–6783.

Darr, A., Gogina, M., Zettler, M.L., 2014. Detecting hot-spots of bivalve biomass in the south-western Baltic Sea. J. Mar. Syst. 134, 69–80.

Diaz, R.J., Rosenberg, R., 1995. Marine benthic hypoxia: A review of its ecological effects and the behavioural responses of benthic macrofauna. Oceanogr. Mar. Biol. 33, 245–303.

Diaz, R.J., Rosenberg, R., 2008. Spreading dead zones and consequences for marine ecosystems. Science 321, 926–9.

Diaz, R.J., Rosenberg, R., 2011. Introduction to environmental and economic consequences of hypoxia. Int. J. Water Resour. Dev. 27, 71–82.

Dries, R.R., Theede, H., 1974. Sauerstoffmangelresistenz mariner Bodenvertebraten aus der westlichen Ostsee. Mar. Bio. 25, 327–333.

Emeis, K.-C., Struck, U., Blanz, T., Kohly, A., Voβ, M., 2003. Salinity changes in the central Baltic Sea (NW Europe) over the last 10000 years. Holocene 13, 411–421.

Fedonkin, M.A., Waggoner, B.M., 1997. The Late Precambrian fossil Kimberella is a mollusc-

like bilaterian organism. Nature 388, 868–871.

Filipsson, H.L., Nordberg, K., 2004. Climate variations, an overlooked factor influencing the recent marine environment. An example from Gullmar Fjord, Sweden, illustrated by benthic foraminifera and hydrographic data. Estuaries 27, 867–881.

Fraiser, M.L., Bottjer, D.J., 2007. When bivalves took over the world. Paleobiology 33, 397–413.

Fröhlich, L., Siebert, V., Huang, Q., Thébault, J., Jochum, K.P., Schöne, B.R., 2022a. Deciphering the potential of Ba/Ca, Mo/Ca and Li/Ca profiles in the bivalve shell *Pecten maximus* as proxies for the reconstruction of phytoplankton dynamics. Ecol. Indic. 141, 109121.

Fröhlich, L., Siebert, V., Walliser, E.O., Thébault, J., Jochum, K.P., Chauvaud, L., Schöne, B.R., 2022b. Ba/Ca profiles in shells of *Pecten maximus* – A proxy for specific primary producers rather than bulk phytoplankton. Chem. Geol. 593, 120743.

Gillikin, D.P., Wanamaker, A.D., Andrus, C.F.T., 2019. Chemical sclerochronology. Chem. Geol. 526, 1–6.

Giomi, F., Barausse, A., Steckbauer, A., Daffonchio, D., Duarte, C.M., Fusi, M., 2023. Oxygen dynamics in marine productive ecosystems at ecologically relevant scales. Nat. Geosci. 16, 560–566.

Golikov, A.N., Scarlato, O.A., 1973. Method for indirectly defining optimum temperatures of inhabitancy for marine cold-blooded animals. Mar. Bio. 20, 1–5.

Goldberg, E.D., 1975. The mussel watch programme – a first step in global marine monitoring. Mar. Pollut. Bull. 6, 111–114

Gooday, A.J., Bernhard, J.M., Levin, L.A., Suhr, S.B., 2000. Foraminifera in the Arabian Sea oxygen minimum zone and other oxygen-deficient settings: taxonomic composition, diversity, and relation to metazoan faunas. Deep Sea Res. Part I Oceanogr. Res. Pap. 47, 25–54.

Gooday, A.J., Levin, L.A., Aranda da Silva, A., Bett, B.J., Cowie, G.L., Dissard, D., Gage, J.D., Hughes, D.J., Jeffreys, R., Lamont, P.A., Larkin, K.E., Murty, S.J., Schumacher, S., Whitcraft, C., Woulds, C., 2009. Faunal responses to oxygen gradients on the Pakistan margin: A comparison of foraminiferans, macrofauna and megafauna. Deep Sea Res. Part II: Top. Stud. Oceanogr. 56, 488–502.

Goreau, T.F., Goreau, N.I., Goreau, T.J., 1979. Corals and coral reefs. Sci. Am. 241, 124–137.

Gröcke, D.R., Gillikin, D.P., 2008. Advances in mollusc sclerochronology and sclerochemistry: tools for understanding climate and environment. Geo-Mar. Lett. 28, 265–268.

Groeneveld, J., Filipsson, H.L., Austin, W.E.N., Darling, K., McCarthy, D., Quintana Krupinski, N.B., Bird, C., Schweizer, M., 2018. Assessing proxy signatures of temperature, salinity, and hypoxia in the Baltic Sea through foraminifera-based geochemistry and faunal assemblages. J. Micropalaeontol. 37, 403–429.

Gustafsson, B.G., Schenk, F., Blenckner, T., Eilola, K., Meier, H.E., Muller-Karulis, B., Neumann, T., Ruoho-Airola, T., Savchuk, O.P., Zorita, E., 2012. Reconstructing the development of Baltic sea eutrophication 1850–2006. Ambio 41, 534–548.

Gustafsson, B.G., Westman, P., 2002. On the causes for salinity variations in the Baltic Sea during the last 8500 years. Paleoceanography 17, 12–1–12–14.

Hardisty, D.S., Riedinger, N., Planavsky, N.J., Asael, D., Andren, T., Jorgensen, B.B., Lyons, T.W., 2016. A Holocene history of dynamic water column redox conditions in the Landsort Deep, Baltic Sea. Am. J. Sci. 316, 713–745.

Harper, E.M., 1998. The fossil record of bivalve molluscs. In: The adequacy of the fossil record. Ed. by S. K. Donovan and C. R. C. Paul. Chichester, UK: John Wiley & Sons, 243–267.

Hatch, M.B.A., Schellenberg, S.A., Carter, M.L., 2013. Ba/Ca variations in the modern intertidal bean clam *Donax gouldii*: An upwelling proxy? Palaeogeogr. Palaeoclimatol. Palaeoecol. 373, 98–107.

Hem, J.D., 1963. Chemical equilibria affecting the behavior of manganese in natural water. International Association of Scientific Hydrology. Bulletin 8, 30–37.

Holland, H.A., Schone, B.R., Marali, S., Jochum, K.P., 2014. History of bioavailable lead and iron in the Greater North Sea and Iceland during the last millennium – A bivalve sclerochronological reconstruction. Mar. Pollut. Bull. 87, 104–116.

IOC-UNESCO, 2022. State of the Ocean Report, Pilot edition. Paris, IOC-UNESCO (IOC Technical Series, 173), Paris.

Jagnow, B., Gosselck, F., 1987. Bestimmungsschlüssel für die Gehäuseschnecken und Muscheln der Ostsee. Mitteilungen aus dem Museum für Naturkunde in Berlin. Zoologisches Museum und Institut für Spezielle Zoologie (Berlin) 63, 191–268.

Jilbert, T., Slomp, C.P., 2013a. Iron and manganese shuttles control the formation of authigenic phosphorus minerals in the euxinic basins of the Baltic Sea. Geochim. Cosmochim. Acta 107, 155–169.

Jilbert, T., Slomp, C.P., 2013b. Rapid high-amplitude variability in Baltic Sea hypoxia during the Holocene. Geology 41, 1183–1186.

Jorissen, F.J., Fontanier, C., Thomas, E. Chapter seven paleoceanographical proxies based on deep-sea benthic foraminiferal assemblage characteristics. Proxies in Late Cenozoic

Paleoceanography, 2007, 263–325 pp.

Kabel, K., Moros, M., Porsche, C., Neumann, T., Adolphi, F., Andersen, T.J., Siegel, H., Gerth, M., Leipe, T., Jansen, E., Sinninghe Damsté, J.S., 2012. Impact of climate change on the Baltic Sea ecosystem over the past 1,000 years. Nat. Clim. Change. 2, 871–874.

Keeling, R.E., Kortzinger, A., Gruber, N., 2010. Ocean deoxygenation in a warming world. Ann. Rev. Mar. Sci. 2, 199–229.

Keigwin, L.D., 1996. The little ice age and medieval warm period in the Sargasso Sea. Science 274, 1504–1508.

Kemp, A.E.S., 1996. Laminated sediments as palaeo-indicators. Geological Society, London, Special Publications 116, vii-xii.

Kiihlmorgen-Hille, G., 1963. Quantitative Untersuchungen der Bodenfauna in der Kieler Bucht und ihre jahreszeitlichen Veränderungen. Kieler Meeresforschungen 19, 42–66.

Kocot, K.M., Cannon, J.T., Todt, C., Citarella, M.R., Kohn, A.B., Meyer, A., Santos, S.R., Schander, C., Moroz, L.L., Lieb, B., Halanych, K.M., 2011. Phylogenomics reveals deep molluscan relationships. Nature 477, 452–6.

Kõuts, M., Maljutenko, I., Elken, J., Liu, Y., Hansson, M., Viktorsson, L., Raudsepp, U., 2021. Recent regime of persistent hypoxia in the Baltic Sea. Environ. Res. Commun. 3, 075004.

Kube, J., Powilleit, M., Warzocha, J., 1996. The importance of hydrodynamic processes and food availability for the structure of macrofauna assemblages in the Pomeranian Bay (Southern Baltic Sea). Archiv für Hydrobiologie 213–228.

Kuliński, K., Rehder, G., Asmala, E., Bartosova, A., Carstensen, J., Gustafsson, B., Hall, P.O.J., Humborg, C., Jilbert, T., Jürgens, K., Meier, H.E.M., Müller-Karulis, B., Naumann, M., Olesen, J.E., Savchuk, O., Schramm, A., Slomp, C.P., Sofiev, M., Sobek, A., Szymczycha, B., Undeman, E., 2022. Biogeochemical functioning of the Baltic Sea. Earth Syst. Dyn. 13, 633–685.

Langlet, D., Alunno-Bruscia, M., Rafélis, M., Renard, M., Roux, M., Schein, E., Buestel, D., 2006. Experimental and natural cathodoluminescence in the shell of *Crassostrea gigas* from Thau lagoon (France): ecological and environmental implications. Mar. Ecol. Prog. Ser. 317, 143–156.

Lazareth, C.E., Putten, E.V., André, L., Dehairs, F., 2003. High-resolution trace element profiles in shells of the mangrove bivalve *Isognomon ephippium*: a record of environmental spatio-temporal variations? Estuar. Coast. Shelf Sci. 57, 1103–1114.

Lenz, C., Jilbert, T., Conley, D., Wolthers, M., Slomp, C., 2015. Are recent changes in sediment

manganese sequestration in the euxinic basins of the Baltic Sea linked to the expansion of hypoxia? Biogeosciences 12, 4875–4894.

Limburg, K.E., Breitburg, D., Swaney, D.P., Jacinto, G., 2020. Ocean deoxygenation: A primer. One Earth 2, 24–29.

Lutz, R.A., Goodsell, J.G., Mann, R., Castagna, M., 1981. Experimental culture of the ocean quahog, *Arctica islandica*. J. World Aquac. Soc. 12, 196–205.

Marali, S., Schöne, B.R., 2015. Oceanographic control on shell growth of *Arctica islandica* (Bivalvia) in surface waters of Northeast Iceland – Implications for paleoclimate reconstructions. Palaeogeogr. Palaeoclimatol. Palaeoecol. 420, 138–149.

Marali, S., Schöne, B.R., Mertz-Kraus, R., Griffin, S.M., Wanamaker, A.D., Butler, P.G., Holland, H.A., Jochum, K.P., 2017a. Reproducibility of trace element time-series (Na/Ca, Mg/Ca, Mn/Ca, Sr/Ca, and Ba/Ca) within and between specimens of the bivalve *Arctica islandica* – A LA-ICP-MS line scan study. Palaeogeogr. Palaeoclimatol. Palaeoecol. 484, 109–128.

Marali, S., Schöne, B.R., Mertz-Kraus, R., Griffin, S.M., Wanamaker, A.D., Matras, U., Butler, P.G., 2017b. Ba/Ca ratios in shells of *Arctica islandica* – Potential environmental proxy and crossdating tool. Palaeogeogr. Palaeoclimatol. Palaeoecol. 465, 347–361.

Marchitto, T.M., Jones, G.A., Goodfriend, G.A., Weidman, C.R., 2000. Precise temporal correlation of holocene mollusk shells using sclerochronology. Quat. Res. 53, 236–246.

Mann, R., 1989. Larval ecology of *Arctica islandica* on the inner continental shelf of the eastern United States. J. Shellfish Res. 8, 464.

Middelburg, J.J., Delange, G.J., Vanderweijden, C.H., 1987. Manganese solubility control in marine pore waters. Geochim. Cosmochim. Acta 51, 759–763.

Morton, B., 2011. The biology and functional morphology of *Arctica islandica* (Bivalvia: Arcticidae) – A gerontophilic living fossil. Mar. Biol. Res. 7, 540–553.

Moss, D.K., Surge, D., Khaitov, V., 2018. Lifespan and growth of *Astarte borealis* (Bivalvia) from Kandalaksha Gulf, White Sea, Russia. Polar Biol. 41, 1359–1369.

Moss, D.K., Surge, D., Zettler, M.L., Orland, I.J., Burnette, A., Fancher, A., 2021. Age and growth of *Astarte borealis* (Bivalvia) from the southwestern Baltic Sea using secondary ion mass spectrometry. Mar. Biol. 168, 1–11.

Murakami-Sugihara, N., Shirai, K., Hori, M., Amano, Y., Fukuda, H., Obata, H., Tanaka, K., Mizukawa, K., Sano, Y., Takada, H., Ogawa, H., 2019. Mussel shell geochemical analyses reflect coastal environmental changes following the 2011 Tohoku tsunami. ACS Earth Space Chem. 3, 1346–1352.

Murray, J.W., 2006. Ecology and applications of benthic foraminifera. Cambridge university press.

Nordberg, K., Gustafsson, M., Krantz, A.L., 2000. Decreasing oxygen concentrations in the Gullmar Fjord, Sweden, as confirmed by benthic foraminifera, and the possible association with NAO. J. Mar. Res. 23, 303–316.

Oeschger, R., 1990. Long-term anaerobiosis in sublittoral marine invertebrates from the western Baltic Sea: Halicryptus spinulosus (Priapulida) *Astarte borealis* and *Arctica islandica* (Bivalvia). Mar. Ecol. Prog. Ser. 59, 133-143.

Oeschger, R., Storey, K.B., 1993. Impact of anoxia and hydrogen sulphide on the metabolism of *Arctica islandica* L. (Bivalvia). J. Exp. Mar. Bio. Ecol. 170, 213–226.

Oschmann, W., 2009. Sclerochronology: editorial. International Journal of Earth Sciences 98, 1–2.

Österblom, H., Hansson, S., Larsson, U., Hjerne, O., Wulff, F., Elmgren, R., Folke, C., 2007. Human-induced trophic cascades and ecological regime shifts in the Baltic Sea. Ecosystems 10, 877–889.

Pakhomova, S.V., Hall, P.O.J., Kononets, M.Y., Rozanov, A.G., Tengberg, A., Vershinin, A.V., 2007. Fluxes of iron and manganese across the sediment – water interface under various redox conditions. Mar. Chem. 107, 319–331.

Papadomanolaki, N.M., Dijkstra, N., van Helmond, N.A.G.M., Hagens, M., Bauersachs, T., Kotthoff, U., Sangiorgi, F., Slomp, C.P., 2018. Controls on the onset and termination of past hypoxia in the Baltic Sea. Palaeogeogr. Palaeoclimatol. Palaeoecol. 490, 347–354.

Panfili, J., de Pontual, H.,Troadec, H., Wright, P.J., 2002. Manual of fish sclerochronology. Brest, France: Ifremer-IRD coedition, 464 pp.

Peharda, M., Schöne, B.R., Black, B.A., Corrège, T., 2021. Advances of sclerochronology research in the last decade. Palaeogeogr. Palaeoclimatol. Palaeoecol. 570, 110371.

Peterson, K.J., Butterfield, N.J., 2005. Origin of the Eumetazoa: testing ecological predictions of molecular clocks against the Proterozoic fossil record. Proc. Natl. Acad. Sci. U.S.A. 102, 9547–52.

Phleger, F.B., Soutar, A., 1973. Production of benthic foraminifera in three east Pacific oxygen minima. Micropaleontology, 110–115.

Prendergast, A.L., Versteegh, E.A.A., Schöne, B.R., 2017. New research on the development of high-resolution palaeoenvironmental proxies from geochemical properties of biogenic carbonates. Palaeogeogr. Palaeoclimatol. Palaeoecol. 484, 1–6.

Rabalais, N.N., Diaz, R.J., Levin, L.A., Turner, R.E., Gilbert, D., Zhang, J., 2010. Dynamics

and distribution of natural and human-caused hypoxia. Biogeosciences 7, 585-619.

Reusch, T.B.H., Dierking, J., Andersson, H.C., Bonsdorff, E., Carstensen, J., Casini, M., Czajkowski, M., Hasler, B., Hinsby, K., Hyytiainen, K., Johannesson, K., Jomaa, S., Jormalainen, V., Kuosa, H., Kurland, S., Laikre, L., MacKenzie, B.R., Margonski, P., Melzner, F., Oesterwind, D., Ojaveer, H., Refsgaard, J.C., Sandstrom, A., Schwarz, G., Tonderski, K., Winder, M., Zandersen, M., 2018. The Baltic Sea as a time machine for the future coastal ocean. Sci. Adv. 4, eaar8195.

Reynolds, D.J., Scourse, J.D., Halloran, P.R., Nederbragt, A.J., Wanamaker, A.D., Butler, P.G., Richardson, C.A., Heinemeier, J., Eiriksson, J., Knudsen, K.L., Hall, I.R., 2016. Annually resolved North Atlantic marine climate over the last millennium. Nat. Commun. 7, 13502.

Risk, M.J., Burchell, M., de Roo, K., Nairn, R., Tubrett, M., Forsterra, G., 2010. Trace elements in bivalve shells from the Río Cruces, Chile. Aquat. Biol. 10, 85–97.

Rue, E.L., Smith, G.J., Cutter, G.A., Bruland, K.W., 1997. The response of trace element redox couples to suboxic conditions in the water column. Deep Sea Res. Part I Oceanogr. Res. Pap. 44, 113–134.

Sampaio, E., Santos, C., Rosa, I.C., Ferreira, V., Portner, H.O., Duarte, C.M., Levin, L.A., Rosa, R., 2021. Impacts of hypoxic events surpass those of future ocean warming and acidification. Nat. Ecol. Evol. 5, 311–321.

Saniewski, M., Zalewska, T., Krasniewski, W., 2022. Benthic macroinvertebrates as reference indicators for monitoring of anthropogenic isotope ^{137}Cs contamination in the marine environment. Environ. Sci. Pollut. Res. 29, 13822–13834.

Savchuk, O.P., Wulff, F., Hille, S., Humborg, C., Pollehne, F., 2008. The Baltic Sea a century ago – a reconstruction from model simulations, verified by observations. J. Mar. Syst. 74, 485–494.

Schinke, H., Matthaus, W., 1998. On the causes of major Baltic inflows – An analysis of long time series. Cont. Shelf Res. 18, 67–97.

Schmiedl, G., Mitschele, A., Beck, S., Emeis, K.-C., Hemleben, C., Schulz, H., Sperling, M., Weldeab, S., 2003. Benthic foraminiferal record of ecosystem variability in the eastern Mediterranean Sea during times of sapropel S5 and S6 deposition. Palaeogeogr. Palaeoclimatol. Palaeoecol. 190, 139–164.

Schöne, B.R., 2013. *Arctica islandica* (Bivalvia): A unique paleoenvironmental archive of the northern North Atlantic Ocean. Glob. Planet. Change. 111, 199–225.

Schöne, B.R., Gillikin, D.P., 2013. Unraveling environmental histories from skeletal diaries –

Advances in sclerochronology. Palaeogeogr. Palaeoclimatol. Palaeoecol. 373, 1–5.

Schöne, B.R., Houk, S.D., Castro, A.D.F., Fiebig, J., Oschmann, W., Kroncke, I., Dreyer, W., Gosselck, F., 2005. Daily growth rates in shells of *Arctica islandica*: Assessing sub-seasonal environmental controls on a long-lived bivalve mollusk. Palaios 20, 78–92.

Sepkoski, J.J., 1981. A factor analytic description of the Phanerozoic marine fossil record. Paleobiology 7, 36–53.

Snowball, I.F., 1993. Geochemical control of magnetite dissolution in subarctic lake sediments and the implications for environmental magnetism. J. Quat. Sci. 8, 339–346.

Sohlenius, G., Emeis, K.C., Andren, E., Adren, T., Kohly, A., 2001. Development of anoxia during the Holocene fresh-brackish water transition in the Baltic Sea. Mar. Geol. 177, 221–242.

Sohlenius, G., Westman, P.E.R., 1998. Salinity and redox alternations in the northwestern Baltic proper during the late Holocene. Boreas 27, 101–114.

Stocker, T., Plattner, G.K., Dahe, Q., 2014. IPCC climate change 2013: the physical science basis – findings and lessons learned. Egu General Assembly Conference 17003 pp.

Stecher III, H.A., Krantz, D.E., Lord III, C.J., Luther III, G.W., Bock, K.W., 1996. Profiles of strontium and barium in *Mercenariu mercenariu* and *Spisula solidissima* shells. Geochim. Cosmochim. Acta 60, 3445–3456.

Steinhardt, J., Butler, P.G., Carroll, M.L., Hartley, J., 2016. The application of long-lived bivalve sclerochronology in environmental baseline monitoring. Front. Mar. Sci. 3, 176.

Sternbeck, J., Sohlenius, G., Hallberg, R.O., 2000. Sedimentary trace elements as proxies to depositional changes induced by a Holocene fresh-brackish water transition. Aquat. Geochem. 6, 325–345.

Strahl, J., Brey, T., Philipp, E.E., Thorarinsdottir, G., Fischer, N., Wessels, W., Abele, D., 2011. Physiological responses to self-induced burrowing and metabolic rate depression in the ocean quahog *Arctica islandica*. J. Exp. Biol. 214, 4223–33.

Taylor, A.C., 1976. Burrowing behaviour and anaerobiosis in the bivalve *Arctica islandica* (L.). J. Mar. Biol. Assoc. U. K. 56, 95–109.

Tebo, B.M., 1991. Manganese (II) oxidation in the suboxic zone of the Black Sea. Deep Sea Res. Part I Oceanogr. Res. Pap. 38, S883–S905.

Theede, H., 1973. Comparative studies on the influence of oxygen deficiency and hydrogen sulphide on marine bottom invertebrates. Neth. J. Sea Res. 7, 244–252.

Theede, H., Ponat, A., Hiroki, K., Schlieper, C., 1969. Studies on the resistance of marine bottom invertebrates to oxygen-deficiency and hydrogen sulphide. Mar. Biol. 2, 325–

337.

Trutschler, K., Samtleben, C., 1988. Shell growth of *Astarte elliptica* (Bivalvia) from Kiel Bay (Western Baltic Sea). Mar. Ecol. Prog. Ser. 42, 155–162.

Tyson, R.V., Pearson, T.H. 1991. Modern and ancient continental shelf anoxia: an overview. Geological Society, London, Special Publications, 58, 1-24.

van Helmond, N.A.G.M., Jilbert, T., Slomp, C.P., 2018. Hypoxia in the Holocene Baltic Sea: Comparing modern versus past intervals using sedimentary trace metals. Chem. Geol. 493, 478–490.

Vander Putten, E., Dehairs, F., Keppens, E., Baeyens, W., 2000. High resolution distribution of trace elements in the calcite shell layer of modern *Mytilus edulis*: environmental and biological controls. Geochim. Cosmochim. Acta 64, 997–1011.

Vaquer-Sunyer, R., Duarte, C.M., 2008. Thresholds of hypoxia for marine biodiversity. Proc. Natl. Acad. Sci. U.S.A. 105, 15452–15457.

Vendrasco, M.J., Checa, A.G., Heimbrock, W.P., 2019. Remarkable preservation of shell microstructures from the Late Ordovician of the Cincinnati Arch region, USA, and the success of nacre among Ordovician mollusks. J. Paleontol. 93, 658–672.

von Oertzen, J.A.V., Schulz, S., 1973. Beitrag zur geographischen Verbreitung und ökologischen Existenz von Bivalviern der Ostsee. Beitr. Meereskunde 32, 75–88.

Wanamaker, A.D., Heinemeier, J., Scourse, J.D., Richardson, C.A., Butler, P.G., Eiríksson, J., Knudsen, K.L., 2008. Very long-lived mollusks confirm 17th century AD tephra-based radiocarbon reservoir ages for North Icelandic shelf waters. Radiocarbon 50, 399–412.

Wanamaker, A.D., Hetzinger, S., Halfar, J., 2011. Reconstructing mid- to high-latitude marine climate and ocean variability using bivalves, coralline algae, and marine sediment cores from the Northern Hemisphere. Palaeogeogr. Palaeoclimatol. Palaeoecol. 302, 1–9.

Witbaard, R., Duineveld, G.C.A., De Wilde, P.A.W.J., 1997. A Long-Term Growth Record Derived from *Arctica islandica* (Mollusca, Bivalvia) from the Fladen Ground (Northern North Sea). J. Mar. Biol. Assoc. U. K. 77, 801-816.

Winter, J.E., 1969. Über den Einfluß der Nahrungskonzentration und anderer Faktoren auf Filtrierleistung und Nahrungsausnutzung der Muscheln *Arctica islandica* und *Modiolus modiolus*. Mar. Biol. 4, 87–135.

Zettler, M.L., 2001. Recent geographical distribution of the *Astarte borealis* species complex, its nomenclature and bibliography (Bivalvia: Astartidae). Schriften zur Malakozoologie 18, 1–14.

Zettler, M.L., 2002. Ecological and morphological features of the bivalve *Astarte borealis*

(Schumacher, 1817) in the Baltic Sea near its geographical range. J. Shellfish Res. 21, 33–40.

Zettler, M.L., Bonsch, R., Gosselck, F., 2001. Distribution, abundance and some population characteristics of the ocean quahog, *Arctica islandica* (Linnaeus, 1767), in the Mecklenburg Bight (Baltic Sea). J. Shellfish Res. 20, 161–169.

Zhao, L., Walliser, E.O., Mertz-Kraus, R., Schöne, B.R., 2017. Unionid shells (*Hyriopsis cumingii*) record manganese cycling at the sediment-water interface in a shallow eutrophic lake in China (Lake Taihu). Palaeogeogr. Palaeoclimatol. Palaeoecol. 484, 97–108.

Zillén, L., Conley, D.J., 2010. Hypoxia and cyanobacteria blooms - are they really natural features of the late Holocene history of the Baltic Sea? Biogeosciences 7, 2567–2580.

Zillén, L., Conley, D.J., Andrén, T., Andrén, E., Björck, S., 2008. Past occurrences of hypoxia in the Baltic Sea and the role of climate variability, environmental change and human impact. Earth Sci. Rev. 91, 77–92.

Zillén, L., Snowball, I., Sandgren, P., Stanton, T., 2003. Occurrence of varved lake sediment sequences in Värmland, west central Sweden: lake characteristics, varve chronology and AMS radiocarbon dating. Boreas 32, 612–626.

2 Material and Methods

2.1 Sample collection

For this study, twenty-two specimens of three bivalve species (*A. islandica*, *A. borealis*, *A. elliptica*) were collected from five stations (i.e., St12, MB2, O4, FBR36 and FBR06) located in different areas of the Baltic Sea (Table 2.1; see map in Fig. 2.1). All live-collected bivalves were initially sacrificed in formalin and subsequently preserved in 70 vol% ethyl alcohol.

In Chapter 3, six specimens of *A. islandica* collected by bottom dredging in the Mecklenburg Bight (St12) on 25 October 2001. Shells of studied specimens lived in a water depth of 25 m. The soft parts of these bivalves were removed in the laboratory in winter 2019/20.

In Chapter 4, eleven specimens were chosen, including five of *A. islandica* and three each of *A. elliptica* and *A. borealis*. All specimens were obtained from Fehmarn Belt with van Veen grabs on 29 June 2020. Specimens of *A. islandica* and *A. elliptica* lived in 21 m depth (FBR36), and *A. borealis* came from 18 m (FBR06). They were eviscerated in the laboratory in the winter of 2020.

Four *A. islandica* collected in Chapter 5 sampled from St12 (25m, N=3) and FBR36 (21m, N=1), respectively. They were already used in previous Chapters.

In Chapter 6, ten specimens of *A. islandica* collected at similar water depths in Mecklenburg Bight, stations O4 (23.5 m, N = 2), MB2 (24 m, N = 3) and St12 (25 m, N = 5). Specimens from MB2 and O4 were collected alive on 22 June 1996 and during November 1904, respectively, and stored in museum collections. Specimens from St12 were already used in Chapter 3.

After carefully removing the soft tissue in the laboratory, the empty shell was washed with tap water and air-dried. I have performed sclerochronological analysis of shell growth patterns and their geochemical properties.

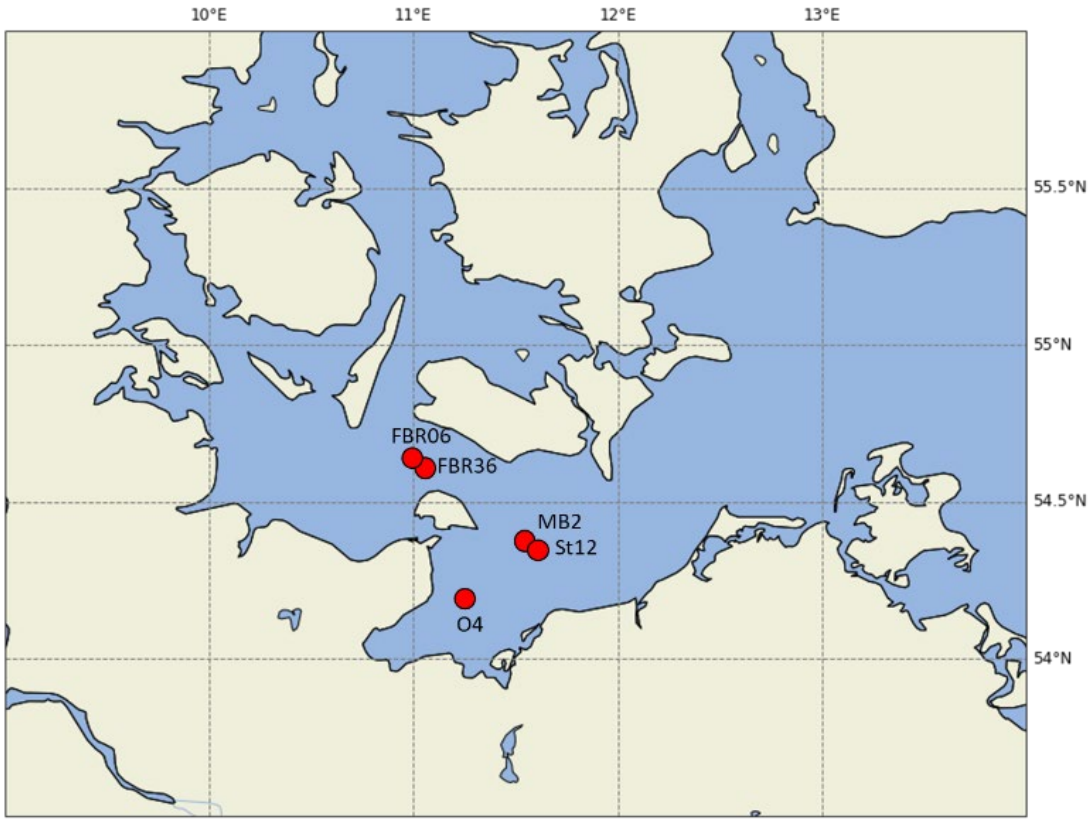

Figure 2.1 Map showing sampling locations (St12, MB2, O4, FBR36 and FBR06) in the Baltic Sea.

Table 2.1 Overview of studied bivalves. Last character of ID denotes left (L) or right (R) valve. [a] H-hinge, VM-ventral margin; [b] MPIC-Max Planck Institute for Chemistry; JGU-Johannes Gutenberg University of Mainz.

Taxon	Specimen ID	Ontogen. age (yr)	LA-ICP-MS	
			#spots [a, b]	cal. yrs, ontog. yrs
Mecklenburg Bight (St12): 54°18′59.50″N, 011°33′00.00″ E; 25 m				
Arctica islandica	MLZ-St12-A2L+R	19	42 [H, MPIC]	
Arctica islandica	MLZ-St12-A4R	19	48 [H, JGU] 329 [VM, JGU]	1987-2001, 5-19
Arctica islandica	MLZ-St12-A5R	15	44 [H, JGU] 326 [VM, JGU]	1991-2001, 5-15
Arctica islandica	MLZ-St12-A6R	14	42 [H, JGU] 373 [VM, JGU]	1991-2001, 4-14
Arctica islandica	MLZ-St12-A7L	7	25 [H, JGU] 183 [VM, JGU]	1997-2001, 3-7
Arctica islandica	MLZ-St12-A9L+R	8	26 [H, JGU] 151 [VM, JGU]	1998-2001, 5-8

Mecklenburg Bight (MB2): 54°19´55.75″ N, 011°29´52.95″E; 24m				
Arctica islandica	HR-MB2-96-A1L	12	38 [H, MPIC]	1988-1995, 3-12
Arctica islandica	HR-MB2-96-A3L	15	49 [H, MPIC]	1984-1995, 3-14
Arctica islandica	HR-MB2-96-A4L	20	56 [H, MPIC]	1979-1995, 3-19
Mecklenburg Bight (O4): 54°10´N, 011°16´E; 23.5m				
Arctica islandica	MOL 8215_04.XI.O4-A1L	65	406 [VM, JGU]	1845-1903, 6-64
Arctica islandica	MOL 8215_04.XI.O4-A2L	59	354 [VM, JGU]	1856-1902, 11-56
Fehmarn Belt (FBR36): 54°18′59.50″N, 011°33′00.00″E; 21m				
Arctica islandica	MLZ-FBR36-A4L	41	480 [VM, JGU]	1983-2020, 4-41
Arctica islandica	MLZ-FBR36-A6L	9	207 [VM, JGU]	2015-2020, 4-9
Arctica islandica	MLZ-FBR36-A7L	10	202 [VM, JGU]	2012-2020, 3-10
Arctica islandica	MLZ-FBR36-A15L	10	393 [VM, JGU]	2012-2020, 3-10
Astarte elliptica	MLZ-FBR36-A16L	21	441 [VM, JGU]	2005-2020, 6-21
Astarte elliptica	MLZ-FBR36-A8L	21	170 [VM, JGU]	2004-2020, 5-20
Astarte elliptica	MLZ-FBR36-A9L	27	134 [VM, JGU]	2003-2015, 10-21
Astarte elliptica	MLZ-FBR36-A10L	30	197 [VM, JGU]	1997-2015, 7-24
Fehmarn Belt (FBR06): 54°37′01.20″N, 011°00′36.00″E; 18m				
Astarte borealis	MLZ-FBR06-A1L	50	210 [VM, JGU]	1978-2019, 8-49
Astarte borealis	MLZ-FBR06-A2L	52	163 [VM, JGU]	1981-2019, 13-51
Astarte borealis	MLZ-FBR06-A3L	47	190 [VM, JGU]	1981-2018, 8-45

2.2 Sclerochronological methods

2.2.1 Shell cross-section preparation

One valve of each species was mounted on plexiglass cubes and wrapped in a protecting layer of WIKO metal epoxy resin. After the epoxy had cured, along the axis of maximum growth, two (or more) ca. 2- to 3-millimeter-thick sections were cut from the umbo to the commissure and perpendicular to the growth lines by using a low-speed saw with a 0.4-millimeter-thick low-concentration diamond-coated saw blade. Afterward, shell slabs were mounted on glass slabs and ground with grit SiC power of 800 and 1200 on glass plate respectively, and polished with 1 µm Al_2O_3 suspension on a Buehler MasterTex cloth. Between each grinding and polishing step, the shell cross-sections were ultrasonically cleaned with tap water. One cross-section was

selected for growth pattern analysis, whereas the other one was subsequently used for in-situ chemical analysis.

2.2.2 Shell growth pattern analysis

In polished cross-sections, growth lines (i.e., periods of slow growth) appear as dark lines and growth increments (i.e., periods of fast growth) as white bands under reflected light. This difference is produced by changes in the growth rates that alter the proportion of organic matrix compounds (Lutz and Rhoads, 1977) and/or the texture and regularity of the crystal microstructure (Ropes et al., 1984) in the shell. To better recognize shell growth patterns, cross-sections were stained using Mutvei's solution for ca. 18 min under constant stirring at 37 to 40 °C (Mutvei, 1979; Schöne et al., 2005). This agent simultaneously etches the carbonate of the shells, preserves organic matters and stains acid mucopolysaccharides and glycosaminoglycans (acid mucosubstances and acetic mucins) blue (Steedman, 1950). Since the growth lines are richer in organics, they stain darker blue and are more etch-resistant than the carbonate dominated portions between adjacent growth lines under a reflected light microscope. To analyzed shell growth patterns, etched and dyed thick-sections were viewed under a binocular microscope (Olympus SZX16) equipped with sectoral (= one-quarter) dark-field right-light illumination (Schott VisiLED MC1000) and photographed with a digital camera (Canon EOS 600D). Growth increments widths were determined in the hinge plate and ventral margin with the digital image processing software, Panopea (© Peinl & Schöne). The annual shell growth patterns provided a framework by which chemical data were placed in accurate temporal context.

2.2.3 Geochemical analysis

The remaining unetched, polished cross-sections were used for in-situ chemical analysis of the shell carbonate. The concentrations of elements were determined by laser ablation-inductively coupled plasma-mass spectrometry (LA-ICP-MS) in spot model at the Max Planck Institute for Chemistry (MPIC) at Mainz or at the Institute of Geoscience, Johannes Gutenberg University of Mainz (JGU) (Table 2.1).

Spots with a diameter of 55 to 65 µm and a midpoint of 80 to 90 µm were placed along the ventral margin of the shell (inner portion of the outer shell layer) as well as the axes of maximum growth in the hinge plate (Table 2.1). Accuracy and precision of all LA-ICP-MS analyses were assessed by measuring different reference materials as quality control materials (QCMs). At both institutes, USGS MACS-3 was used, and at the JGU USGS BCR-2G as well.

Reference values were taken from the GeoReM database (preferred complied values, http://georem.mp ch-mainz.gwdg.de/; Jochum et al., 2005, 2011). For data measured at the MPIC, the synthetic glass, NIST SRM 612, was used to calibrate the element concentrations of the shell samples and signals of the measurements were monitored in time-resolved mode and processed using an in-house Excel spreadsheet (Jochum et al., 2007; Mischel et al., 2017). For the measurements performed at JGU, NIST SRM 610 and 612 were used as calibration material. The time-resolved signals were processed using LAtools (Branson et al., 2019). For both data reduction strategies and to compute molar element-to-calcium ratios (µmol/mol), ^{43}Ca served as the internal standard, applying for samples with a Ca content of 380,000 µg/g (Marali et al., 2017).

By using periodic growth patterns as a time gauge, the geochemical data of the shells were placed in a precise temporal context. Mathematical resampling was required to adjust the LA spots to a common resolution to allow direct comparison of geochemical data. The compilation of long-term environmental data was used to assess how well geochemical parameters of the shells record the occurrence and intensity of hypoxia in the studied localities.

Reference

Branson, O., Fehrenbacher, J., Vetter, L., Sadekov, A.Y., Eggins, S.M., Spero, H.J., 2019. LAtools: A data analysis package for the reproducible reduction of LA-ICP-MS data. Chem. Geol. 504, 83–95

Jochum, K.P., Nohl, U., Herwig, K., Lammel, E., Stoll, B., Hofmann, A.W., 2005. GeoReM: a new geochemical database for reference materials and isotopic standards. Geostand. Geoanal. Res. 29, 333–338.

Jochum, K.P., Stoll, B., Herwig, K., Willbold, M., 2007. Validation of LA-ICP-MS trace element analysis of geological glasses using a new solid-state 193 nm Nd:YAG laser and matrix-matched calibration. J. Anal. At. Spectrom. 22, 112.

Jochum, K.P., Weis, U., Stoll, B., Kuzmin, D., Yang, Q., Raczek, I., Jacob, D.E., Stracke, A., Birbaum, K., Frick, D.A., Günther, D., Enzweiler, J., 2011. Determination of reference values for NIST SRM 610–617 glasses following ISO guidelines. Geostand. Geoanal. Res. 35, 397–429.

Lutz, R.A., Rhoads, D.C., 1977. Anaerobiosis and a theory of growth line formation. Science 198, 1222–1227.

Marali, S., Schöne, B.R., Mertz-Kraus, R., Griffin, S.M., Wanamaker, A.D., Butler, P.G., Holland, H.A., Jochum, K.P., 2017. Reproducibility of trace element time-series (Na/Ca, Mg/Ca, Mn/Ca, Sr/Ca, and Ba/Ca) within and between specimens of the bivalve *Arctica islandica* – A LA-ICP-MS line scan study. Palaeogeogr. Palaeoclimatol. Palaeoecol. 484, 109–128.

Mischel, S.A., Mertz-Kraus, R., Jochum Klaus, P., Scholz, D., 2017. TERMITE: An R script for fast reduction of laser ablation inductively coupled plasma mass spectrometry data and its application to trace element measurements. Rapid Comm. Mass Spec. 31, 1079–1087.

Ropes J.W., Jones, D.S., Murawski S,A., Serchuk, F. M., Ambrose Jearld, J.R.,1984. Ocean quahogs, *Arctica islandica* Linné. Fish. Bull. 82, 1.

Schöne, B.R., Dunca, E., Fiebig, J., Pfeiffer, M., 2005. Mutvei's solution: An ideal agent for resolving microgrowth structures of biogenic carbonates. Palaeogeogr. Palaeoclimatol. Palaeoecol. 228, 149–166.

Steedman, H.F., 1950. Alcian blue 8GS: a new stain for mucin. J. Cell Sci. 91, 477–479.

3 Mn/Ca in shells of *Arctica islandica* (Baltic Sea) – A potential proxy for ocean hypoxia?

Bernd R. Schöne[1], Xizhi Huang[1], Michael L. Zettler[2], Liqiang Zhao[3], Regina Mertz-Kraus[1], Klaus Peter Jochum[4], Eric O. Walliser[1]

[1] Institute of Geosciences, University of Mainz, Mainz, Germany
[2] Leibniz Institute for Baltic Sea Research Warnemünde, Rostock, Germany
[3] College of Fisheries, Guangdong Ocean University, Zhanjiang, China
[4] Climate Geochemistry Department, Max Planck Institute for Chemistry, Mainz, Germany

Schöne, B.R., Huang, X., Zettler, M.L., Zhao, L., Mertz-Kraus, R., Jochum, K.P., and Walliser, E.O. (2021). Mn/Ca in shells of *Arctica islandica* (Baltic Sea) – A potential proxy for ocean hypoxia? *Estuarine, Coastal and Shelf Science*, *251*, 107257.

This manuscript was published in the journal "*Estuarine, Coastal and Shelf Science*". I contributed to the sample preparation and measurements, collected and organized data, developed part of the methodology, and helped with the interpretation of the results. This work was supported by the DFG grant to BRS [SCHO793/22].

Authors' contributions:

BRS: Conceptualization, Data curation, Formal analysis, Funding acquisition, Investigation, Methodology, Project administration, Supervision, Validation, Visualization, Writing –

original draft preparation; Writing – review and editing

XZH: Data curation, Methodology, Formal analysis

MLZ: Resources, Writing – review and editing

LQZ: Conceptualization, Methodology

RMK: Resources, Validation, Writing – review and editing

KPJ: Resources, Validation

EOW: Investigation, Supervision, Validation, Visualization, Writing – review and editing

Abstract

Oxygen depletion threatens an increasing number of shallow water environments, specifically habitats below the seasonal halocline in coastal settings of the Baltic Sea. To understand the natural variations of dissolved oxygen levels on seasonal and inter-annual time-scales prior to the instrumental era, high-resolution archives are urgently required. The present study evaluates the potential use of Mn/Ca values in shells of the bivalve, *Arctica islandica* to infer concentrations of past dissolved oxygen concentrations. This study is based on laser ablation – inductively coupled plasma – mass spectrometry (LA-ICP-MS) data of six contemporaneous specimens and demonstrates that background variations of shell Mn/Ca are inversely linked to dissolved oxygen concentrations in the water column ($r = -0.68$; $R^2 = 0.46$, $p < 0.0001$), which in turn are coupled to the amount of dissolved Mn. The regular seasonal changes were superimposed by sharp Mn/Ca peaks, most likely resulting from the ingestion of a large amount of Mn-rich organic particles. The availability of such particles can increase due to the resuspension of food particles by strong bottom currents or alternatively, result from increased particle flux from surface waters after major river discharges and subsequent phytoplankton blooms. Besides sharp Mn/Ca peaks, often accompanied by sharp Ba/Ca peaks and increased shell growth rate. In addition, after exceptional major barotropic inflows from the North Sea, the biogeochemical steady-state conditions remained disturbed for up to ca. two years, because the redox-sensitive elements were removed from the water column by oxygenated waters, and it took time for them to build up again in the water column. Therefore, subsequent to such Major Baltic Inflows (MBIs), dissolved Mn levels and shell Mn/Ca values were strongly reduced despite summertime low- oxygen conditions. As demonstrated here, Mn/Ca data of *A. islandica* shells can potentially serve as a proxy for dissolved oxygen levels in the water column. To further develop this proxy, a set of additional environmental and physiological proxies such as shell Ba/Ca values and growth rate should be critically assessed and used in combination with shell Mn/Ca.

3.1 Introduction

Oxygen depletion threatens an increasing number of nearshore shallow-water ecosystems (Vaquer-Sunyer and Duarte 2008). Severe and prolonged low-oxygen conditions can be lethal for aquatic organisms and destroy benthic communities (Karlson et al., 2002; Diaz and Rosenberg 2008) with repercussions for the entire food web (Zillén et al., 2008). Low levels of dissolved oxygen (DO) can also alter the biogeochemical cycles of nutrients by enhancing the release of phosphorus and nitrogen from the sediment into the overlying water column which promotes eutrophication and amplifies oxygen undersaturation (Österblom et al., 2007). Despite significant differences in low-oxygen tolerance among species, the threshold of DO below which most marine organisms greatly suffer or perish is, on average, approx. 2.3 mg/L (corresponding to 1.6 mL/L or 72.2 µmol/L) (Vaquer-Sunyer and Duarte 2008). This concentration delimits normoxic from hypoxic waters. Since the solubility of gases in water depends on a number of factors including temperature and salinity, the threshold of hypoxia is now defined by a DO saturation of 30 % (Rabalais et al., 2010). Sticking to the aforementioned DO concentration of 2.3 mg/L, this DO saturation threshold would be attained, for example, at 17.8 °C and 35.0 PSU, or 22.0 °C and 21.9 PSU (computed with the equation by Benson and Krause, 1984).

One of the largest and best studied oxygen-deficient zones in the world is located in the Baltic Sea, where the spatial extent, intensity and duration of hypoxia below the halocline has increased strikingly during the last century and continues to do so, both in deeper offshore settings and shallow nearshore (coastal) environments (Conley et al., 2009, 2011; Carstensen et al., 2014a). However, due to temporally and spatially incomplete observational data, coastal hypoxia of the Baltic Sea (typically a seasonal phenomenon; Bonsdorff, 2006) is poorly characterized and its causes are not entirely clear. Potential driving forces include anthropogenic eutrophication (Conley et al., 2007), meteorological and hydrological conditions (e.g., wind speed, horizontal advection, vertical mixing, climate-controlled pulses of barotropic inflows from the North Sea, so-called Major Baltic Inflows, MBIs) as well as global warming (Kabel et al., 2012; Caballero-Alfonso et al., 2015). With a more robust dataset and knowledge of past DO levels it would be possible to (i) determine pre-anthropogenic baseline conditions and quantify the natural DO dynamics (Sohlenius et al., 2001; Zillén et al., 2008), (ii) elucidate the processes leading to hypoxia and estimate the anthropogenic contribution to the expansion of oxygen-minimum zones (Andrén et al., 2000; Carstensen et al., 2014a), and (iii) set restoration targets and timetables (Carstensen et al., 2014b; Caballero-Alfonso et al., 2015). Up until now, information on the history of bottom water hypoxia prior to the instrumental era relies

almost exclusively on DO proxies archived in sediments such as foraminifera (Nordberg et al., 2000; Filipsson and Nordberg 2004) and diatom assemblages (Witkowski and Pempkowiak, 1995; Westman and Sohlenius, 1999), magnetic properties of sediments (Reinholdsson et al., 2013) and redox-sensitive elements in bulk sediment (Jilbert and Slomp 2013). In particular, Mn/Ca values of benthic foraminifera are increasingly used to reconstruct paleo-DO levels (Groeneveld and Filipsson 2013; Groeneveld et al., 2018; Guo et al., 2019).

Manganese (Mn) is a redox-sensitive element that occurs in its dissolved form (as Mn^{2+}) under reducing conditions and predominantly in its particulate form (e.g., as pyrolusite, MnO_2) when oxygen is present (e.g., Hem, 1963; Balzer, 1982; Rue et al., 1997). Dissolved manganese is mainly transported to the ocean by rivers (Ahl, 1977) and diffuses out of the sediment (Sundby et al., 1981; Roitz et al., 2002). Mn^{2+} then becomes oxidized in the water column (Pakhamova et al., 2007), adsorbed to particles (Hunt, 1983), or taken up by bacteria (Sunda and Huntsman, 1987, 1990) and phytoplankton (Sunda and Huntsman, 1983, 1985; Tebo et al., 2004; Dellwig et al., 2010). Once these organic and inorganic particles accumulate at the seafloor, manganese can be remobilized as soon as reducing conditions emerged in the sediment due to benthic respiration (Froehlich et al., 1979; Graf et al., 1982; Millward et al., 1998). Mn^{2+} builds up in the pore water, diffuses across the sediment-water interface (Tebo, 1991; Pakhamova et al., 2007) and gradually increases in concentration in the water column as the DO concentration declines (Groeneveld et al., 2018). Furthermore, Mn^{2+} is released from decaying organic particles while they sink to the seafloor (Freitas et al., 2006).

Although sediment cores can provide unrivaled information on century and millennial-scale DO trends, data on seasonal and inter-annual DO changes and hypoxic events is still scarce. Developing long, temporally well-constrained, high-resolution DO proxy archives that can overcome many of the existing limitations is thus an essential research need. In fact, bivalves fulfil many of these requirements and could serve as more powerful DO recorders than foraminifera or mobile archives like fish (e.g., Limburg et al., 2011). Many species including *A. islandica* attain a lifespan of decades or even centuries and record environmental changes in their shells in chronological order (e.g., Leipe et al., 2005; Schöne 2013). Growth patterns ensure that each shell portion can be placed in precise temporal context. As in foraminifera, Mn/Ca ratios of bivalve shells change proportionately to the concentration of ambient Mn^{2+} (e.g., Jeffree et al., 1995; Markich et al., 2002; Freitas et al., 2006; Lartaud et al., 2010), the biologically most available form of manganese (Campbell, 1995) (for more detail on Mn uptake pathways, see Discussion). Furthermore, many bivalves, specifically *A. islandica* are extremely tolerant against low DO levels and can survive the temporary lack of oxygen (anoxia) and

presence of hydrogen sulfide (euxinia) (Theede et al., 1969; Taylor, 1976; Oeschger, 1990; Oeschger and Storey, 1993; Strahl et al., 2011). For that reason, *A. islandica* is widely distributed in low-oxygen settings of the Baltic Sea (e.g., Zettler et al., 2001) and continues to monitor ambient DO levels when other, less tolerant species have already passed away. In addition, the pristine Mn/Ca signal encoded in bivalve shells has a great potential to withstand diagenetic alteration, because the majority of Mn^{2+} is covalently bound to the carbonate fraction and substitutes for Ca^{2+} in the crystal lattice of $CaCO_3$. To ensure that the large Mn ion (atomic radius: 161 pm) fits into aragonitic bivalve shells, the crystal structure is locally distorted, which results in an octahedral coordination of Mn as in calcite (Soldati et al., 2016), the diagenetically most resistant polymorph of $CaCO_3$.

Existing bivalve sclerochonological studies mainly used shell Mn/Ca values to reconstruct soil erosion and river discharge (e.g., Lazareth et al., 2003; Barats et al., 2008; Risk et al., 2010; Van Plantinga and Grossman 2019) or phytoplankton blooms (e.g., Vander Putten et al., 2000; but see Freitas et al., 2006). Only a single study employed such data as a proxy for pore water DO content (Zhao et al., 2017). No attempt has yet been made to estimate DO levels in the water column based on bivalve shell Mn/Ca values. The present study addresses this very issue by using shells of *A. islandica* collected alive from the Baltic Sea. High-resolution, temporally well-constrained shell Mn/Ca data (LA-ICP-MS data) from the hinge plates and ventral margins of six specimens were compared to available instrumental records of DO. Results of our study pave the way to establish a long-term, high-resolution archive for past DO levels and hypoxic events in shallow ocean waters.

3.2 Material and methods

Six specimens of *A. islandica* were collected alive during a cruise with the R/V "Alexander von Humholdt" by means of dredging from 25 m water depth in the Mecklenburg Bight, NW Rostock (54°18'59.5"N 11°33'00.0"E; Fig. 3.1) on 25 October 2001, immediately sacrificed in formalin and subsequently preserved in 70 vol% ethyl alcohol. In preparation for sclerochronological analysis, these specimens were eviscerated in winter 2019/20, the shells washed with tap water and air-dried.

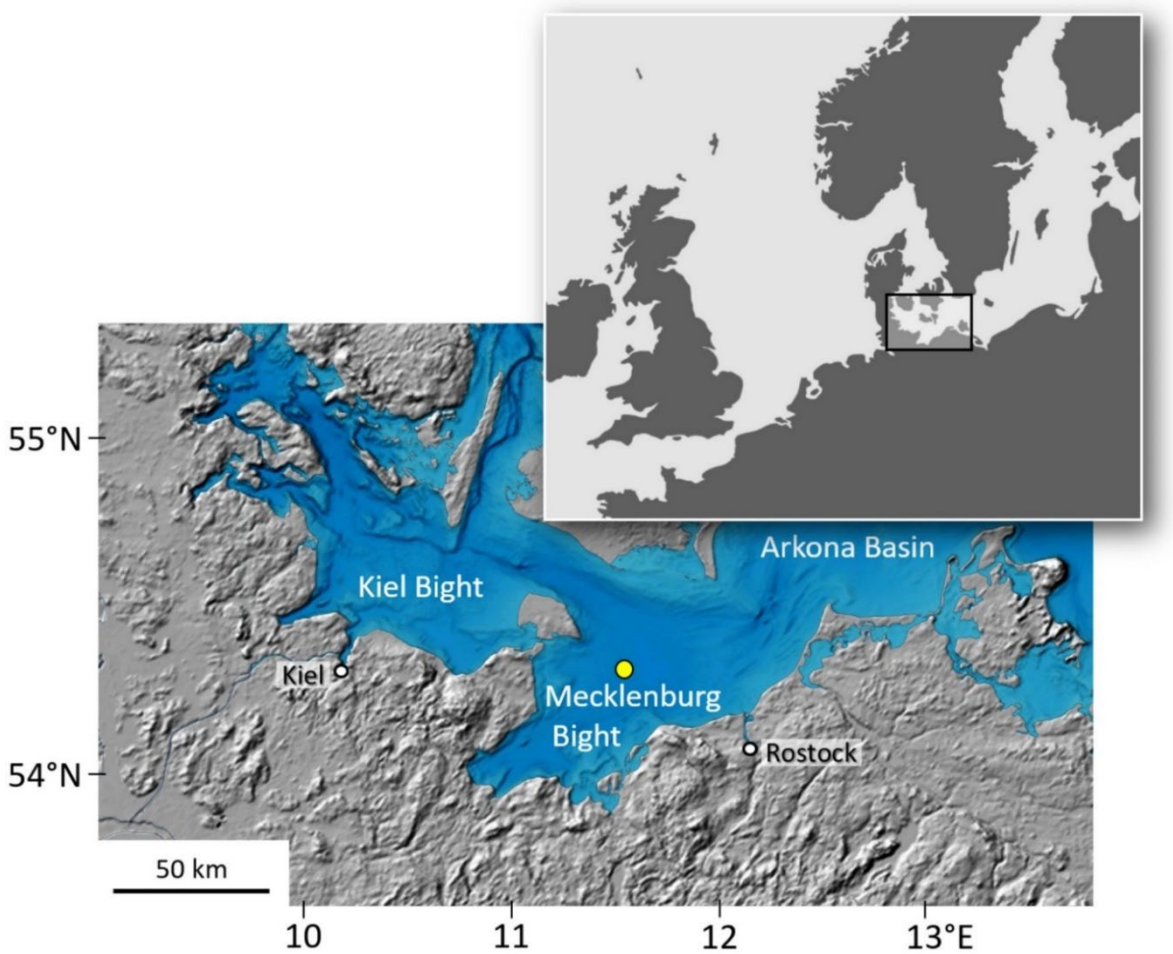

Figure 3.1 Map showing locality (yellow circle) where sampling has been conducted and instrumental records came from (station TF0012). Map sources: inlet (upper right) modified after http://www.mygeo.info; bathymetry map modified after http://data.bshc.pro (Baltic Sea Bathymetry Database); last access: Oct 27, 2020. (For interpretation of the references to color in this figure legend, the reader is referred to the Web version of this article.)

3.2.1 Sample preparation

One valve of each specimen (Table 3.1) was mounted to an acrylic glass cube with a fast curing plastic welder (WIKO Multi Power 03) and the outer and inner shell surfaces along the axis of maximum growth from the umbo to the ventral margin were coated with a approx. 1 cm wide and approx. 2 mm thick protective layer of WIKO metal epoxy resin 05. After ca. three hours curing time, from that axis two 3 mm thick slabs were cut with a low-speed precision saw (Buehler Isomet 1000) equipped with a 0.4 mm thick diamond-coated saw blade (Buehler IsoMet Blade 15LC) at 175 to 225 rpm. Both shell slabs were mounted on glass slides with the mirroring sides facing upward using metal epoxy. Cross-sectioned shell slabs were ground on glass plates with F800 and F1200 grit SiC powder suspended in water and then polished with an Al_2O_3 suspension (1 µm grain size) on Buehler Microfloc cloth. After each of these steps, the specimens were ultrasonically cleaned with tap water.

Table 3.1 List of specimens of the bivalve, *Arctica islandica* from Mecklenburg Bight, Baltic Sea, used in this study including analytical approaches. All specimens were collected alive and sacrificed on 25 October 2001. Last character of ID denotes left (L) or right (R) valve. AIWA = annual increment width analysis.

Specimen ID MLZ-St12-…	Ontogenetic age (yr); AIWA: # increments	$\delta^{18}O_{shell}$ (‰) covered time (Year CE)	LA-ICP-MS: #; Start growing season (Year CE)	
			Hinge	Ventral margin
A2L		1989-1992		
A2R	19; 16		42; 1984/85	
A4R	19; 16		48; 1985/86	329; 1987/88
A5R	15; 12		44; 1988/89	326; 1991/92
A6R	14; 11		42; 1989/90	373; 1990/91
A7L	7; --		25; 1984/85	183; 1997/98
A9L		1994-1997		
A9R	8; 5		26; 1996/97	151; 1988/89

3.2.2 Growth pattern analysis

For growth pattern analysis (Fig. 3.2+3.3), one polished section was immersed in Mutvei's solution (Schöne et al., 2005a) for 18 min at 37-40 °C under constant stirring, gently rinsed in deionized water and then dried from air for ca. six hours. All steps were performed under a fume hood. Etched and dyed thick-sections were viewed under a binocular microscope (Olympus SZX16) equipped with sectoral dark-field ring-light illumination (Schott VisiLED MC1000; best results were achieved with one-quarter illumination) and documented with a Canon EOS 600D digital camera. Annual increment widths (= distances between consecutive

annual growth lines) were determined in the hinge (Fig. 3.3) to the nearest approx. 1 µm using the custom-made image processing software (Panopea, © Peinl & Schöne). Following standard sclerochronological methods (Cook and Peters, 1997; Helama et al., 2006; Butler et al 2013; Schöne 2013; Schöne et al., 2020), annual increment width chronologies were corrected for heteroscedasticity by means of adaptive power transformation, age-detrended with stiff, monotonically decreasing cubic spline functions, standardized and then arithmetically averaged to form a stacked chronology (Fig. 3.4) which could then be compared, e.g., to environmental variables (Fig. 3.5). Note, only chronologies with a length of at least five years were included in the stacked record, because proper age-detrending was impossible in shorter chronologies.

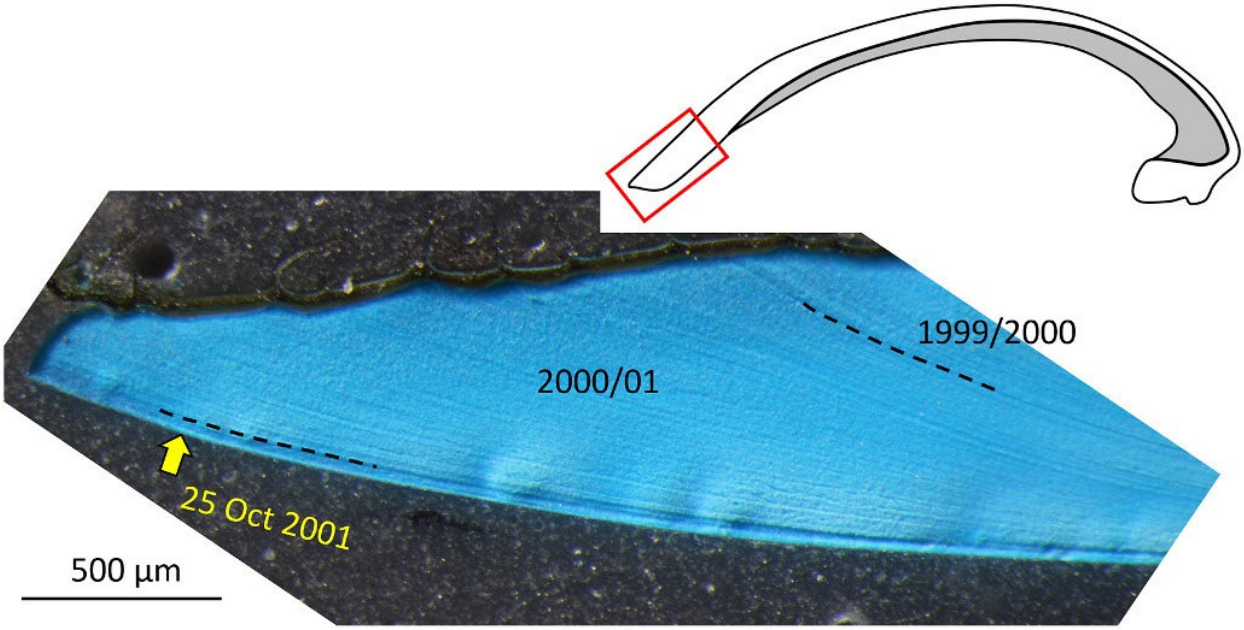

Figure 3.2 Annual growth lines (dashed) near the ventral margin of an *Arctica islandica* specimen (MLZ- St12-A4R) from Mecklenburg Bight, Baltic Sea. Red box in sketch illustrates the position in the shell where this photo was taken (white = outer shell layer; grey = inner shell layer). The portion between last annual growth line and the ventral margin formed approximately between mid-September and 25 Oct 2001, i.e., date of collection (= death; yellow arrow). Compared to specimens from other well-oxygenated sites in the North Atlantic, this ca. nineteen-year-old specimen is remarkably thin. The darker blue color after staining with Mutvei‘s solution indicates a larger proportion of organic macromolecules stained by Alcian Blue.

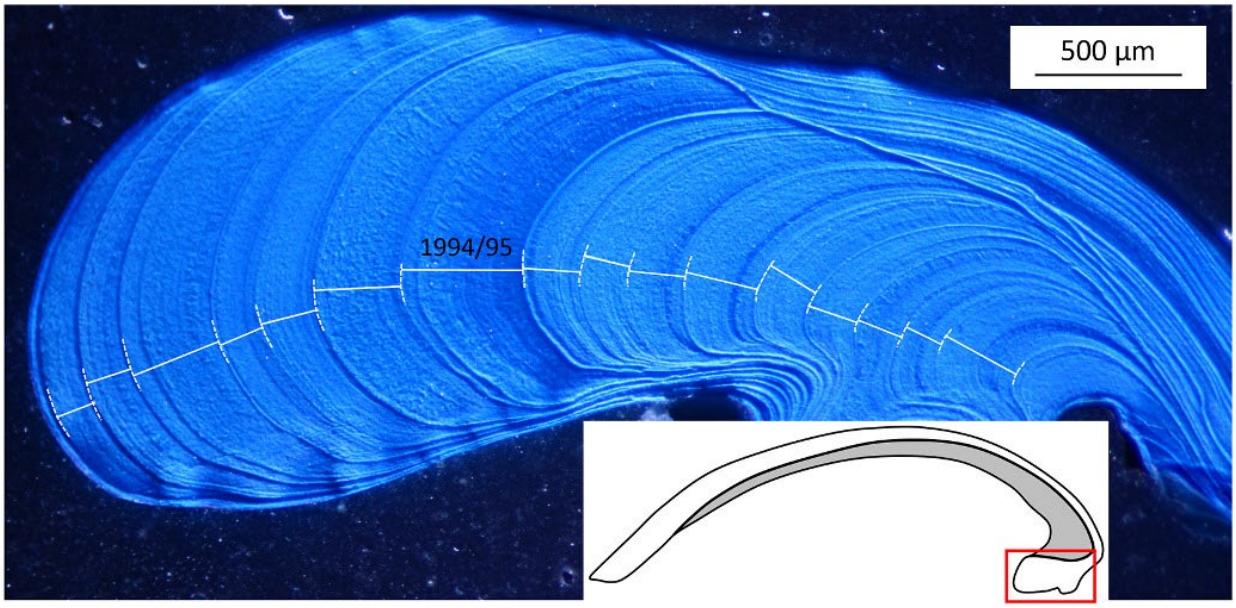

Figure 3.3 Annual growth increments (straight lines) and annual growth lines (dashed) in the hinge plate of an *Arctica islandica* specimen (MLZ-St12-A4R) from Mecklenburg Bight, Baltic Sea. Red box in sketch illustrates the position in the shell where this photo was taken (white = outer shell layer; grey = inner shell layer). In contrast to the ventral margin, the widths of all annual increments can be measured as perpendiculars in the hinge plate. Note the particularly broad increment of the growing season 1994/95. The darker blue color after staining with Mutvei‘s solution indicates a larger proportion of organic macromolecules stained by Alcian Blue. On the outer shell surface and in polished sections prior to staining (not shown here), this darker blue-stained portion is brownish suggesting a larger proportion of pigments.

3.2.3 In-situ element analysis

The other polished shell slab was used to determine the chemical composition using laser ablation – inductively coupled plasma – mass spectrometry (LA-ICP-MS) in spot mode. In this paper, only Mn and Ba are reported and discussed. Additional chemical properties are given in the Supplements. One shell hinge (MLZ-St12-A2R) was analyzed at the Max Planck Institute for Chemistry, Mainz (MPIC), all remaining samples at the Institute of Geosciences, Johannes Gutenberg University of Mainz (JGU) (Table 3.1).

At the MPIC, a 213 nm Nd:YAG laser (UP-213 NewWave) coupled to a Thermo Fisher Element2 single collector sector-field ICP-MS (run at low-mass resolution mode) was used. Spots with a diameter of 55 µm and a spacing of 90 µm (measured between the midpoints of the LA spots) were placed along the axis of maximum growth in the hinge plate of specimen MLZ-St12-A2R. Laser energy density was approx. 15.7 J/cm^2. Background intensities were measured for 12 s, and times for ablation and washout were 60 s and 30s.

The system at JGU consisted of a 193 nm ArF Excimer laser (ESI NWR193) coupled to an Agilent 7500ce quadrupole ICP-MS. Spots with a diameter of 65 µm and a midpoint spacing of 85 µm were placed along the ventral margins of the shells (inner portion of the outer shell

layer) as well as the axes of maximum growth in the hinge plates of the remaining specimens. Laser repetition rate was 10 Hz and the laser energy on the samples approx. 3 J/cm^2. Each analysis consisted of 15 s of background, 30 s of ablation and 20 s of washout.

Accuracy and precision of all LA-ICP-MS analyses were assessed by measuring different reference materials as quality control materials (QCMs). At both institutes, USGS MACS-3 was used, and at the JGU USGS BCR-2G as well. For data measured at the MPIC, the synthetic glass, NIST SRM 612, was used to calibrate the element concentrations of the shell samples and the remaining reference materials using the preferred values available at the GeoReM database (http://georem.mpch-mainz.gwdg.de/, application version 20; last access: 27 Oct 2020; Jochum et al., 2005, 2011). Signals of the measurements were monitored in time-resolved mode and processed using an in-house Excel spreadsheet (Jochum et al., 2007). Details of the calculations are given in Mischel et al. (2017). For the measurements performed at the JGU, NIST SRM 610 and 612 were used as calibration material. The time-resolved signals were processed using LAtools (Branson et al., 2019). For both data reduction strategies and to computer molar element/Ca ratios of *A. islandica* shells, ^{43}Ca was used as the internal standard, applying for the samples a Ca content of 380,000 µg/g according to Marali et al. (2017), and the values reported in the GeoReM database for the QCMs and calibration material. Element concentrations determined for the QCMs are given in Table 3.2. To compute molar element/Ca ratios of *A. islandica* shells, we assumed a calcium concentration of 380,000 µg/g (see Marali et al. 2017).

Table 3.2 Average concentration and standard deviations (1σ) of manganese (Mn) and barium (Ba) in reference materials USGS MACS-3 and USGS BCR-2G were determined at MPIC and JGU during chemical analysis of *Arctica islandica* specimen MLZ-St12-A2R and the remaining five specimens, respectively. Reference (Ref.) values were taken from the GeoReM database (preferred complied values, http://georem.mpch-mainz.gwdg.de/, application version 20; Jochum et al. 2005, 2011).

Specimen ID: MLZ-St12-… →			A2R	A4R	A5R	A6R	A7L	A9R
Reference material ↓	Element (µg/g)	Ref. values	Measured values					
USGS MACS-3	Mn	512 ± 25	444 ± 18	522 ± 11	516 ± 10	513 ± 11	527 ± 11	517 ± 10
	Ba	59.6 ± 1.4	56.4 ± 1.0	61.1 ± 5.2	60.4 ± 2.3	60.0 ± 9.0	63.0 ± 2.7	61.8 ± 5.7
USGS BCR-2G	Mn	1550 ± 70		1570 ± 22	1551 ± 18	1549 ± 24	1582 ± 23	1549 ±28
	Ba	683 ± 7		711 ± 24	713 ±17	703 ± 23	718 ± 16	704 ± 15

3.2.4 Stable oxygen isotope analysis of shell aragonite

The remaining valves of two specimens (MLZ-St12-A2L and -A9L) were used for oxygen isotope analysis. Since the studied shells were only approx. 300 µm thick, sampling in cross-section would have been extremely challenging and resulted in significant time-averaging. Therefore, carbonate powder (aragonite) was obtained by hand from the outer shell surface using a conical SiC drill bit operated in a milling device that was firmly attached to a microscope. Nearly equidistant sample swaths (length, width and depth of approx. 1 cm, 100 µm and 10 – 20 µm, respectively) were taken parallel to the growth patterns and yielded approx. 30 to 60 µg of shell powder. Samples were dissolved in He-flushed 12 mL borosilicate exetainers at 72 °C using a 99.9 % phosphoric acid. After two hours reaction time, the released CO_2 gas was measured in a Thermo Fisher MAT 253 continuous flow-gas source isotope ratio mass spectrometer coupled to a GasBench II. Stable isotope ratios were calibrated against an NBS-19 calibrated Carrara Marble ($\delta^{18}O = -1.91‰$) distributed by IVA Analysentechnik GmbH & Co. KG. Results are expressed as parts per thousand (‰) with respect to the Vienna Pee Dee Belemnite isotope scale (V-PDB). The long-term accuracy based on blindly measured NBS-19 samples (N = 421) is better than 0.04 ‰ for $\delta^{18}O$. Note that no correction was applied for differences in acid fractionation factors of the reference material (calcite) and shells (aragonite); for details see Füllenbach et al. (2015). Shell oxygen isotope data were used to temporally contextualize the shell record and determine the seasonal timing and rate of shell growth (for details see next section).

3.2.5 Temporal alignment of the chemical data

A major prerequisite for the interpretation of chemical or physical properties measured in bivalve shells is to place the data into precise temporal context and determine the time covered by each sample. This approach is mandatory because the timing and rate of biomineralization varies through seasons and years in response to physiological processes and environmental conditions (e.g., Schöne 2008). Consequently, different shell portions and samples taken from the shell represent different amounts of time. To compute averages of the growing seasons (henceforth referred to as ‘annual averages’), weighted averages need to be computed from the intra-annual chemical data (instead of arithmetic means; Schöne et al., 2004). This requires knowledge of the relative proportion of time covered by each LA spot which can be inferred from the species-/site-specific seasonal growth curve.

The seasonal growth model of *A. islandica* for the study locality was constructed

according to the method described by Schöne et al. (2007) and Peharda et al. (2019). In brief, measured shell oxygen isotope ($\delta^{18}O_{shell}$) values of specimen MLZ-St12-A9L were arranged– in the order at which they were measured – until they closely matched the shape of the instrumental water temperature curve as well as the predicted shell oxygen isotope curve ($\delta^{18}O_{shell\ predicted}$) of 1994-1997 (Fig. 3.6A-D). The latter was computed using the paleothermometry equation of Grossman and Ku (1986; including a PDB-SMOW scale correction of -0.27 ‰ according to Gonfiantini et al., 1995) solved for $\delta^{18}O_{shell}$:

$$\delta^{18}O_{shell\ predicted} = \frac{20.60+4.34\times(\delta^{18}O_{water}-0.27)-T}{4.34}, \quad (1)$$

where $\delta^{18}O_{shell\ predicted}$ is given relative to V-PDB and $\delta^{18}O_{water}$ relative to V-SMOW, and temperature is reported in degree Celsius. The $\delta^{18}O_{water}$ values were reconstructed from measured salinity data using the freshwater mixing line by Schöne et al. (2005b; Eq. 2):

$$\delta^{18}O_{water} = 0.30 \times S - 10.36. \quad (2)$$

Since the calendar date of each isotope sample as well as the distances between subsequent sampling positions are known, the rate of seasonal shell growth could be easily determined (Fig. 3.6E+F).

3.2.6 Resampling of LA-ICP-MS data

To directly compare element data of different years and specimens with each other, it was necessary to mathematically adjust the number data points in each year to a common resolution (e.g., Schöne 2008; Hallman et al 2011). This approach was necessary because LA-ICP-MS data from years with higher temporal resolution would otherwise show larger amplitudes than samples from annual increments with fewer samples. Once the date of midpoint of each LA spot was determined, linear interpolation was used to compute an uninterrupted time-series with daily resolution. Then, the new time-series was resampled at regular intervals such that twelve samples were available for each annual increment and each sample thus represented one month of growth (Fig. 3.11).

3.2.7 Instrumental data

Instrumental data of temperature, salinity and dissolved oxygen concentration were obtained

from the data base provided by the Leibniz Institute for Baltic Sea Research Warnemünde, IOW from their website at https://odin2.io-warnemuende.de/ (last access: 25 October 2020) for the closest station next to the locality where the bivalves were collected, i.e., station TF0012 (54°18'54.00"N, 011°33'00.00"E; 20 m water depth; Fig. 3.1). The data were taken at irregular time intervals and are incomplete (Fig. 3.9). Therefore, linear interpolation was used to compute an artificial, uninterrupted time-series with daily resolution (see Figure DO in Supplements). For time intervals during which T, S and DO data were measured, DO saturation (see Figure DO in Supplements) were computed using the conversion by Benson and Krause (1984).

It would have been superior to compare the shell Mn/Ca data to DO saturation rather than DO concentration. However, due to the scarcity of instrumental temperature and salinity data, DO saturation could only be computed for a short time interval. As revealed by Figure DO in the Supplements, DO concentration, and DO saturation curves were largely similar justifying the comparison with DO concentration. For a more rigorous evaluation, future work should target DO saturation.

Mean daily river discharge data (station Bad Suelze 1) were obtained from obtained from the Federal Institute of Hydrology from their website at https://portal.grdc.bafg.de (last access: 30 Oct 2020). From these data, growing season averages (Sep_t-Aug_{t+1}) were calculated (Fig. 3.12). Note that largest riverine fluxes occurred in winter. Data on Major Baltic inflows (barotropic inflows) came from Mohrholz (2018; https://dx.doi.org/10.12754/data-2018-0004, last access: 30 Oct 2020). Phytoplankton data were provided by Norbert Wasmund (pers. communication 2020, IOW, Warnemünde, Germany).

3.3 Results

Studied specimens of *A. islandica* were between ca. seven and nineteen years old (Table 3.1). Shortly before the shell margin (= most recently formed shell portion) at the ventral margin and the hinge, all studied specimens showed an annual growth line, followed by a newly forming annual growth increment (Fig. 3.2). Annual growth lines were particularly well developed in the hinge (Fig. 3.3) and thus, distances between consecutive growth lines (= annual growth increment widths) were measured in this shell portion. Note, in *A. islandica*, the first two to four years of life – in contrast to the ventral margin – are typically not represented by the hinge record; annual increment chronologies are thus shorter than the lifespan of the respective specimen (Table 3.1). By visual assessment, ontogenetic age-detrended (weighted) annual increment chronologies of studied specimens showed noticeable synchronicity (Fig. 3.4). Fastest annual shell growth occurred during 1994/95, 1998/99 and 1991/92, and slowest during 1993/94 and 1997/98 (Fig. 3.4). The arithmetically averaged chronology computed from these series covered the growing seasons of 1985/86 to 2000/2001 and exhibited a significant positive correlation to DO during November – March ($r = 0.76$, $R^2 = 0.58$, $p = 0.0006$) and a significant negative correlation to DO in summer (June – August; $r = 0.60$, $R^2 = 0.36$, $p = 0.0139$; Fig. 3.5).

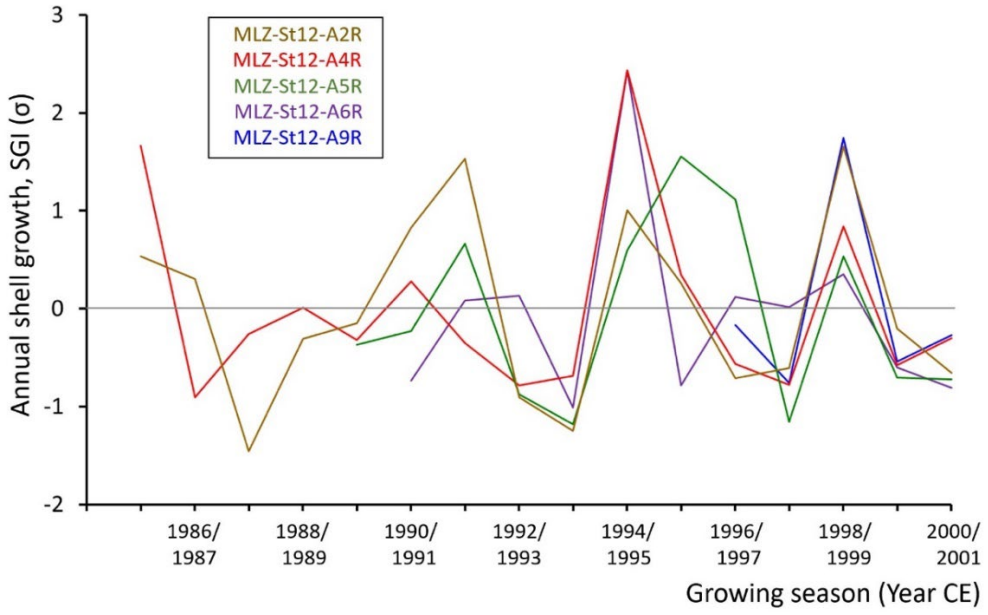

Figure 3.4 Annual shell growth curves (standardized increment width, SGI) of five *Arctica islandica* specimens from Mecklenburg Bight, (Station 12, 20 m water depth), Baltic Sea. Note that specimen A7 was only four years old and too short to be included here (detrending issues). Details on the detrending method are explained in section 2.2.

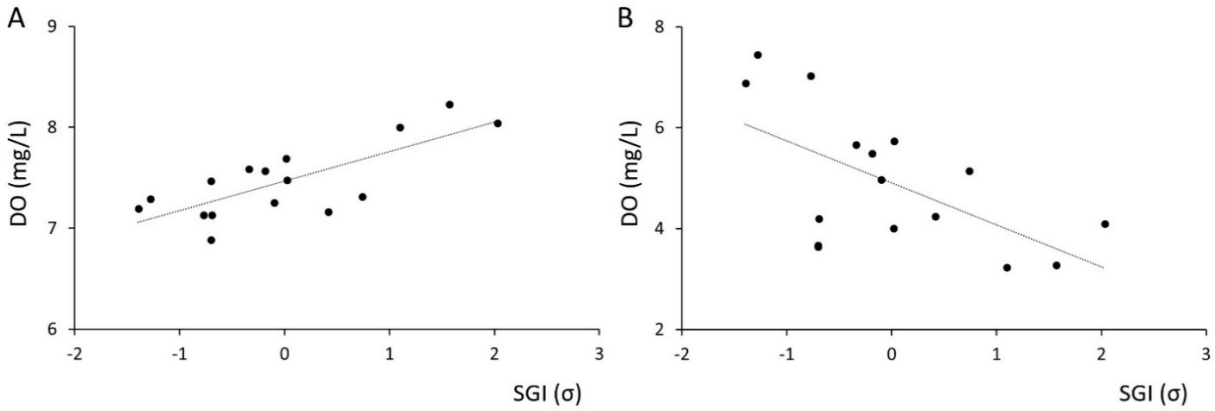

Figure 3.5 Annual shell growth (standardized growth increment, SGI, width) of *Arctica islandica* (growing season 1985/86 to 2000/01) compared to concentration of dissolved oxygen in the water column at Mecklenburg Bight (Station 12, 20 m water depth), Baltic Sea. Details on the detrending method are explained in section 2.2.

3.3.1 Seasonal growth model

Shell oxygen isotope values of specimen MLZ-St12-A9L covered the time interval of 1994 to 1997 and showed distinct seasonal oscillations ranging between -2.50 and +0.07 ‰ (Fig. 3.6A+B), i.e., a roughly similar range and level as given by $\delta^{18}O_{shell\ predicted}$ (Fig. 3.6B). As in other hitherto studied *A. islandica* specimens (e.g., Schöne et al., 2005b; Schöne 2013), annual growth lines were detected near the most negative $\delta^{18}O_{shell}$ values (Fig 3.6A+B). As revealed by the clear bias toward higher $\delta^{18}O_{shell}$ values, a significant proportion of each annual increment formed during the colder part of year (Fig 3.6A+B). Once the $\delta^{18}O_{shell}$ values were cross dated with the shape of the instrumental water temperature and $\delta^{18}O_{shell\ predicted}$ curves, each isotope sample was temporally constrained and allowed us to determine the seasonal timing and rate of shell growth. The arithmetic average of two complete growing seasons (1994/95 and 1995/96) served as the seasonal growth model (Fig. 3.6E+F) that was subsequently used to place the chemical record into temporal context and provide the basis to compute weighted annual Mn/Ca averages. Following this model, studied *A. islandica* specimens from Mecklenburg Bight grew at slowest rates and formed annual growth lines during September/October. Therefore, biomineralization rates increased steadily and reached highest levels between January and March, then declined and showed a second, but much less pronounced peak between June and August (Fig. 3.6E). The validity of the seasonal growth model was verified with $\delta^{18}O_{shell}$ data of specimen MZL-ST12-A2L (Fig. 3.6A-F). As shown in Figures 3.6E and F, the average growth curves of the two specimens are nearly identical, but differ much stronger from a growth model that assumes unchanged growth rate (linear shell growth) throughout the growing season.

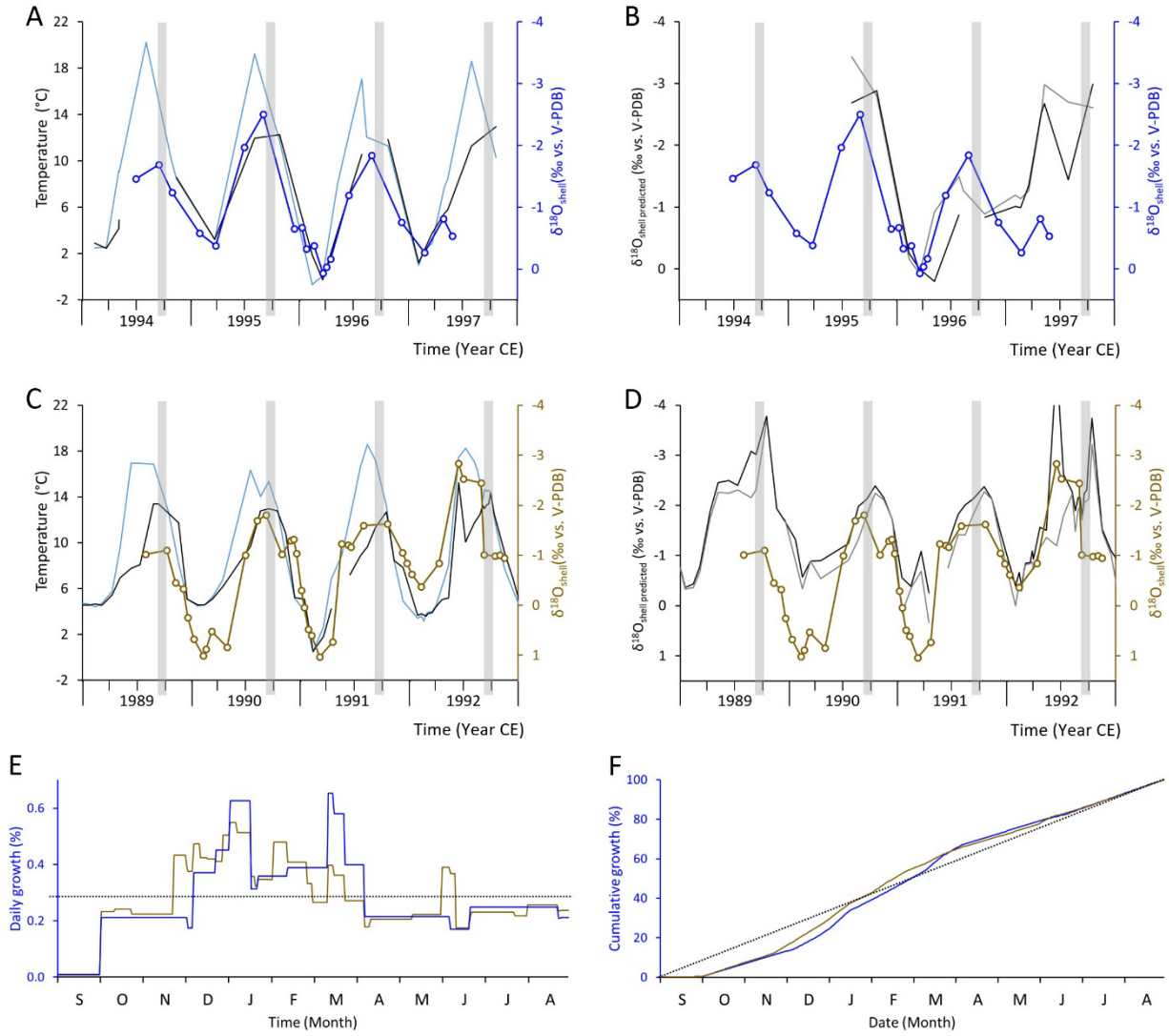

Figure 3.6 Shell oxygen isotope-based construction of the seasonal growth model for *Arctica islandica* from Mecklenburg Bight, Baltic Sea. The $\delta^{18}O_{shell}$ data (note reverted axis) of specimens MLZ-St12-A9L (A+B) and MLZ-St12-A2L (C+D) fluctuate seasonally. To place the data into temporal context, the $\delta^{18}O_{shell}$ values were aligned to show the best agreement with the shape of the instrumental water temperature curves at 20 m water depth (A+C; black curves) as well as predicted shell oxygen isotope values (B+D; black = $\delta^{18}O_{shell\ predicted}$ at 20m; grey at 15 m [B] and 25 m [D]). For comparison, water temperatures above the halocline are depicted in A and C (light blue curves; A: 5m, B: 1m). Within each cycle, a larger number of data falls into the first part of the growing season suggesting fast growth during winter and spring. This observation also becomes clear from the average daily growth curves (E) and the cumulative daily growth curves (F). Data from specimen MLZ-St12-A9L are consistently shown in red, and such of MLZ-St12-A2L in deep blue. The growth curve of specimen MLZ-St12-A9L was used to temporally align all shell records, while data from MLZ-St12-A2L was used to verify the model. As revealed by E and F, the two growth curves are very similar to each other, but greatly differ from a linear growth model (dotted lines) that assumes unchanged growth rates through different seasons. Grey vertical bars denote the annual growth lines.

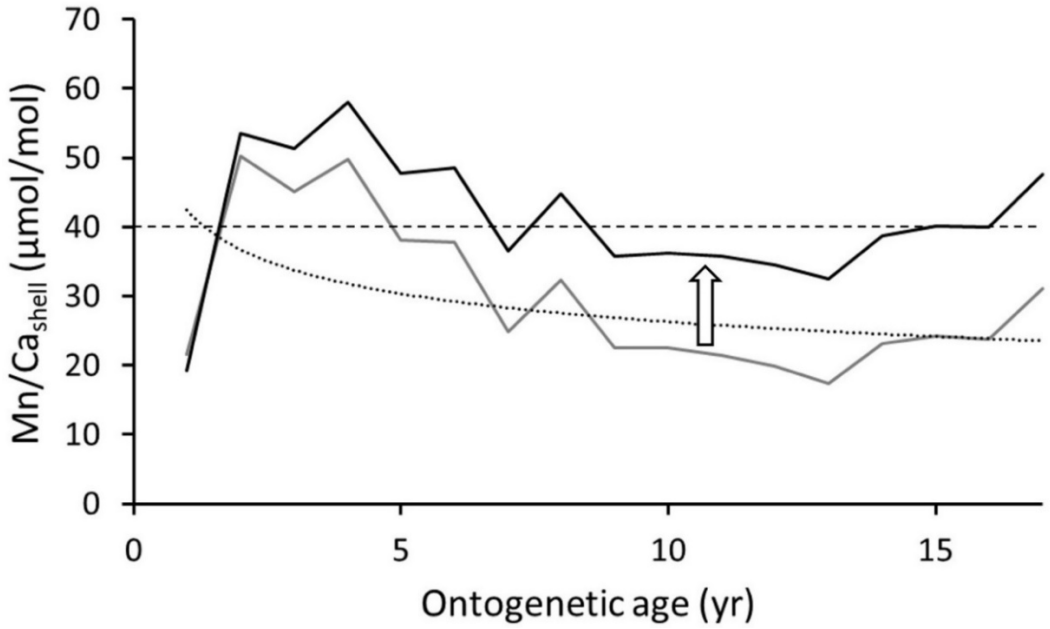

Figure 3.7 Average Mn/Ca$_{shell}$ curve (grey), measured in the hinges of six studied *Arctica islandica* specimens (hinge plates) from Mecklenburg Bight, Baltic Sea, plotted against ontogenetic age. The inherent age trend was estimated with a power function (dotted line) und removed from the individual Mn/Ca$_{shell}$ time-series. For this purpose, the level at the beginning of the time-series (approx. 40 µmol/mol; dashed line) was set an anchor point and Mn/Ca$_{shell}$ values at year n were elevated by the difference between this anchor point and the trend curve at year n. To illustrate the method, here, the annual Mn/Ca$_{shell}$ mean curve was detrended (black)

3.3.2 Mn/Ca

Weighted annual Mn/Ca curves of the hinge revealed distinct ontogenetic trends toward lower values with increasing age (Fig. 3.7). Before further analyses of the curves, inherent age trends were thus removed. For this purpose, annually averages from all six studied specimens were plotted against ontogenetic age and the decline in growth rate estimated with a power function ($Mn/Ca = 42.396 \times age^{-0.208}$), which was subsequently used to detrend each Mn/Ca series. Instead of producing dimensionless (= standardized indices) Mn/Ca values, the level at the beginning of the time-series (approx. 40 µmol/mol) was set as an anchor point and lifted the Mn/Ca values at year n was increased by the difference between this anchor point and the predicted growth value at year n (Fig. 3.7). It should be added that this age trend-removal technique has the disadvantage of making the detrended Mn/Ca series depend on the initial Mn/Ca level which needs to be considered in subsequent approaches to develop a proxy to quantify past oxygen concentrations. When rearranged by calendar time, the age-detrended Mn/Ca values of the six studied specimens showed moderate agreement with conspicuous positive peaks in 1987, 1991 and 1997/98 (Fig. 3.8A). Apparently, age trends were insufficiently removed from the two shortest series (Fig, 3.8A).

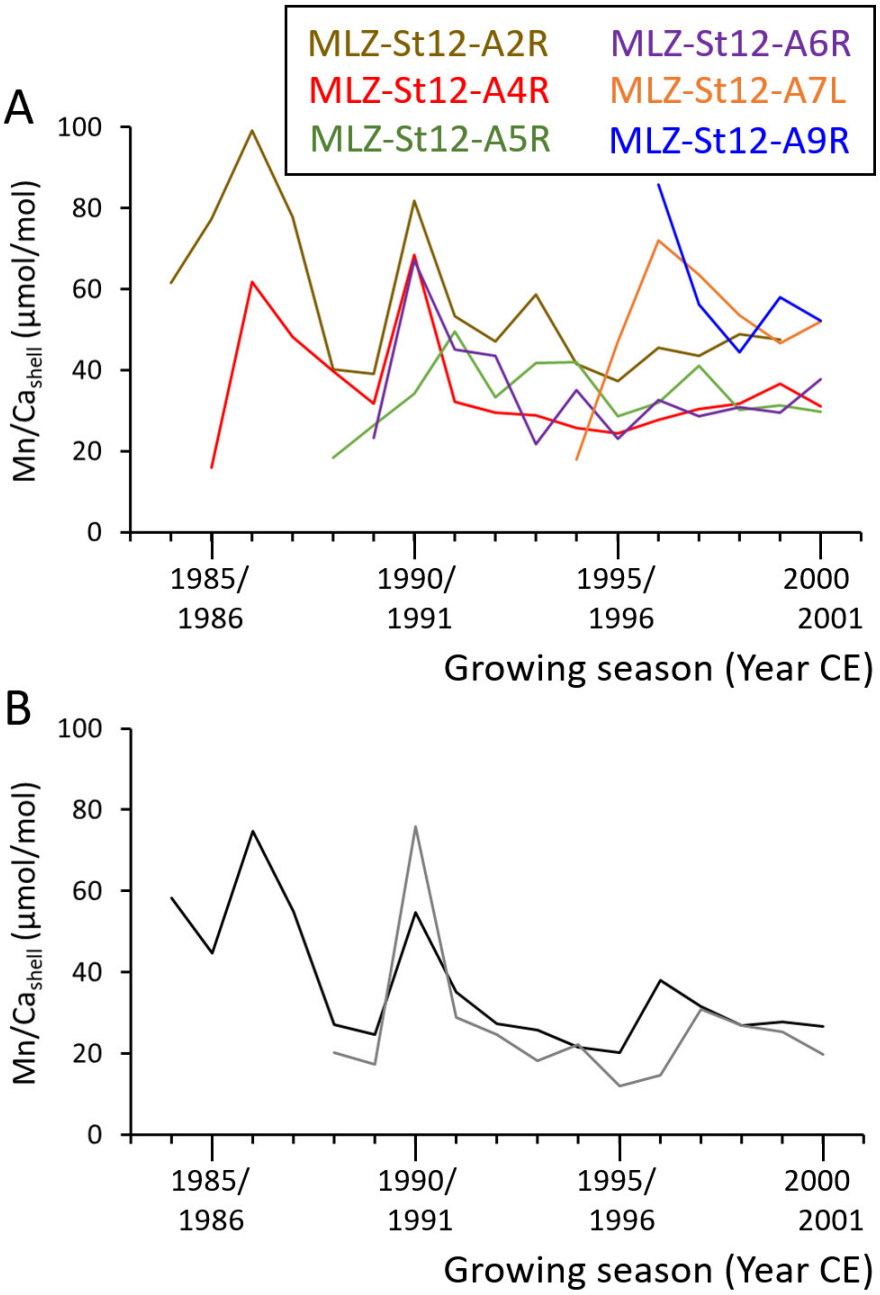

Figure 3.8 Detrended Mn/Ca$_{shell}$ curves (hinge data) of *Arctica islandica* from Mecklenburg Bight, Baltic Sea, plotted against calendar year. (A) Individual Mn/Ca$_{shell}$ curves of the six studied specimens. (B) Arithmetically averaged Mn/Ca$_{shell}$ curves from the hinge plates (black) and ventral margins (grey) compare well to each other and show strong synchrony.

Mn/Ca data of the ventral margin were detrended in the same way as the hinge data. The weighted annual Mn/Ca curves of the two shell portions compared well to each other, i.e., they showed similar curve shapes (Fig. 3.8B). The detrended annual data of the ventral margin were, on average, only approx. 6 % lower than the hinge. However, in 1991 specimens deviated from the hinge, on average, by approx. 30 %, and in this case, the hinge was depleted in Mn relative to the ventral margin (Fig. 3.8B). Weighted annual Mn/Ca data were weakly negatively

correlated to DO concentration during spring (March – May) (hinge: r = - 0.23, p = 0.3677; ventral margin: r = -0.57, p = 0.0415).

Due to overall faster shell growth, the ventral margin (outer shell layer) provided much higher resolved intra-annual data than the hinge and thus an insight into seasonal element/Ca variations. Yet, the series is typically shorter than the hinge data, because closer to the umbo, the outer shell layer becomes so thin that proper sampling with the laser becomes impossible and time-averaging increases strongly. Subseasonal Mn/Ca patterns are exemplarily described for specimen MLZ-St12-A4L, which provided the longest record (Fig. 3.9). Despite strong high-frequency variability, the Mn/Ca curve revealed distinct seasonal oscillations with typical values of approx. 50 µmol/mol during summer (DO concentrations of approx. 2 – 4 mg/L) and approx. 30 µmol/mol during winter (DO concentration approx. 8 – 9 mg/L). The only exception occurred in summer 1995, when Mn/Ca remained at approx. 30 µmol/mol despite a DO concentration of only 3 mg/L. During the preceding winter, Mn/Ca reached values of 90 µmol/mol. Highest overall Mn/Ca values were attained in summer 1991 (> 300 µmol/mol). If the exceptional years and the high-frequency components remained unconsidered, the seasonal variations (= background variations) were – by visual comparison – inversely linked to DO concentration (Fig. 3.9). In Figure 3.10 this relationship is quantified demonstrating that background Mn/Ca variations can explain 46 % of the variability in DO (r = –0.68; R^2 = 0.46, $p < 0.0001$).

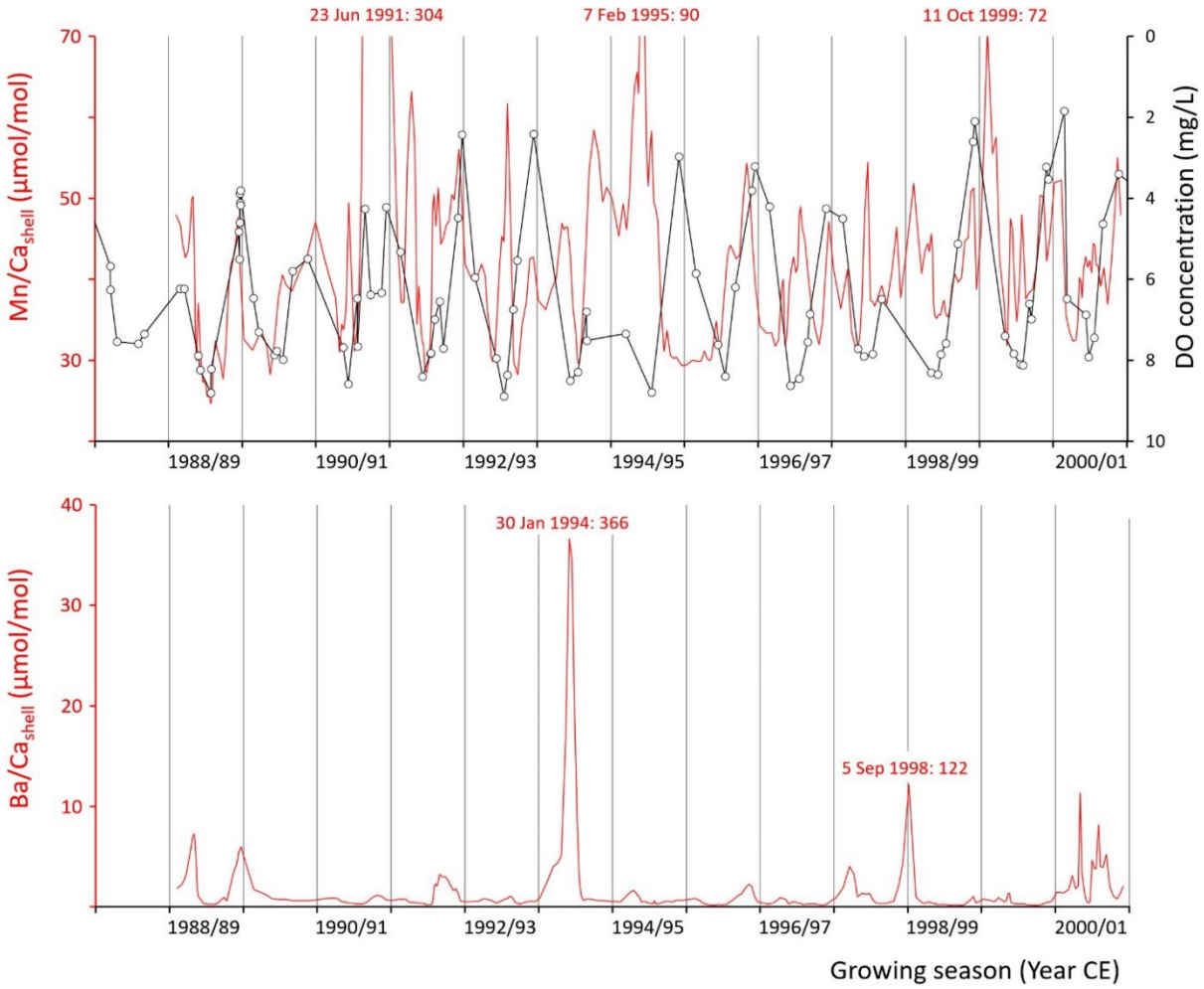

Figure 3.9 Temporally aligned element/Ca$_{shell}$ data from the outer shell layer (ventral margin) of *Arctica islandica* specimen MLZ-St12-A4R from Mecklenburg Bight, Baltic Sea. In the upper panel, age-detrended Mn/Ca$_{shell}$ is plotted versus DO concentration (open circles = measured values; connecting lines represent linearly interpolated DO values; note reversed axis). Background Mn/Ca$_{shell}$ variations are inversely correlated to DO and thus dissolved Mn in the water column. Only during 1995, dissolved Mn levels remained low, possible as a result of a major biogeochemical disturbance induced by strong river discharge in winter 1993/94. This riverine influx possibly triggered a major diatom bloom that caused a strong Ba enrichment in the shells in early 1994 (lower panel). Episodic Mn/Ca$_{shell}$ peaks likely result from particulate Mn (ingested Mn-rich organic particles).

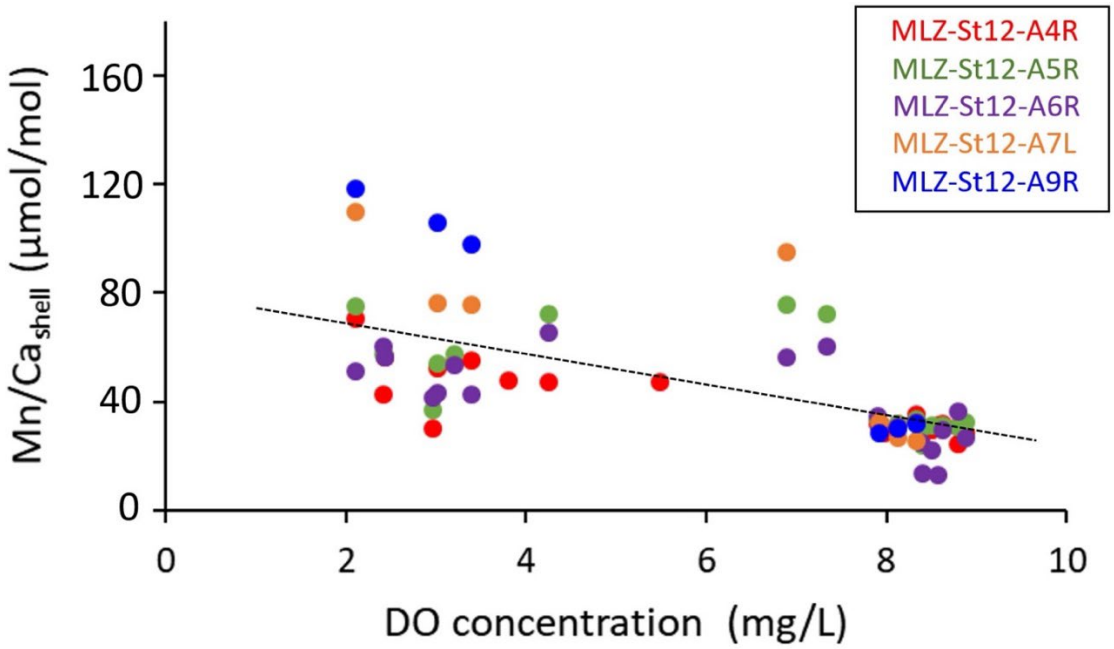

Figure 3.10 Correlation between Mn/Ca_{shell} (ventral margin data) of *Arctica islandica* specimens from Mecklenburg Bight, Baltic Sea, and dissolved oxygen concentration. Due to the high-frequency Mn/Ca variability, the focus was placed on seasonal minima and maxima. Years with unusually high or missing Mn enrichment were omitted. Dotted line represents the regression curve.

To directly compare all five ventral margin Mn/Ca chronologies with each other, some mathematical transformations were required. Besides removal of ontogenetic age trends, it was necessary to correct for differences in time-averaging (the time represented by each LA spot varied between approx. 3 and 44 days). A lower sampling resolution and larger time-averaging in narrower annual increments would result in truncated amplitudes relative to such from broader annual increments. Furthermore, the ontogenetically younger specimens MLZ-St12-A7L and -A9L showed markedly higher Mn/Ca values than the three older specimens (which were not completely removed by age-detrending: Fig. 3.11). Removal of ontogenetic age trends was accomplished in the same manner as described above for annual growth data. To account for differences in time-averaging, the chronologies were mathematically resampled to a common resolution given by the annual increment with the lowest number of data points, i.e., twelve samples per year. After resampling, each sample reflected the same amount of time allowing to directly compare data points within and among years and specimens. Age-detrended and resampled Mn/Ca series, in particular those of the three older specimens, were in remarkably good agreement and showed a high level of synchronicity, specifically at the background level (Fig. 3.11). Major peaks occurred in summer 1991 and winter 1997/98. The latter was only developed in one of the four specimens covering this time interval. At visual inspection, the average resampled Mn/Ca curve showed a similar inverse relationship with DO

concentration as the raw curve of MLZ-St12-A4L (Fig. 3.9, 3.12). With the exception of summer 1995, high shell Mn/Ca values occurred during summer, low values in winter (Fig. 3.9, 3.12). Although mathematical re-sampling resulted in a smoothed time-series, the chronology was still noisy, i.e., contained a strong high-frequency component (Fig. 3.12). Considering the incomplete instrumental data, it would not make much sense to conduct a regression analysis of the monthly resolved Mn/Ca data and interpolated monthly DO data. As before, only the seasonal extremes were studied yielding a similar result as before: When outliers were omitted (summers 1991+1995, winter 1997), shell Mn/Ca and DO were still significantly negatively correlated to each other ($r = -0.77$, $p < 0.05$).

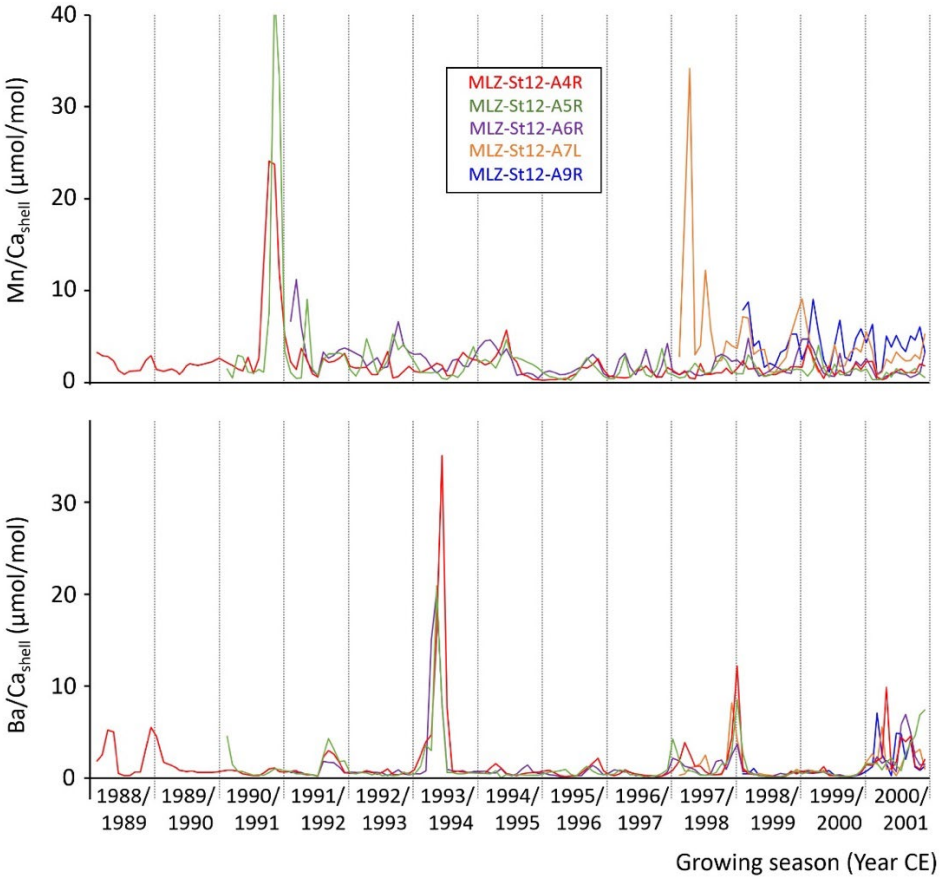

Figure 3.11 Temporally aligned and resampled element/Ca$_{shell}$ data from the outer shell layer (ventral margin) of five *Arctica islandica* specimens from Mecklenburg Bight, Baltic Sea. The Mn/Ca$_{shell}$ data in the upper panel were also age-detrended. Note, running similarity between the element/Ca$_{shell}$ series. Whereas all contemporaneous specimens showed Ba/Ca$_{shell}$ peaks, typically of nearly identical height, the Mn/Ca$_{shell}$ peaks were not always developed in all specimens (e.g., growing season 1997/98).

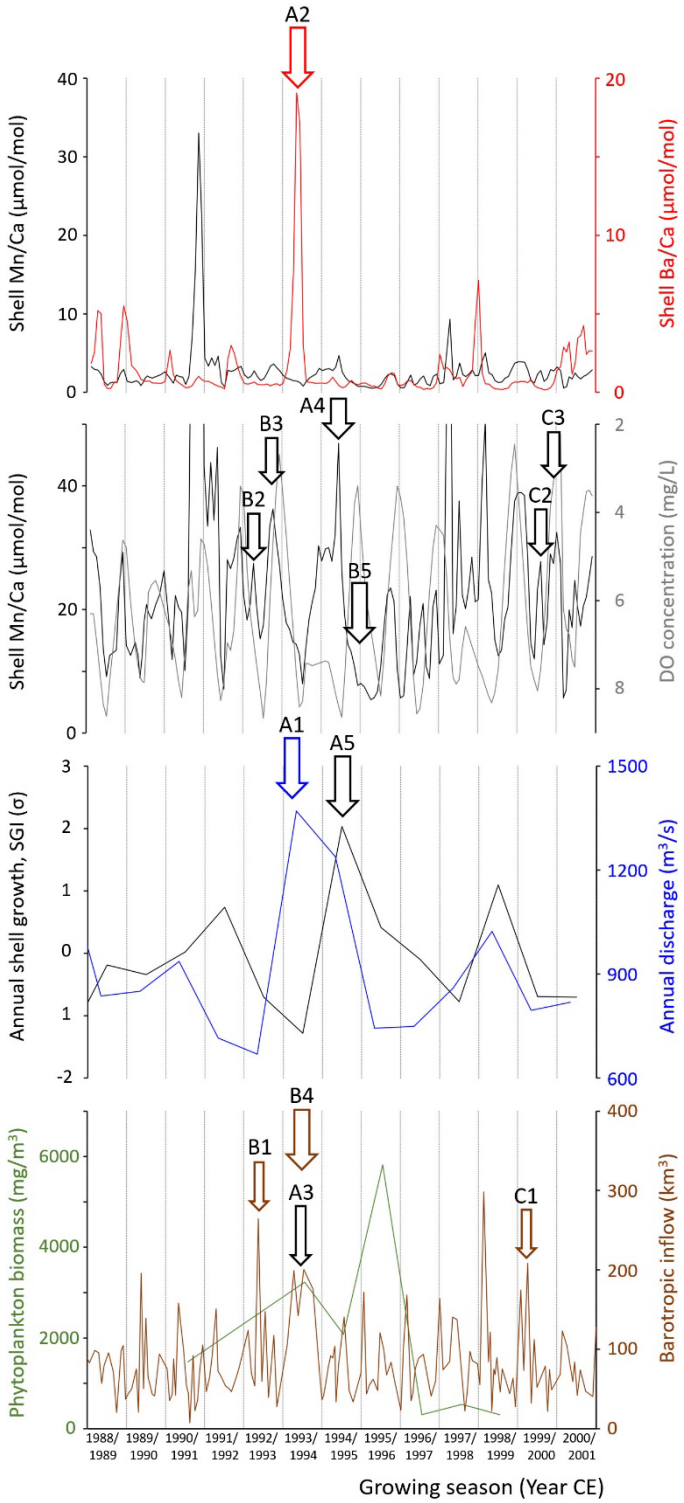

Figure 3.12 Temporally aligned and resampled element/Ca_{shell} data from the outer shell layer (ventral margin) of *Arctica islandica* from Mecklenburg Bight, Baltic Sea in comparison with various different instrumental data sets. The Mn/Ca_{shell} data were also age-detrended. The Mn and Ba series represent the arithmetic averages of five contemporaneous specimens. The second panel from above shows the Mn/Ca_{shell} data from the upper panel, but with a focus on the background variation for better comparison with monthly DO concentration (note reverted axis). As in Figure 3.9, an inverse relationship with DO is apparent. Arrows with characters and numbers indicate assumed mechanisms that can explain the element/Ca_{shell} data. The following are hypotheses. A major river discharge in winter 1993/94 (A1) resulted in an increase of dissolved Ba in the water which was registered by all bivalves (A2). In addition, the river water increased the nutrient load in the coastal waters which triggered a phytoplankton (diatom?) bloom in early 1994 (A3; only moderately well developed in instrumental records due to limited measurement frequency). However, the subsequent downward flux of Mn-rich food particles was only recorded by the bivalves once the seasonal halocline disrupted, and not only resulted in a shell Mn/Ca peak (A4) but also in a boost of shell growth (A5). Major Baltic inflows in early 1993 (B1) and 1994 (B4) not only lead to increased availability of particulate Mn (as a result of stronger bottom water currents and resuspension of organic particles) that was recorded in the shells in the form of elevated Mn levels (B3), but also caused a major biogeochemical disturbance. The barotropic inflows carried oxygenated waters to the Baltic Sea which scavenged dissolved Mn. It took more than two years until dissolved Mn levels reestablished. During 1995 dissolved Mn levels in the water column were very low (B5) despite DO was strongly reduced. A smaller MBI in winter 1999/2000 also caused slightly elevated availability particulate Mn (C2) and removed larger proportions of dissolved Mn from the water column through oxidation (C3).

3.3.3 Ba/Ca

Ba/Ca data of the ventral margin revealed sharp peaks, specifically in winter 1994 und late summer 1998 (Fig. 3.9). The Ba/Ca series of the five studied specimens were remarkably similar to each other, specifically after mathematical re-sampling (Fig. 3.11B). Note that no age-detrending was required. The high synchronicity among the studied specimens not only included the aforementioned peaks, but also the great majority of the numerous smaller excursions (Fig. 3.11). As such, Ba/Ca served as an independent verification of the cross-dating of the growth increment series confirming the temporal alignment of the shell records.

3.4 Discussion

As demonstrated by the results, shells of *Arctica islandica* can serve as a high-resolution archive of past dissolved oxygen levels and bottom hypoxia. Mn/Ca values in shells of specimens from the Mecklenburg Bight, Baltic Sea oscillated on seasonal timescales and were inversely proportional to DO concentrations. Accordingly, highest Mn/Ca values were typically recorded during the warm season when seasonal stratification prevented the ventilation of bottom waters below the halocline, and lowest values during winter. However, these regular changes were superimposed by three additional shell Mn/Ca features caused by other environmental factors, namely extreme peaks in certain years, a strong high-frequency variability, and missing Mn enrichment in one summer despite oxygen depletion.

3.4.1 Pathways of Mn from the environment into bivalve shells

Manganese in bivalve shells can derive from dissolved Mn (e.g., Hawkes et al., 1996; Markich et al., 2002; Langlet et al., 2007; Lartaud et al., 2010) and particulate Mn (suspended organic particle ingestion: Bilos et al., 1998; Vander Putten et al., 2000; Lazareth et al., 2003; Langlet et al., 2007). Like many other ions, Mn^{2+} is taken up by bivalves predominantly along with water inhaled through the siphons. It can also enter the body fluids across the mantle epithelia by diffusion (e.g., Stewart, 1984). Bivalves can also ingest Mn-rich particulate organic matter, which dissolves during digestion and releases Mn^{2+} into the body fluids. Irrespective of the source, the manganese ions eventually reach the site of biomineralization and become incorporated – almost exclusively (i.e., some Mn is possibly linked to the shell organic matrix, see Takesue et al., 2008; Freitas et al., 2009) – into the carbonate fraction of the shell (Soldati et al., 2016), which has important implications for its use as a paleo-DO archive (see

Introduction). As demonstrated by previous studies, changes in the amount of dissolved manganese in the water column were reflected in the shell composition within less than a week (Jeffree et al., 1995: 2-6 days), i.e., shell Mn/Ca registers DO changes in the water column without significant lag. The same time frame may apply to particulate Mn after digestion, i.e., once the manganese has been converted to the reduced, bioavailable form. However, shell Mn/Ca signals resulting from particulate Mn do not necessarily reflect the time when Mn-rich organic particles reached the seafloor for the first time, but also the ingestion of re-suspended food particles that settled at the seafloor in previous years and accumulated through time.

3.4.2 Seasonal shell Mn/Ca variations and high-frequency oscillations

Seasonal variations are the most prominent low-frequency component of the shell Mn/Ca series in the studied *A. islandica* specimens. Most certainly, shell Mn/Ca variations resulted from regular changes in dissolved Mn in the ambient water and thus, seasonal DO fluctuations in the water column, rather than changes in the amount of ingested Mn-rich particles or Mn^{2+} (and DO) variations in the pore water of the sediment. This interpretation is supported by the strong coherency of the shell Mn/Ca curves from different specimens (Fig. 3.11), the running similarity and correlation of shell Mn/Ca and DO data of the water column (Fig. 3.9, 3.10), as well as previous observations according to which Mn/Ca values of bivalve shells closely mirror levels of dissolved Mn in the ambient water (e.g., Jeffree et al., 1995; Langlet et al., 2007; Lartaud et al., 2010). If particulate Mn would be the main driver for changing seasonal Mn levels in the shell, a strong correlation should exist between shell Mn/Ca values and seasonal shell growth rate. This is because a larger amount of ingested Mn-rich food particles requires an accelerated filter rate, and the shell Mn/Ca values would likely vary among specimens due to individual differences in feeding rate and food processing. This is because a large amount of ingested Mn-rich food particles requires an accelerated filter growth, which is intimately linked to increased food uptake and metabolic activity resulting in faster growth. However, no such correlation was observed here (compare shapes of the seasonal shell growth rate, Fig. 3.6E, and seasonal shell Mn/Ca data, Fig. 3.9: curves are shifted against each other), and was neither in most previous studies (Freitas et al., 2006, 2009; Carrè et al., 2006; but Langlet et al., 2007). Likewise, it seems unlikely that Mn^{2+} reaching the body fluids by transmembrane diffusion from pore water plays a significant role, although this may apply to infaunal freshwater bivalves (Zhao et al., 2017). If that was the case here, shell Mn/Ca curves would resemble much lower running similarity with DO values of the water column.

Although a decent visual inverse agreement exists between background shell Mn/Ca

data (i.e., leaving exceptional peaks and missing signals unconsidered) and DO, a regression analysis would yield low r-values, unless only the seasonal minima and maxima of both variables were plotted against each other (Fig. 3.10). The predominant reason for this discrepancy lies in the vastly different temporal resolution of the two data sets. Whereas DO measurements were only completed a few times per year (and at different dates in every year) and represent short-term snapshots, the shell Mn/Ca data represents a nearly uninterrupted record of dissolved Mn concentration. Our approach to linearly interpolate missing DO data helps to identify and visualize overall trends, but can impossibly reconstruct the actual DO variability. How strongly the oxygen levels can change within a few days is shown by more frequent measurements completed between 14 and 23 August 1989. During these ten days, the DO concentration fluctuated back and forth between 3.81 and 5.50 mg/L, and the largest difference between consecutive days equaled 1.62 mg/L (18 Aug 1989: 5.50 mg/L; 19 Aug 1989: 3.88 mg/L; Fig. 3.9). Hence, the synchronous, high-frequency variations of the shell Mn/Ca data most certainly result from high-frequency DO oscillations in the ambient water.

3.4.3 Peaks in shell Mn/Ca

In contrast to the regular seasonal variations, the exceptional shell Mn/Ca peaks, e.g., during summer 1991, winters 1991/92 and 1994/95, spring 1993 etc. can hardly be explained by sole changes in ambient DO (Fig. 3.9). Firstly, no such peak in shell Mn/Ca was observed in years during which the DO concentrations were even lower than in years where strong Mn enrichment was observed (e.g., summers 1992, 1995, 1999, Fig. 3.9). Secondly, at the study locality, hypoxia is limited to the warm season. Consequently, shell Mn enrichment in during winter and spring cannot result from extremely low DO. Thirdly, Mn/Ca peaks were not coherently developed in all studied specimens, i.e., in some years, peaks in shell Mn/Ca were only detected in one or few individuals, but missing in others; in addition, peak heights variedly significantly among specimens (e.g., during 1998, Fig. 3.11). These arguments suggest that shell Mn/Ca peaks were caused by particulate Mn, rather than changes in dissolved Mn levels. Inconsistent peaks among specimens could be indicative of Mn-rich organic particles being only available for a short time interval during which some specimens were not feeding at all or less than others. Unfortunately, there is not sufficient high-resolution environmental data to test this hypothesis.

The amount of food supply at the seafloor can be increased, for example, by an elevated flux of Mn-rich organic particles from surface to bottom waters following a major phytoplankton bloom, which in turn can be triggered by strong terrestrial runoff. Strong river discharge is not only associated with the influx of nutrients, but also Ba-rich sediments. In the

estuarine mixing zone, the barium gets desorbed from the clayey particles leading to elevated levels of dissolved Ba in coastal waters (Li and Chan, 1979). Riverine discharge events can then be recorded in the shells in the form of Ba/Ca peaks resulting either from increased dissolved Ba levels in the water (similar observations were reported from corals: McCulloch et al., 2003) or the ingestion of Ba-rich phytoplankton, specifically diatoms (Stecher et al., 1996; Vander Putten et al., 2000; Lazareth et al., 2003; Thébault et al., 2009), the most important component at the basis of the trophic pyramid (e.g., Sarthou et al., 2005). Actually, all studied bivalves showed a strong, synchronous Ba enrichment in their shells during winter 1994 (Jan/Feb) (Fig. 3.11, 3.12: "A2") that followed shortly after the strongest river discharge event recorded during the studied time interval (Fig. 3.12: "A1). After some moderate shell Mn/Ca rise during spring and summer 1994, values increased noticeably during winter 1994/95 (Fig. 3.12: "A4). Due to the lack of DO data from summer 1994 (Fig. 3.11, 12), it remains unclear if these elevated Mn concentrations in the shell resulted exclusively from the ingestion of Mn-rich organic particles or dissolved Mn as well. However, significantly faster shell growth rates in 1994/95 point to increased food levels (Fig. 3.12: "A5"). The observed temporal lag between the phytoplankton bloom in surface waters during spring (Fig. 3.12: "A3") and the elevated shell Mn levels in the following cold season does not come at surprise in a seasonally stratified habitat. The temporally developed halocline serves as a barrier that separates surface from bottom waters. Due to the scarcity of instrumental data, it is also not possible to verify the link between shell Ba content and diatom blooms. For example, silicate consumption, a proxy for diatom biomass, does not support our interpretation (Wasmund et al., 2013) and neither was a significant increase recorded in total phytoplankton biomass (Fig. 3.12: "A3"). The reservation must be made that all these data were only taken episodically, represent snapshots, and most likely have missed the maximum phase of phytoplankton blooms in some years. However, given the short time span between the river discharge and barium enrichment in the shells, the shell Ba/Ca peak may also have primarily resulted from increased amounts of dissolved Ba in the water (e.g., due to river discharge) rather than the ingestion of Ba-rich diatom frustules.

Another possibility to raise the amount of Mn-rich particles available for uptake by bivalves is resuspension of food particles by strong bottom currents. Actually, some of the smaller peaks in shell Mn/Ca, e.g., early 1993 (Fig. 3.12: "B2") and 1999 (Fig. 3.12: "C2"), occurred shortly after the strongest barotropic inflows during the time covered by the bivalve shell record (see list of MBIs in Mohrholz 2018). Such events resulted in the inflow of oxygen-rich saline waters from the North Sea into the Baltic Sea, which increased bottom current strength and modified the redox state beneath the halocline. Subsequently, dissolved Mn was

oxidized and precipitated at the seafloor as particulate Mn. Growth of bacteria further intensified the decline in Mn^{2+} content in the water column. This may explain the slightly lower than expected shell Mn/Ca values during summers 1993 and 1999 (Fig. 3.12: “B3” + “C3”).

3.4.4 Summer 1995: Low shell Mn/Ca values despite DO depletion

One remaining feature of the shell Mn/Ca curves is more challenging to interpret. During the warm season of 1995, all five studied specimens showed unexpectedly low shell Mn/Ca values (Fig. 3.9, Fig. 3.12: “B5”). The typical seasonal rise in shell manganese failed to appear although instrumental data indicated low DO concentrations (Fig. 3.9, 3.12). An erroneous temporal alignment can be precluded with certainty, because a distinct annual growth line was developed in all specimens separating the growing seasons of 1994/95 and 1995/96. More importantly, the $\delta^{18}O_{shell}$ values of specimen MLZ-St12-A9L covering this very time interval confirm the temporal alignment (Fig. 3.6). Assuming that shell Mn/Ca serves as a faithful proxy for dissolved and particulate Mn, concentrations of dissolved Mn in the water column remained extremely low during summer 1995 despite oxygen depletion. In addition, no significant Mn-rich organic particles seem to have been ingested at that time; this would also have materialized as elevated shell Mn/Ca values. In the absence of instrumental records on dissolved or particulate manganese concentrations, it can be speculated about the reasons for the low shell Mn/Ca values in 1995. Our interpretation is based on a numerical simulation by Yakushev et al. (2011) according to which strong barotropic inflow events can disturb biogeochemical properties in the ocean so severely that the reestablishment of steady-state conditions may take up to 2 years. Actually, the MBI cluster of the winters 1993 and 1994 (Fig. 3.12: “B1” + “B4”) has resulted in a striking oxygenation of the eastern Baltic Sea (Pohl and Hennings, 1999) during which dissolved Mn could be efficiently scavenged from the water column. Following the model by Yakushev et al. (2011), we suggest that Mn^{2+} levels then continued to remain low in the water column until late 1995 (Fig. 3.12: “B5”). The oxygenation events were superimposed by a freshwater discharge event (Fig. 3.12: “A1”) and subsequent phytoplankton bloom in 1993/94 that resulted in an increased downward flux of particulate Mn once the halocline disappeared in fall. The increased food supply then propelled shell growth in the following year (Fig. 3.12: “A3”). Similarly diminished shell Mn levels (Fig. 3.12: “C3”) were observed after the moderate MBIs in winters 1998/99 and 1999/2000 (Fig. 3.12: “C1”).

To summarize, shell Mn/Ca data of *A. islandica* from Mecklenburg Bight reflect the dissolved Mn concentration of bottom water, but also the occasional flux of particulate Mn from surface waters and/or increased hydrodynamic energy near the sea floor and associated

resuspension of particulate Mn. Analysis of shell Ba/Ca values and shell growth rate may help to distinguish the two sources of Mn in order to interpolate prevailing DO conditions during growth. To verify the hypotheses presented above (see also summarizing model in Figure 3.13) and establish shell Mn/Ca as a proxy for past DO content in shallow marine settings, tank experiments under controlled conditions or a detailed monitoring study are strongly recommended. Such studies could also determine the DO threshold below which *A. islandica* produces disturbance lines in its shell, ceases to biomineralize and stops to record environmental conditions. At the study locality, DO levels seems to have remained above this threshold, because no major disturbance lines were observed that were indicative of extended low-oxygen-related growth cessation.

3.4.5 Hinge plate records

Due to its condensed growth record, the hinge does not closely approach the same high-resolution environmental proxy data set as the ventral margin. Notwithstanding, the hinge comes with some advantages for sclerochronology-based paleoenvironmental reconstructions. For example, the growth pattern geometry of the hinge significantly facilitates the construction of annual increment width chronologies, because the growth increment widths can always be measured as perpendiculars between subsequent growth lines, specifically in ontogenetically young shell portions (Fig. 3.3). Furthermore, some trace elements (Sr, Mg) are strongly linked to the prevailing microstructure or processes controlling their formation (Schöne et al., 2013). Element analyses should therefore be completed in the microstructurally most uniform shell portion, i.e., the hinge plate, instead of the ventral margin. The latter is microstructurally much more complex (see Ropes et al., 1984; Dunca et al., 2009) than the hinge plate (Schöne, 2013). As demonstrated in Figure 3.8, the annual shell Mn/Ca data of the hinge and ventral margin show a robust running similarity and, on average, similar ratios in both shell portions suggesting that the shell microstructure has only little effect on the incorporation of Mn in the shell. Mn/Ca data from different shell portions with different microstructure can thus be faithfully compared with each other, and the high-resolution Mn record from the ventral margin should be largely unbiased by microstructural changes. Further studies should still address this issue in more detail. For reasons explained in section 4.2 (high-frequency variability, Mn/Ca peaks etc.), a regression analysis between weighted annual shell Mn/Ca values and annual DO concentration data would not provide useful information.

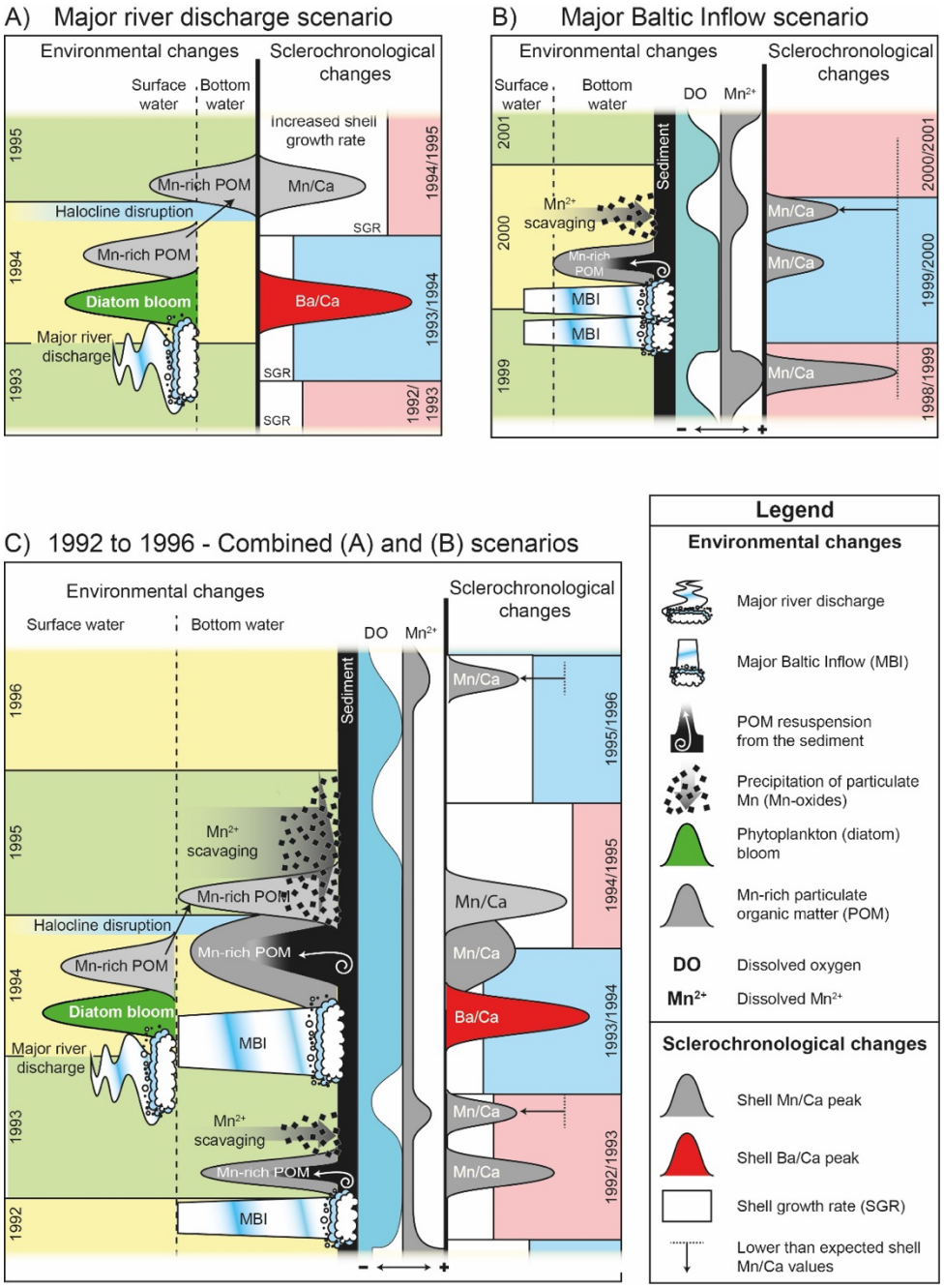

Fig. 3.13. Model based on Figure 3.12 explaining the link between Mn, Ba and growth rate of shells of *Arctica islandica* from Mecklenburg Bight, Baltic Sea and environmental conditions.

Annual increment width series of the studied specimens showed a strong agreement with each other suggesting that shell growth was controlled by external forcings as in other species. Most certainly temperature and food availability play a major role in this regard, but there was not sufficient instrumental data to verify this here. Additionally, the main focus of the present study was oxygen availability and therefore the relationship between shell growth and DO was addressed. Annual increments were significantly broader when more oxygen was available during November – March, but narrower if the oxygen levels were higher during summer (Fig.

3.5). At first, shell production during the cold season may sound counterintuitive, but *A. islandica* is one the few species, that grow continuously to grow, though at reduced rate, during the entire cold season (Schöne et al., 2005b). It is hypothesized here, that winter growth in *A. islandica* increases when more oxygen is available, because fewer food competitors are active at that time. The opposite may be the case during summer. Then, a larger number of consumers benefit from better oxygenation of the water column, which leads to food competition and, consequently, slower growth rate in *A. islandica* and probably other species as well.

3.4.6 Required data treatment: Temporal alignment, age-detrending, resampling

The present study would not have been possible without precise temporal alignment of the chemical data measured in the shells, removal of inherent ontogenetic age-related trends and mathematical resampling. These data treatments ensure that existing synchronicity between the time-series can be detected and each sample represents the same amount of time. Otherwise, peaks would be out of phase, and seasonal amplitudes of shells sampled with higher resolution would appear larger than those sampled with lower resolution. As exemplified in Figure 3.11, precisely dated, age-detrended and resampled chemical time-series of the studied specimens not only exhibit strong synchronicity (that would not be apparent prior to the mathematical conversion; see Supplements for data prior to detrending and resampling), and the chemical properties are also less variable among specimens. Aside from reflecting individual physiological controls (see also Freitas et al., 2006), the remaining differences may partly be explained by variations of the seasonal growth rate among specimens and ontogenetic years. Our seasonal growth model may not be perfect, but the two versions of the seasonal growth model based on different calendar years and specimens are nearly identical (Fig. 3.6E+F). Weighted annual averages based on these two growth models differ much less from each other than arithmetic annual averages (compare growth curves in Fig. 3.6E+F). It should be noted that the precision of the seasonal growth model hinges on the temporal resolution of the environmental data. Given the limited frequency at which temperature and salinity were measured (on average, six times per year; max. fourteen times per year), our seasonal growth model likely comes with an estimated error or ca. one to two months.

3.5 Summary and conclusions

Shell Mn/Ca values of *A. islandica* from the Baltic Sea can potentially be used to quantify the past DO concentrations in the ambient water and reconstruct hypoxic events. However, aside from variations in dissolved Mn, the shell Mn/Ca data also reflect changes in ontogenetic age and particulate Mn in the ambient environment. The latter can be easily identified, because they leave extreme Mn/Ca peaks in the shell, which stand out significantly (>> 50 µmol/mol) from the regular seasonal variations (approx. 30 to 50 µmol/mol, corresponding DO concentrations: 8.9 to 1.8 mg/L) resulting from changes in Mn^{2+} and DO concentration in the water column. Prior to any analyses, it is required to place the the shell Mn/Ca data in precise temporal context and mathematically remove inherent ontogenetic age-related trends. If values of different years and specimens are compared with each other, data need to be mathematically resampled so that each sample represents the same amount of time. In order to obtain more reliable results, a transfer function capable of reconstructing paleo-DO concentrations from shell Mn/Ca data should also consider growth increment widths as a measure of food supply and shell Ba/Ca peaks as possible indicators of river discharge events and/or phytoplankton blooms. Tank experiments under controlled conditions could help to further constrain the transfer function.

3.6. Supplementary data

Supplementary data to this article can be found online at https://doi.org/10.1016/j.ecss.2021.107257.

References

Ahl, T., 1977. River discharges of Fe, Mn, Cu, Zn, and Pb into the Baltic Sea from Sweden. Ambio Spec. Rep. 5, 219–228.

Andrén, E., Andrén, T, Kunzendorf, H., 2000. Holocene history of the Baltic Sea as a background for assessing records of human impact in the sediments of the Gotland Basin. Holocene 10, 687–702.

Balzer, W., 1982 On the distribution of iron and manganese at the sediment/water interface: thermodynamic versus kinetic control. Geochim. Cosmochim. Acta 46, 1153–1161.

Barats, A., Amouroux, D., Pécheyran, C., Chauvaud, L., Donard, O.F.X., 2008. High-frequency archives of Manganese inputs to coastal waters (Bay of Seine, France) resolved by the LA-ICP-MS analysis of calcitic growth layers along scallop shells (*Pecten maximus*). Environ. Sci. Technol. 42, 86–92.

Benson, B.B., Krause, D. Jr., 1984. The concentration and isotopic fractionation of oxygen dissolved in freshwater and seawater in equilibrium with the atmosphere. Limnol. Oceanogr. 29, 620–632.

Bilos, C., Colombo, J.C. and Presa, M.J., 1998. Trace metals in suspended particles, sediments and Asiatic clams (*Corbicula fluminea*) of the Río de la Plata Estuary, Argentina. Environ. Pollut. 99, 1–11.

Bonsdorff, E., 2006. Zoobenthic diversity-gradients in the Baltic Sea: Continuous post-glacial succession in a stressed ecosystem. J. Exp. Mar. Biol. Ecol. 330, 383–391.

Branson, O., Fehrenbacher, J., Vetter, L., Sadekov, A.Y., Eggins, S.M., Spero, H.J., 2019. LAtools: A data analysis package for the reproducible reduction of LA-ICPMS data. Chem. Geol. 18962.

Caballelero-Alfonso, A.M., Carstensen, J., Conley, D.J., 2015. Biogeochemical and environmental drivers of coastal hypoxia. J. Mar. Syst. 141, 190–199.

Carré, M, Bentaleb, I., Bruguier, O., Ordinola, E., Barrett, N.T., Fontugne, M., 2006. Calcification rate influence on trace element concentrations in aragonitic bivalve shells: Evidences and mechanisms. Geochim. Cosmochim. Acta 70, 4906–4920.

Carstensen, J., Andersen, J.H., Gustafsson, B.G., Conley, D.J., 2014a. Deoxygenation of the Baltic Sea during the last century. Prox. Nat. Acad. Sci. 111, 5628–5633.

Carstensen, J., Conley, D.J., Bonsdorff, E., Gustafsson, B.C., hietanen, S., Janas, U., Jilbert, T., Maximov, A., Norkko, A., Norkko, J., Reed, D.C., Slomp, C.P., Timmermann, K., Voss., M., 2014b. Hypoxia in the Baltic Sea: Biogeochemical cycles, benthic fauna, and management. Ambio 43, 26–36.

Conley, D.J., Björck, S., Bonsdorff, E., Carstensen, J., Destouni, G., Gustafsson, B.G., Hietanen, S., Kortekaas, M., Kuosa, H., Meier, M., Müller-Karulis, B., Nordberg, K., Nürnberg, G., Norkko, A., Pitkänen, H., Rabalais, N.N., Rosenberg, R., Savchuk, O.P., Slomp, C.P., Voss, M., Wulff, F., Zillén, L., 2009. Hypoxia-related processes in the Baltic Sea. Environ. Sci. Technol. 43, 3412–3420.

Conley, D.J., Carstensen, J., Ærtebjerg, G., Bondo Christensen, P., Dalsgaard, T., Hansen, J.L.S., Josefson, A.B., 2007. Long-term changes and impact of hypoxia in Danish coastal waters. Ecol. Applicat. 17, S165–S184.

Conley, D.J., Carstensen, J., Aigars, J., Axe, P., Bonsdorff, E., Eremina, T., Haahti, B.-M., Humborg, C., Jonsson, P., Kotta, J., Lännegren, C., Larsson, U., Maximov, A., Medina, M.R., Lysiak-Pastuszak, E., Remeikaite-Nikiene, N., Walve, J., Wilhelms, S., Zillén, L., 2011. Hypoxia is increasing in the coastal zone of the Baltic Sea. Environ. Sci. Technol. 45, 6777–6783.

Dellwig, O., Schnetger, B., Brumsack, H.-J., Grossart, H.-P., Umlauf, L., 2012. Dissolved reactive manganese at pelagic redoxclines (part II): Hydrodynamic conditions for accumulation. J. Mar. Syst. 90, 31–41.

Diaz, R.J., Rosenberg, R., 2008. Spreading dead zones and consequences for marine ecosystems. Science 321, 926–929.

Dunca, E., Mutvei, H., Göransson, P., Mörth, C.-M., Schöne, B.R., Whitehouse, M.J., Elfman, M., Baden, S.P., 2009. Using ocean quahog (*Arctica islandica*) shells to reconstruct palaeoenvironment in Öresund, Kattegat and Skaggerak, Sweden. International J. Earth Sci. 98, 3–17.

Filipsson, H.L., Nordberg, K., 2004. A 200 year environmental record of a low oxygen fjord, Sweden, elucidated by benthic foraminifera, sediment characteristics and hydrographic data. J. Foram. Res. 34, 277–293.

Freitas, P.S., Clarke, L.J., Kennedy, H., Richardson, C.A., Abrantes, F., 2006. Environmental and biological controls on elemental (Mg/Ca, Sr/Ca and Mn/Ca) ratios in shells of the king scallop *Pecten maximus*. Geochim. Cosmochim. Acta 70, 5119–5133.

Freitas, P.S., Clarke, L.J., Kennedy, H., Richardson, C.A., 2009. Ion microprobe assessment of the heterogeneity of Mg/Ca, Sr/Ca and Mn/Ca ratios in *Pecten maximus* and *Mytilus edulis* (bivalvia) shell calcite precipitated at constant temperature. Biogeosci. 6, 1209–1227.

Froehlich, P.N., Klinkhammer, G.P., Bender, M.L., Luedtke, N.A., Heath, G.R., Cullen, D., Dauphin, P., Hammond, D., Hartman, B., Maynard, V., 1979. Early oxidation of organic

matter in pelagic sediments of the eastern equatorial Atlantic: suboxic diagenesis. Geochim. Cosmochim. Acta 43, 1075–1090.

Füllenbach, C.S., Schöne, B.R., Mertz-Kraus, R., 2015. Strontium/lithium ratio in aragonitic shells of *Cerastoderma edule* (Bivalvia) – a new potential temperature proxy for brackish environments. Chem. Geol. 417, 341–355.

Gonfiantini, R., Stichler,W., Rozanski, K., 1995 Standards and intercomparison materials distributed by the International Atomic Energy Agency for stable isotope measurements (IAEA-TECDOC-825), International Atomic Energy Agency (IAEA), Vienna, Austria, 13–29, available at: https://www-pub.iaea.org/MTCD/publications/PDF/te_825_prn.pdf (last access: 26 Oct., 2020)

Graf, G., Bengtsson, W., Diesner, U., Schulz, R., Theede, H., 1982. Benthic response to sedimentation of a spring phytoplankton bloom: Process and budget. Mar. Biol. 67, 201–208.

Groeneveld, J., Filipsson, H.L., 2013. Mg/Ca and Mn/Ca ratios in benthic foraminifera: the potential to reconstruct past variations in temperature and hypoxia in shelf regions. Biogeosci. 10, 5125–5138.

Groeneveld, J., Filipsson, H.L., Austin, W.E.N., Darling, K., McCarthy, D., Krupinski, N.B.Q., Bird, C., Scweizer, M., 2018. Assessing proxy signatures of temperature, salinity, and hypoxia in the Baltic Sea through foraminifera-based geochemistry and faunal assemblages. J. Micropalaeontol. 37, 403–429.

Grossman, E.L., Ku, T.-L., 1986. Oxygen and carbon isotope fractionation in biogenic aragonite; temperature effects, Chem. Geol. Isot. Geosci. Sect., 59, 59–74.

Guo, X., Xu, B., Burnett, W., Yu, Z., Yang, S., Huang, X., Wang, F., Nan, H., Yao, P., Sun, F., 2019. A potential proxy for seasonal hypoxia: LA-ICP-MS Mn/Ca ratios in benthic foraminifera from the Yangtze River Estuary. Geochim. Cosmochim. Acta 245, 290–303.

Hallmann, N., Schöne, B.R., Irvine, G.V., Burchell, M., Cokelet, E.D., Hilton, M., 2011. An improved understanding of the Alaska Coastal Current: The application of a bivalve growth-temperature model to reconstruct freshwater-influenced paleoenvironments. Palaios 26, 346–363.

Hawkes, G.P., Day, R.W., Wallace, M.W., Nugent, K.W., Bettiol, A.A., Jamieson, D.N., Williams, M.C., 1996. Analyzing the growth and form of mollusc shell layers, in situ, by cathodoluminescence microscopy and Raman spectroscopy. J. Shellf. Res. 15, 659–666.

Hem, J.D., 1963. Chemical equilibria and rates of manganese oxidation. U.S. Geol. Surv. Water Supply Pap. 1667-A, A1–A64.

Hunt, C.D., 1983. Incorporation and deposition of Mn and other trace metals by flocculent organic matter in a controlled marine ecosystem. Limnol. Oceanogr. 28, 302–308.

Jeffree, R.A., Markich, S.J., Lefebvre, F., Thellier, M., Ripoll, C., 1995. Shell microlaminations of the freshwater bivalve *Hyridella depressa* as an archival monitor of manganese water concentration: Experimental investigation by depth profiling using secondary ion mass spectrometry (SIMS). Experientia 51, 838–848.

Jilbert, T., Slomp, C.P., 2013. Rapid high-amplitude variability in Baltic Sea hypoxia during the Holocene. Geology 41, 1183–1186.

Jochum, K.P., Nohl, U., Herwig, K., Lammel, E., Stoll, B., Hofmann, A.W., 2005. GeoReM: a new geochemical database for reference materials and isotopic standards. Geostand. Geoanal. Res. 29, 333–338.

Jochum, K.P., Stoll, B., Herwig, K., Willbold, M., 2007. Validation of LA-ICP-MS trace element analysis of geological glasses using a new solid-state 193 nm Nd:YAG laser and matrix-matched calibration. J. Anal. At. Spectrom. 22, 112.

Jochum, K.P., Weis, U., Stoll, B., Kuzmin, D., Yang, Q., Raczek, I., Jacob, D.E., Stracke, A., Birbaum, K., Frick, D.A., Günther, D., Enzweiler, J., 2011. Determination of reference values for NIST SRM 610–617 glasses following ISO guidelines. Geostand. Geoanal. Res. 35, 397–429.

Kabel, K., Moros, M., Porsche, C., Neumann, T., Adolphi, F., Joest Andersen, T., Siegel, H., Gerth, M., Leipe, T., Jansen, E., Sinninghe Damsté, J.S., 2012. Impact of climate change on the Baltic Sea ecosystem over the past 1,000 years. Nature Clim. Change 2, 871–874.

Karlson, K., Rosenberg, R., Bonsdorff, E., 2002. Temporal and spatial large-scale effects of eutrophication and oxygen deficiency of benthic fauna in Scandinavian and Baltic waters – A review. Oceanogr. Mar. Biol. Annu. Rev. 40, 427–489.

Langlet, D., Alleman, L.Y., Plisnier, P.D., Hughes, H., André, L., 2007. Manganese content records seasonal upwelling in Lake Tanganyika mussels. Biogeosci. 4, 195–203.

Lartaud, F., De Rafélis, M., Ropert, M., Emmanuel, L., Geairon, P., Renard, M., 2010. Mn labelling of living oysters: artificial and natural cathodoluminescence analyses as a tool for age and growth rate determination of *C. gigas* (Thunberg, 1793) shells. Aquacult. 300, 206–217.

Lazareth, C.E., Vander Putten, E., André, L., Dehairs, F., 2003. High-resolution trace element profiles in shells of the mangrove bivalve *Isognomon ephippium*: a record of environmental spatio-temporal variations? Estuar. Coastl. Shelf Sci. 57, 1103–1114.

Leipe, T., Kersten, M., Heise, S., Pohl, C., Witt, G., Liehr, G., Zettler, M., Tauber, F., 2005.

Ecotoxicity assessment of natural attenuation effects at a historical dumping site in the western Baltic Sea. Mar. Pollut. Bull. 50, 446–459.

Li, Y.-H., Chan, L.-H., 1979. Desorption of Ba and ^{226}Ra from river-borne sediments in the Hudson estuary. Earth Planet. Sci. Lett. 43, 343–350.

Limburg, K.E., Olson, C., Walther, Y., Dale, D., Slomp, C.P., Høie, H., 2011. Tracking Baltic hypoxia and cod migration over millennia with natural tags. Proc. Nat. Acad. Sci., 108, E177–E182.

Longerich, H.P., Jackson, S.E., Günther, D., 1996. Laser ablation inductively coupled plasma mass spectrometric transient signal data acquisition and analyte concentration calculation. J. Anal. At. Spectrom. 11, 899–904.

Marali, S., Schöne, B.R., Mertz-Kraus, R., Griffin, S.M., Wanamaker Jr., A.D., Butler, P.G., Holland, H.A., Jochum, K.P., 2017. Reproducibility of trace element variations (Na/Ca, Mg/Ca, Mn/Ca, Sr/Ca, and Ba/Ca) within and between specimens of the bivalve *Arctica islandica* – a LA-ICP-MS line scan study. Palaeogeogr. Palaeoclimatol. Palaeoecol. 484, 109–128.

Markich, S.J., Jeffree, R.A., Burke, P.T., 2002. Freshwater bivalve shells as archival indicators of metal pollution from a copper-uranium mine in tropical northern Australia. Environ. Sci. Technol. 36, 821–832.

McCulloch, M.T., Fallon, S., Wyndham, T., Hendy, E., Lough, J., Barnes, D., 2003. Coral record of increased sediment flux to the inner Great Barrier Reef since European settlement. Nature 421, 727–730.

Millward, G.E., Morris, A.W., Tappin, A.D., 1998. Trace metals at two sites in the southern North Sea: Results from a sediment resuspension study. Cont. Shelf Res. 18, 1381–1400.

Mischel, S.A., Mertz-Kraus, R., Jochum Klaus, P., Scholz, D., 2017. TERMITE: An R script for fast reduction of laser ablation inductively coupled plasma mass spectrometry data and its application to trace element measurements. Rapid Comm. Mass Spec. 31, 1079–1087.

Mohrholz, V., 2018. Major Baltic Inflow statistics – Revisited. Front. Mar. Sci. 5, 384.

Nordberg, K, Gustafsson, M, Krantz, A.-L., 2000. Decreasing oxygen concentrations in the Gullmar Fjord, Sweden, as confirmed by benthic foraminifera, and the possible association with NAO. J. Mar. Syst. 23, 303–316.

Oeschger, R., 1990. Long-term anaerobiosis in sublittoral marine invertebrates from the Western Baltic Sea: *Halicryptus spinulosus* (Priapulida), *Astarte borealis* and *Arctica islandica* (Bivalvia). Mar. Ecol. Prog. Ser. 59, 133–143.

Oeschger, R., Storey, K.B., 1993. Impact of anoxia and hydrogen sulphide on the metabolism of *Arctica isiandica* L. (Bivalvia). J. Exp. Mar. Biol. Ecol. 170, 213–226.

Österblom, H., Hansson, S., Larsson, U., Hjerne, O., Wulff, F., Elmgren, R., Folke, C., 2007. Human-induced trophic cascades and ecological regime shifts in the Baltic Sea. Ecosyst. 10, 877–889.

Pakhamova, S.V., Hall, P.O.J., Kononets, M.Y., Rozanov, A.G., Tengberg, A., Vershinin, A.V., 2007. Fluxes of iron and manganese across the sediment–water interface under various redox conditions. Mar. Chem. 107, 319–331.

Peharda, M., Walliser, E.O., Markulin, K., Purroy, A., Uvanović, H., Janekovic, I., Župan, I., Vilibic, I., Schöne, B.R., 2019. *Glycymeris pilosa* (Bivalvia) – A high-potential geochemical archive of the environmental variability in the Adriatic Sea. Marine Environmental Research 150, 104759.

Pohl, C., Hennings, U., 1999. The effect of redox processes on the partitioning of Cd, Pb, Cu, and Mn between dissolved and particulate phases in the Baltic Sea. Mar. Chem. 65, 41–53.

Rabalais, N.N., Díaz, R.J., Levin, L.A., Turner, R.E., Gilbert, D., Zhang, J., 2010. Dynamics and distribution of natural and human-caused hypoxia. Biogeosci. 7, 585–619.

Reinholdsson, M., Snowball, I., Zillén, L., Lenz, C., Conley, D.J., 2013. Magnetic enhancement of Baltic Sea sapropels by greigite magnetofossils. Earth Planet. Sci. Lett. 366, 137–150.

Risk, M.J., Burchell, M., de Roo, K., Nairn, R., Tubrett, M., Forsterra, G., 2010. Trace elements in bivalve shells from the Río Cruces, Chile. Aquat. Biol. 10, 85–97.

Roitz, J.S., Flegal, A.R., Bruland, K.W., 2002. The biogeochemical cycling of Manganese in San Francisco Bay: Temporal and spatial variations in surface water concentrations. Estuar. Coast. Shelf Sci. 54, 227–239.

G., Timmermans, K. R., Blain, S., Tréguer, P., 2005. Growth physiology and fate of diatoms in the ocean: a review. J. Sea Res. 53, 25–42.

Ropes, J.W., Jones, D.S., Murawski, S.A., Serchuk, F.M., Jearld, A. Jr., 1984. Documentation of annual growth lines in ocean quahogs, Arctica islandica Linné. Fish. Bull. 82, 1–19.

Rue, E.L., Smith, G.J., Cutter, G.A., Bruland, K.W., 1997. The response of trace element redox couples to suboxic conditions in the water column. Deep-Sea Res. I 44, 113–134.

Schöne, B.R., 2008. The curse of physiology – Challenges and opportunities in the interpretation of geochemical data from mollusk shells. Geo-Mar. Lett. 28, 269–285.

Schöne, B.R., 2013. *Arctica islandica* (Bivalvia): A unique paleoenvironmental archive of the northern North Atlantic Ocean. Global Planet. Change 111, 199–225.

Schöne, B.R., Freyre Castro, A.D., Fiebig, J., Houk, S.D., Oschmann, W., Kröncke, I., 2004. Sea surface water temperatures over the period 1884-1983 reconstructed from oxygen isotope ratios of a bivalve mollusk shell (*Arctica islandica*, southern North Sea). Palaeogeogr. Palaeoclimatol. Palaeoecol. 212, 215–232.

Schöne, B.R., Dunca, E., Fiebig, J., Pfeiffer, M., 2005a. Mutvei's solution: an ideal agent for resolving microgrowth structures of biogenic carbonates. Palaeogeogr. Palaeoclimatol. Palaeoecol. 228, 149–166.

Schöne, B.R., Houk, S.D., Freyre Castro, A.D., Fiebig, J., Kröncke, I., Dreyer, W., Oschmann, W., 2005b. Daily growth rates in shells of *Arctica islandica*: Assessing subseasonal environmental controls on a long-lived bivalve mollusk. Palaios 20, 78–92.

Schöne, B.R., Rodland, D.L., Wehrmann, A., Heidel, B., Oschmann, W., Zhang, Z., Fiebig, J., Beck, L., 2007. Combined sclerochronologic and oxygen isotope analysis of gastropod shells (*Gibbula cineraria*, North Sea): life-history traits and utility as a high-resolution environmental archive for kelp forests. Mar. Biol. 150, 1237–1252.

Schöne, B.R., Radermacher, P., Zhang, Z., Jacob, D.E., 2013. Crystal fabrics and element impurities (Sr/Ca, Mg/Ca, and Ba/Ca) in shells of *Arctica islandica* – Implications for paleoclimate reconstructions. Palaeogeogr. Palaeoclimatol. Palaeoecol. 373, 50–59.

Sohlenius, G., Emeis, K.-C., Andrén, E., Andrén, T., Kohly, A., 2001. Development of anoxia during the Holocene fresh-brackish water transition in the Baltic Sea. Mar. Geol. 177, 221–242.

Soldati, A.L., Jacob, D.E., Glatzel, P., Swarbrick, J.C., Geck, J., 2016. Element substitution by living organisms: the case of manganese in mollusc shell aragonite. Sci. Rep. 6, 22514.

Stecher, H.A., Krantz, D.E., Lord, C.J., Luther, G.W., Bock, K.W., 1996. Profiles of strontium and barium in *Mercenaria mercenaria* and *Spisula solidissima* shells. Geochim. Cosmochim. Acta 60, 3445–3456.

Stewart, M.G., 1984. Permeability and epidermal transport. In: Bereiter-Hahn, J., Matoltsy, A.G., Richards, K.S. (Eds.), Biology of the Integument. 1 Invertebrates. Springer, Berlin, pp. 486–501.

Strahl, J., Dringen, R., Schmidt, M.M., Hardenberg, S., Abele, D., 2011. Metabolic and physiological responses in tissues of the long-lived bivalve *Arctica islandica* to oxygen deficiency. Comp. Biochem. Physiol. A158, 513–519.

Sunda, W.G., Huntsman, S.A., 1983. Effect of competitive interactions between manganese and copper on cellular growth in estuarine and oceanic species of the diatom *Thalassiosira*. Limnol. Oceanogr. 28, 924–934.

Sunda, W.G., Huntsman, S.A., 1985. Regulation of cellular manganese and manganese transport rates in the unicellular alga *Chlamydomonas*. Limnol. Oceanogr. 30, 71–80.

Sunda, W.G., Huntsman, S.A., 1987. Microbial oxidation of manganese in a North Carolina estuary. Limnol. Oceanogr. 32, 552–564.

Sunda, W.G., Huntsman, S.A., 1990. Diel cycles in microbial manganese oxidation and manganese redox speciation in coastal waters of the Bahama Islands. Limnol. Oceanogr. 35, 325–338.

Sundby, B., Silverberg, N., Chesselet, R., 1981. Pathways of manganese in an open estuarine system. Geochim. Cosmochim. Acta 45, 293–307.

Takesue, R.K., Bacon, C.R., Thompson, J.K., 2008. Influences of organic matter and calcification rate on trace elements in aragonitic estuarine bivalve shells. Geochim. Cosmochim. Acta 72, 5431-5445.

Taylor, A.C., 1976. Burrowing activity and anaerobiosis of the bivalve *Arctica islandica* (L.). J. Mar. Biol. Ass. U.K. 56, 95–105.

Tebo, B.M., Bargar, J.R., Clement, B.G., Dick, G.J., Murray, K.J., Parker, D., Verity, R., Webb, S.M., 2004. Biogenic manganese oxides: properties and mechanisms of formation. Annu. Rev. Earth Planet. Sci. 32, 287–328.

Thébault, J., Chauvaud, L., L'Helguen, S., Clavier, J., Barats, A., Jacquet, S., Pécheyran, C., Amouroux, D., 2009. Barium and molybdenum records in bivalve shells: geochemical proxies for phytoplankton dynamics in coastal environments? Limnol. Oceanogr. 54, 1002–1014.

Theede, H., Ponat, A., Hiroki, K., Schlieper, C., 1969. Studies on the resistance of marine bottom invertebrates to oxygen-deficiency and hydrogen sulphide. Mar. Biol. 2, 325–337.

Vander Putten, E., Deharis, F., Keppens, E., Baeyens, W., 2000. High resolution distribution of trace elements in the calcite shell layer of modern *Mytilus edulis*: Environmental and biological controls. Geochim. Cosmochim. Acta 64, 997–1011.

VanPlantinga, A.A., Grossman, E.L., 2019. Trace elements in mussel shells from the Brazos River, Texas: environmental and biological control. Biogeosci. Disc.

Vanquer-Sunyer, R., Duarte, C.M., 2008. Thresholds of hypoxia for marine biodiversity. Proc. Nat. Acad. Sci. 105, 15453–15457.

Wasmund, N., Nausch, G., Feistel, R., 2013. Silicate consumption: an indicator for long-term trends in spring diatom development in the Baltic Sea. J. Plankton Res. 35, 393–406.

Westman, P., Sohlenius, G., 1999. Diatom stratigraphy in five offshore sediment cores from the northwestern Baltic proper implying large scale circulation changes during the last 8500

years. J Paleolimnol. 22, 53–69.

Witkowski, A., Pempkowiak, J., 1995. Reconstructing the development of human impact from diatoms and ^{210}Pb sediment dating (the Gulf of Gdansk-southern Baltic Sea). Geographia Polonica 65, 63–78.

Yakushev, E.V., Kuznetsov, I.S., Podymov, O.I., Burchard, H., Neumann, T., Pollehne, F., 2011. Modeling the influence of oxygenated inflows on the biogeochemical structure of the Gotland Sea, central Baltic Sea: Changes in the distribution of manganese. Comp. Geosci. 37, 398–409.

Zettler, M.L., Bönsch, R., Gosselck, F., 2001. Distribution, abundance, and soem population characteristics of the ocean quahog, *Arctica islandica* (Linnaeus, 1767) in the Mecklenburg Bight (Baltic Sea).J. Shellf. Res. 20, 161–169.

Zhao, L., Walliser, E.O., Mertz-Kraus, R., Schöne, B.R., 2017. Unionid shells (*Hyriopsis cumingii*) record manganese cycling at the sediment-water interface in a shallow eutrophic lake in China (Lake Taihu). Palaeogeogr. Palaeoclimatol. Palaeoecol. 484, 97–108.

Zillén, L., Conle, D.J., Andrén, T., Andrén, E., Björck, S., 2008. Past occurrences of hypoxia in the Baltic Sea and the role of climate variability, environmental change and human impact. Earth-Sci. Rev. 91, 77–92.

Corrigenda:

Where shell Mn/Ca is compared to DO, the latter are given in mL/L, not mg/L (text in sections 3.2, 4.2 and 5; Fig. 5, 9, 10, 12).

Mn/Ca_{shell} data in Figure 11 (upper panel) need to be multiplied by 10.

Heading of section 4.4 should read: “4.4 Summer 1995: low shell …”

4 High-resolution reconstruction of dissolved oxygen levels in the Baltic Sea with bivalves – a multi-species comparison (*Arctica islandica*, *Astarte borealis*, *Astarte elliptica*)

Bernd R. Schöne[1], Xizhi Huang[1], Anne Jantschke[1], Regina Mertz-Kraus[1], Michael L. Zettler[2]

1 Institute of Geosciences, University of Mainz, Mainz, Germany
2 Leibniz Institute for Baltic Sea Research Warnemünde, Rostock, Germany

Schöene, B.R., Huang, X., Jantschke, A., Mertz-Kraus, R., and Zettler, M.L. (2022). High-resolution reconstruction of dissolved oxygen levels in the Baltic Sea with bivalves – a multi-species comparison (*Arctica islandica*, *Astarte borealis*, *Astarte elliptica*). Frontiers in Marine Science, 9, 820731.

This manuscript was published in the journal "*Frontiers in Marine Science*". I contributed to the sample preparation, performed the measurements, collected and synthesized the data, developed part of the methodology, and helped with the interpretation of the results. This work was supported by the DFG grant to BRS [SCHO793/22]; The sampling cruise was financed as part of the LEGRA project funded by the Federal Agency for Nature Conservation (BfN) (FKZ 3519532202).

Authors' contributions:

BRS: Conceptualization, Data curation, Formal analysis, Investigation, Methodology, Project administration, Supervision, Validation, Visualization, Writing-original draft Preparation; Writing-review and editing.

XZH: Sample preparation, Data curation, Methodology, Formal analysis.

AJ: Writing-review and editing.

RMK: Resources, Writing-review and editing.

MLZ: Resources, Writing-review and editing.

Abstract

An increasing area of shallow-marine benthic habitats, specifically in the Baltic Sea, is affected by seasonal oxygen depletion. To place the current spread of oxygen deficiency into context and quantify the contribution of anthropogenic ecosystem perturbation to this development, high-resolution archives for the pre-instrumental era are needed. As recently demonstrated, shells of the bivalve mollusk, *Arctica islandica* fulfil this task with molar Mn/Ca_{shell} ratios as proxies for dissolved oxygen (DO) levels in the water column. Since the ocean quahog is inhomogeneously distributed in the Baltic Sea and may not be present in museum collections or found throughout sedimentary sequences, the present study evaluated whether two other common bivalves, *Astarte elliptica* and *Astarte borealis* can be used interchangeably or alternatively as proxy DO recorders. Once mathematically resampled and corrected for shell growth rate-related kinetic effects and (some) vital effects, Mn/Ca_{shell} data of all three species (age ten onward in *A. islandica*) were statistically significantly ($p < 0.0001$) linearly and inversely correlated to DO concentration in the free water column above seafloor ($r = –0.66$ to $–0.75$, corresponding to 43 to 56 % explained variability). *A. elliptica* may provide slightly more precise DO data (1σ error of ±1.5 mL/L) than *A. islandica* or *A. borealis* (±1.6 mL/L), but has a shorter lifespan. Both *Astarte* species show a stronger correlation with DO than *A. islandica*, because their biomineralization seems to be less severely hampered by oxygen and salinity stress. In turn, *A. islandica* grows faster resulting in less time-averaged data. During youth, the ocean quahog typically incorporates a disproportionately large amount of manganese into its shell, possibly because food intake occurs directly at the sediment-water interface where Mn-rich porewater diffuses out of the sediment. With increasing age, however, *A. islandica* seems to generate a gradually stronger inhaling water current and takes in a larger proportion of water farther away from the fluffy layer. As demonstrated here, all three studied species can be used as DO archives, though species-specific limitations should be kept in mind.

4.1 Introduction

Severe oxygen deficiency endangers aquatic ecosystems potentially resulting in dead zones. When dissolved oxygen (DO) concentration falls below approx. 2.3 mg/L (≙ 1.6 mL/L or 72 µmol/L; Vaquer-Sunyer and Duarte, 2008; equivalent to approx. 30 % DO saturation; Rabalais et al., 2010) – the transition from normoxic to hypoxic waters –, most invertebrates and fish can no longer properly respire (Herreid, 1980). As a consequence, diversity decreases, food webs collapse and biogeochemical cycles change, which in turn can further fuel oxygen depletion (Österblom et al., 2007), eventually until all free oxygen is consumed, and anoxic conditions and dead zones emerge.

As indicated by abundant dark grey and black shale deposits, widespread depletion or absence of DO near the seabed has been a common and recurring phenomenon during Earth history (Tyson and Pearson, 1991; Arthur and Sageman, 1994) and continues to do so. Since the beginning of the 20th century, oxygen-deficiency has significantly expanded and now also threatens nearshore coastal environments (Conley et al., 2009; Carstensen et al., 2014; Fennel and Testa, 2019). Despite extensive research – predominantly in the Baltic Sea, one of the largest marine low-oxygen settings – the mechanisms and ultimate causes of coastal hypoxia are still not well understood, but likely include anthropogenic eutrophication that propelled primary production and increased the flux of organic carbon to the seafloor (Conley et al., 2007; Carstensen et al., 2014). This deficit of knowledge is largely attributed to incomplete instrumental data and lack of suitable high-resolution archives. Whereas DO trends on time-scales of centuries and millennia can be reconstructed from sediment cores (Jokinen et al., 2018), annually and better resolved, temporally well-constrained archives are still scarce. Besides fish otoliths (Limburg et al., 2011) and foraminifera (Groeneveld and Filipsson, 2013), shells of the marine bivalve mollusk, *Arctica islandica* have recently been identified as interannually to seasonally resolved in-situ archives of oxygen deficiency with manganese-to-calcium (Mn/Ca) molar ratios serving as a proxy for DO in the overlying water body (DO measured some decimeters away from the seafloor) (Schöne et al., 2021).

Due to its long lifespan and presence of annual growth patterns (Jones, 1980; Butler et al., 2013; Schöne, 2013) the ocean quahog, *A. islandica* can potentially serve as an accurately dated DO archive spanning several decades or centuries. The DO history may be assessed on even longer time-scales if Mn/Ca_{shell} data of live-caught specimens from museum collections were used and/or crossdated specimens were studied. For the latter purpose, annual increment width series of specimens with overlapping lifespan are combined based on similar growth patterns to form longer chronologies that cover many generations of bivalves (Butler et al., 2013;

Black et al., 2019). Its tolerance against severe oxygen depletion (Theede et al., 1969; Taylor, 1976; Oeschger, 1990; Oeschger and Storey, 1993; Strahl et al., 2011) makes the ocean quahog an ideal DO archive. However, its biogeographic distribution is not uniform in the Baltic Sea (Zettler et al., 2001; Darr et al. 2014). Therefore, it would be extremely useful if different bivalve species could be used interchangeably or alternatively to reconstruct the spatial and temporal development of DO.

Here, we have studied if *Astarte borealis* and *Astarte elliptica* record DO in a similar way as *A. islandica* and thus serve as alternative DO archives. According to existing laboratory experiments, *Astarte* spp. is slightly more tolerant against low DO than *A. islandica* (Theede, 1973; Dries and Theede, 1974) and more widely distributed in the Baltic Sea (Darr et al., 2014). Specimens of all three species were recently collected alive in the same region of the Fehmarn Belt, Baltic Sea. Data obtained herein on *A. islandica* (ontogenetic age range: 9 – 41 yrs; water depth: 21 m; DO range: 2.8 – 9.4 mL/L; temporal coverage: 1983 – 2020) supplemented such of a previous study of the same species from Mecklenburg Bight (7 – 19 yrs; 25 m; 1.8 – 8.9 mL/L; 1987 – 2001) (Table 4.1). Particular attention was paid to the relationship between DO and Mn/Ca_{shell}, ontogenetic Mn/Ca_{shell} trends, lifespan, timing and rate of seasonal shell growth and clarity of growth patterns necessary to temporally align the chemical data measured in the shells. Results of this study will be of great relevance to reconstruct multiregional DO trends through time in the Baltic Sea. Given the broad biogeographic distribution of *A. elliptica* (Abbott and Morris, 1995) and *A. borealis* (Zettler, 2001) outside the Baltic Sea, similar studies on water oxygenation trends can likely be conducted at many other localities.

4.2 Materials and methods

Five specimens of *A. islandica* and three specimens of each, *A. elliptica* and *A. borealis*, were collected alive at Fehmarn Belt near the halocline on 29 June 2020 with van Veen grabs during cruise EMB239 with the R/V Elisabeth Mann Borgese (Table 4.1; Fig. 4.1). *A. islandica* and *A. elliptica* co-occurred in 21 m (median grain size: 114 µm, organic content: 1.65 wt%), and *A. borealis* came from 18 m water depth (median grain size: 961 µm, organic content: 2.43 wt%) (Fig. 4.1, Table 4.1). Immediately after collection, specimens were sacrificed in formalin and then preserved in 70 vol% ethanol. In the laboratory, soft parts were removed with a knife and empty shells washed with soap and water. Data obtained herein were combined with such of a previous study on live-collected *A. islandica* specimens from Mecklenburg Bight (Fig. 4.1; for details see Schöne et al., 2021). Relevant data of the bivalves and the physical environmental parameters at both study regions are provided in Table 4.1.

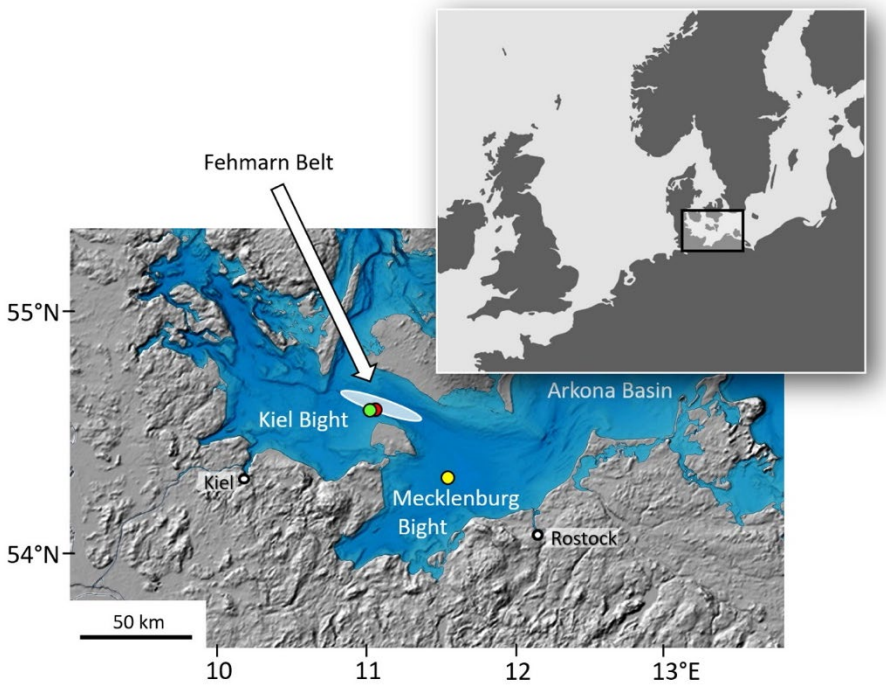

Figure 4.1 Map showing sample localities in the Bay of Mecklenburg (yellow circle: St12, 54°18′59.50″N, 011°33′00.00″ E, 25 m water depth) and Fehmarn Belt (green circle: FBR36, 54°35'52.80"N, 010°51'28.80"E, 21 m; red circle: FBR06, 54°37'01.20"N, 011°00'36.00"E, 18 m). White oval denotes area where instrumental records came from. Map sources: inlet (upper right) modified after http://www.mygeo.info; bathymetry map modified after http://data.bshc.pro (Baltic Sea Bathymetry Database); last access: 27 Oct. 2021.

Table 4.1 List of bivalves from the Baltic Sea used in the present study along with basic environmental data (monthly temperature, T, salinity, S, dissolved oxygen concentration, DO conc., and DO saturation, DO sat.). All specimens were collected alive (Fehmarn Belt: 29 June 2020; Mecklenburg Bight: 25 October 2001). Last character of ID denotes left (L) or right (R) valve. Isotope samples in parentheses denote number of samples used to construct the seasonal age model. For details on the age model of specimens from Mecklenburg Bight, see Schöne et al. (2021).

Specimen ID	Taxon	Ontogenetic age (yr)	#$\delta^{18}O$ samples	LA-ICP-MS: #spots, cal. yrs, ontog. yrs
Fehmarn Belt (FBR36): 54°18′59.50″N, 011°33′00.00″ E; 21m;				
1983-2020: T: -0.4–14.6°C; S: 10.9–26.5; DO conc.: 3.0–9.4 mL/L; DO sat.: 32.1–77.9 %				
MLZ-FBR36-A4L	*Arctica islandica*	41		480, 1983–2020, 4–41
MLZ-FBR36-A5R	*Arctica islandica*	38	79 (43)	
MLZ-FBR36-A6L	*Arctica islandica*	9		207, 2015–2020, 4–9
MLZ-FBR36-A7L	*Arctica islandica*	10		202, 2012–2020, 3–10
MLZ-FBR36-A15L	*Arctica islandica*	10		393, 2012–2020, 3–10
MLZ-FBR36-A16L	*Arctica islandica*	21		441, 2005–2020, 6–21
MLZ-FBR36-A8L	*Astarte elliptica*	21	180 (70)	170, 2004–2020, 5–20
MLZ-FBR36-A9L	*Astarte elliptica*	27		134, 2003–2015, 10–21
MLZ-FBR36-A10L	*Astarte elliptica*	30		197, 1997–2015, 7–24
Fehmarn Belt (FBR06): 54°37'01.20"N, 011°00'36.00"E; 18m;				
1978-2019: T: -0.4–16.2°C; S: 10.9–26.8; DO conc.: 2.8–9.2 mL/L; DO sat.: 28.3–80.2 %				
MLZ-FBR06-A1L	*Astarte borealis*	50		210, 1978–2019, 8–49
MLZ-FBR06-A2L	*Astarte borealis*	52		163, 1981–2019, 13–51
MLZ-FBR06-A3L	*Astarte borealis*	47	175 (31)	190, 1981–2018, 8–45
Mecklenburg Bight (St12): 54°18′59.50″N, 011°33′00.00″ E; 25 m;				
T: -0.5–16.9°C; S: 14.9–28.9; DO conc.: 2.0–8.9 mL/L; DO sat.: 24.5–77.1 %				
MLZ-St12-A4R	*Arctica islandica*	19		329, 1987–2001, 5–19
MLZ-St12-A5R	*Arctica islandica*	15		326, 1991–2001, 5–15
MLZ-St12-A6R	*Arctica islandica*	14		373, 1991–2001, 4–14
MLZ-St12-A7L	*Arctica islandica*	7		183, 1997–2001, 3–7
MLZ-St12-A9R	*Arctica islandica*	8		151, 1998–2001, 5–8

4.2.1 Sample preparation

Samples were prepared according to standard sclerochronological techniques described recently in Schöne et al. (2021). Briefly, covered with a protective layer of metal epoxy resin, shells were cut along the axis of maximum growth with a low-speed saw at 175 to 225 rpm and a water-cooled 0.4 mm thick, diamond-coated saw blade (low diamond concentration blade, Buehler IsoMet 15LC). From that axis, two ca. 3 mm-thick slabs were cut, which were affixed (with metal epoxy) to glass slides with the cutting surfaces facing upward. These surfaces were then ground on F800 and F1200 grit SiC powder and highly polished with 1 µm Al_2O_3 suspension on a Buhler Microfloc cloth. After each step, samples were ultrasonically rinsed with tap water and then air-dried.

4.2.2 Growth pattern analysis

For shell growth pattern analysis, one polished section of each specimen was immersed in Mutvei's solution for 17 min under constant stirring at 37 to 40 °C, then gently rinsed in deionized water and air-dried under the fume hood for ca. six hours (Schöne et al., 2005a). Mutvei-stained sections were viewed under a binocular microscope equipped with sectoral (= one-quarter) darkfield ring-light illumination (Schott VisiLED MC1000) and photographed with a Canon EOS 600D digital camera (Fig. 4.2A upper panel + B). In addition, the other, unstained polished slab was studied under brightfield illumination (Fig. 4.2A lower panel + C) as well as under a stereomicroscope (Zeiss Axio Imager.A1m) with circular polarized reflected light in conjunction with a differential interference contrast prism (henceforth "C-DIC method"; Danz & Gretscher, 2004) (Supplements). The C-DIC method was particularly useful to cross-verify annual growth patterns in *Astarte* spp.

Growth pattern analyses fulfilled two tasks. They were used to determine the ontogenetic ages of the studies specimens (Table 4.1) and to assign calendar years to annual increments (= portions between annual growth lines). Annual increment widths (Supplements) were measured to the nearest approx. 10 µm using the in-house software package Panopea (© Peinl and Schöne). These data were compared to weighted element-to-Ca averages (i.e., regression analyses were conducted) to reveal potential growth rate-related kinetic effects. In *A. elliptica* intra-annual growth patterns were visible after immersion in Mutvei's solution (Fig. 4.2B). The changing widths of intra-annual growth increments agreed at large with changing seasonal growth rates inferred from the oxygen isotope alignment approach (see below). Mutvei-stained sections also facilitated the study of the geometry of internal shell growth patterns (e.g., Fig. 4.2B) which is crucial to understand time-averaging of samples taken from the shells and to construct more precise seasonally resolved chemical chronologies.

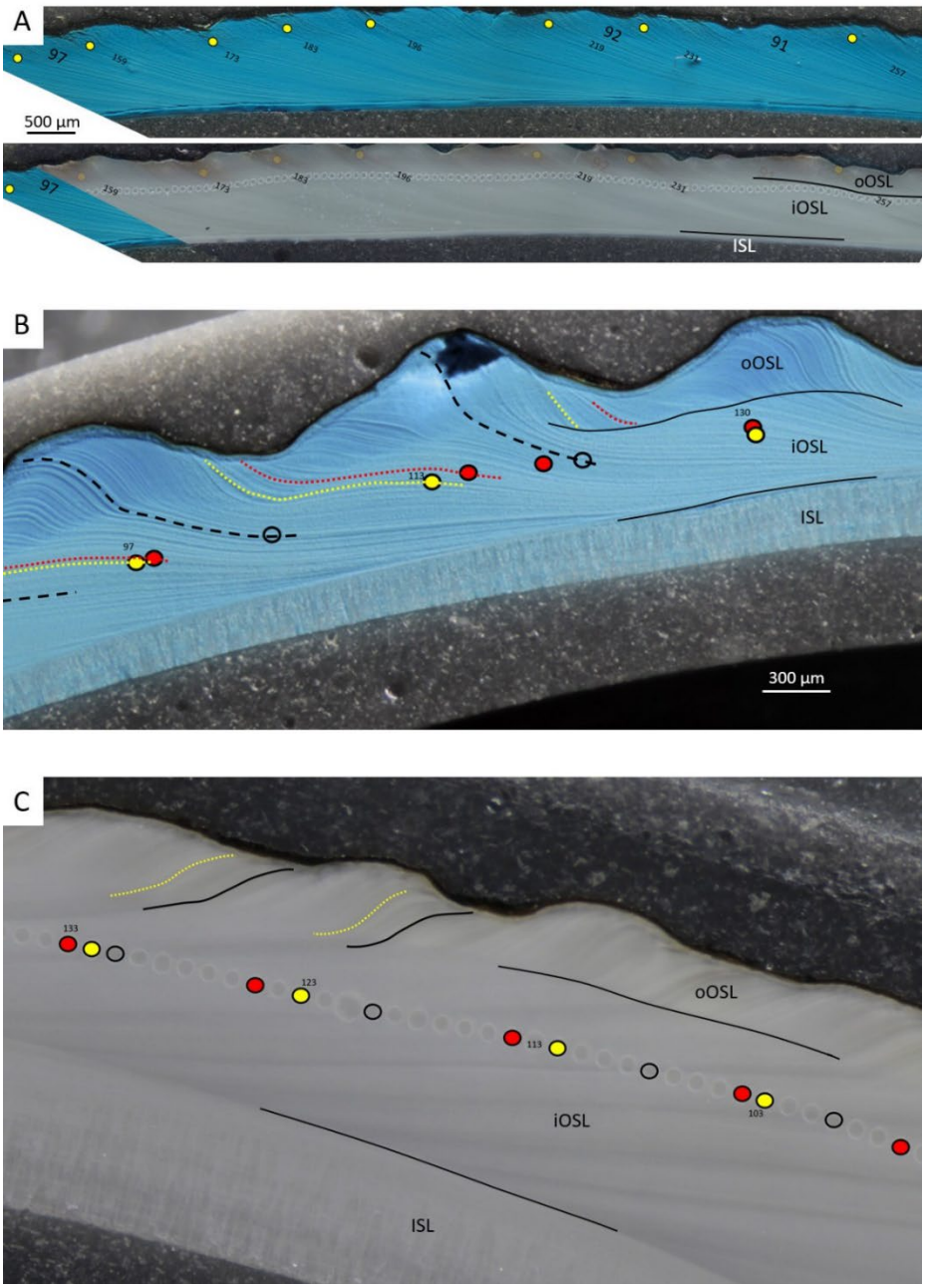

Figure 4.2 Growth patterns in shells of *Arctica islandica* (A, specimen MLZ-FBR36-A4L), *Astarte elliptica* (B, MLZ-FBR36-A9L) and *Astarte borealis* (C, MLZ-FBR06-A1L). (**A, upper panel + B**) = sectoral darkfield illumination; (**A, lower panel and C**) = brightfield illumination (with partly numbered LA-ICP-MS spots). Open yellow circles and lines indicate seasonal magnesium peaks, red circles (LA-ICP-MS spots) and lines stand for manganese peaks, and black circles in *Astarte* spp. denote Mn minima. Bold numbers in **A** = calendar years (e.g., "97" = 1997). In *A. islandica*, only one annual growth line is developed which forms in late fall and is associated with the seasonal Mg peak. In Mutvei-stained sections (**A upper panel**), the annual growth lines were often difficult distinguish from disturbance lines. In such cases, comparison with polished cross-sections (**A lower panel**) were a great help, because distinct brown annual bands were occasionally developed with the Mg maxima occurring in their center. In *Astarte* spp., two annual growth lines can be distinguished which delimit a dark band (dark blue after immersion in Mutvei's solution, **B**, and grey in polished sections, **C**), i.e., a faint, Mg-rich line at the beginning and a distinct Mg-depleted line at the end. The dark band consisted of a series of very narrow intra-annual growth lines indicating slow winter growth. Intra-annual growth lines approached the outer shell surface at an increasingly steep angle toward the end of the growth band. With the beginning of the new growing season (lighter blue or grey in **B** and **C**, respectively), the angle became much shallower indicating fast shell growth. Faint black lines were used show the boundary between the different shell layers, i.e., the outer and inner portions of the

outer shell layer (oOSL, iOSL) and inner shell layer (ISL). Note that the ISL in *A. islandica* is almost completely dissolved (**A**), whereas both astartids show thick inner shell layers. In *A. elliptica*, the spiral rides of the outer shell sculpture (approx. one per year) are mirrored in the wavy boundary between the two sublayers of the OSL (**B**), whereas the boundary between the oOSL and iOSL in *A. borealis* is much less wavy (**C**).

4.2.3 Shell oxygen isotope analysis

As described above, shell oxygen isotope data were used to temporally contextualize the growth record, determine the timing of growth line formation, and ascertain the changing rate of seasonal shell growth. Since *A. islandica* from the Baltic Sea tends to be very thin-shelled compared to conspecific specimens from well-oxygenated and fully marine sites (e.g., Arntz and Weber, 1970), and the growth patterns of *A. elliptica* exhibit strong undulations, sampling in these two species was completed on the outer shell surface of specimens MLZ-FBR36-A5 (*A. islandica*; N=79) and MLZ-FBR36-A8 (*A. elliptica*; N=72). In *A. borealis* (MLZ-FBR06-A3), aragonite powder samples (N=173) were micromilled from cross-sections (for a graphic representation of the sampling methods see Peharda et al., 2019). Prior to sampling, the periostracum (and adhering manganese oxides) and the outermost portion of the external shell surface were physically removed with grinding paper (P320 to P800) and/or a glass fiber brush. Aragonite powder samples were obtained by hand from the outer shell surface using a conical SiC drill bit operated in a milling device that was firmly attached to a binocular microscope. In case of surface milling, approx. 1 cm long sample swaths (approx. 100 µm wide and 20 µm deep) were taken at nearly equidistant intervals parallel to the growth patterns.

Each milling step yielded approx. 30 to 70 µg of aragonite powder. Samples were reacted with water-free phosphoric acid for two hours in He-flushed 12 mL borosilicate exetainers at 72 °C. CO_2 gas in the headspace was measured in a Thermo Fisher MAT 253 continuous flow – isotope ratio mass spectrometer coupled to a GasBench II. Stable isotope ratios were calibrated against an NBS-19 calibrated Carrara Marble ($\delta^{18}O$ = −1.91 ‰) distributed by IVA Analysentechnik GmbH & Co. KG. Results are given in per mil (‰) relative to the Vienna Pee Dee Belemnite isotope scale. The 1σ long-term accuracy based on blindly measured NBS-19 samples (N = 421) is better than 0.04 ‰ for $\delta^{18}O$. Differences in acid fractionation factors of the reference material (calcite) and shells (aragonite) remained unconsidered, because the data were used in conjunction with the paleothermometry equation by Grossman & Ku (1986) which likewise did not consider these acid fractionation factors (for more detailed explanation see methods section in Füllenbach et al., 2015: section 3.4).

4.2.4 In-situ chemical analysis: LA-ICP-MS

The chemical composition of the shells was measured in the remaining polished slabs by means of laser ablation – inductively coupled plasma – mass spectrometry (LA-ICP-MS) in spot mode. In this paper, the focus was placed on manganese (Mn), and reference was given to barium (Ba) and magnesium (Mg) values. For some additional elements (Li, B, Na, K, Sr), the reader is referred to Supplements. Analyses were completed with a 193 nm ArF Excimer laser (ESI NWR193) coupled to an Agilent 7500ce quadrupole ICP-MS. Spots with a diameter of 55 µm and a midpoint spacing of 85 µm were placed along the ventral margins of the shells, within the inner portion of the outer shell layer. Laser repetition rate was 10 Hz. The laser energy on the samples attained approx. 3 J/cm^2. Each analysis consisted of 15 s of background, 30 s of ablation, and 20 s of washout time. Accuracy and precision of the data were assessed through comparison with reference materials USGS MACS-3 and BCR-2G as well as JCt-1 as quality control materials (QCMs) (Supplements). NIST SRM 610 and 612 were used as calibration materials. Preferred values for calibration and reference materials were taken from the GeoReM database (http://georem.mpch-mainz.gwdg.de/, application version 30; last access: 15 May 2021; Jochum et al., 2005, 2011). ^{43}Ca was used as the internal standard. The time-resolved signals were processed using LAtools (Branson et al., 2019). To compute molar element-to-Ca ratios, a Ca concentration of 380,000 µg/g was assumed following Marali et al. (2017a).

To compare the shell element chemical data of different specimens or species with each other, or compare the shell element chemistry with environmental data, a set of mathematical transformations is required which are described in the following two sections. Firstly, it needs to be ensured that each data point represents the same amount of time and that a calendar axis is added to the data (section 2.5). Secondly, trends related to ontogenetic age or growth rate as well as vital effects controlling the incorporation of elements into the shell need to be mathematically eliminated as effectively as possible (section 2.6).

4.2.5 Seasonal shell growth models and mathematical resampling

The timing and rate of shell growth typically varies through ontogeny as well as between specimens, species and localities. Equally sized samples taken from the shells thus represent different amounts of time. Likewise, the time interval between consecutive samples differs, even if sampling was completed at the same spacing. To enable a direct comparison of the chemical data, mathematical resampling is crucially required (Schöne, 2008; Hallmann et al., 2011). It will adjust the data to a common resolution. The first step is to properly align the growth record based on the species-specific seasonal age model. Once the precise date of the

center of each sample (e.g., LA spot) is known, missing data between samples can be obtained by linear interpolation. The resulting curve is then resampled to obtain an uninterrupted artificial time-series with daily resolution, which can be used, for instance, to compute monthly or annual averages.

Here, the species-specific and locality-specific timing and rate of seasonal shell growth was determined with the stable oxygen isotope method described by Schöne et al. (2007). For this purpose, measured $\delta^{18}O_{shell}$ values were arranged in consecutive order until the best fit was achieved with the shape of the predicted shell oxygen isotope curve (pseudo-$\delta^{18}O_{shell}$ curve). The latter was computed from instrumental temperature, T, and $\delta^{18}O_{water}$ values using the paleothermometry equation by Grossman and Ku (1986; with a PDB-SMOW scale correction of –0.27 ‰ following Gonfiantini et al., 1995) solved for predicted $\delta^{18}O_{shell}$:

(1) $$\delta^{18}O_{shell\ predicted} = \frac{20.60 + 4.34 \times (\delta^{18}O_{water} - 0.27) - T}{4.34}.$$

In the absence of direct measurements of $\delta^{18}O_{water}$, respective values were estimated from instrumental salinity data, S, using the local freshwater mixing line (Schöne et al., 2005b):

(2) $$\delta^{18}O_{water} = 0.30 \times S - 10.36.$$

Based on the known distances and time intervals between the isotope samples, daily growth curves were computed. For comparison with each other, the growth curves were normalized. Then, the seasonal growth curves of several years for which at least eight samples were available (*A. islandica* MLZ-FBR36-A5: 4 seasonal growth curves; *A. elliptica* MLZ-FBSCR36-A8: 7 curves; *A. borealis* MLZ-FBR06-A3: 4 curves; full data set given in Supplements) were arithmetically averaged to obtain species-specific seasonal growth models (Fig. 4.3). Cumulative (normalized) growth curves formed the basis to add a time axis to the LA-ICP-MS data. Based on the relative position of a LA-ICP-MS spot within the annual growth increment (center of the annual growth line = zero), the cumulative growth curve provided the corresponding calendar date.

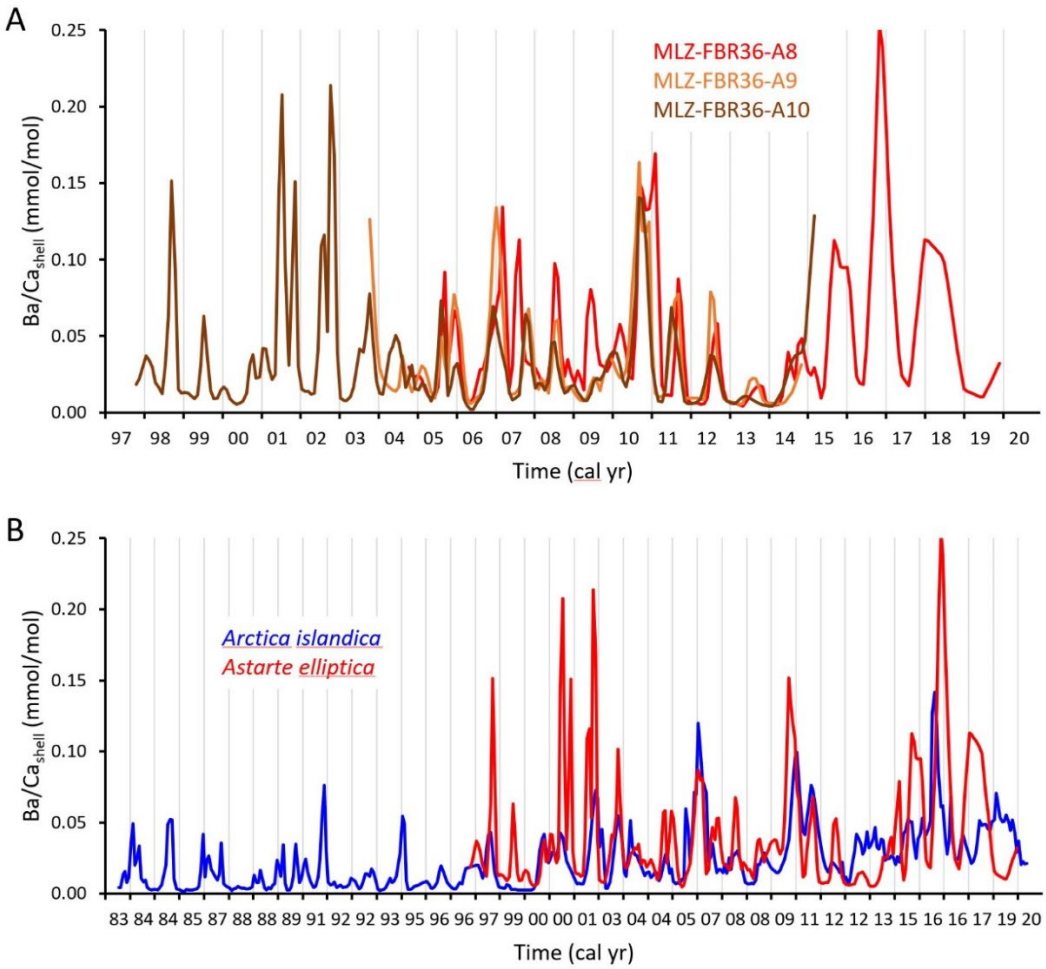

Figure 4.3 Monthly Ba/Ca$_{shell}$ chronologies validate the proper temporal alignment of the shell data. Chronologies show a strong running similarity between specimens of the same species (example from *A. elliptica*) (**A**) as well as across species boundaries (**B**). Chronologies in **B** represent the average of five specimens of *A. islandica* and three specimens of *A. elliptica*, respectively.

4.2.6 Detrending of Mn/Ca$_{shell}$ data

For calibration and comparison with environmental data, ontogenetic age-related trends (Fig. 4.5) were mathematically removed from each Mn/Ca$_{shell}$ series. For this purpose, the monthly Mn/Ca$_{shell}$ data of each specimen were first plotted against ontogenetic age and the decline through life estimated with exponential functions. Following our previous study (Schöne et al., 2021), instead of producing dimensionless Mn/Ca$_{shell}$ data, the Mn/Ca$_{shell}$ level at the intercept (age zero) was set as an anchor point, and the monthly Mn/Ca$_{shell}$ values of later stages of life increased by the difference (offset) between this anchor point and the predicted Mn/Ca$_{shell}$ value at the respective stage of life. Note, that we also tested a species-specific detrending approach as in Schöne et al. (2021), by which the average ontogenetic Mn/Ca$_{shell}$ trend computed from all conspecific specimens was used to detrend the individual chronologies, but the resulting

Mn/Ca_{shell} data were linked less strongly to DO than by employing the age trend of each individual specimen.

To account for growth rate-related effects, annual (= growing season averages) Mn/Ca_{shell} data were plotted against annual increment widths. From such crossplots, species-specific linear regression models were computed. As in the detrending technique described earlier, an anchor point was selected (for each species), here, the broadest increment, and the difference between this anchor point and the predicted Mn/Ca_{shell} value for the respective annual increment added to its monthly Mn/Ca_{shell} values. Note that through this treatment, the Mn/Ca_{shell} of slower growing shell portions were artificially lifted to higher levels as if no Mn/Ca_{shell} decline had occurred in later, slower growing stages of life. In case of *A. islandica*, new data from Fehmarn Belt were combined with such from our previous study at Mecklenburg Bight (Schöne et al., 2021). We refrained from adjusting the monthly data to monthly growth rate differences, because intra-annual increment curves were not available and the seasonal growth models were not deemed precise enough for this purpose.

To consider both Mg/Ca_{shell} and growth rate-related effects on shell manganese content, raw Mn/Ca_{shell} data were first plotted against Mg/Ca_{shell} values. The relationship between the two elements was estimated with species-specific exponential equations. The Mn/Ca_{shell} value at the lowest Mg/Ca_{shell} value (of each species) was chosen as the anchor point and the offset from the anchor point to the predicted value added to the Mn/Ca_{shell} value. Subsequently, the data were corrected for growth rate-related trends following the description above.

As in our previous study at the Bay of Mecklenburg (Schöne et al., 2021), only the seasonal Mn/Ca_{shell} extremes (this time: species averages) were compared to respective seasonal DO minima and maxima. This approach predominantly accounts for the incompleteness of instrumental data, in particular DO. Research cruises (during which respective measurements were completed) were often conducted during times of the occurrence of seasonal hypoxia or close to the time of the year where highest oxygenation occurred. Therefore, the seasonal DO extremes were most reliably recorded. The complete dataset (monthly pairs of Mn/Ca_{shell} vs. DO) is provided in the Supplements.

4.2.7 Instrumental data

Instrumental data (temperature, salinity, DO concentration) were obtained from the Leibniz Institute for Baltic Sea Research Warnemünde, IOW, from their website at https://odin2.io-warnemuende.de/ as well as the Baltic Nest Institute from their website at http://nest.su.se/ (last

access: 25 March 2021) for stations and water depths in the vicinity of the shell collection sites (Fig. 4.1). It needs to be pointed out that the instrumental data were not conducted at the seafloor where the bivalves dwelled and inhaled water, but some decimeters away from the seafloor. Here, the Mn/Ca and DO values of the water likely differed from such directly at the sediment-water interface where the bivalves lived, but were co-varied with such. This piece of information needs to be kept in mind during data interpretation. Since the environmental data were temporally incomplete, linear interpolation was applied to fill gaps. The resulting curves were then resampled at daily resolution. From these values, monthly and annual averages were computed for comparison with the chemical data of the shells. To construct the seasonal shell growth model, long-term daily averages were computed. Due to insufficient instrumental temperature and salinity data required to compute DO saturation data from DO concentration values (Benson and Krause, 1984), the latter were reported instead. As demonstrated in Schöne et al. (2021), DO concentration and DO saturation curves are largely similar in this region of the Baltic Sea justifying the comparison of Mn/Ca_{shell} with DO concentration.

4.3 Results

4.3.1 Lifespan and annual shell growth

In all three studied species, annual growth lines were discernable with sectoral darkfield illumination after immersion in Mutvei's solution (Fig. 4.2). The old-grown *A. islandica* specimen MLZ-FBR-A4 also showed distinct brown annual bands and lines in the polished ventral margin when viewed with brightfield illumination (Fig. 4.2A, lower panel). Specifically in younger ocean quahogs, the annual growth patterns were often more clearly developed in the hinge portions (condensed growth record) than the ventral margin, and used to validate the ventral margin growth record. The occurrence of disturbance lines (reflecting non-periodic interruptions or slow-down of shell growth) in the ocean quahogs made the recognition of annual growth lines a challenging task. As long as the cutting axis was exactly perpendicular to the growth lines, the C-DIC method provided an alternative means to detect annual growth lines in polished sections (Supplements). The annual nature of the growth patterns was confirmed by periodic Mg/Ca_{shell} and $\delta^{18}O_{shell}$ oscillations which were also reported from numerous other bivalve species (Jones and Quitmyer, 1996; Kubota et al., 2017; Hausmann et al., 2019) including *A. islandica* (Schöne, 2013; Shirai et al., 2014). The presence and proper recognition of annual growth patterns was further evidenced by coherent Ba/Ca_{shell} chronologies, both among conspecific specimens and across species boundaries (Fig. 4.3). Ba/Ca_{shell} typically agrees well among specimens from the same site (Gillikin et al., 2006) and thus serves as a crossdating tool (Marali et al., 2017b), although the environmental drivers of Ba/Ca_{shell} change in *A. islandica* remain largely unknown.

In contrast to *A. islandica*, which formed just one annual growth line per year (Fig. 4.2A), after immersion in Mutvei's solution, both *Astarte* species showed two growth lines per year delimiting a dark blue-stained growth band (Fig. 4.2B+C). The first, faint line occurred at the beginning of this growth band and was associated with the seasonal Mg/Ca_{shell} maximum, whereas a second, stronger growth line was observed at the end of the dark blue band and associated with the seasonal Mg/Ca_{shell} minimum. According to annual growth pattern analysis, the ontogenetic ages ranged between 9 and 52 years (Table 4.1; respective annual counts were done in the ventral margins supported by data of the hinges). *A. borealis* attained the longest lifespan, followed by *A. islandica* (maximum of 41 years) and *A. elliptica* (27 years).

Compared to their sizes, the shells of *A. islandica* were notably thin. For example, specimen MLZ-FBR36-A4 measured 6 cm in height, but the shell was barely 1 mm thick (measured half way between the hinge and the ventral margin; Fig. 4.2A). As shown in Figure

4.2A, the inner shell layer was extremely thin and showed signs of erosion. Relative to their overall size, both *Astarte* species, however, had thicker shells (MLZ-FBR36-A9L: 2.1 cm height; 1.2 mm thickness measured half way between the hinge and ventral margin; Fig. 4.2B+C).

4.3.2 Timing and rate of seasonal shell growth

As revealed by the stable oxygen isotope alignment technique, the timing and rate of seasonal shell growth at Fehmarn Belt differed slightly among the three studied species (Fig. 4.4). *A. islandica* mainly grew shell between December and August of the following year. Growth was retarded during the remainder of the growing season. The annual growth line (Mg-rich) formed between mid-October and mid-November (Fig. 4.2A, 4.4A), i.e., ca. two months after the seasonal temperature maximum, which is largely in agreement with previous observations (Schöne, 2013). For comparison, the seasonal growth model from Mecklenburg Bight is also depicted in Figure 4.4A (pale blue) demonstrating that the growth line formation occurred several weeks earlier than at Fehmarn Belt. In *A. elliptica* and *A. borealis*, a Mg-rich growth line (compare Fig. 4.2B+C) formed nearly contemporaneously with that in the ocean quahog, i.e., between mid-October and end of November (Fig. 4.4B+C). A second growth line (compare Fig. 4.2B+C) was associated with the seasonal Mg minimum and laid down in January/February, i.e., near the end of a slow growth period (Fig. 4.4B+C). The latter was visually expressed as a dark grey (or dark blue-stained) growth band (compare Fig. 4.2B+C). Previous studies likewise concluded the dark growth band in these two astartids formed during the cold season (Trutschler and Samtleben, 1988; Moss et al., 2021). The cumulative growth curves of the studied species were not particularly sinusoidally shaped (Fig. 4.4), reflecting that shell growth rates did not vary a lot throughout the year. Accordingly, weighted monthly (annual) averages of trace element data do not deviate significantly from arithmetic averages.

A. elliptica was the only species that revealed intra-annual growth patterns clearly enough to be studied (Fig. 4.2B). The $\delta^{18}O_{shell}$-based reconstruction of the seasonal growth curve (Fig. 4.4B) of this species compared well to the changing width of the intra-annual growth increments (Fig. 4.2B). Narrowest intra-annual increments occurred between the Mg-rich and the Mg-poor growth lines, i.e., within the dark blue-stained growth band. The growth lines in this shell portion approached the outer shell surface at a very steep angle. Thereafter, the shells were stained lighter blue by Mutvei's solution (= less organics, relatively more $CaCO_3$), the intra-annual increments broadened and the angle between intra-annual growth lines and the shell surface decreased reflecting faster shell growth (compare Fig. 4.2B). Since the time

represented by intra-annual growth increments remains unresolved and the intra-annual growth lines could not always be unequivocally identified, the intra-annual increment widths were not measured. Noteworthy, the striking sculpture of the outer shell surface of *A. elliptica* (compare Fig. 4.2B) provided an approximate estimate of the ontogenetic age of the specimens. In many instances, one spiral ridge formed per year (but see Trutschler and Samtleben, 1988).

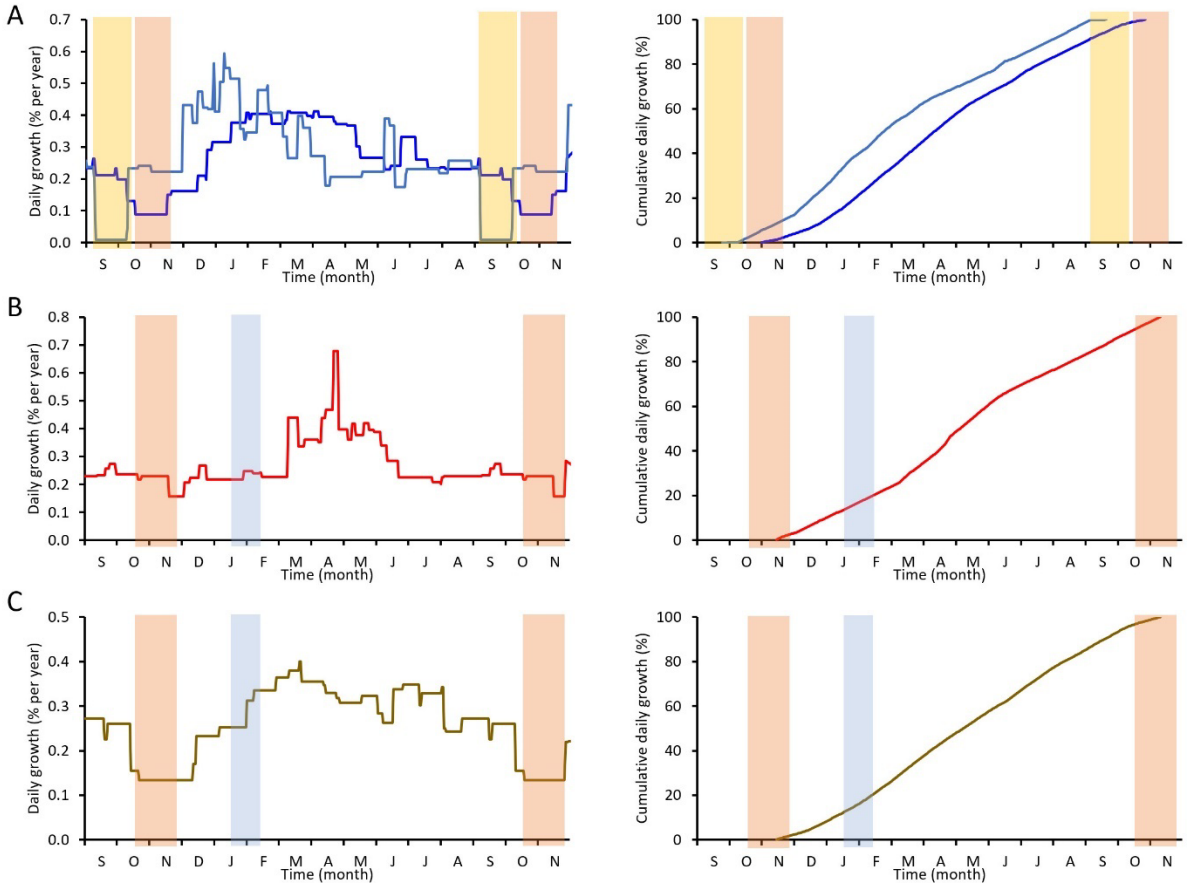

Figure 4.4 Seasonal growth models of the three studied species based on the oxygen isotope alignment technique. Left panel: daily growth rates, right panel: cumulative growth curves. (**A**) *A. islandica*, station FBR36 (Fehmarn Belt) is brilliant blue, St12 (Mecklenburg Bight) in pale blue; (**B**) *A. elliptica*, FBR36; (**C**) *A. borealis*, FBR06 (Fehmarn Belt). Vertical bars represent annual growth lines. Red, yellow = Mg-rich line at Fehmarn Belt and Mecklenburg Bight, respectively; blue = Mg-depleted growth line. In *Astarte* spp., the red and blue lines delimit a grey (or Mutvei blue-stained) growth band. Data from Mecklenburg Bight taken from Schöne et al. (2021).

4.3.3 Mn/Ca$_{shell}$ chronologies

In all three studied species, Mn/Ca$_{shell}$ values showed a non-linear decrease during ontogeny (Fig. 4.5). In *A. islandica* this decrease was associated with a distinct decline in seasonal variability (Fig. 4.5A). For example, this species attained monthly averages of up to approx. 220 µmol/mol and seasonal ranges of nearly 200 µmol/mol between age three and six (months

36 and 72) and lowest values of 1 µmol/mol and seasonal ranges of less than 5 µmol/mol at age 36 (month 432) (Fig. 4.5A). In *A. elliptica*, monthly maxima and seasonal swings during youth (age six to nine, month 72 to 108) remained well below that of the ocean quahog and equaled 120 µmol/mol and up to approx. 80 µmol/mol, respectively, and all-time minima of 5 µmol/mol were reached at age 23 (month 276) (Fig. 4.5A). Similar values were measured in coeval *A. islandica* specimens. *A. borealis* reached highest Mn/Ca_{shell} values of 114 µmol/mol at the age of eight (month 96), ca. 40 µmol/mol at age 23 (month 276), and a minimum of 6 µmol/mol at age 35 (month 420). Highest seasonal amplitudes during youth barely exceeded 45 µmol/mol (Fig. 4.5A). In contrast to Mn/Ca_{shell} values, Mg/Ca_{shell} values increased non-linearly through lifetime (Fig. 4.6). For greater clarity, only one of the longest chronologies of each species is depicted in Figure 4.6. Note strong seasonal oscillations (in sufficiently resolved years) as in Mn/Ca_{shell} chronologies.

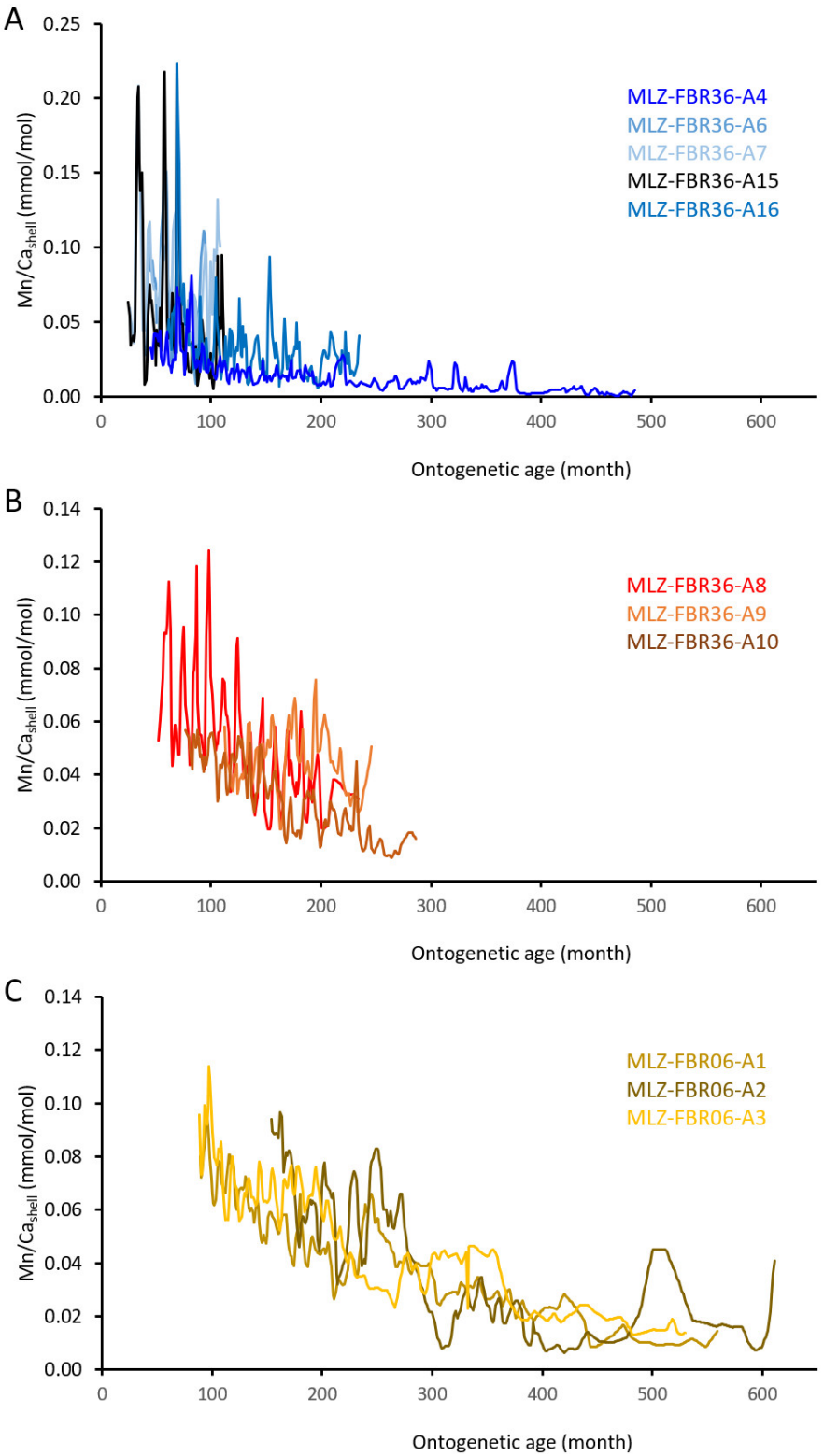

Figure 4.5 Mn/Ca$_{shell}$ chronologies (monthly resolution) reveal striking ontogenetic trends. (**A**) *A. islandica*; (**B**) *A. elliptica*; (**C**) *A. borealis*.

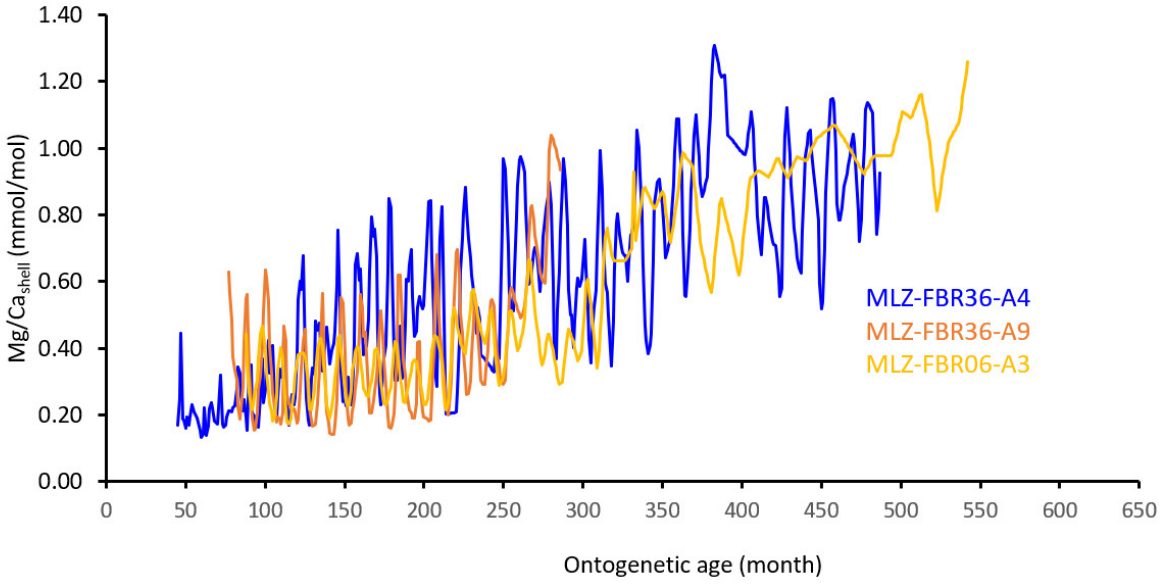

Figure 4.6 Mg/Ca_{shell} chronologies (monthly resolution) of long-lived specimens of *A. islandica* (MLZ-FBR36-A4), *A. elliptica* (MLZ-FBR36-A9) and *A. borealis* (MLZ-FBR06-A3) reveal distinct seasonal oscillations and a gradual increase through lifetime.

When this ontogenetic age-related trend was mathematically removed (and the data plotted against calendar year), the detrended Mn/Ca_{shell} curves not only revealed significant differences in level and seasonal variance between conspecific specimens as well as between species, but also some degree of running similarity (Fig. 4.7). For example, in the 2010s, *A. islandica* specimen A4 barely exceeded 29 µmol/mol, whereas specimen A16 fluctuated between 43 and 131 µmol/mol (Fig. 4.7A). The three remaining specimens from Fehmarn Belt were in closer agreement with each other and ranged between 37 and 280 µmol/mol (Fig. 4.7A). Similar discrepancies in level were observed in the two *Astarte* species (Fig. 4.7B+C). *A. elliptica* specimens A9 and A10 were in close agreement, specifically during 2004 and 2011, while specimen A8 showed, on average, approx. 20 µmol/mol higher values than the other two individuals and more than two to three times larger seasonal amplitudes (Fig. 4.7B). In some years (mid 1990s), monthly Mn/Ca_{shell} values of different *A. borealis* specimens deviated by nearly 750 % (40 µmol/mol), while specimens MLZ-FBR06-A1 and A3 were much closer together (Fig. 4.7C).

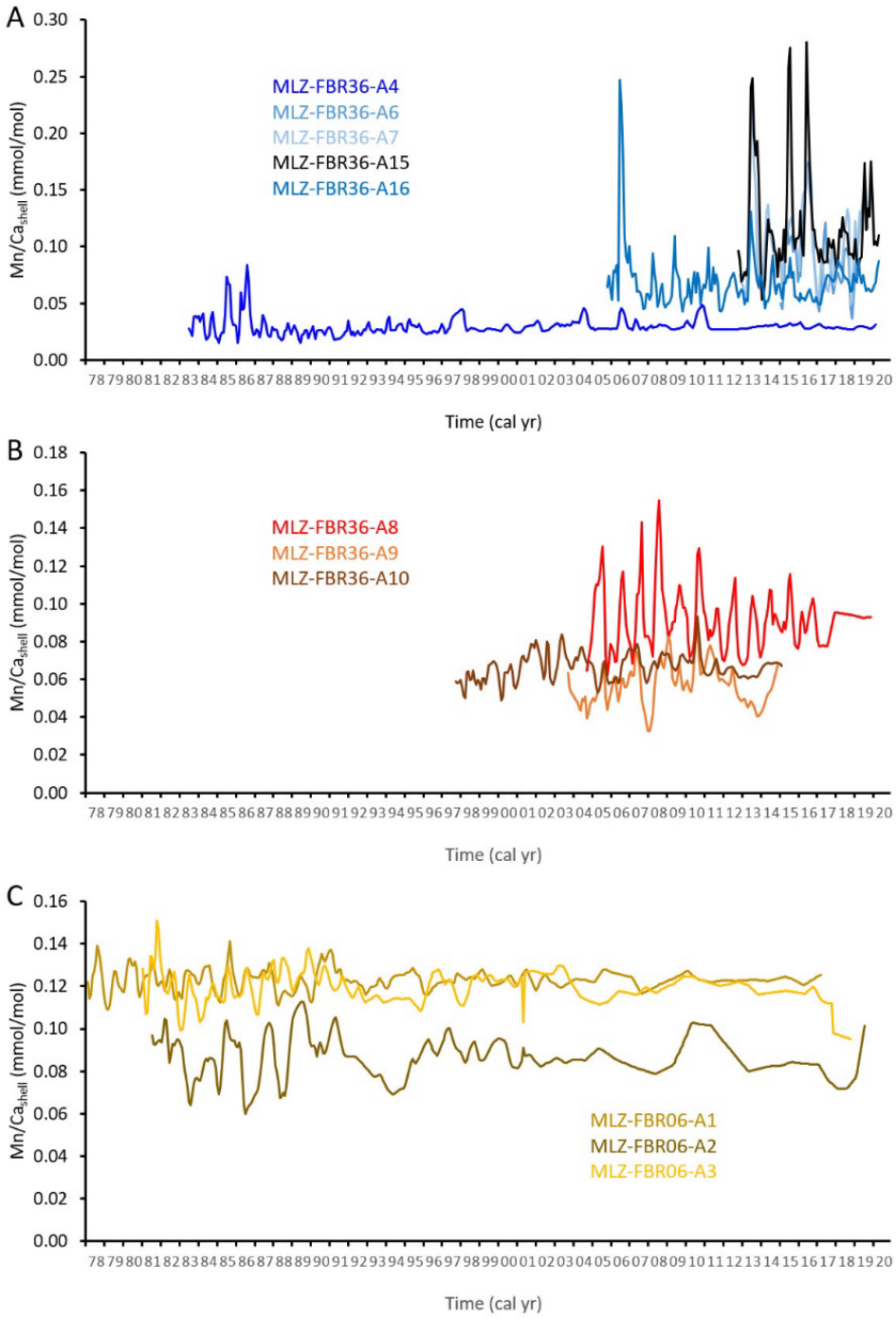

Figure 4.7 After removal of ontogenetic age-related trends (compare Fig. 5), Mn/Ca$_{shell}$ chronologies (monthly resolution) reveal distinct differences between conspecific specimens during the same calendar year. (**A**) *A. islandica*; (**B**) *A. elliptica*; (**C**) *A. borealis*.

Aside from ontogenetic age, Mn/Ca$_{shell}$ data were also statistically significantly ($p < 0.0001$) correlated to annual growth rate (Fig. 4.8A-C) as well as other trace impurities (Supplements) which are governed by vital effects in *A. islandica* and numerous other species (e.g., Lorens and Bender, 1980; Palacios et al., 1994; Wanamaker et al., 2008; Wanamaker and

Gillikin, 2019). The covariation between trace impurities suggests similar physiological effects have controlled the incorporation of these elements into the shell carbonate. In a first step, we targeted the correlation with growth rate. The strongest relationship between growth rate and Mn/Ca_{shell} was found in *A. borealis* ($r = 0.83$; $p < 0.0001$, also for all subsequently given r-values) and some weaker covariation in *A. islandica* ($r = 0.60$) and *A. elliptica* ($r = 0.58$). Once these growth rate-related kinetic effects were mathematically eliminated, the Mn/Ca_{shell} chronologies were in much closer agreement (Fig. 4.9).

Mg/Ca_{shell} molar ratios were chosen for the second detrending step, because they showed the strongest correlation with growth rate-detrended Mn/Ca_{shell} among all measured element-to-Ca ratios (Fig. 4.8D-F). This approach followed previous successful attempts to remove vital effects from a desired element-to-Ca ratio by normalization with another biologically controlled element-to-Ca value. Examples include Mn/Ca vs. Mg/Ca in fish otoliths (Limburg et al., 2011) as well as Li/Ca vs. Sr/Ca or Mg/Ca in foraminifera, cold-water corals and bivalves (Bryan and Marchitto, 2008; Case et al., 2010; Füllenbach et al, 2015; Rollion-Bard and Blamart, 2015). The double detrending approach (annual growth rate and Mg/Ca_{shell}) further constrained the similarity between the Mn/Ca_{shell} curves and shifted them slightly closer together; Supplements) and more importantly, increased the agreement between Mn/Ca_{shell} and DO, as outlined in the following.

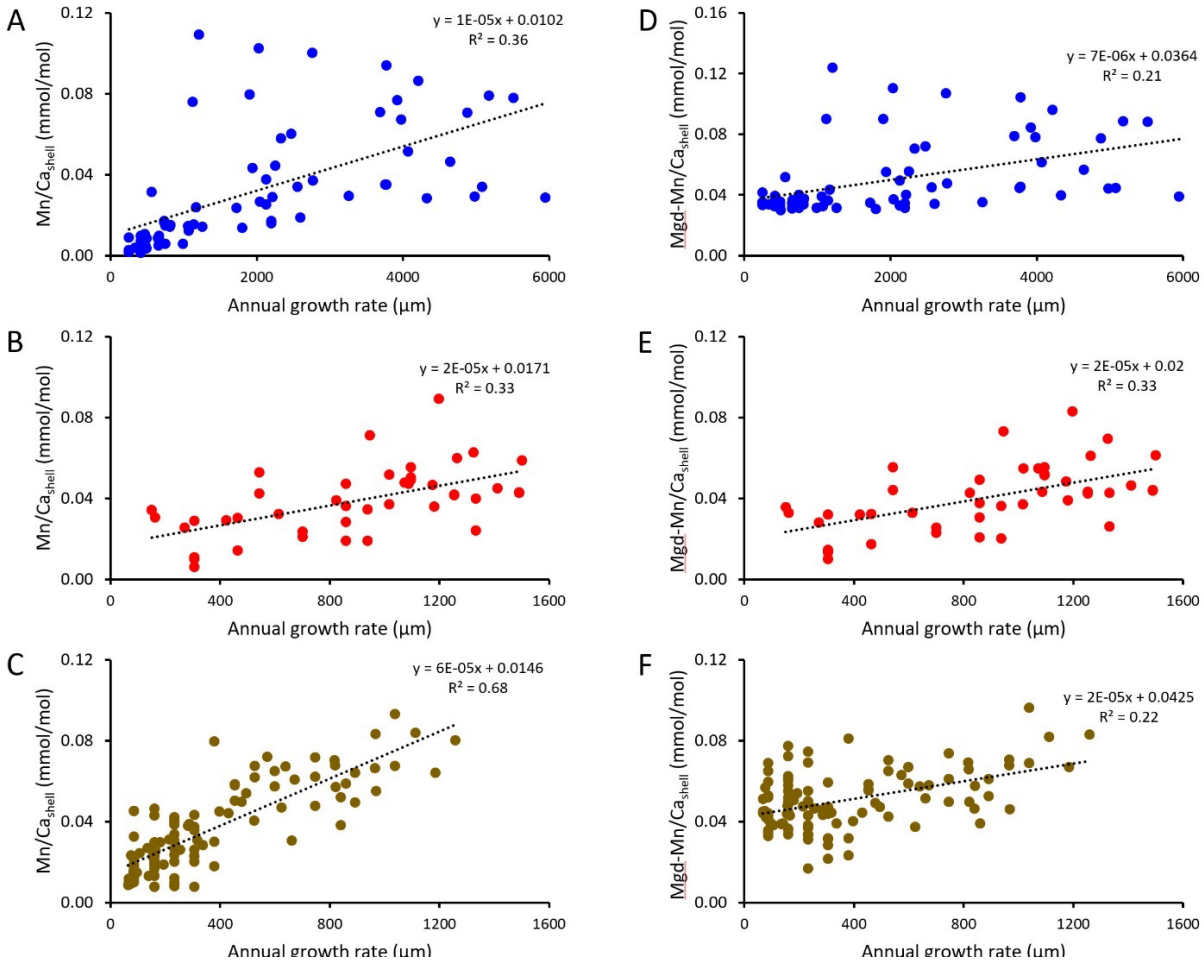

Figure 4.8 Relationship between monthly Mn/Ca_{shell} and annual growth rate before (A-C) and after detrending with Mg/Ca_{shell} data (D-F). (**A+D**) *A. islandica*, station FBR36; (**B+E**) *A. elliptica*, FBR36; (**C+F**) *A. borealis*, FBR06. All *p*-values better than 0.008.

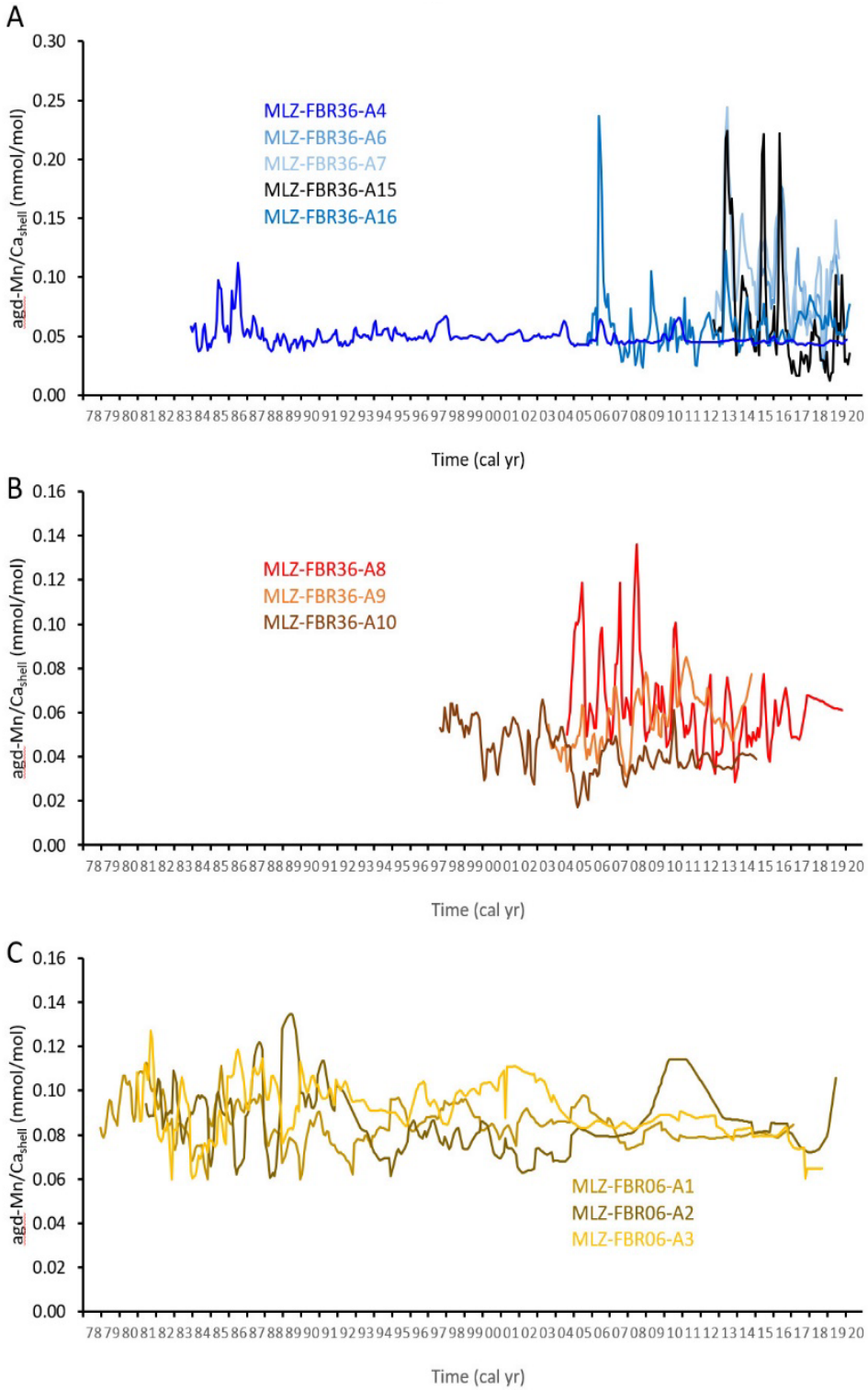

Figure 4.9 After removal of annual growth rate-related trends (compare Fig. 8A-C), Mn/Ca$_{shell}$ chronologies (monthly resolution; agd = annual growth rate detrended) plotted closer together and revealed a larger degree of running similarity. (**A**) *A. islandica*; (**B**) *A. elliptica*; (**C**) *A. borealis*.

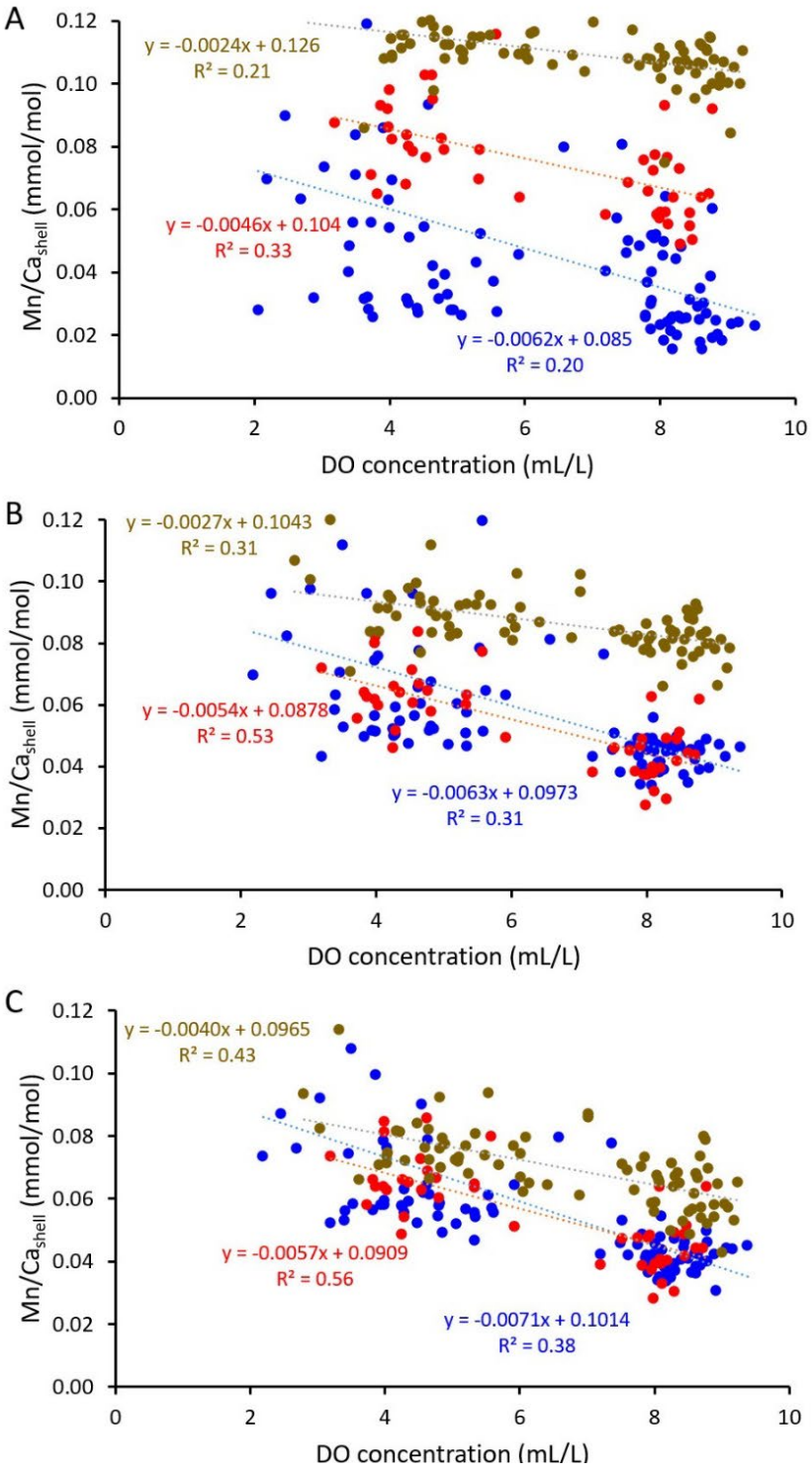

Figure 4.10 Effect of different detrending techniques on the relationship between Mn/Ca_{shell} of bivalves dwelling at seafloor and DO concentration measured some decimeters above seafloor. (**A**) Ontogenetic age trends removed; (**B**) Annual growth rate-detrended and (**C**) double detrended data, i.e., correlation between Mn/Ca_{shell} with annual growth rate and Mg/Ca_{shell} mathematically eliminated. Blue = *A. islandica*; red = *A. elliptica*; brown = *A. borealis*.

4.3.4 Relationship between Mn/Ca_{shell} data and DO concentration

To evaluate the effect of the different detrending methods, Mn/Ca_{shell} data of bivlaves dwelling at the seafloor were compared with DO concentration measured some decimeters above seafloor (Fig. 4.10). Ontogenetic age-detrended Mn/Ca_{shell} data revealed only moderate linear correlations with seasonal DO extremes (R_{adj}^2 range between 0.20 and 0.33), and the relationships varied notably between species, i.e., both the slopes and intercept deviated notably from each other (Fig. 4.10A). Annual growth rate-detrending brought the species-specific regression lines much closer together, specifically that of *A. islandica* and *A. elliptica*, and also resulted in more coherent relationships between Mn/Ca_{shell} and DO concentration (R_{adj}^2 range between 0.31 and 0.53) (Fig. 4.10B). The double-detrending approach further substantiated the correlations (R_{adj}^2 of *A. islandica* = 0.38, *A. elliptica* = 0.56, and *A. borealis* = 0.43) (Fig. 4.10C).

Despite double-detrending, however, the cross-plot of DO vs. Mn/Ca_{shell} of *A. islandica* still exhibited a relatively large scatter which accounted for the relatively low R^2 values (Fig. 4.10C). This largely resulted from a strong non-linear (here: exponential) relationship of Mn/Ca_{shell} with DO in the younger shell portions of specimens MLZ-FBR36-A6, A7, A15 and A16 (Fig. 4.11A). However, data of specimen MLZ-FBR-A4 plotted near the data of all specimens from Mecklenburg Bight (St12), i.e., individual differences rather than locality-specific differences prevailed (Fig. 4.11A). A linear regression was performed on the DO concentrations and the logarithm-transformed Mn/Ca_{shell} data to explore their potential significant relationship provided by *p*-values (see Supplements). For all except two specimens (FBR36-A16 and St12-A7), *p* was better than 0.05. In contrast, after the age of ten, Mn/Ca_{shell} data of all *A. islandica* were strongly linearly correlated to DO ($R_{adj}^2 = 0.56$; $p < 0.0001$) (Fig. 4.11B). More importantly, the regression lines of the three species showed more similar slopes if data from the first nine years of life of the ocean quahog were omitted (*A. islandica*: –39 instead of –71, *A. elliptica*: –57, and *A. borealis*: –40 µmol/mol Mn/Ca_{shell} per mL/L DO) (Fig. 4.11B). When the data of all three species were combined in a single linear regression model, the adjusted R^2 value equaled 0.27, whereas a combination of *A. islandica* and *A. elliptica* provided a much higher adjusted R^2 value of 0.53. The *p*-values of all linear regression analyses were smaller than 0.0001 unless otherwise stated (Supplements).

Tentative predictive models for the three studied species are depicted in Figure 4.12. As above, for *A. islandica* only data from age ten onward were considered. According to these models, Mn/Ca_{shell} data of *A. elliptica* can provide the most precise DO estimates, i.e., ±1.5 mL/L. Slightly larger 1σ uncertainties are involved when *A. islandica* or *A. borealis* are used (both: ±1.6 mL/L DO). A combination of data from *A. elliptica* and *A. islandica* is associated

with an uncertainty of ±1.5 mL/L DO, and a mix of all studied specimens comes with an uncertainty of ±1.7 mL/L DO (Supplements). Following these transfer functions, in *A. islandica*, *A. elliptica* and *A. borealis*, an increase by 10 µmol/mol Mn/Ca_{shell} reflects a decrease in DO by 1.44, 0.98, and 1.08 mL/L, respectively.

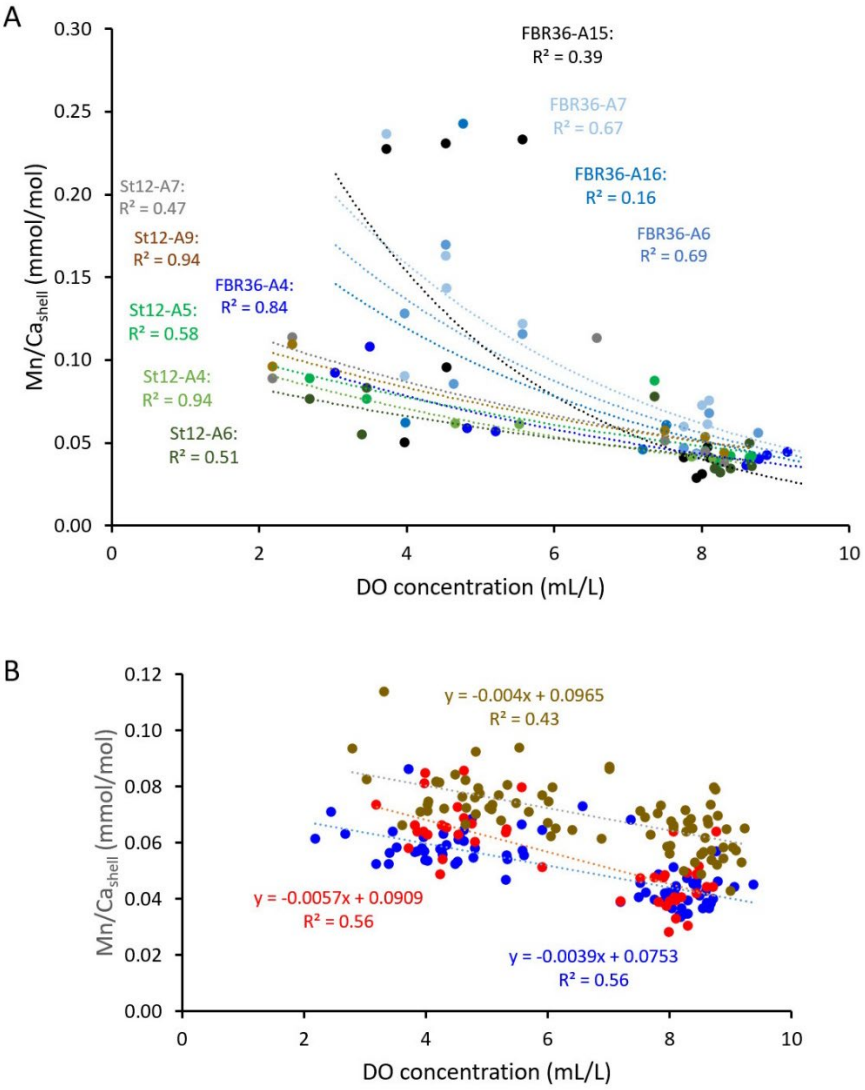

Figure 4.11 (A) During early ontogeny (below age 10), Mn/Ca_{shell} revealed non-linear relationships (here exponential fits used), even after double-detrending (= correlation between Mn/Ca_{shell} with both annual growth rate and Mg/Ca_{shell} mathematically eliminated). Trends varied between specimens, not localities. St12 = Mecklenburg Bight, FBR36 = Fehmarn Belt. (B) If the data from shell portions formed prior to age 10 were omitted, the relationship between Mn/Ca_{shell} of *A. islandica* and DO concentration measured some decimeters above seafloor became much stronger (compare Fig. 10C).

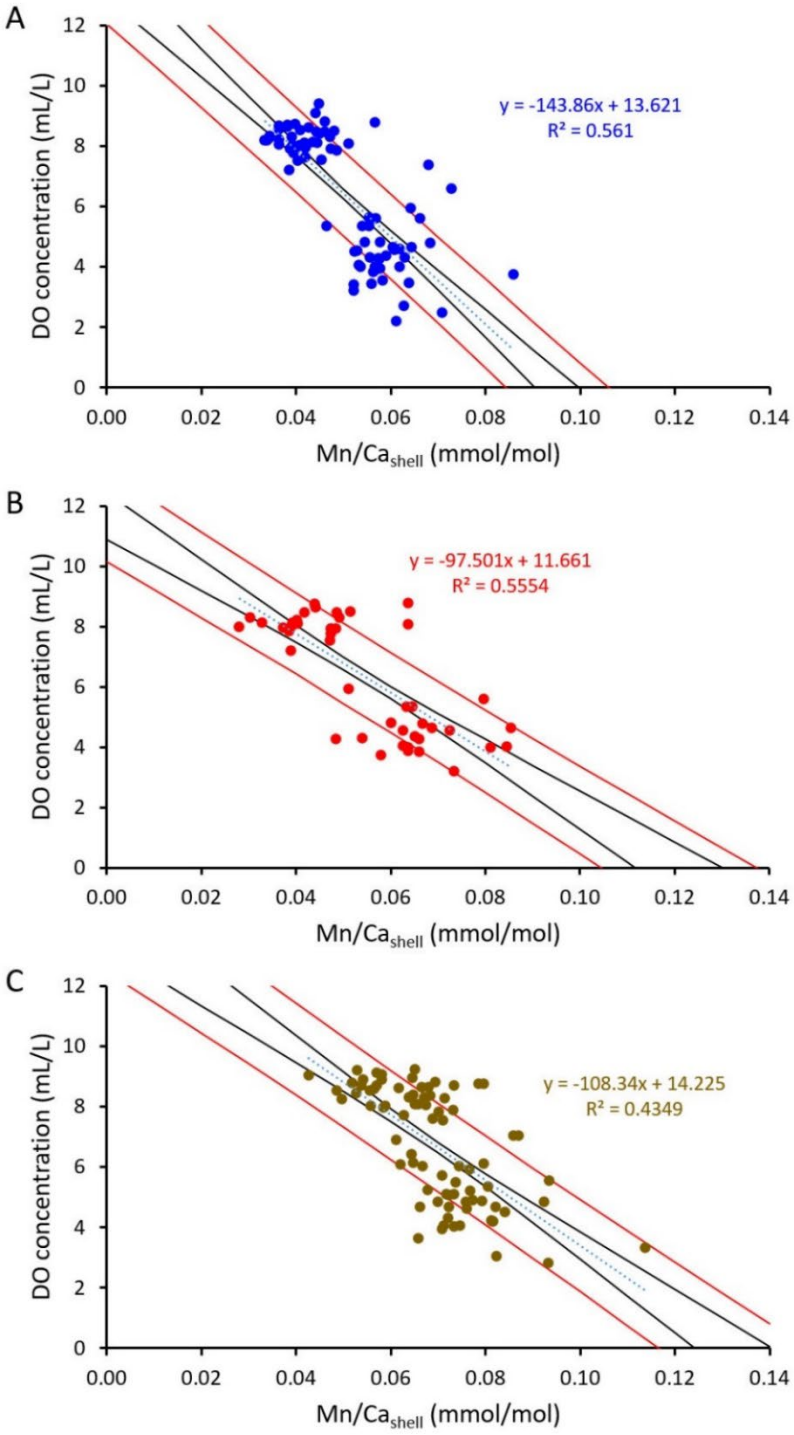

Figure 4.12 Tentative models to predict DO concentration some decimeters above seafloor using Mn/Ca$_{shell}$ values of the three studied bivalve species. (**A**) *A. islandica*; (**B**) *A. elliptica*; (**C**) *A. borealis*. Black curves = 95 % confidence intervals of the regression lines; red curves = 1σ prediction intervals. *A. elliptica* can provide slightly more precise DO data (±1.5 mL/L) than *A. islandica* or *A. borealis* (±1.6 mL/L).

4.4 Discussion

The present study adds further support to the hypothesis that molar Mn/Ca data of bivalve shells can provide temporally well-constrained records of DO in the free water column (Zhao et al., 2017a; Schöne et al., 2021). Like other redox-sensitive elements, manganese becomes dissolved (as Mn^{2+}) under reducing conditions (Hem, 1963, Balzer, 1982; Rue et al., 1997) and – against thermodynamic expectations – can remain for a while in this bioavailable form even under the presence of oxygen (Tebo, 1991), possibly mediated by organic substances (Kremling and Petersen, 1978). Relative to permanently well-oxygenated settings in the North Atlantic, manganese was significantly enriched in studied bivalve shells from the Baltic Sea (this study and Schöne et al., 2021). For example, shells of *A. islandica* from nearshore coastal sites in NE Iceland contained, on average, only 2 µmol/mol Mn/Ca_{shell} and extremes barely reached 5 µmol/mol (Marali et al., 2017a). In contrast, respective values in conspecific specimens from the Fehmarn Belt and Mecklenburg Bight were, on average, 21 times higher (approx. 42 µmol/mol), and peaks (undetrended monthly data) can attain more than 300 µmol/mol Mn/Ca_{shell} (Schöne et al., 2021).

As shown here, besides *A. islandica* two other species, i.e., *A. elliptica* and *A. borealis* can likewise serve as proxy archives for dissolved oxygen levels in the water column. Once corrected for shell growth rate-related kinetic effects and (some) vital effects, Mn/Ca_{shell} data (age ten onward in *A. islandica*) of bivalves living at the seafloor are statistically significantly ($p < 0.0001$) correlated to DO concentration measured some decimeters above the sediment surface ($r = -0.66$ to -0.75, corresponding to 43 to 56 % explained variability) (Fig. 4.12). According to the tentative models developed here, *A. elliptica* can provide slightly more precise DO data (±1.5 mL/L) than *A. islandica* or *A. borealis* (±1.6 mL/L).

4.4.1 Advantages and disadvantages of the three studied species for DO reconstructions

The prediction interval (Fig. 4.12) certainly is a relevant criterion to determine which species might be the most suitable archive to reconstruct DO, but no major differences were observed between the three species (uncertainties of ±1.5 to 1.6 mL/L DO). Several other aspects should be considered as well including longevity, continued shell production under low DO levels and fluctuating salinity, distinctness of annual growth lines, growth pattern geometry and temporal resolution.

Shells of the ocean quahog were considerably thinner than at most other sites outside

the Baltic Sea. For example, the oldest specimen hardly measured more than one millimeter in thickness (Fig. 4.2A). Predominantly, this resulted from a very thin, severely eroded or even missing inner shell layer (Fig. 4.2A; see also Schöne, 2013). Like the two *Astarte* species, to survive under hostile environmental conditions, the ocean quahog switches into an anaerobic metabolism during which acidic metabolites are generated which are subsequently neutralized by the dissolution of inner shell surfaces (Crenshaw, 1980; Oeschger, 1990; Oeschger and Storey, 1993). However, *A. islandica* can also undergo self-induced anaerobiosis without a clear external trigger (Taylor 1976; Oeschger, 1990). Perhaps, the ocean quahog thus spent more time in anaerobiosis than the other two species, and consequently, its shell experienced stronger dissolution of inner shell surfaces. With thinner, more fragile shells, the bivalve is less well protected against predators and possibly prone to damage by bottom-trawling (Rumohr and Krost, 1991) and may thus not attain the extraordinary lifespan reported from well-oxygenated sites in the North Atlantic, i.e., up to over 500 years (Schöne, 2013; Butler et al., 2013). At least, the ontogenetic age of the oldest and largest specimen (Table 1), arbitrarily selected for the present study, remained well beyond the longevity for which *A. islandica* is renowned. Studied *A. borealis* attained higher ages than *A. islandica* (Table 1).

While all three studied species can survive hypoxic, anoxic and even euxinic conditions for several months (Theede et al., 1969; Weigelt & Rumohr, 1986; Oeschger, 1990; Oeschger and Storey, 1993) and resist large salinity swings (von Oertzen and Schlungbaum, 1972; von Oertzen 1973), biomineralization rates of *A. islandica* were more severely affected by adverse environmental conditions than such of *Astarte* spp. Annual growth patterns of *A. islandica* were much more difficult to identify than typically at well-oxygenated, fully marine sites and less distinct than in the two Astartidae. In the ventral margin, the annual growth lines were only faintly developed and could hardly be distinguished from disturbance lines (Fig. 4.2A). It thus took considerable efforts to temporally contextualize the shell portions of the ocean quahog in this region. Besides disturbance lines, several other findings suggested *A. islandica* experienced physiological stress as outlined in the following. With a maximum shell size increase of 6 mm per year it grew four to five times faster than *Astarte* spp., but annual growth rates remained approx. two to four times below that observed in this species at well-oxygenated, stenohaline sites in the North Atlantic (e.g., up to 20 mm per year around the coasts of the British Isles; personal observation, BRS). While food supply was certainly not a limiting growth factor, because the Baltic Sea is heavily eutrophicated (Conley et al., 2007), variable salinity and low-oxygen stress (Table 1) could have adversely affected shell production rates. The ocean quahog survives salinity stress better than *Astarte* (von Oertzen and Schlungbaum, 1972; von Oertzen

1973), but likely on the expense of a reduced biomineralization rate. If more energy needs to be devoted to osmoregulation, less energy is available for growth and reproduction. Furthermore, the physiological resistance of *A. islandica* against oxygen deficiency and hydrogen sulfide is significantly lower than that of the *Astarte* spp. (von Oertzen and Schlungbaum, 1972; von Oertzen 1973; Theede, 1973; Dries & Theede, 1974). Therefore, it appears likely that salinity fluctuations, low oxygen levels and more frequent anaerobiosis resulted in lower biomineralization rates in the ocean quahog and eventually the formation of numerous disturbance lines.

Both *Astarte* species seem to have coped better with the hostile environmental conditions, at least the biomineralization processes did not seem to have been impacted as much. The shells were thick (see also Oeschger, 1990; Rumohr and Krost, 1991) and the inner shell layers fully developed without signs of significant dissolution. Judging from fewer disturbance lines, the biomineralization process was also less frequently interrupted. Thus, their shells may provide a more reliable and more complete record of the ocean oxygenation than the ocean quahog. The recognition of annual growth lines was much easier in the astartids, specifically in *A. elliptica*. Besides the presence of blue-stained annual bands and lines after immersion in Mutvei's solution, sharp Mg/Ca_{shell} peaks and troughs aided in the identification of the annual growth lines in this species. Note that these Mg (as well as Sr) enrichments did not coincide with the coldest or warmest season suggesting that Mg and Sr were not primarily governed by temperature.

While *A. elliptica* can provide slightly more precise DO estimates than the other two species (Fig. 4.12), the disadvantage is its relatively short lifespan of only twenty years or so (Table 4.1). Furthermore, strong undulations of the outer shell layer that mirrored spiral ridges of the outer shell surface (Fig. 4.2B), made sampling a challenging task and often resulted in strongly time-averaged chemical data. Such difficulties were not encountered in *A. borealis* (Fig. 4.2C). This species only showed a weak wavy sculpture that barely affected the geometry of growth patterns in the outer shell layer. *A. borealis* attained the longest lifespan of the studied species (Table 4.1), which is an important prerequisite to assess the long-term trends or quasi-decadal cycles of ocean ventilation.

If the advantages and disadvantages of the studied species are weighed up against each other and more than a single species is available for DO reconstructions, preference should be given to the two *Astarte* species, because the growth patterns are easier to identify than in the ocean quahog facilitating the temporal alignment of the LA spots. Since the shell formation remained largely unimpeded by salinity and low oxygen stress, the studied astartids offer better

chances to record the most extreme deoxygenation events. If the most precise DO estimates are needed, *A. elliptica* should be given preference, whereas long-term trends may be easiest obtained from *A. borealis*. Mn/Ca_{shell} data of *A. islandica* and *A. elliptica* may be combined to infer DO levels, because the transfer functions of both species were nearly identical (Fig. 4.12B+C; Supplements).

4.4.2 Mn/Ca_{shell} serve as a proxy for DO levels in the water column

The covariation between detrended Mn/Ca_{shell} and DO concentration suggests that the primary source for this metal in the shell was dissolved Mn^{2+}, i.e., hydrated ions, complexes or colloids rather than particulate Mn. The strongest Mn enrichment was observed in shell portions formed between July and September, i.e., contemporaneously with the lowest oxygen levels in the water column, but several months after the primary production maximum and associated downward flux of Mn-rich organic particles, and several months before the halocline disrupted giving way to increased bottom currents that may have stirred up Mn-bearing particles from the sea floor. Sharp Mn/Ca_{shell} peaks as previously reported from *A. islandica* of Mecklenburg Bight (Schöne et al., 2021) could potentially be derived from digested particulate Mn. However, the seasonal Mn/Ca_{shell} oscillations that covary with DO support a predominant dissolved source of this metal. Controlled laboratory experiments in future studies would certainly be useful to shed light on the relative importance of the different Mn sources.

In-situ analyses would also be useful to clarify the degree to which the incorporation of this metal into the shell is controlled by biological effects and whether equilibrium with Mn^{2+} in the ambient water is attained at some stage of life. As the concentration of Mn^{2+} (as well as DO) at the very position where the food intake takes place is unknown (note again, in the present study and in Schöne et al., 2021, Mn/Ca_{shell} values were compared to DO concentration some decimeters above the seafloor), not even a rough estimate on the magnitude of the vital effects and its change through lifetime is possible. With their extremely short siphons (e.g., Morton, 2011), the studied endobenthic bivalves inhaled water directly from the sediment-water interface, i.e., where dissolved Mn diffuses out of the sediment (Sundby et al., 1981; Roitz et al., 2002) and mixes with the overlaying water body. The highest Mn^{2+} concentrations (and lowest DO levels) within the water column occur just here, at the sediment-water interface and gradually decline with increasing distance from the sediment surface while DO levels rise (e.g., Kremling and Petersen, 1978). At least, the strong correlation between detrended Mn/Ca_{shell} values recorded at the seafloor and DO levels measured some decimeters away from the sediment surface suggests that the Mn^{2+} concentrations and DO levels in the water column

changed proportionately to that in the fluffy layer at the seabed which has important implications for the use of this proxy. Subsequent studies should evaluate if and how strongly the relationship of DO (and Mn/Ca) within the coelomic fluid of the bivalves (containing inhaled water), directly at the sediment-water interface and different heights above the seafloor varies over time. With such knowledge, it may also be possible to further constrain the relationship between DO and Mn/Ca_{shell} values. Furthermore, if the relationship between DO within the coelomic fluid and at various heights above seafloor is known, it may also become possible to estimate bottom DO concentrations from Mn/Ca_{shell} values.

The concentration of dissolved manganese near the sediment-water interface typically can vary among localities, depending on DO level, duration of oxygen deficiency, amount of Mn-rich particles at the sea floor, bottom currents etc. (Limburg et al., 2011). For example, Groeneveld et al. (2018) reported water column Mn/Ca values of approx. 5 µmol/mol at 5 mL/L DO and above, and more than 200 µmol/mol at 2 mL/L DO at Hanö Bay. However, in the Kattegat, $Mn/Ca_{seawater}$ values remained below 23 µmol/mol even near the normoxic/hypoxic boundary (Groeneveld et al., 2018). In the present study, the DO vs. Mn/Ca_{shell} data from Mecklenburg Bight and Fehmarn Belt fitted very well to each other (and were thus combined in the same prediction model) suggesting similar Mn fluxes into the water column. Subfossil shells from the same region should thus provide reasonable estimates on past DO levels in the water column some decimeters above seafloor.

Porewater Mn^{2+} may have reached the site of biomineralization also through the mantle epithelia and foot. When gaping, a small portion of the mantle is constantly engulfed by porewater. In addition, when the animal digs into the sediment, the foot comes into contact with porewater. Hence, there were chances for diffusive transmembrane ion transport from the porewater into the blood and eventually the calcifying fluid. However, the amounts of ions reaching the internal fluids through intercellular diffusion are small relative to active transmembrane ion transport (Carré et al., 2006) and most certainly remain far below the ion supply from the water column considering filtration rates, e.g., up to 7 L/h in the ocean quahog (Winter, 1969). The large amounts of water passing through the mantle coelom will likely dilute and remove most of the ions that arrived via diffusion from porewater before they can reach the calcifying fluid.

Furthermore, the strong correlation between detrended Mn/Ca_{shell} and DO implies that the water inhaled through the siphons was the major contributor of Mn^{2+} (and other ions) in the shells rather than diffusion from porewater. In contrast to the water column, oxygen levels in the porewater likely did not vary notably on seasonal time-scales, specifically in the mud/fine-

silt-dominated, organic-rich sediment in which *A. borealis* lived. Dissolved Mn concentrations in the porewater should thus have remained nearly invariant over time and were very likely much higher than above the sediment surface. Furthermore, larger, ontogenetically older, deeper digging specimens would have been exposed to much higher Mn concentrations than younger specimens would, but the opposite was observed: The highest Mn concentrations were measured in shell portions formed during youth.

4.4.3 Controls on Mn incorporation into the shells

Faster growing shell portions contained larger amounts of manganese than slower growing shell portions (Fig. 4.8A-C). Similar trends have previously been reported from two aragonitic shells from Peru, *Mesodesma donacium* and *Chione subrugosa*, and were ascribed to growth rate-related kinetic effects (Carré et al., 2006). At first sight, this finding indeed points to kinetic processes as it agrees well with results from synthetically precipitated aragonite (Kumagai, 1978). A possible explanation is that faster precipitation is associated with the coprecipitation of ions that would otherwise not fit into the orthorhombic crystal lattice of aragonite, e.g., monovalent ions (Rollion-Bard and Blamart, 2015) or divalent ions that are more than 15 % larger or smaller than Ca^{2+} (114 pm) (Kretz, 1982) thereby resulting in a larger number of lattice defects (Amiel et al., 1973). Ba^{2+}, Mn^{2+} and Mg^{2+} belong to the latter group. The ion radius of high-spin Mn^{2+}, which is present in bivalve shell aragonite (Soldati et al., 2016; Son et al. 2019), measures 83 pm, Mg^{2+} 72 pm, and Ba^{2+} 147 pm (Speer, 1983). To accommodate Mn^{2+} in the crystal lattice of aragonite, local calcite coordination domains are generated so that Mn^{2+} is coordinated by a CO_3-octahedron (e.g., Soldati et al., 2016). The same process likely ensures that Mg^{2+} can be accommodated in the aragonitic crystal lattice.

Following this rationale, faster growing shell portions should not only contain more Mn^{2+}, but also larger amounts of Na^+, Li^+, K^+, Mg^{2+} etc., because these ions are present in the calcifying fluid and nearly as highly concentrated as in the ambient seawater (e.g., Crenshaw, 1972; Lorens and Bender, 1980; Wada and Fujinuki, 1976). While the two Peruvian bivalves cited earlier fulfilled this expectation, and shell Sr/Ca, Ba/Ca, and Mg/Ca were positively coupled to growth rate as well (Carré et al., 2006), the opposite was found in the present study for Sr/Ca_{shell} and Mg/Ca_{shell}, specifically in old-grown specimens (Fig. 4.6). These two element-to-Ca ratios were thus inversely correlated to Mn/Ca_{shell} suggesting vital effects played a more important role during Mn incorporation into the shell aragonite than processes prevailing in abiotic systems.

This interpretation is further supported, firstly, by the fact that many trace impurities in

bivalve shells remain far below concentrations expected for equilibrium precipitation. For example, Mg/Ca_{shell} values in aragonitic bivalve shells such as *A. islandica* range between approx. 0.2 to 1.3 mmol/mol (Schöne et al., 2011; and data herein), whereas seawater contains 5.5 mol/mol. Based on experimentally determined distribution coefficients for Mg/Ca in synthetic aragonite provided by Gaetani and Cohen (2006), between 5 °C and 15 °C, the shells should contain approx. 81.95 to 9.35 mmol/mol. As no direct measurements of Mn/Ca values are available from the water near the seabed where the bivalves fed, no reliable conclusions can be drawn on the degree of a possible disequilibrium for this metal in shell aragonite. Secondly, lattice distortions can also be physiologically induced in biominerals by the insertion of proteins into the crystal lattice (Pokroy et al., 2006), perhaps as a response to manganese enrichment in the ambient water and the requirement for detoxification (see below). Thirdly, in abiogenic systems, interactions between ions in the calcifying solution can prevent the incorporation of some and favor the incorporation of other ions into the $CaCO_3$ crystal lattice (Okumura and Kitano, 1986; Dromgoole and Walter, 1990). For example, Mg^{2+} competes more successfully than Mn^{2+} for adsorption sites on growing crystal surfaces of calcite and suppresses the incorporation of Mn^{2+} into the crystal lattice (Dromgoole and Walter, 1990). Assuming the few reports on the chemistry of the extrapallial fluid (Crenshaw, 1972; Lorens and Bender, 1980; Wada and Fujinuki, 1976) are correct and kinetics are the same as in pure calcite, the studied shells, more specifically the calcite domains in the aragonite should be almost devoid of Mn^{2+}. However, the opposite clearly is the case, pointing to a significant participation of vital effects during shell growth.

Whereas vital effects can result in much lower distribution coefficients than expected for thermodynamic equilibrium, trace elements such as Sr^{2+} are still incorporated into the shell proportional to that in the water (Zhao et al., 2017b). Based on the findings herein, this also applies to Mn^{2+}, a major prerequisite to employ this trace metal as a DO proxy in bivalves. The proportionate increase of Mn^{2+} in the shells may also reflect attempts to detoxify, i.e., to remove unwanted ions from the body fluids either by pumping them out of the mantle coelom or by using the shell as a recycle bin. Mn^{2+} is one these 'unwanted' ions, because it can be toxic for bivalves at elevated concentration as it interferes with neurotransmitters that control the beating of the cilia of the gills (Nelson et al., 2018).

After mathematical detrending for growth rate-related kinetic effects as well as vital effects that affected the incorporation of both Mg^{2+} and Mn^{2+} into the shell, the Mn/Ca_{shell} data agreed much better with DO (Fig. 4.10C). However, during early ontogeny (< age 10), *A. islandica* shells still contained much larger amounts of Mn^{2+}, than during later stages of life,

and large individual differences in juvenile Mn^{2+} enrichment were observed (Fig. 4.11A). Possible reasons include microhabitat differences, e.g., variations in Mn flux from the seabed into the overlaying water body, or physiological differences among specimens. In addition, older specimens likely produced a much stronger current through their siphons and thus sucked in water farther away from the sediment-water interface where Mn^{2+} concentrations were lower than directly at the seabed, while young specimens with weaker muscles accessed a larger proportion of water from the fluffy layer. Individual fitness may account for differences in juvenile Mn^{2+} enrichment among specimens. Another possibility is that older specimens were more effective in removing unwanted ions from body fluids including the site of biomineralization and thus contained lower amounts of Mn^{2+} than younger specimens. Some juveniles may have invested more energy into shell growth rather than a chemically cleaner shell. As in abiogenic aragonite, larger amounts of trace impurities, specifically Mg^{2+} can increase the hardness of the shells (Boon et al., 2019); presumably, the same applies to Mn^{2+}. However, at the same this makes them more amenable to fractures, because the shells become more brittle, less elastic. Yet, this disadvantage may outweigh the danger of being eaten by a predator due insufficient body size.

It remains unclear whether such Mn enrichment during youth also occurs in *Astarte* spp., because respective shells portions could hardly be sampled due to the peculiar growth pattern geometry and/or a thin outer shell layer in early ontogeny. Judging from the few data of specimens MLZ-FBR-A8 and A10 as well as MLZ-FBR06-A1 and A3, Mn^{2+} is not as strongly elevated in shells of young *Astarte* spp. than in the ocean quahog. Pending confirmation of this finding, astartids may be more efficient in excluding Mn from incorporation into the shell carbonate than the ocean quahog. Alternatively, they generate a stronger current through their siphons during youth than coeval specimens of *A. islandica* resulting in the uptake of water farther away from Mn-enriched fluffy layer.

The relationship between detrended Mn/Ca_{shell} values (above the age of ten) and DO levels in the water column varied only slightly between *A. islandica* and *A. elliptica* (Fig. 4.10C) suggesting that largely similar mechanisms were at work during manganese uptake, transport and incorporation into the shell. However, *A. borealis* incorporated, on average, approx. 20 µmol/mol more manganese in its shell than the other two species (Fig. 4.10C). These differences could reflect species-specific vital effects controlling the incorporation of trace impurities into the shell or site-specific differences in porewater Mn^{2+} fluxes, bottom currents etc. In light of similar transfer functions for co-occurring bivalves belonging to different genera, i.e., *A. islandica* and *A. elliptica*, site-specific differences in Mn availability do not seem unlikely to

explain the higher level in *A. borealis*.

4.4.4 Detrending

The double-detrending approach eliminated a significant proportion of physiological and growth rate-related kinetic effects (Fig. 4.10C), but was uncapable of removing the heteroscedastic noise from the Mn/Ca_{shell} chronologies of *A. islandica*, i.e., the decreasing Mn/Ca_{shell} amplitudes with increasing ontogenetic age and slower shell growth (Fig. 4.5A). In dendrochronology and bivalve sclerochronology, annual growth rates typically exhibit a strong heteroscedasticity, which can be mathematically eliminated with an adaptive power transformation (Cook and Peters, 1997). Briefly, the local mean and variance of annual increment widths are linearly correlated when plotted in logarithmic space. A data-adaptive power transformation of these data can be used to normalize the raw data based on the slope of the regression line and produce variance-stabilized (= homoscedastic) growth data (see step-by-step explanation in Cook and Peters, 1997, and for application in sclerochronology see Schöne, 2013). A similar approach could theoretically be used to remove the heteroscedasticity from the Mn/Ca_{shell} chronologies provided they were at least as long as the that of specimen MLZ-FBR36-A4. This is because a broad spectrum of log mean vs. log variance pairs were needed for each specimen to obtain a robust regression line and slope for the variance correction. Notably, a data-adaptive power transformation can only be performed on individual chronologies, because the absolute changes of Mn/Ca_{shell} values during different ontogenetic ages in the same specimen must be known. As shown in Figures 4.5A, 4.7A and 4.9A, during early stages of life, studied specimens of *A. islandica* showed large differences in seasonal Mn/Ca_{shell} amplitudes making it impossible to predict how the Mn/Ca_{shell} curves would develop during subsequent years. Furthermore, due to strong individual differences in Mn/Ca_{shell} amplitudes of coeval specimens (Fig. 4.11A), no common non-linear relationship exists between DO concentration and Mn/Ca data of shell portions produced until the age of ca. nine. Therefore, no reliable method currently exists to infer DO from shells of ontogenetically young specimens of *A. islandica*. Since the Mn/Ca_{shell} chronologies were largely homoscedastic from age ten onward (Fig. 4.5A) and no variance correction was required, it seems justified to simply disregard the data from the first nine years of life in the prediction model for *A. islandica* (Fig. 4.12A).

Growth rate-related kinetics demonstrably affected the Mn/Ca_{shell} data (Fig. 4.8A-C). In the present study, removal of growth rate-related trends was exclusively accomplished on the basis of annual shell growth rates, i.e., (resampled) daily and monthly Mn/Ca_{shell} data were

detrended with the annual growth value of the respective growing season. Ideally, daily growth rates should have been used to detrend Mn/Ca_{shell} data. However, daily increment width data were not available and the generalized seasonal growth model may not perfectly reflect the actual daily growth rates in each year. To avoid large errors resulting from the use of inappropriate (interpolated) daily growth data, the annual increment widths were used instead.

4.5 Summary and conclusion

Manganese-to-Ca ratios in shells of all three studied bivalves from the Baltic Sea, *A. islandica*, *A. elliptica* and *A. borealis* can provide robust information (1σ error of ±1.5 to 1.6 mL/L) on the concentration of dissolved oxygen in the water column some decimeters above seafloor using species-specific transfer functions. Once the raw data were temporally contextualized with an appropriate seasonal age model and corrected for differences in time-averaging, the resampled Mn/Ca_{shell} chronologies require detrending, ideally the mathematical elimination of both the correlation with annual growth rate and Mg/Ca_{shell} values. This treatment removes a large proportion of vital (and potentially kinetic) effects. Due to specimen-specific non-linear relationships between DO and Mn/Ca_{shell} as well as strong heteroscedasticity of Mn/Ca_{shell}, data from the first nine years of life of *A. islandica* should not be used for DO reconstructions. Findings of the present study provide the basis to reconstruct inter-annual trends of seasonal DO extremes in nearshore coastal environments of the Baltic Sea during the most recent centuries.

4.6 Supplements material

The Supplementary Data for this article can be found online at:
https://www.frontiersin.org/articles/10.3389/fmars.2022.820731/full#supplementary-material

References

Abbott, R. T., Morris, P. A., 1995. A Field Guide to Shells: Atlantic and Gulf Coasts and the West Indies. New York, Houghton Mifflin, 512 pp.

Amiel, A. J., Friedman, G. M., Miller, D. S., 1973. Distribution and nature of trace elements in modern aragonitic corals. Sedimentol. 20, 47–64.

Arntz, W. E., Weber, W., 1970. *Cyprina islandica* L. (Mollusca, Bivalvia) als Nahrung von Dorsch und Kliesche in der Kieler Bucht. Ber. Dt. Wiss. Komm. 2, 193–209.

Arthur, M. A., Sageman, B. B., 1994. Marine black shales: depositional mechanisms and environments of ancient deposits. Annu. Rev. Earth Planet. Sci. 22, 499–551.

Balzer, W., 1982 On the distribution of iron and manganese at the sediment/water interface: thermodynamic versus kinetic control. Geochim. Cosmochim. Acta 46, 1153–1161.

Benson, B.B., Krause, D. Jr., 1984. The concentration and isotopic fractionation of oxygen dissolved in freshwater and seawater in equilibrium with the atmosphere. Limnol. Oceanogr. 29, 620–632.

Berner, R. A., 1975. The role of magnesium in the crystal growth of calcite and aragonite from sea water. Geochim. Cosmochim. Acta 39, 489–504.

Black, B. A., Andersson, C., Butler, P. G., Carroll, M., DeLong, K. L., Reynolds, D. J., Schöne, B. R., Scourse, J., van der Sleen, P., Wanamaker, A. D., Witbaard, R., 2019. The revolution in marine paleoecology and paleoclimatology. Biology Letters 15, 20180665.

Boon, M., Rickard, W. D. A., Rohl, A. L., Jones, F., 2019. Stabilization of aragonite: role of Mg^{2+} and other impurity ions. Cryst. Growth Des. 20, 5006–5017.

Branson, O., Fehrenbacher, J., Vetter, L., Sadekov, A.Y., Eggins, S.M., Spero, H.J., 2019. Latools: a data analysis package for the reproducible reduction of LA-ICPMS data. Chem. Geol. 504, 83–95.

Bryan, S. P., Marchitto, T. M., 2008. Mg/Ca-temperature proxy in benthic foraminifera: new calibrations from the Florida Straits and a hypothesis regarding Mg/Li. Paleoceanogr 23, PA2220.

Butler, P.G., Wanamaker Jr., A.D., Scourse, J.D., Richardson, C.A., Reynolds, D.J., 2013. Variability of marine climate on the North Icelandic Shelf in a 1357-year proxy archive based on growth increments in the bivalve *Arctica islandica*. Palaeogeogr. Palaeoclimatol. Palaeoecol. 373, 141–151.

Carré, M., Bentaleb, I., Bruguier, O., Ordinola, E., Barrett, N. T., Fontugne, M., 2006. Calcification rate influence on trace element concentrations in aragonitic bivalve shells: Evidences and mechanisms. Geochim. Cosmochim. Acta 70, 4906–4920.

Case, D. H., Robinson, L. F., Auro, M. E., Gagnon, A. C., 2010. Environmental and biological controls on Mg and Li in deep-sea scleractinian corals. Earth Planet. Sci. Lett. 300, 215–225.

Carré, M, Bentaleb, I., Bruguier, O., Ordinola, E., Barrett, N.T., Fontugne, M., 2006. Calcification rate influence on trace element concentrations in aragonitic bivalve shells: Evidences and mechanisms. Geochim. Cosmochim. Acta 70, 4906–4920.

Carstensen, J., Andersen, J.H., Gustafsson, B.G., Conley, D.J., 2014. Deoxygenation of the Baltic Sea during the last century. Prox. Nat. Acad. Sci. 111, 5628–5633.

Conley, D.J., Björck, S., Bonsdorff, E., Carstensen, J., Destouni, G., Gustafsson, B.G., Hietanen, S., Kortekaas, M., Kuosa, H., Meier, M., Müller-Karulis, B., Nordberg, K., Nürnberg, G., Norkko, A., Pitkänen, H., Rabalais, N.N., Rosenberg, R., Savchuk, O.P., Slomp, C.P., Voss, M., Wulff, F., Zillén, L., 2009. Hypoxia-related processes in the Baltic Sea. Environ. Sci. Technol. 43, 3412–3420.

Conley, D.J., Carstensen, J., Ærtebjerg, G., Bondo Christensen, P., Dalsgaard, T., Hansen, J.L.S., Josefson, A.B., 2007. Long-term changes and impact of hypoxia in Danish coastal waters. Ecol. Applicat. 17, S165–S184.

Cook, E. R., Peters, K., 1997. Calculating unbiased tree-ring indices for the study of climatic and environmental change. Holocene 7, 361–370.

Crenshaw, M. A., 1972. Inorganic composition of molluscan extrapallial fluid. Biol Bull 143, 506–512.

Crenshaw, M.A., 1980. Mechanisms of shell formation and dissolution. In: Rhoads, D. C., Lutz, R. A. (Eds.), Skeletal Growth of Aquatic Organisms: Biological Records of Environmental Change. Plenum Press, New York, pp. 115–132.

Danz, R., Gretscher, P., 2004. C–DIC: a new microscopy method for rational study of phase structures in incident light arrangement. Thin Solid Films 462–463, 257–262.

Darr, A., Gogina, M, Zetler, M. L., 2014. Detecting hot-spots of bivalve biomass in the south-western Baltic Sea. J. Mar. Syst. 134, 69–80.

Dries. R. R., Theede, H., 1974. Sauerstoffmangelresistenz mariner Bodenvertebralen aus der Westlichen Ostsee. Mar. Biol. 25, 327–333.

Dromgoole, E. L., Walter, L. M., 1990. Inhibition of calcite growth rates by Mn2+ in $CaCl_2$ solutions at 10, 25, and 50°C. Geochim. Cosmochim. Acta 54, 2991–3000.

Fennel, K., Testa, J. M., 2019. Biogeochemical controls on coastal hypoxia. Annu. Rev. Mar. Sci. 11, 105–130.

Füllenbach, C.S., Schöne, B.R., Mertz-Kraus, R., 2015. Strontium/lithium ratio in aragonitic

shells of *Cerastoderma edule* (Bivalvia) – a new potential temperature proxy for brackish environments. Chem. Geol. 417, 341–355.

Gaetani, G. A., Cohen, A. L., 2006. Element partitioning during precipitation of aragonite from seawater: A framework for understanding paleoproxies. Geochim. Cosmochim. Acta 70, 4617–4634.

Gillikin, D.P., Dehairs, F., Lorrain, A., Steenmans, D., Baeyens, W., André, L., 2006. Barium uptake into the shells of the common mussel (*Mytilus edulis*) and the potential for estuarine paleo-chemistry reconstruction. Geochim. Cosmochim. Acta 70, 395–407.

Gonfiantini, R., Stichler,W., Rozanski, K., 1995 Standards and intercomparison materials distributed by the International Atomic Energy Agency for stable isotope measurements (IAEA-TECDOC-825), International Atomic Energy Agency (IAEA), Vienna, Austria, 13–29, available at: https://www-pub.iaea.org/MTCD/publications/PDF/te_825_prn.pdf (last access: 1 Nov. 2022)

Groeneveld, J., Filipsson, H.L., 2013. Mg/Ca and Mn/Ca ratios in benthic foraminifera: the potential to reconstruct past variations in temperature and hypoxia in shelf regions. Biogeosci. 10, 5125–5138.

Groeneveld, J., Filipsson, H.L., Austin, W.E.N., Darling, K., McCarthy, D., Krupinski, N.B.Q., Bird, C., Scweizer, M., 2018. Assessing proxy signatures of temperature, salinity, and hypoxia in the Baltic Sea through foraminifera-based geochemistry and faunal assemblages. J. Micropalaeontol. 37, 403–429.

Grossman, E.L., Ku, T.-L., 1986. Oxygen and carbon isotope fractionation in biogenic aragonite; temperature effects, Chem. Geol. Isot. Geosci. Sect., 59, 59–74.

Hallmann, N., Schöne, B.R., Irvine, G.V., Burchell, M., Cokelet, E.D., Hilton, M., 2011. An improved understanding of the Alaska Coastal Current: The application of a bivalve growth-temperature model to reconstruct freshwater-influenced paleoenvironments. Palaios 26, 346–363.

Hausmann, N., Robson, H. K., Hunt, C., 2019. Annual growth patterns and interspecimen variability in Mg/Ca records of archaeological *Ostrea edulis* (European oyster) from the Late Mesolithic site of Conors Island. Open Quat. 5, 9.

Hem, J.D., 1963. Chemical equilibria and rates of manganese oxidation. U.S. Geol. Surv. Water Supply Pap. 1667-A, A1–A64.

Herreid, C. F. II, 1980. Hypoxia in invertebrates. Comp. Biochem. Physiol. 67A, 311–320.

Jochum, K.P., Nohl, U., Herwig, K., Lammel, E., Stoll, B., Hofmann, A.W., 2005. GeoReM: a new geochemical database for reference materials and isotopic standards. Geostand.

Geoanal. Res. 29, 333–338.

Jochum, K.P., Stoll, B., Herwig, K., Willbold, M., 2007. Validation of LA-ICP-MS trace element analysis of geological glasses using a new solid-state 193 nm Nd:YAG laser and matrix-matched calibration. J. Anal. At. Spectrom. 22, 112.

Jochum, K.P., Weis, U., Stoll, B., Kuzmin, D., Yang, Q., Raczek, I., Jacob, D.E., Stracke, A., Birbaum, K., Frick, D.A., Günther, D., Enzweiler, J., 2011. Determination of reference values for NIST SRM 610–617 glasses following ISO guidelines. Geostand. Geoanal. Res. 35, 397–429.

Jokinen, S. A., Virtasalo, J. J., Jilbert, T., Kaiser, J., Dellwig, O., Arz, H. W., Hänninen, J., Arppe, L., Collander, M., Saarinen, T., 2018. A 1500-year multiproxy record of coastal hypoxia from the northern Baltic Sea indicates unprecedented deoxygenation over the 20th century. Biogeosci 15, 3975–4001.

Jones, D.S., 1980. Annual cycle of shell growth increment formation in two continental shelf bivalves and its paleoecologic significance. Paleobiology 6, 331–340.

Jones, D. S., Quitmyer, I. R., 1996. Marking time with bivalve shells: oxygen isotopes and season of annual increment formation. Palaios 11, 340–346.

Kremling, K., Petersen, H., 1978. The distribution of Mn, Fe, Zn, Cd and Cu in Baltic seawater; a study on the basis of one anchor station. Mar. Chem. 6, 155-170.

Kubota, K., Shirai, K., Murakami-Sugihara, N., Seike, K., Hori, M., Tanabe, K., 2017. Annual shell growth pattern of the Stimpson's hard clam *Mercenaria stimpsoni* as revealed by sclerochronological and oxygen stable isotope measurements. Palaeogeogr. Palaeoclimatol. Palaeoecol. 465, 307–315.

Kumagai, T., 1978. Coprecipitation of manganese with calcium carbonate. Bull. Inst. Chem. Res. Kyoto Univ. 56, 280–285.

Kretz, R., 1982. A model for the distribution of trace elements between calcite and dolomite. Geochim. Cosmochim. Acta 46, 1979–1981.

Limburg, K.E., Olson, C., Walther, Y., Dale, D., Slomp, C.P., Høie, H., 2011. Tracking Baltic hypoxia and cod migration over millennia with natural tags. Proc. Nat. Acad. Sci., 108, E177–E182.

Lorens, R. B., Bender, M. L., 1980. The impact of solution chemistry on *Mytilus edulis* calcite and aragonite. Geochim Cosmochim Acta 44, 1265–1278.

Marali, S., Schöne, B. R., Mertz-Kraus, R., Griffin, S. M., Wanamaker, A. D. Jr., Matras, U., Butler, P. G., 2017b. Ba/Ca ratios in shells of *Arctica islandica* – Potential environmental proxy and crossdating tool. Palaeogeogr. Palaeoclimatol. Palaeoecol. 465, 347–361.

Marali, S., Schöne, B.R., Mertz-Kraus, R., Griffin, S.M., Wanamaker Jr., A.D., Butler, P.G., Holland, H.A., Jochum, K.P., 2017a. Reproducibility of trace element variations (Na/Ca, Mg/Ca, Mn/Ca, Sr/Ca, and Ba/Ca) within and between specimens of the bivalve *Arctica islandica* – a LA-ICP-MS line scan study. Palaeogeogr. Palaeoclimatol. Palaeoecol. 484, 109–128.

Meyer, H. J., 1984. The influence of impurities on the growth rate of calcite. J. Crystal Growth 66, 639–646.

Morton, B., 2011. The biology and functional morphology of *Arctica islandica* (Bivalvia: Arcticidae): a gerontophilic living fossil. Mar. Biol. Res. 7, 540–553.

Moss, D. K., Surge, D., Zettler, M. L., Orland, I. J., Burnette, A., Fancher, A., 2021. Age and growth of Astarte borealis (Bivalvia) from the southwestern Baltic Sea using secondary ion mass spectrometry. Mar. Biol. 168, 133.

Nelson, M., Adams, T., Ojo, C., Carroll, M. A., Catapane, E. J., 2018. Manganese toxicity is targeting an early step in the dopamine signal transduction pathway that controls lateral cilia activity in the bivalve mollusc *Crassostrea virginica*. Comp. Biochem. Physiol. C Toxicol. Pharmacol. 213, 1–6.

Oertzen, J.-A. von, 1973. A biotic potency and physiological resistance of shallow and deep water bivalves. Oikos Suppl. 15, 261–266.

Oertzen, J.-A. von, Schlungbaum, G., 1972. Experimentell-ökologische Untersuchungen über O_2-Mangel- und H_2S-Resistenz an marinen Evertebraten der westlichen Ostsee. Beitr. Meereskd. 29, 79–91.

Oeschger, R., 1990. Long-term anaerobiosis in sublittoral marine invertebrates from the Western Baltic Sea: *Halicryptus spinulosus* (Priapulida), *Astarte borealis* and *Arctica islandica* (Bivalvia). Mar. Ecol. Prog. Ser. 59, 133–143.

Oeschger, R., Storey, K.B., 1993. Impact of anoxia and hydrogen sulphide on the metabolism of *Arctica isiandica* L. (Bivalvia). J. Exp. Mar. Biol. Ecol. 170, 213–226.

Okumura, M., Kitano, Y., 1986. Coprecipitation of alkali metal ions with calcium carbonate. Geochim. Cosmochim. Acta 50, 49–58.

Österblom, H., Hansson, S., Larsson, U., Hjerne, O., Wulff, F., Elmgren, R., Folke, C., 2007. Human-induced trophic cascades and ecological regime shifts in the Baltic Sea. Ecosyst. 10, 877–889.

Palacios, R., Orensanz, J. M., Armstrong, D. A., 1994. Seasonal and lifelong variation of Sr/Ca ratio in shells of *Mya arenaria* from Grays Harbor (Washington) — an ancillary criterion in demographic studies. Estuarine, Coastal and Shelf Science 39, 313–327.

Peharda, M., Walliser, E. O., Markulin, K., Purroy, A., Uvanović, H., Janekovic, I., Župan, I., Vilibic, I. and Schöne, B. R. 2019. *Glycymeris pilosa* (Bivalvia) – A high-potential geochemical archive of the environmental variability in the Adriatic Sea. Mar. Environ. Res. 150, 104759.

Pokroy, B., Fitch, A. N., Lee, P. L., Quintana, J. P., Caspi, E. N., Zolotoyabko, E., 2006. Anisotropic lattice distortions in the mollusk-made aragonite: A widespread phenomenon. J. Struct. Biol. 153, 145–150.

Rabalais, N.N., Díaz, R.J., Levin, L.A., Turner, R.E., Gilbert, D., Zhang, J., 2010. Dynamics and distribution of natural and human-caused hypoxia. Biogeosci. 7, 585–619.

Roitz, J.S., Flegal, A.R., Bruland, K.W., 2002. The biogeochemical cycling of Manganese in San Francisco Bay: Temporal and spatial variations in surface water concentrations. Estuar. Coast. Shelf Sci. 54, 227–239.

Rollion-Bard, C., Blamart, D., 2015. Possible controls on Li, Na, and Mg incorporation into aragonite coral skeletons. Chem. Geol. 396, 98–111.

Rue, E.L., Smith, G.J., Cutter, G.A., Bruland, K.W., 1997. The response of trace element redox couples to suboxic conditions in the water column. Deep-Sea Res. I 44, 113–134.

Rumohr, H., Krost, P., 1991. Experimental evidence of damage to benthos by bottom trawling with special reference to *Actica islandica*. Meeresforsch. 33, 340–345.

Sanjuan, B., Girard, J. P., 1996. Review of kinetic data on carbonate mineral precipitation. BRGM Rep. R39062, 91pp. http://infoterre.brgm.fr/rapports/RR-39062-FR.pdf (last access: 2 Nov. 2021)

Schöne, B.R., 2008. The curse of physiology – Challenges and opportunities in the interpretation of geochemical data from mollusk shells. Geo-Mar. Lett. 28, 269–285.

Schöne, B.R., 2013. *Arctica islandica* (Bivalvia): A unique paleoenvironmental archive of the northern North Atlantic Ocean. Global Planet. Change 111, 199–225.

Schöne, B.R., Dunca, E., Fiebig, J., Pfeiffer, M., 2005a. Mutvei's solution: an ideal agent for resolving microgrowth structures of biogenic carbonates. Palaeogeogr. Palaeoclimatol. Palaeoecol. 228, 149–166.

Schöne, B.R., Houk, S.D., Freyre Castro, A.D., Fiebig, J., Kröncke, I., Dreyer, W., Oschmann, W., 2005b. Daily growth rates in shells of *Arctica islandica*: Assessing subseasonal environmental controls on a long-lived bivalve mollusk. Palaios 20, 78–92.

Schöne, B.R., Rodland, D.L., Wehrmann, A., Heidel, B., Oschmann, W., Zhang, Z., Fiebig, J., Beck, L., 2007. Combined sclerochronologic and oxygen isotope analysis of gastropod shells (*Gibbula cineraria*, North Sea): life-history traits and utility as a high-resolution

environmental archive for kelp forests. Mar. Biol. 150, 1237–1252.

Schöne, B. R., Zhang, Z., Radermacher, P., Thébault, J., Jacob, D., Nunn, E. V., Maurer, A.-F., 2011. Sr/Ca and Mg/Ca ratios of ontogenetically old, long-lived bivalve shells (*Arctica islandica*) and their function as paleotemperature proxies. Palaeogeogr. Palaeoclimatol. Palaeoecol. 302, 52–64.

Schöne, B.R., Huang, X., Zettler, M.L., Zhao, L., Mertz-Kraus, R., Jochum, K.P., Walliser, E.O., 2021. Mn/Ca in shells of *Arctica islandica* (Baltic Sea) – A potential proxy for ocean hypoxia? Estuar. Coast. Shelf Sci. 251, 107257.

Shirai, K., Schöne, B. R., Miyaji, T., Radermacher, P., Krause, R. A. Jr., Tanabe, K., 2014. Assessment of the mechanism of elemental incorporation into bivalve shells (*Arctica islandica*) based on elemental distribution at the ultrastructural scale. Geochim. Cosmochim. Acta 126, 307–320.

Soldati, A.L., Jacob, D.E., Glatzel, P., Swarbrick, J.C., Geck, J., 2016. Element substitution by living organisms: the case of manganese in mollusc shell aragonite. Sci. Rep. 6, 22514.

Son, S., Newton, A. G., Jo, K.-n., Lee, J.-Y., Kwon, K. D., 2019. Manganese speciation in Mn-rich CaCO3: A density functional theory study. Geochim. Cosmochim. Acta 248, 231–341.

Speer, J. A., 1983. Crystal chemistry and phase relations of orthorhombic carbonates. Reviews in Mineralogy 11, 145–225.

Strahl, J., Dringen, R., Schmidt, M.M., Hardenberg, S., Abele, D., 2011. Metabolic and physiological responses in tissues of the long-lived bivalve *Arctica islandica* to oxygen deficiency. Comp. Biochem. Physiol. A158, 513–519.

Sundby, B., Silverberg, N., Chesselet, R., 1981. Pathways of manganese in an open estuarine system. Geochim. Cosmochim. Acta 45, 293–307.

Taylor, A.C., 1976. Burrowing activity and anaerobiosis of the bivalve *Arctica islandica* (L.). J. Mar. Biol. Ass. U.K. 56, 95–105.

Tebo, B.M., 1991. Manganese(II) oxidation in the suboxic zone of the Black Sea. Deep-Sea Res. 38, Suppl. 2, S883–S905.

Theede, H., 1973. Comparative studies on the influence of oxygen deficiency and hydrogen sulphide on marine bottom invertebrates. Neth. J. Sea Res. 7, 244–252.

Theede, H., Ponat, A., Hiroki, K., Schlieper, C., 1969. Studies on the resistance of marine bottom invertebrates to oxygen-deficiency and hydrogen sulphide. Mar. Biol. 2, 325–337.

Trutschler, K., Samtleben, C., 1988. Shell growth of *Astarte elliptica* (Bivalvia) from Kiel Bay (Western Baltic Sea). Mar. Ecol. Prog. Ser. 42, 155–162.

Tyson, R. V., Pearson, T.H., 1991. Modern and ancient continental shelf anoxia: an overview. Geol. Soc. London Spec. Publ. 58, 1–24.

Vanquer-Sunyer, R., Duarte, C.M., 2008. Thresholds of hypoxia for marine biodiversity. Proc. Nat. Acad. Sci. 105, 15453–15457.

Wada, K., Fujinuki, T., 1976. Biomineralization in bivalve molluscs with emphasis on the chemical composition of the extrapallial fluid. In: N. Watabe, K.M. Wilbur (Eds.), The Mechanisms of Mineralization in the Invertebrates and Plants. Univ South Carolina Press, 175–190.

Wanamaker, A.D. Jr., Gillikin, D. P., 2019. Strontium, magnesium, and barium incorporation in aragonitic shells of juvenile *Arctica islandica*: Insights from temperature controlled experiments. Chem. Geol. 526, 117–129.

Wanamaker, A. D. Jr., Kreutz, K. J., Wilson, T., Borns, H. W. Jr., Introne, D. S., Feindel, S., 2008. Experimentally determined Mg/Ca and Sr/Ca ratios in juvenile bivalve calcite for *Mytilus edulis*: implications for paleotemperature reconstructions. Geo-Mar. Lett. 28, 359–368.

Weigelt, M., Rumohr, H., 1986. Effects of wide range oxygen depletion on benthic fauna and demersal fish in Kiel Bay 1981-1983. Meeresforsch. 31, 124–136.

Winter, J. E., 1969. Über den Einfluß der Nahrungskonzentration und anderer Faktoren auf Filtrierleistung und Nahrungsausnutzung der Muscheln *Arctica islandica* und *Modiolus modiolus*. Mar. Biol. 4, 87–135.

Zettler, M. L., 2001. Recent geographical distribution of the *Astarte borealis* species complex, its nomenclature and bibliography (Bivalvia: Astartidae). Schr. Malakozool. 8, 1–14.

Zettler, M.L., Bönsch, R., Gosselck, F., 2001. Distribution, abundance, and some population characteristics of the ocean quahog, *Arctica islandica* (Linnaeus, 1767) in the Mecklenburg Bight (Baltic Sea). J. Shellf. Res., 20, 161–169.

Zhao, L., Walliser, E.O., Mertz-Kraus, R., Schöne, B.R., 2017a. Unionid shells (*Hyriopsis cumingii*) record manganese cycling at the sediment-water interface in a shallow eutrophic lake in China (Lake Taihu). Palaeogeogr. Palaeoclimatol. Palaeoecol. 484, 97–108.

Zhao, L., Schöne, B. R., Mertz-Kraus, R., 2017b. Controls on strontium and barium incorporation into freshwater bivalve shells (*Corbicula fluminea*). Palaeogeogr. Palaeoclimatol. Palaeoecol. 465, 386–394.

5 Shell microstructures (disturbance lines) of *Arctica islandica* (Bivalvia): a potential proxy for severe oxygen depletion

Nils Höche[1], Michael L. Zettler[2], Xizhi Huang[1], Bernd R. Schöne[1]

1 Institute of Geosciences, University of Mainz, Mainz, Germany
2 Leibniz Institute for Baltic Sea Research Warnemünde, Rostock, Germany

Höche, N., Zettler, M.L., Huang, X., and Schöne, B.R. (2023). Shell microstructures (disturbance lines) of *Arctica islandica* (Bivalvia): a potential proxy for severe oxygen depletion. Frontiers in Marine Science, 10, 1219716.

This manuscript was published in the journal "*Frontiers in Marine Science*". I contributed to the formal analysis, the interpretation and discussion of the results, the review and editing of the final manuscript. This work was supported by the DFG grant to BRS [SCHO793/22-1] and [SCHO793/23-1].

Authors' contributions:

NH: Data curation, Formal analysis, Investigation, Methodology, Validation, Visualization, Writing – original draft, Writing-review and editing.

MLZ: Resources, Writing-review and editing.

XZH: Formal analysis, Writing-review and editing.

BRS: Conceptualization, Formal analysis, Funding acquisition, Investigation, Methodology, Project administration, Resources, Supervision, Validation, Visualization, Writing – original draft, Writing-review and editing,

Abstract

The spread of oxygen deficiency in nearshore coastal habitats endangers benthic communities. To better understand the mechanisms leading to oxygen depletion and eventually hypoxia, predict the future development of affected ecosystems, hypoxia, predict the future development of affected ecosystems and define suitable mitigation strategies requires detailed knowledge of the dissolved oxygen (DO) history. Suitable high-resolution DO archives covering coherent time intervals of decades to centuries include bivalve shells. Here, we explored if the microstructure, specifically, disturbance lines, in shells of *Arctica islandica* from the western Baltic Sea can be used as an alternative or complementary proxy to Mn/Ca_{shell} to track the frequency and severity of past low-DO events. Disturbance lines differ from periodic annual growth lines by the presence of fine complex crossed lamellae instead of irregular simple prisms. Aside from a qualitative assessment of microstructural changes, the morphology of individual biomineral units (BMU) was quantitatively determined by artificial intelligence-assisted image analysis to derive models for DO reconstruction. As demonstrated, Mn-rich disturbance lines can provide a proxy for past deoxygenation events (i.e., DO < 45 µmol/L), but it currently remains unresolved if low-DO leads to microstructurally distinct features that differ from those caused by other environmental stressors. At least in studied specimens from the Baltic Sea and Iceland, neither low temperature, salinity near the lower physiological tolerance nor food scarcity resulted in disturbance lines. With decreasing DO supply, disturbance lines seem to become more prominent, contained more Mn and consisted of increasingly smaller and more elongated BMUs with a larger perimeter-to-area ratio. Although the relationship between DO and BMU size or elongation was statistically significant, the explained variability (< 1.5 %) was too small and the error too large to reconstruct DO values. BMU parameters may reveal a closer relationship with DO if studied in three dimensions and if the DO content was determined at high-resolution, directly at the position where the bivalves lived, something that future work should address.

6.1 Introduction

There is growing concern about the rapid spread of bottom hypoxia in nearshore coastal habitats (Conley et al., 2009; Carstensen et al., 2014a; Fennel and Testa, 2019). Severe oxygen depletion can have deleterious effects on marine biodiversity and ecosystem functioning (Karlson et al., 2002; Vaquer-Sunyer and Duarte, 2008; Zillén et al., 2008). Specifically, dissolved oxygen (DO) levels below 2.3 mg/L (equivalent to 1.7 mL/L or 71.9 µmol/L at 1 atm and 10 °C) are lethal for most biota (Vaquer-Sunyer and Duarte, 2008) as proper breathing is then no longer possible (Herreid, 1980). This DO threshold marks the transition from normoxia to hypoxia. Furthermore, deoxygenation can result in an enhanced porewater efflux of nutrients into the overlying water body, which further increases eutrophication leading to enhanced primary production, organic carbon export to the seafloor and subsequent oxygen loss in bottom waters (Conley et al., 2007; Österblom et al., 2007; Carstensen et al., 2014a).

In order to better comprehend the mechanisms leading to oxygen depletion (Andrén et al., 2000; Carstensen et al., 2014b), identify the ecosystem baseline (Sohlenius et al., 2001; Zillén et al., 2008), predict the future development of oxygen availability and define proper mitigation and ecosystem restoration strategies (Carstensen et al., 2014a; Caballero-Alfonso et al., 2015), a detailed knowledge of the DO history on seasonal to decadal time-scales is required. However, even in the Baltic Sea, the largest and best studied oxygen-depleted setting (Carstensen and Conley, 2019), this is not the case. The ultimate causes for coastal deoxygenation remain incompletely understood mainly due to short and incomplete instrumental data sets (online database of the Leibnitz-Institut für Ostseeforschung Warnemünde, 2021, at https://odin2.io-warnemuende.de/; last access: 20 Nov. 2022) and low-resolution proxy archives (e.g., Westman and Sohlenius, 1999; Filipsson and Nordberg, 2004; Osterman et al., 2005; Jilbert and Slomp, 2013). While sediments provide extremely valuable insights into the long-term DO trends and cycles (Jilbert and Slomp, 2013), little is known on short-term fluctuations of bottom-water oxygen supply. Suitable high-resolution DO archives obtained by geochemical analysis include fish otoliths (Limburg et al., 2011) and, as recently demonstrated, shells of bivalve mollusks (Zhao et al., 2017; Schöne et al., 2021, 2022).

As shown by numerous studies, shells of bivalves can serve as very powerful, temporally well-constrained in-situ archives providing information on seasonal to inter-annual changes of environmental conditions – including DO – over coherent time intervals of decades to centuries (Weidman et al., 1994; Witbaard et al., 1997; Wanamaker Jr et al., 2012; Lohmann and Schöne, 2013; Reynolds et al., 2017; Edge et al., 2021). The shells of the sessile animals

grow on a periodic basis resulting in a distinct pattern of alternating growth increments (fast growth) and lines or band (slow growth) which can be used to place each shell portion into precise temporal context and determine the ontogenetic age of the bivalves (Belding, 1910; Jones, 1980). According to sclerochronological analyses, some species such as *Arctica islandica* attain a lifespan of nearly 400 to more than 500 years (Schöne et al., 2005a; Wanamaker Jr et al., 2008; Butler et al., 2013). Environmental changes experienced during life are recorded in the shells in the form of variable growth increment widths, chemical and microstructural properties (e.g., Epstein and Lowenstam, 1953; Jones et al., 1989; Milano et al., 2017). For example, when exposed to physiological stress (i.e., temperature, DO outside physiological tolerance), *A. islandica* forms disordered microstructures and a large number of disturbance lines in its shell (Dunca et al., 2009; Höche et al., 2021, 2022a). Furthermore, shell Mn/Ca ratios are negatively correlated to DO in the water column, because sedimentary manganese can be remobilized under reducing conditions, i.e., absence of oxygen (Schöne et al., 2021, 2022). Few species such as *A. islandica* are also highly tolerant against low oxygen supply and can survive in the complete absence of oxygen (anoxia) and even presence of H_2S (euxinia) for several weeks or months (Theede et al., 1969; Dries and Theede, 1974; Oeschger, 1990). Under such hostile conditions, they leave their valves closed and switch to an anaerobic metabolism (Theede et al., 1969; Oeschger, 1990). The generated acidic metabolites are then neutralized by the dissolution of inner shell surfaces (Crenshaw and Neff, 1969; Crenshaw, 1980). Specimens from the Baltic Sea thus tend to be very thin (< 1.5 mm) and fragile with the inner shell layer and parts of the inner portion of outer shell layer missing (pers. communication Weigelt cited in Oeschger, 1990; Schöne, 2013).

In the present study, we explored if the shell microstructure, specifically, disturbance lines can be used as an alternative or complementary proxy to Mn/Cashell values to track the number and severity of past low-oxygen events. So far, descriptions of microstructural changes in shells of bivalves from stressful environments remain descriptive (Clark, 1974; Kennish and Olsson, 1975; Dunca et al., 2009; Cardoso et al., 2013; Höche et al., 2021) and no detailed microstructural comparison of shells from oxygen-depleted and normoxic environments has been undertaken. For that purpose, here, the microstructure properties of *A. islandica* shells from NE Iceland (well-oxygenated habitat) were compared to specimens from the western Baltic Sea (Mecklenburg Bight, Fehmarn Belt) which were exposed to seasonally recurring oxygen depletion, occasionally hypoxia. Aside from a qualitative assessment of microstructural changes, the morphology of individual biomineral units (size, elongation, solidity, perimeter-to-size ratio, and coverage) was quantitatively determined by means of artificial intelligence-

assisted image analysis to derive models for the reconstruction of DO. Results of our study can help to obtain better insights into the historical development of low-oxygen environments.

5.2 Material and methods

Eight *A. islandica* specimens were collected alive between 2001 and 2020 by dredging from two different regions in the North Atlantic realm, namely the western Baltic Sea (n = 4; three specimens from Mecklenburg Bight, one specimen from Fehmarn Belt) and NE Iceland (n = 4; Þistilfjörður) (Table 5.1; Fig. 5.1). All specimens were used for microstructure analyses via scanning electron microscopy (SEM). SEM analysis was preferred over more sophisticated analytical techniques such as EBSD, high-resolution electron backscatter diffraction (used, e.g., by Karney et al., 2012), in order to study large areas of shell in adequate time. In addition, we were interested in identifying a method that can be applied by a large number of laboratories, i.e., SEM is more often available than EBSD machines. In three specimens per region, individual biomineral units (BMUs) were quantitatively characterized, and in the remaining specimen, the microstructure was qualitatively described (Table 5.1). All except one specimen from NE Iceland were used in previous studies targeting the element chemistry (in particular, Mn/Ca_{shell} and Ba/Ca_{shell}) and the seasonal timing and rate of shell growth (see Table 5.1 and references provided in table caption).

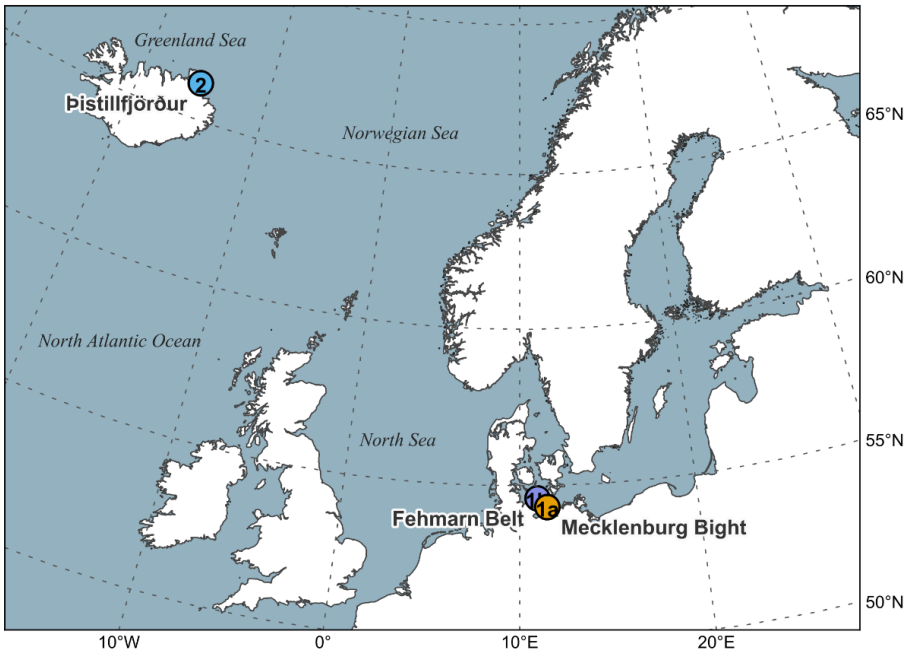

Figure 5.1. Map showing the regions where *Arctica islandica* specimens were collected. (1) Western Baltic Sea, (2) NE Iceland.

Table 5.1. List of *Arctica islandica* shells used in present study. Wd = water depth; BMU morphometry = morphometric analysis of individual biomineral units (quantitative analysis) of specimens ultra-polished with 60 nm Buehler MasterMet suspension; qualitative analysis was done on polished sections etched for 10 seconds in 1 M HCl. Cal. = calendar. Shells used previously for sclerochronological analyses: a = Schöne et al. (2021): Mn/Ca_{shell}, Ba/Ca_{shell}, seasonal timing and rate of shell growth (STR), annual shell growth in hinge (ASGh); b = Schöne et al. (2022): Mn/Ca_{shell}, Ba/Ca_{shell}, STR, ASGh; c = Höche et al. (2022): STR, morphometry of individual biomineral units within the annual increment (without disturbance lines and annual growth lines).

Region	Sample site	Specimen ID	Lon/Lat	Wd (m)	Date of death	Cal. years studied	#SEM images	Microstructure analysis
1: W Baltic Sea	Mecklenburg Bight	MLZ-St12-A4R[a,b,c]	54°18'59.50"N, 011°33'00.00"E	24.8	25.10. 2001	1986 – 2001	247	BMU morphometry
		MLZ-St12-A6R[a,b,c]				1987 – 2000	384	
		MLZ-St12-A7L[a,b]				1997 – 2000	325	
	Fehmarn Belt	MLZ-FBR36-A6R[b]	54°35'53.67"N, 011°00'34.24"E	21	29.06. 2020		1112	Qualitative analysis
2: NE Iceland	Þistilfjörður, NE Iceland	ICE06-6.2-A6R[c]	66°11'22.26"N, 015°21'09.54W	6.6	17.08. 2006	1994 – 2006	566	BMU morphometry
		ICE06-6.2-A11R[c]				2001 – 2006	173	
		ICE06-6.2-A16R[c]				1992 – 2006	154	
		ICE06-6.2-A56R					2519	Qualitative analysis

5.2.1 Sample preparation

For sclerochronological analyses, three ca. 3 mm-thick sections were cut from one valve of each specimen along the axis of maximum growth (Fig. S5.1). One of the sections was used for growth pattern analyses, the mirroring side for in-situ chemical analyses, and the remaining shell slab for microstructure investigations. Before sectioning, the shells were covered along the cutting axis with an approx. 1 – 1.5 cm wide and 0.3 cm thick protective layer of metal epoxy resin (WIKO EpoFix 05). To mount the shells for cutting, acrylic glass blocks were attached to the anterior side of the valves using plastic welder (WIKO Multi Power 03). Specimens were then sliced at approx. 200 rpm using a rotational low-speed saw (Buehler IsoMet 1000) equipped with a 0.4 mm-thick diamond-coated blade (Buehler 15LC 11-4255). After cutting, the shell slabs were ground on glass plates using F800 and F1200 SiC grit powders (suspended in deionized water) and then polished on a polishing cloth (Buehler MasterTex) using a 1 µm Al_2O_3 suspension. After each grinding and polishing step, the samples were

ultrasonically rinsed with deionized water. Sections used for growth pattern analysis were then mounted to glass slides using metal epoxy (WIKO EpoFix 05).

5.2.2 Growth pattern analysis and temporal alignment of the growth record

For growth pattern analysis, one polished slab of each specimen was immersed in Mutvei's solution (Schöne et al., 2005b) for 20 minutes at 37 to 40 °C under constant stirring. This treatment facilitated the recognition of annual growth lines. Stained sections were then photographed with a digital camera (Canon EOS 600D) mounted to a reflected-light binocular microscope (Zeiss Stemi 508). Samples were illuminated with sectoral (= one-quarter) dark-field ring-light illumination (Schott VisiLED MC1000). Growth pattern analyses were carried out on stitched images (Microsoft Image Composite Editor) using the image analysis software ImageJ (Schneider et al., 2012; Schindelin et al., 2015; Rueden et al., 2017). The number of annual increments provided information on the lifespan of the studied specimens and helped to assign each shell portion to a precise calendar year. The time of the year represented by each SEM image was determined based on its the relative position between consecutive annual growth lines and existing seasonal growth models for the study sites (Schöne et al., 2021; Höche et al., 2022a). For details on the seasonal dating procedure see also (Schöne et al., 2021). These growth models not only provided information on the timing of seasonal shell growth, but also on daily growth rates (in %).

5.2.3 Microstructure analysis via SEM

Shell microstructures (see review in, e.g., Checa, 2018) consist of hierarchically organized BMUs which can be rounded as in the homogeneous microstructures (HOM) or needle-shaped as in crossed-lamellar, fine complex crossed-lamellar (FCCL) and crossed-acicular (CA) microstructures. Each BMU is enveloped by intercrystalline and interwoven with intracrystalline organic matrices (proteins, lipids, sugars, etc.) (Bevelander and Nakahara, 1980; Marin et al., 2012).

In the present study, different preparation techniques were employed for qualitative and quantitative analyses (Table 5.1) of the microstructural properties of the shells. For qualitative analyses, the third polished shell section of each specimen was briefly (10 sec.) immersed in diluted (1 M) hydrochloric acid to generate a topographical relief highlighting the BMUs. Immediately after etching, specimens were rinsed with demineralized water and air-dried, and then coated with a 5 nm-thick platinum layer using a sputter coater (Leica EM ACE200). For quantitative BMUs analyses, the same shell slabs were first repolished with 1 µm Al_2O_3

suspension and subsequently ultra-polished with an alkaline polishing agent (Buehler MasterMet, 60 nm grain size) and sputter-coated with Pt.

Microstructure investigations were conducted with a Desktop SEM (Phenom Pro, 3rd generation) equipped with a CeB_6 electron source backscatter electron detector at 10 keV. For qualitative assessment of the HCl-etched shells, mappings of large shell regions were generated automatically by stitching up to 400 individual images together. Each SEM image was taken at approx. 3,500× magnification. Quantitative measurements of the BMU shape were performed on individual SEM images taken at a magnification of approx. 7,500×. When viewed under backscatter SEM, the intercrystalline organic envelopes appeared black, while BMUs appeared in shadings of gray reflecting variations in the amount of intracrystalline organics. This approach greatly facilitated the quantitative BMU analysis.

5.2.4 Automated measurement of the BMU shape

SEM images taken for quantitative analysis of the BMU size and shape were fed into the machine-learning-based image segmentation software ilastik (Berg et al., 2019). For details on how this software can assist in microstructure analysis, the reader is referred to (2022a). In brief, the program classifies each pixel of the SEM images (Fig. S5.2A) as belonging to either a BMU or the interstitial space (= organic envelope, intercrystalline organic matrix) based on user-supplied examples and returns an image where the pixels of each BMU are labeled in an individual color, while the background is labeled black. This color-coded image (Fig. S5.2B) can then be used as an input for automatic particle analysis to obtain the morphological parameters of each BMU. Particle analysis was performed using the python programming language and the scikit-learn image analysis library (as well as with the image analysis software ImageJ using the plugin MorphoLibJ). The trained classifier used by ilastik is available in Höche et al. (2022b).

In addition to the BMU size, width, length, elongation, perimeter and coverage, which have already been studied in prior publications (e.g., Milano et al., 2017; Ballesta-Artero et al., 2018; Höche et al., 2021, 2022a), several novel shape parameters were investigated in the present study, namely (i) the perimeter-to-size ratio of the BMUs, which is a two-dimensional representation of the surface-to-volume ratio of three-dimensional particles and (ii) the BMU solidity, i.e., the size of the BMUs in relation to the size of the smallest convex polygonal envelope of the BMU (= BMU size / size of convex hull; Fig. S5.2C). This value decreases when a smaller proportion of the convex hull is filled out by the BMU, i.e., when the BMU has more crevices that are not filled with $CaCO_3$.

5.2.5 Statistical analyses

For specimens from the Baltic Sea, correlation analysis was performed between morphological parameters of the BMUs and environmental parameters. For this purpose, Spearman's rank correlation was used because BMU morphology data were not consistently normally distributed. In Baltic Sea shells, the properties of microstructures formed under well-oxygenated conditions were compared to such formed during low-oxygen conditions during summer. For this purpose, the time covered by the shell growth records was categorized into 'high-DO' and 'low-DO' intervals based on the oxygenation status during biomineralization. Since we do not know the DO concentration of the water inhaled by the bivalves (see also section 4.1), the average summer DO concentration of the study region (Mecklenburg Bight and Fehmarn Belt) at 5 m above the seafloor (where actual DO measurements were completed), i.e., 5 mL/L, was set as the boundary between 'high-DO' and 'low-DO'. Very likely, the formation of disturbance lines is coupled to the metabolic rate. According to Strahl et al. (2011), in *A. islandica* the metabolic rate decreases markedly below DO values of 5 kPa, which likely corresponds to the threshold set for the categorization into high and low-DO time intervals. An oxygen partial pressure of 5 kPa (measured at 1 atm and 10 °C; Strahl et al., 2011) corresponds to 0.43 mL/L, 1.62 mg/L or 44.93 µmol/L DO assuming the environmental conditions of the Mecklenburg Bight, i.e., a temperature of 7.5 °C, a salinity of 19.3 (averages during the studied time interval) and 24.8 m water depth (converted using Henry's law and the ideal gas constant). Subsequently, all BMU data of the 'low-DO' category were compared to such of the 'high-DO' category using non-parametric Mann-Whitney-U tests. An analogous comparison between low and high-salinity conditions was not performed, because salinity only causes severe stress in *A. islandica* below values of approx. 15 (Hiebenthal et al., 2012). Furthermore, salinity in Mecklenburg Bight only fell below this threshold on 25 days during the entire studied time interval.

5.2.6 Environmental conditions at the study sites

For comparison with the microstructure data, instrumental temperature, salinity, DO and chlorophyll a (Chl *a*) data were acquired for Þistilfjörður, NE Iceland, and Mecklenburg Bight, western Baltic Sea (Table 5.1). In case of Þistilfjörður, temperature data were obtained from Grímsey station (Hanna et al., 2006), and salinity data taken from satellite measurements (Gaillard et al., 2016). High-resolution DO time-series were not available for the site at NE Iceland, but given that the habitat belongs to the well-agitated surface water body and the sandy substrates prevail, permanent well-oxygenated conditions can be assumed. According to the World Ocean Atlas (https://www.ncei.noaa.gov; last access: 21 Nov. 2022), surface waters in

that region contained ca. 0.35 mol O_2 per g, corresponding to 11.2 mg/L or 4.9 mL/L O_2 at the water depth in which the bivalves lived, i.e., 6.6 m, and the local water temperature (see below). For Mecklenburg Bight, temperature, salinity and DO concentration data were taken from *in-situ* measurements in a water depth of 20 m at Station 12 (Zettler et al., 2017; online database, reference Leibnitz-Institut für Ostseeforschung Warnemünde, 2021, at https://odin2.io-warnemuende.de/, last access: 20 Nov. 2022), located ca. 172 m NW of the sampling site. Note, these DO data may overestimate the actual oxygen availability at the seafloor where the bivalves dwelled (see also discussion in Schöne et al., 2022). Within the timespan covered by the shell records (1986 – 2006; Table 5.1) the instrumental DO dataset (Fig. 5.2) comprises 179 points of data (on average, ca. nine per year), with 20 of them falling into summer months (i.e., one per year). All environmental datasets are provided in (Höche et al., 2022b).

The water at the study site at Mecklenburg Bight was, on average, >3 °C warmer than at NE Iceland (7.4 ± 3.5 °C vs 4.3 ± 2.3 °C; 1983 – 2012), but significantly lower in salinity (19.4 ± 2.7 vs 34.4 ± 0.2) and contained highly variable amounts of dissolved oxygen (2.0 – 8.9 mL/L vs ca. 4.2 – 5.1 mL/L) (Höche et al., 2022b). Food availability (Chl *a*) was nearly identical at both study sites (Mecklenburg Bight: 1.8 ± 0.7 mg/m^3, NE Iceland: 1.8 ± 0.8 mg/m^3), but more extreme in the Baltic Sea (0 – 10.3 vs 0.6 – 4.7 mg/m^3). Seasonal temperature and salinity amplitudes at Mecklenburg Bight (-0.4 – 16.9 °C; 14.9 – 28.9) clearly exceeded those at NE Iceland (-1.1 – 10.3 °C; 34.4 – 34.7). During summer, the study site at Mecklenburg Bight experienced temperatures as high as 12.2 ± 2.1 °C and salinities, Chl *a* level and DO concentrations of 23.6 ± 2.7, 1.76 ± 0.02 mg/m^3 and 3.0 ± 1.2 mL/L, respectively.

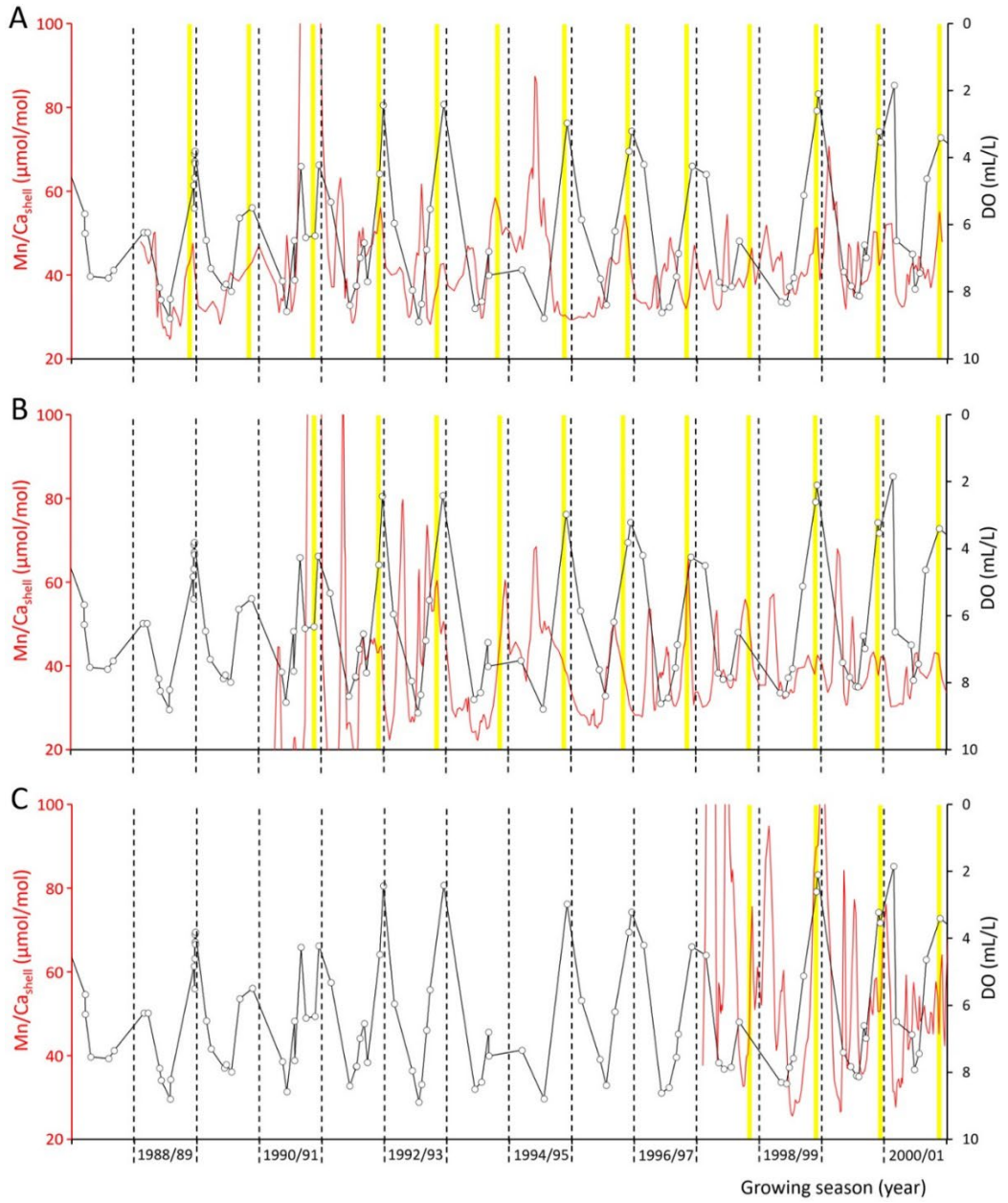

Figure 5.2. Shell Mn/Ca chronologies of the three studied *Arctica islandica* specimens from Mecklenburg Bight (A: MLZ-St12-A4R, B: …-A6R, C: …-A7L) in comparison to levels of dissolved oxygen (DO) measured 5 m above the seafloor. Open circles denote actual DO measurements, black connecting lines represent linearly interpolated DO data. Also shown are annual growth lines (black dashed lines) and disturbance lines (solid yellow lines). Note that the formation of disturbance lines occurs in summer (July / August) and typically falls together with the seasonal DO minimum and shell Mn/Ca maximum.

5.3 Results

After immersion in Mutvei solution, cross-sectioned shells revealed internal growth patterns, i.e., annual growth lines and – in case of specimens from the Baltic Sea – disturbance lines in both the hinge portion and the ventral margin (Fig. 5.3, S5.3+S5.4). Disturbance lines were typically developed shortly before the annual growth lines and typically fell together with the seasonal DO minima and shell Mn/Ca maxima (Fig. 5.2). As outlined further below, the two types of growth lines can be distinguished from each other by means of microstructure analysis. More distinct disturbance lines appeared to be associated with more severe oxygen depletion, but a quantification of this link was not possible. For example, more prominent disturbance lines were observed in summer 1995 and 1999 (i.e., growing seasons 1994/95 and 1998/99), but weaker lines during summer 1996 and 1998, although DO levels dropped to similarly low values in 1996 as in 1995 (Fig. 5.2, 5.3, S5.3+S5.4). In studied specimens from NE Iceland (well-oxygenated habitat), no disturbance lines were developed (see Fig. S5.5).

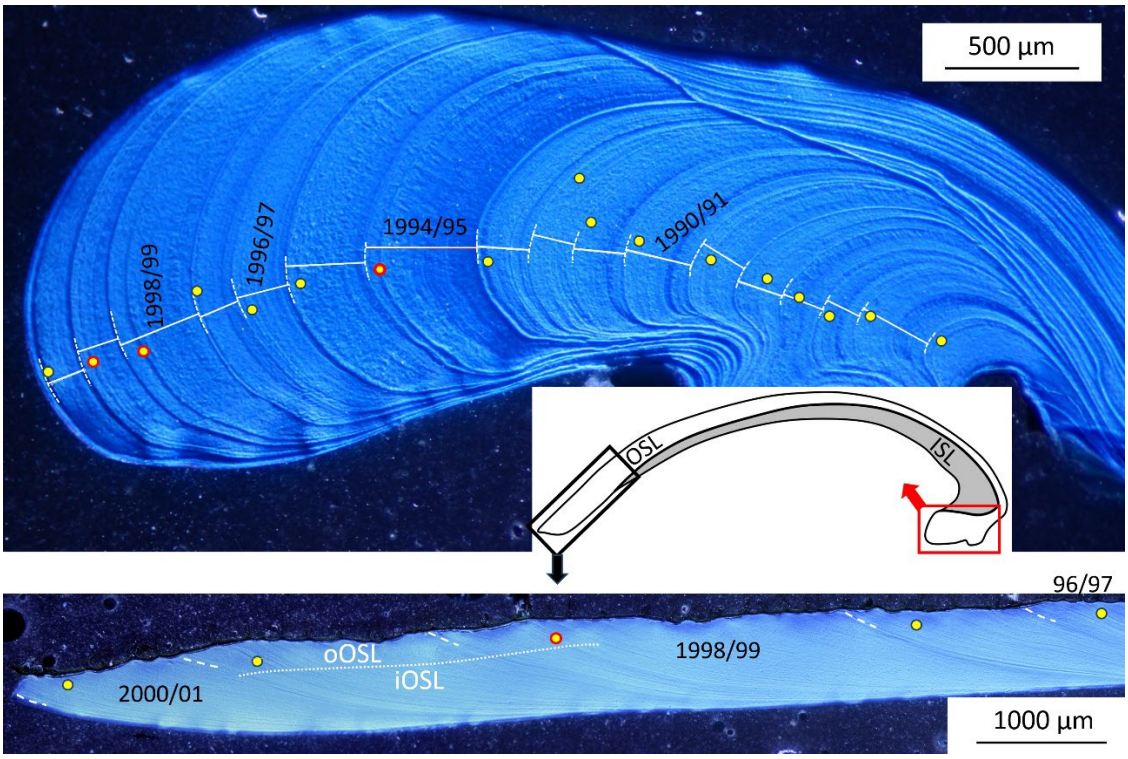

Figure 5.3. Mutvei-stained cross-section of an *Arctica islandica* specimen from Mecklenburg Bight (specimen MLZ-St12-A4R) showing annual growth lines (dashed white lines) and disturbance lines (yellow circles) in the hinge (upper panel) and the ventral margin (lower panel). Circles with red outline denote particularly prominent disturbance lines. OSL = outer shell layer; ISL = inner shell layer; oOSL, iOSL = outer and inner portions of the OSL.

5.3.1 Relationship between shell growth and environmental parameters

In the western Baltic Sea, shells of *A. islandica* grew up to 0.6 % of the annual growth increment within a single day (Höche et al., 2022a). In general, daily growth rates increased with higher oxygen supply (r = 0.55, p < 0.05; Fig. 5.4A). Fastest shell production (0.3 – 0.6 % of annual growth per day) was observed at DO concentrations above ca. 6 mL/L. Below this threshold, however, no more than 0.25 % of the annual growth increment were produced per day. Shell growth was also negatively correlated to water temperature (r = -0.54, p < 0.05; Fig. 5.4B). Fastest growth rates occurred between 2.5 and 5 °C. In contrast, at Iceland, growth rates were weakly positively linked to the water temperature (r = 0.22, p < 0.05), and daily shell growth varied between 0.1 to 1 % of the annual increment (Fig. 5.4B).

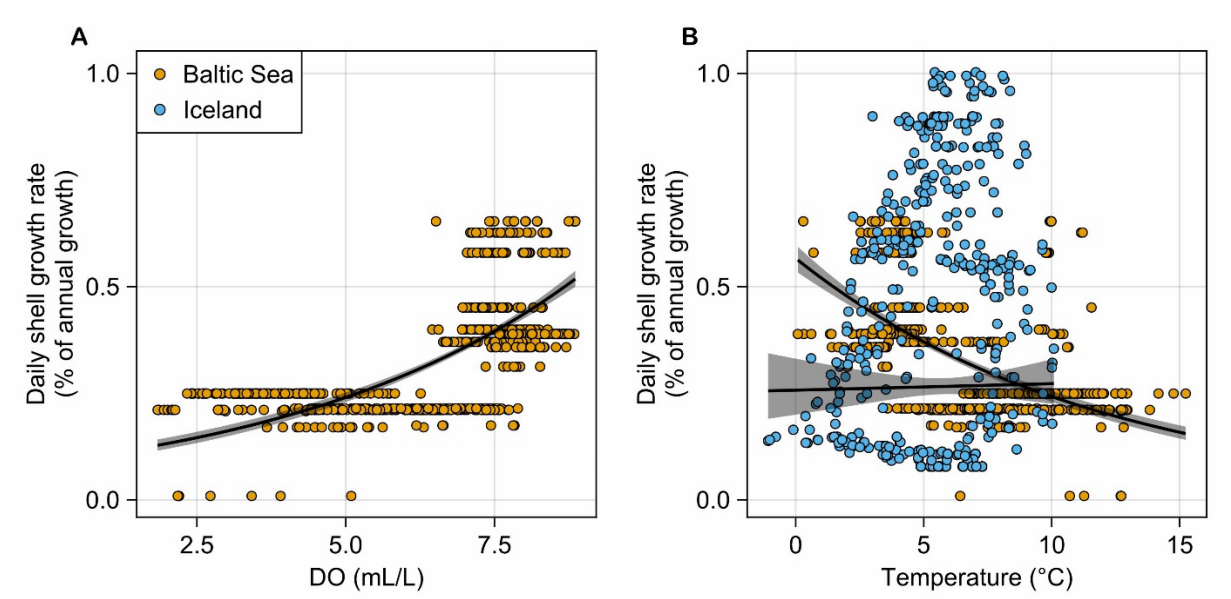

Figure 5.4. Correlation between intra-annual shell growth rate of *Arctica islandica* and environmental variables. Note that data were pooled from three specimens per site and the regression curves thus treat all data points as independent variables. (A) Specimens from the western Baltic Sea (Mecklenburg Bight) grew faster when DO levels were higher. Below DO concentrations of ca. 6 mL/L, shell growth rates were strongly reduced. (B) In the Baltic Sea, shell growth rates decreased with rising water temperature, but the opposite was observed in specimens from NE Iceland (Þistilfjörður). Note, DO concentration was measured 5 m above the sediment surface. Actual DO concentration experienced by the bivalves was much lower due to sedimentary porewater efflux.

6.3.2 Qualitative assessment of microstructural differences between localities

Irrespective of locality, the outer shell layer (OSL) of the ventral margin of the studied specimens (Table 5.1) was subdivided into microstructurally distinct sub-layers (Fig. 5.2), i.e., an outer portion (oOSL) dominated by HOM microstructure (Fig. 5.5A, D, G, J) and an inner portion (iOSL) in which CA microstructure prevailed (Fig. 5.5B, K). From the oOSL/iOSL transition (i.e., boundary between HOM and CA microstructure) toward the myostracum individual BMUs became gradually smaller and more elongated. In the innermost part of the

iOSL, i.e., the slowest growing portion near the myostracum, FCCL microstructure was observed (Fig. 5.5C, L).

In contrast, the hinge plate (portion formed in the outer extrapallial space, i.e., the same from which the oOSL of the ventral margin was precipitated) was microstructurally more uniform than the ventral margin and showed less gradual microstructural transitions (Fig. 5.6). CA microstructure prevailed, with occasional intercalations of FCCL microstructure (Fig. 5.6A, D, G, J). In shells from both study sites, the annual growth lines in the hinge and ventral margin were typically composed of ISP microstructure (e.g., Fig. 5.6B-C, E-F, I, K), but significant differences were detected regarding their relative proportions. In the following, these differences will be described in more detail.

5.3.2.1 Ventral margin

The HOM microstructure of the oOSL of the ventral margin was nearly identical at both localities, i.e., the size and elongation of individual BMUs were virtually indistinguishable (Fig. 5.5D, J). Likewise, irrespective of the habitat, the annual growth lines in the oOSL were composed of ISP microstructure (Fig. 5.5D-F, H-I). However, the annual growth ‘lines’ of the oOSL were much broader in specimens from the western Baltic Sea than in specimens from NE Iceland, especially underneath the periostracum, and are thus better ascribed as annual growth ‘bands’ rather than ‘lines’. The width of these bands decreased gradually from the outer shell surface toward the oOSL/iOSL transition where they attained nearly the same width as in specimens from NE Iceland (from here toward the myostracum referred to as ‘annual growth lines'; Fig. 5.5E-F, H-I).

Shells from the western Baltic Sea and NE Iceland differed more distinctly by the microstructures of the iOSL of the ventral margin than the oOSL (Fig. 5.5B-C, K-L). At both localities, the outer part of the iOSL (i.e., near the transition to the oOSL) was composed of CA microstructure (Fig. 5.5B, K), whereas FCCL dominated the innermost parts (near the myostracum; Fig. 5.5C, L). The appearance of these microstructures, however, differed between the two localities, as did their relative abundance. In specimens from the western Baltic Sea, CA BMUs were typically arranged in layers parallel to the growth front. Adjacent layers were separated from each other by a thin spacing or numerous voids arranged like a string of pearls (Fig. 5.5K). Prior to etching, the latter may have been filled with organic components. This layered arrangement also occurred in shells from Iceland, but it was largely constrained to regions near annual growth lines (Fig. 5.5E-F). Furthermore, specimens from the Baltic Sea contained much more voids within the iOSL than specimens from Iceland.

Locality-specific microstructural differences were also observed in the appearance of the annual growth lines of the iOSL. In Baltic Sea shells, the vicinity of annual growth lines was strongly enriched in organics as indicated by the broad, dark gray shadings in the SEM images (Fig. 5.5H-I), whereas only thin, distinct organic-rich lines were developed in specimens from Iceland (Fig. 5.5E-F). The recognition of annual growth lines was greatly facilitated in Islandic shells for two more reasons. Firstly, BMU sizes differed significantly before and after the annual growth lines, whereas nearly identical BMU sizes were observed in specimens from the Baltic Sea (Fig. 5.5E-F, H-I). Secondly, the annual growth lines in the iOSL of specimens from Iceland were composed of ISP microstructure (as within the oOSL) and thus deviated distinctly from the shell architecture in adjacent shell portions (Fig. 5.5E-F). In contrast, annual growth lines were much less prominent in specimens from the Baltic Sea, because they consisted of the same CA microstructure as the surrounding regions (Fig. 5.5H-I).

Furthermore, specimens from the Baltic Sea contained a large number of disturbance lines, which were missing in specimens from Iceland (and less well developed in the better oxygenated Fehmarn Belt site; Fig. 5.2, 5.4 and 5.5). These disturbance lines (Fig. 5.5L) were easily distinguishable from the annual growth lines (Fig. 5.5E-F, H-I) by the presence of FCCL microstructure, i.e., small, elongated BMUs, which were arranged in two predominant dipping angles (Fig. 5.5L). Disturbance lines were exclusively developed in shell portions that were strongly enriched in manganese (Fig. 5.2) (Schöne et al., 2021), i.e., shell portions that formed in the summer months during which dissolved oxygen in the water dropped markedly (Fig. 5.3).

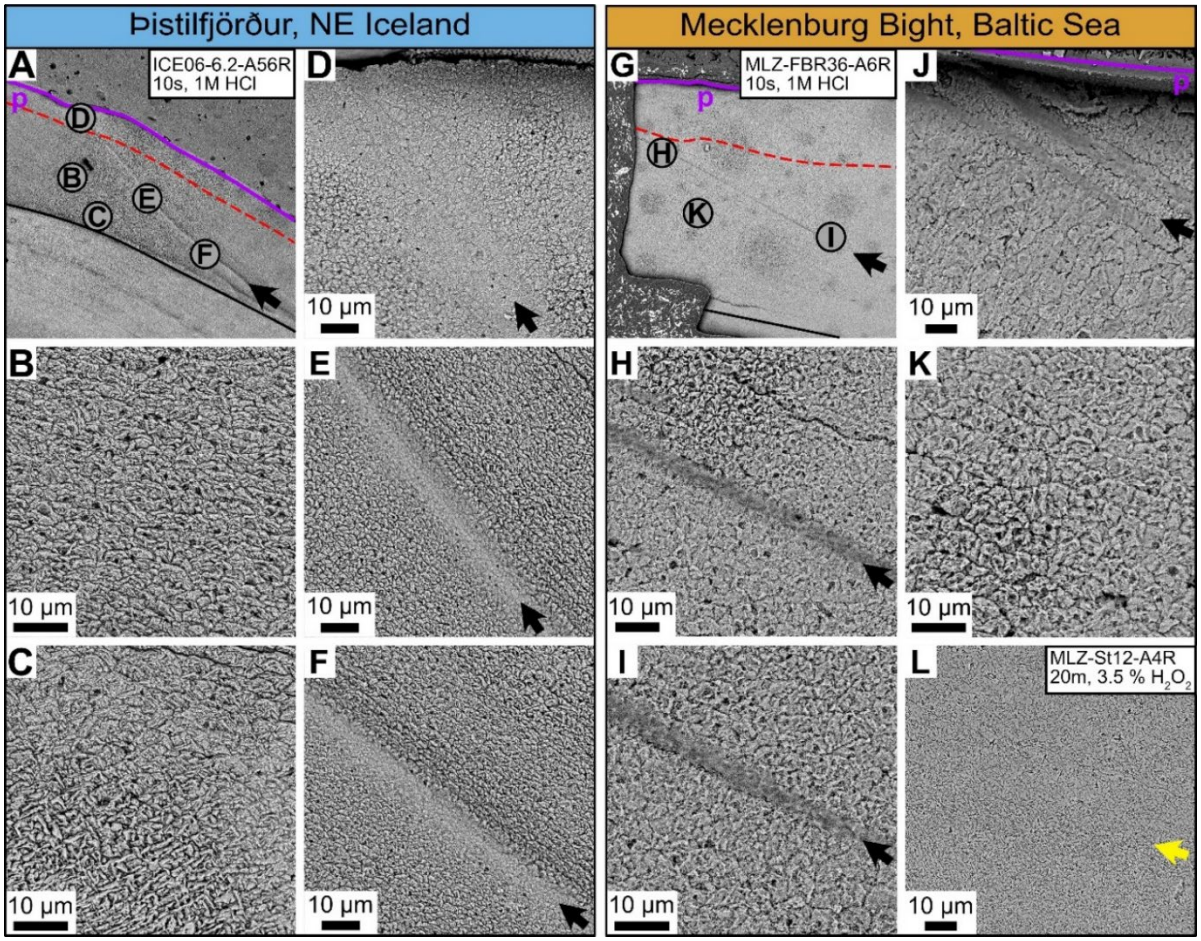

Figure 5.5. Microstructures in the ventral margin of *Arctica islandica* shells. Icelandic shells: left panel, blue header; shells from the Baltic Sea: right panel, orange header. The direction of growth is from the upper right to the lower left in all images. (A, G) SEM overviews showing the position of magnified shell portions (letters in gray circles) as well as the periostracum (p; purple line), the myostracum (black line) and the boundary between the inner and outer portion of the outer shell layer (dashed red line). (B, K) Crossed-acicular and (C, L) fine complex-crossed lamellar microstructures were formed in the annual increments toward the myostracum (bottom of the images). (K-L) Biomineral units (BMUs) in shells from the Baltic Sea were arranged in layers, traced by thin spacings (presumably filled with organics before preparation) and occasionally, voids were arranged like a row of pearls perpendicular to the growth direction. (B-C) This layered BMU arrangement including the voids was missing in shells from Iceland. (D, J) In the outermost portion of the outer shell layer, homogeneous microstructure was formed at both localities, with similar biomineral unit (BMU) morphologies, especially near the periostracum. (E-F) In shells from Iceland, BMU sizes varied strongly before and after an annual growth line (black arrows), but no strong enrichment of organic components was observed (which would be indicated by darker gray shadings). (H-I) In shells from the Baltic Sea, on the other hand, BMU sizes remained nearly unchanged before and after annual growth lines or bands, but the growth lines/bands contained larger amounts of organics and were much broader than at Iceland (dark gray shadings). (L) Disturbance lines (yellow arrow) in the ventral margin of Baltic Sea specimens consisted of fine complex crossed-lamellar microstructures with small and highly elongated BMUs.

5.3.2.2 Hinge

Regardless of locality, in the hinge plate (oOSL), the annual growth lines consisted of irregular simple prisms (Fig. 5.6A-C, E-F, G, I, K), while annual increments were predominantly composed of CA and FCCL microstructures (Fig. 5.6D, J). However, shells from NE Iceland and the western Baltic Sea differed by the relative proportion of these two microstructure types. In specimens from NE Iceland, FCCL microstructure was typically limited to regions adjacent to annual growth lines (Fig. 5.6B, E), whereas in shells from the Baltic Sea this microstructure also occurred within the annual increments (Fig. 5.6G-K).

Although the annual growth lines of the hinge plate of all studied specimens consisted of the same microstructure type (ISP), site-specific differences were observed at higher magnification (Fig. 5.6A-C, E-F, G, I, K). In Icelandic specimens, the irregular simple prisms were broader and much smaller and their boundaries less well-defined than in specimens from the Baltic Sea (Fig. 5.6B-C, E-F). In the latter, the annual growth lines consisted only of one layer of irregular simple prisms with clearly defined boundaries (Fig. 5.6I). Occasionally, the ISP layer was completely missing in specimens from the Baltic Sea and replaced by a thin organic layer (Fig. 5.6K). In addition, specimens from the Baltic Sea sometimes exhibited an extreme form of FCCL microstructure near the annual growth lines of the hinge. This unusual form consisted of highly elongated blocks of acute BMUs, arranged in alternating dipping directions (Fig. 5.6H), closely resembling the appearance of simple crossed-lamellar microstructures.

5.3.3 Quantitative assessment of microstructural differences between localities

The morphology of BMUs was quantitatively assessed in a total of 1,875 SEM images taken in six shells (Table 5.1). In the following, the relationships between different BMU shape parameters will be described. Then, the BMU shape data of the two localities will be contrasted to each other, and finally, for specimens from the Baltic Sea, data of shell regions formed under low and high DO will be compared with each other.

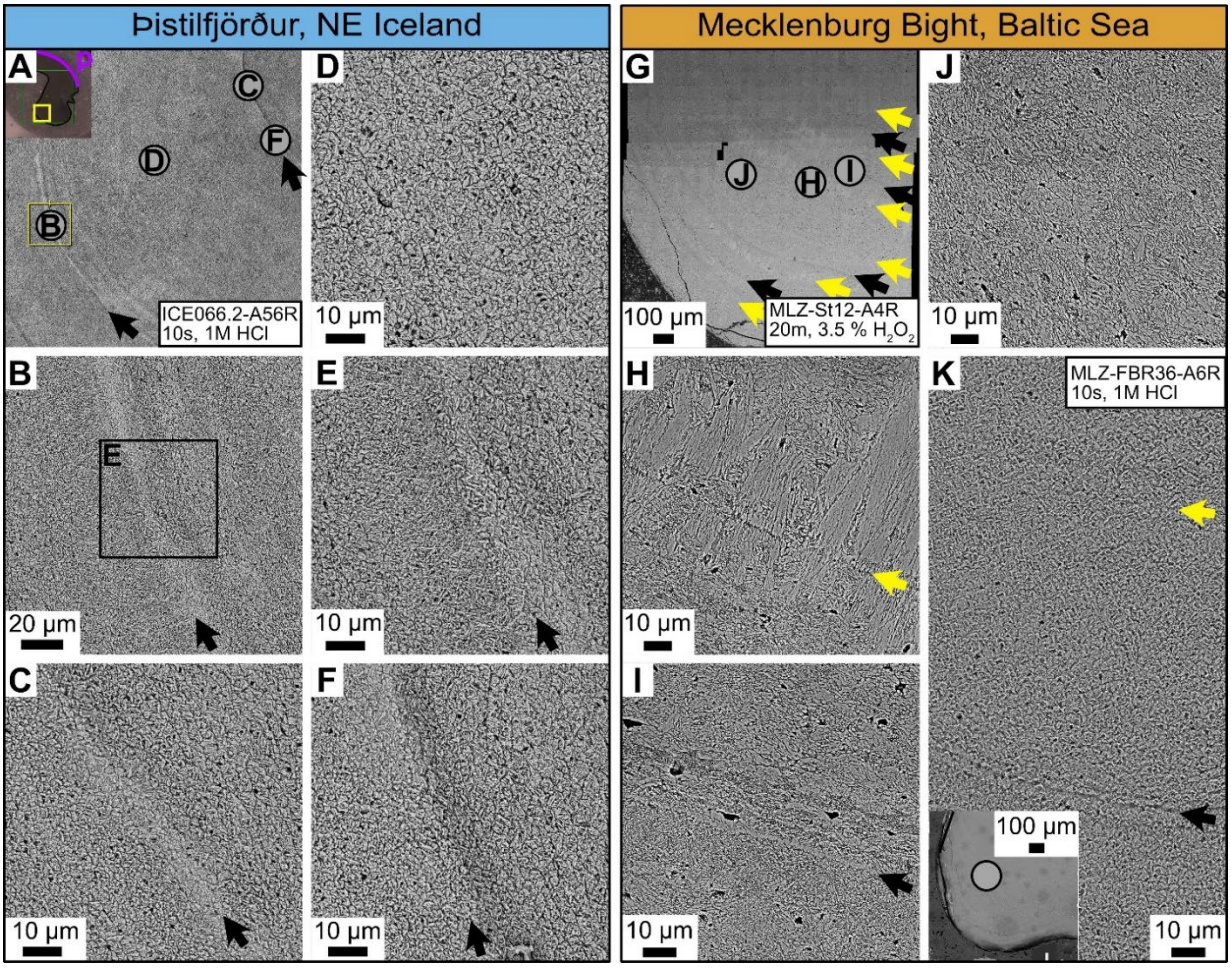

Figure 5.6. Shell microstructures in the hinge plate of *Arctica islandica*. Icelandic shells: left panel, blue header; shells from the Baltic Sea: right panel, orange header. (A, G) SEM overviews showing the position of panels B to F and H to I, respectively (letters in gray circles). The periostracum (p) is indicated by the purple line. (D, J) Within the annual increments, crossed-acicular and fine complex crossed-lamellar microstructures prevailed. Biomineral units (BMUs) in shells from Iceland appeared more rounded than those of shells from the Baltic Sea. The latter were more acute and frequently contained small voids (presumably filled with organics before preparation). (B-C, E-F) Annual growth lines (black arrows) in the hinge plates of Icelandic specimens had the same microstructural appearance as such in the ventral margin, i.e., BMU sizes varied strongly before and after the annual growth lines. (I, K) Annual growth lines of specimens from the Baltic Sea, in contrast, consisted of distinct bands (or layers) of irregular simple prismatic microstructure, and BMUs before and after the annual growth lines exhibited less variability in size than in specimens from Iceland. In addition, BMUs were more acute and elongated at the annual growth lines than in the annual increments. (H, K) Disturbance lines (yellow arrows) in the hinge plate of Baltic Sea specimens consisted of fine complex crossed-lamellar microstructure, interrupted by a thin, organic-rich layer, and occasionally clusters of untypically highly elongated BMUs.

5.3.3.1 Relationship between morphological parameters of BMUs

The size of BMUs of *A. islandica* shells of both localities was weakly but significantly positively correlated to the coverage of BMUs in the SEM images ($0.25 < r < 0.37$, $p < 0.05$), i.e., larger BMUs were associated with narrower interstitial spaces between them and thus less intercrystalline organic matrix (Fig. 5.6A). In addition, the BMU size was antiproportional to BMU elongation ($-0.20 < r < -0.37$, $p < 0.05$), i.e., larger BMUs were more rounded and smaller BMUs more elongated (Fig. 5.6B). The strongest inverse correlation was found between the size and the perimeter-to-size ratio of BMUs ($-0.90 < r < -0.91$, $p < 0.05$) – a parameter that has not yet been studied in the context of bivalve shell microstructures (Fig. 5.7C). Larger BMUs came with smaller perimeter-to-size ratios (Fig. 5.7C). The second newly studied microstructural parameter, the BMU solidity, was also negatively linked to BMU size ($-0.46 < r < -0.47$, $p < 0.05$) meaning that larger BMUs contained larger and more numerous notches and crevices. Larger BMUs thus appeared as less ideally shaped grains than smaller BMUs. All above-mentioned relationships occurred at both sites without obvious site-specific differences.

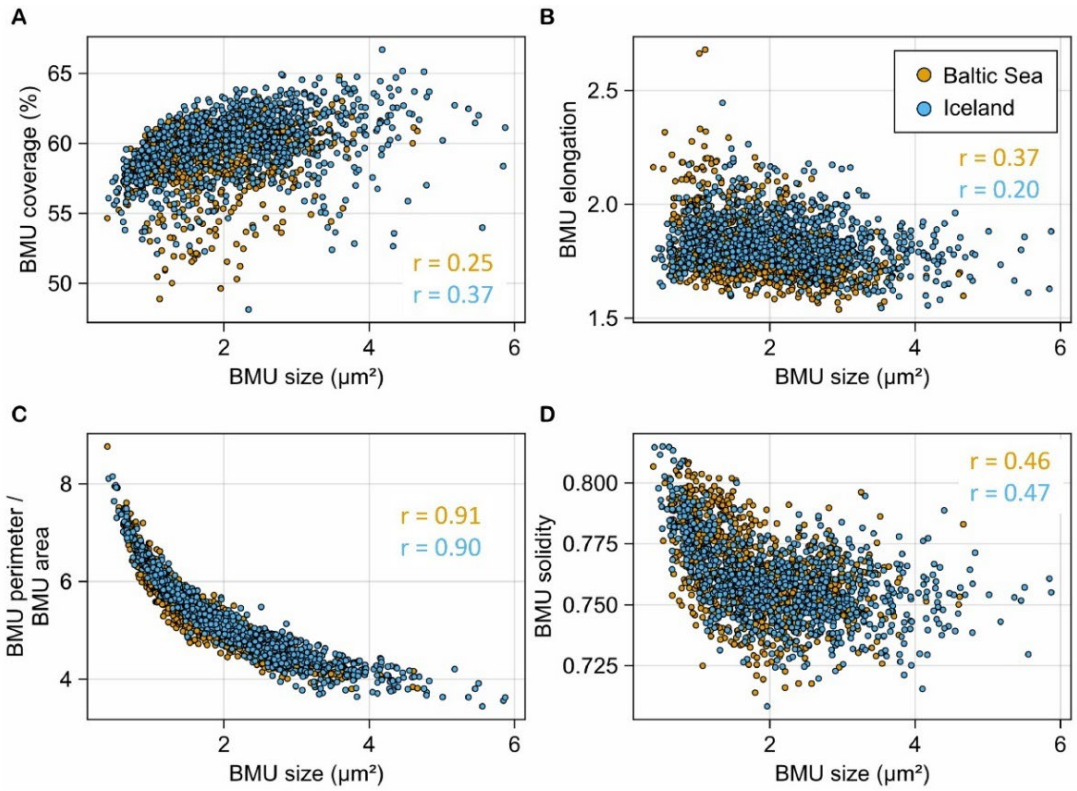

Figure 5.7. Microstructural parameters of six *Arctica islandica* shells (three from Mecklenburg Bight, orange; three from NE Iceland, blue) plotted against each other. (A) Coverage of the biomineral units (BMUs) in the SEM images was positively correlated with the BMU size. (B) BMU elongation, (C) the perimeter-to-area ratio of the BMUs, and (D) the BMU solidity were all negatively correlated with BMU size. All correlations are statistically significant ($p < 0.05$).

5.3.3.2 Site-specific differences in BMU morphology

Typically, BMUs of shells from NE Iceland were significantly larger than those of shells from the Baltic Sea (average of 2.18 versus 1.79 µm^2; Mann-Whitney-U-Test, $p < 0.05$), particularly in the ventral margin (Fig. 5.8A). The elongation of the BMUs of the ventral margin exhibited no significant difference between sites and equaled, on average approx. 1.8 for both sites (Fig. 5.8B). In the hinge, however, the elongation of BMUs differed significantly ($p < 0.05$) between sites. BMUs of specimens from the Baltic Sea were, on average, more elongated (2.0) than in shells from Iceland (1.8; Fig. 5.8B). The average BMU solidity, however, returned statistically indistinguishable values for both sites, i.e., 0.76 (Fig. 5.8C). The perimeter-to-size ratio of the BMUs (= two-dimensional surface area-to-volume ratio) was generally larger in the hinge than in the ventral margin. In both shell portions, perimeter-to-size ratios of BMUs of specimens from the Baltic Sea were significantly larger than those of specimens from Iceland ($p < 0.05$; 5.2 vs 4.5 in the ventral margin and 5.7 vs 5.3 in the hinge, respectively; Fig. 5.8D).

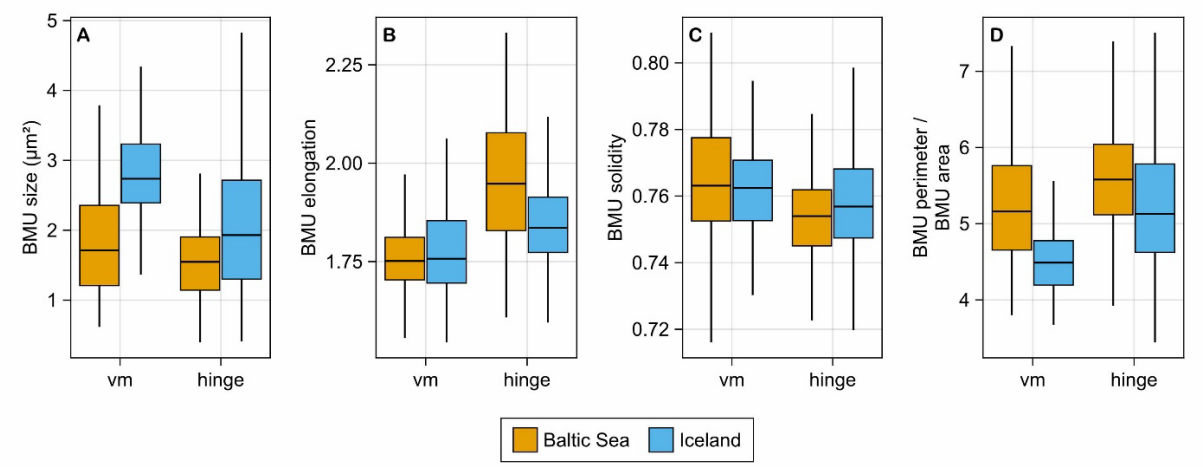

Figure 6.8. Morphological parameters of biomineral units (BMUs) in different shell portions of *Arctica islandica*. (A) BMU size, (B) elongation (C) solidity and (D) perimeter-to-area ratio.

5.3.3.3 Correlation between BMU morphology and environmental parameters as well as shell growth rate

In specimens from the Mecklenburg Bight, BMU elongation and solidity were weakly, but statistically significantly anticorrelated to DO concentration (r = -0.11 and -0.08, respectively; $p < 0.05$; Fig. 5.9). In addition, the BMU solidity was weakly, but significantly negatively correlated to salinity (r = -0.09, $p < 0.05$), while the opposite applied to BMU elongation and salinity (r = 0.12, $p < 0.05$). All other parameters, i.e., the BMU size, perimeter-to-area ratio and solidity were neither significantly linked with DO or salinity. Both BMU size and coverage were inversely coupled with temperature, while the BMU elongation revealed a positive correlation (r = -0.07, -0.11 and 0.16, respectively; $p < 0.05$). The BMU size was also significantly positively linked with the shell growth rate (r = 0.11, $p < 0.05$), whereas the opposite applied to BMU elongation and perimeter-to-area ratio (r = -0.15 and -0.11, respectively; $p < 0.05$).

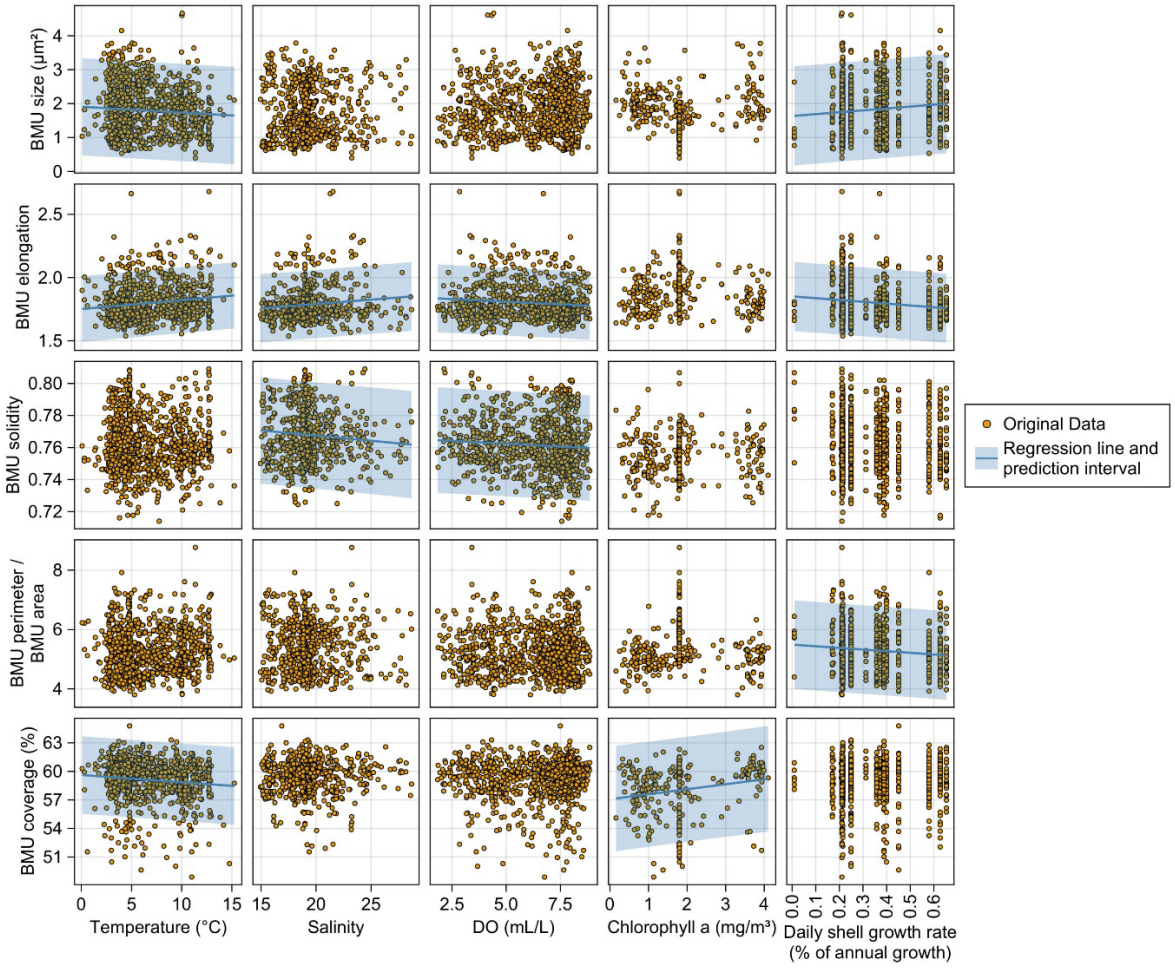

Figure 5.9. Scatterplots illustrating correlations between biomineral unit (BMU) morphology of *Arctica islandica* shells and environmental parameters. Only data of specimens from the Baltic Sea shown. In case of statistically significant correlations between parameters, lines and shaded areas are shown which represent linear regression models and their prediction intervals.

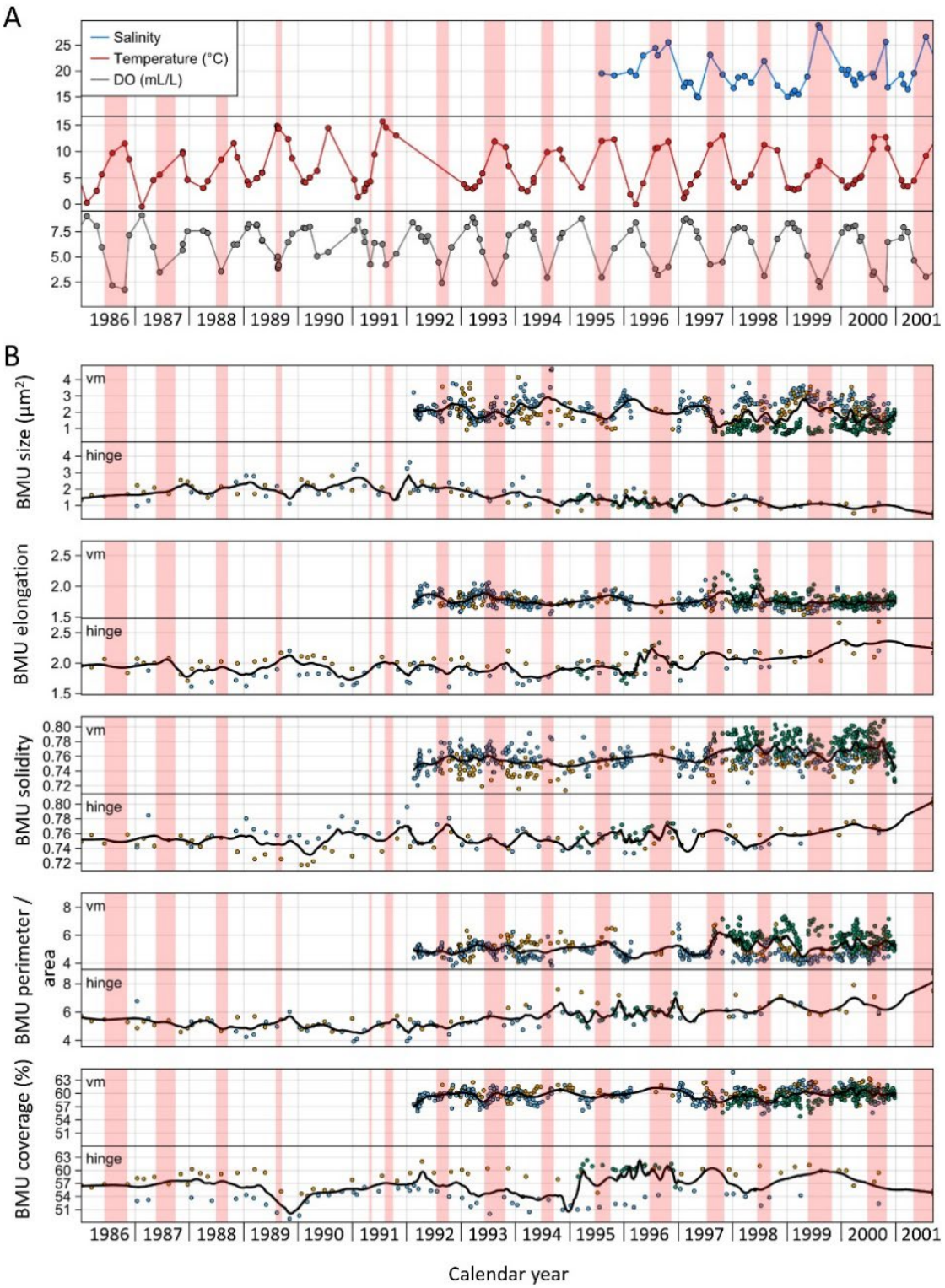

Figure 5.10. Temporal variability of (A) environmental parameters (temperature, salinity and dissolved oxygen) and (B) microstructural parameters of *Arctica islandica*. Only data of specimens from the Baltic Sea shown. (A) Circles represent in-situ measured data and lines represent daily interpolations. **(B)** For biomineral unit (BMU) size, elongation, solidity, and perimeter-to-area, each data point represents the median of all BMUs within one SEM image. Data of different specimens are shown in different colors (blue, orange, green). Curves represent LOESS models computed using a smoothing factor of 0.3 and representing changes of each parameter over time. Solid markers and black curves represent data from the ventral margin, whereas transparent markers and gray curves represent hinge plate data. Areas shaded in red represent time intervals with DO concentrations below 5 mL/L.

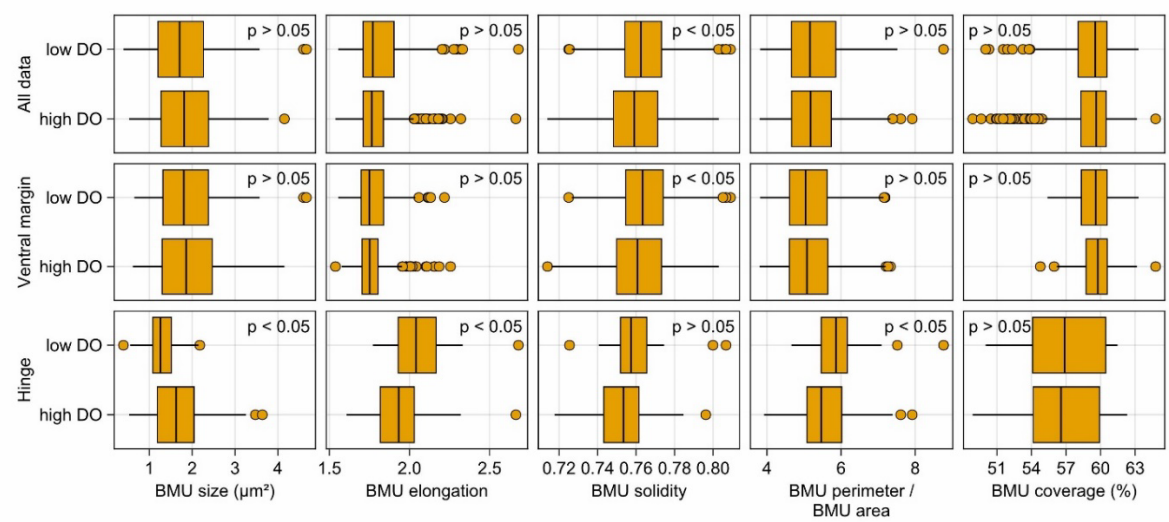

Figure 5.11. Biomineral unit (BMU) morphology of *Arctica islandica* at different dissolved oxygen concentrations. Only data of specimens from the Baltic Sea is shown. A threshold of 7 mL/L dissolved oxygen at the time of formation (≡ 743 µmol/L) was used for classification of BMU data into low and high dissolved oxygen categories.

5.3.3.4 Variations in BMU morphology over time

BMU parameters of specimens from the Baltic Sea exhibited substantial variability through ontogeny (Fig. 5.10). Data from the ventral margin showed similar patterns over time as data from the hinge, but the levels of change in the two shell portions did not always match. BMUs in the hinge were smaller and more elongated, had larger perimeter-to-area ratios and a lower BMU coverage (Figs 7A and 9). In the ventral margin, however, the BMU morphology of different specimens exhibited similar levels and highly synchronous variation through time, except for specimen MLZ-St12-A7L, which had approx. 1.0-1.5 µm^2 smaller and approx. 0.02 (i.e., 2 %) more solid BMUs than the remaining specimens (Fig. 5.10B). Typically, BMUs were largest in winter (~2.8 µm^2 during December and January), and smaller in summer (~1-2 µm^2). However, in year 1994, the annual BMU size maximum already occurred in fall, while in years 1997 to 2000, it occurred later (ca. spring to summer). BMUs were more rounded at the annual boundaries and more elongated during summer, i.e., nearly contemporaneously with the seasonal hypoxia. Exceptions from this pattern occurred during 1994 and 1996, when BMUs remained rounded even during summer. In case of the BMU solidity, perimeter-to-area ratio and coverage, no pronounced seasonal patterns could be identified, and values exhibited much more variation between specimens than for the remaining parameters.

In specimens from the Baltic Sea, several significant morphological differences were observed between BMUs precipitated below and above 5 mL/L DO (Fig. 5.11A). In the ventral margin, BMUs formed at low DO were significantly (Mann-Whitney-U test, $p < 0.05$) more solid (0.765 versus 0.762), whereas all other morphological parameters were unrelated to

oxygenation status. In the hinge plate, on the other hand, BMUs formed below 5 mL/L DO were significantly smaller (1.3 versus 1.7 μm^2), more elongated (2.06 versus 1.93) and had a higher perimeter-to-area ratio (5.95 vs. 5.57 $\mu m/\mu m^2$) than BMUs formed at higher DO concentration.

5.4 Discussion

As indicated by the results of this study, strongly reduced dissolved oxygen availability leads to the formation of disturbance lines in shells of *A. islandica* (Fig. 5.3), associated with a significant enrichment in manganese (Fig. 5.2). Disturbance lines were missing in shells of specimens from well-oxygenated sites at NE Iceland. Note, at this locality, shell manganese concentration remained below detection limit (Schöne et al., 2023). Disturbance lines can be microstructurally distinguished from periodic annual growth lines, because the former consist of fine complex crossed-lamellar microstructure, whereas annal growth lines are made of irregular simple prisms (Fig. 5.5+5.6). As demonstrated by previous studies, the two types of growth lines can also be distinguished by means of trace element analysis, because disturbance lines occur in shell portions that are strongly enriched in manganese, whereas the annual growth lines fall together with sharp Mg/Ca_{shell} peaks (Schöne et al., 2022).

With decreasing oxygen content in the ambient water, the disturbance lines seem to become more prominent (Fig. 5.5+5.6) and contain increasingly smaller and more elongated individual biomineral units with a larger perimeter-to-area ratio (Fig. 5.8–10). However, it was not possible to provide a quantitative relationship between the prominence of disturbance lines and DO values, largely because the oxygen levels in the water were measured too infrequently (see Fig. 5.2). The actual seasonal low-oxygen minima may thus have been missed. Future studies under controlled laboratory experiments and constant monitoring of environmental parameters would be very useful to further explore the relationship between the prominence and microstructural features of disturbance lines in relation to varying DO levels. Such experiments should also be conducted with a larger number of specimens to assess potential individual differences between bivalves. Also, due to a lack of detailed descriptions of the microstructure at disturbance lines (micrometer to nanometer-scale) in previous studies (Pannella and MacClintock, 1968; Clark, 1974; Gaspar et al., 1994; Dunca et al., 2009; Cardoso et al., 2013; Vihtakari et al., 2016), it currently remains unknown if strong oxygen depletion leads to microstructurally distinct disturbance lines that differ from those caused by other environmental stressors (something that controlled rearing experiments could likewise tackle). Unless combined with high-resolution element chemical analyses, disturbance lines can currently not

be employed as an independent proxy for oxygen deficiency. Therefore, it is strongly recommended to verify at least in one specimen of a selected study site that the shell portions containing disturbance lines are enriched in manganese (= a chemical DO proxy in bivalve shells; Schöne et al., 2021, 2022).

5.4.1 Disturbance lines as deoxygenation proxies, verification by Mn/Ca_{shell}

Disturbance lines were exclusively found in specimens from the Baltic Sea, specifically in shell portions formed under severe oxygen depletion during summer (Fig. 5.2+5.3). None of the other environmental variables for which instrumental data were available caused comparable shell growth patterns at any other study locality. For example, the study site at NE Iceland is episodically strongly influenced by nutrient-poor polar waters (Marali and Schöne, 2015). Despite that the bivalves did not form disturbance lines (Fig. S5.5), but just grew slower (Marali and Schöne, 2015). Likewise, no disturbance lines were formed in the present study at temperatures close to zero degrees Celsius or salinities as low as 14.6 (Fig. 5.10), conditions which are well-known to cause physiological stress and slow growth in ocean quahogs (Witbaard et al., 1998; Hiebenthal et al., 2012). In shells from the western Baltic Sea, disturbance lines formed in summer despite water temperatures (-0.5 – 15.9 °C; Fig. 5.10) were near the species-specific optimum (6 to 16 °C; Merril et al., 1969; Witbaard et al., 1998; Cargnelli, 1999) and salinities (16.7 – 28.9 between June and August; Fig. 5.10) well above values that exceed the species-specific tolerance (approx. 10 – 12: von Oertzen and Schulz, 1973; Zettler et al., 2007; Darr et al., 2014). Given that the Baltic Sea is eutrophicated, the bivalves should also not have experienced any lack of food supply that could have led to disturbed shell growth in summer. While high algal densities were reported to negatively affect feeding behavior of *A. islandica* (Winter, 1970), this effect is probably negligible in comparison to the effects of an actual lack of food supply. It is also unlikely that the disturbance lines resulted from predatory attacks. Firstly, growth distortions related to predation are typically associated with distinct notches and damages on the outer shell surface (e.g., Kennish and Loveland, 1980; Gaspar et al., 1994; Ramsay et al., 2001), which were not observed. Secondly, predatory attacks should not be limited to low-DO times, but occur year-round. Thirdly, predation, for instance, by predatory fish (Arntz and Weber, 1970; Rumohr and Krost, 1991), is also common at other localities outside the Baltic Sea as well. The only reasonable remaining environmental factor that could have triggered the formation of the regularly developed disturbance lines in Baltic Sea shells is severe oxygen deficiency. This conclusion is supported by the concurrent enrichment of manganese in the shells as well as an inverse relationship

between the prominence of disturbance lines and DO concentration (and the height of Mn/Ca_{shell} peaks).

The rationale for using Mn/Ca ratios of bivalve shells as a surrogate for DO is as follows. Under reducing conditions (e.g., within the sediment), manganese becomes dissolved in the water column (Hem, 1963; Balzer, 1982; Rue et al., 1997) and biologically available as Mn^{2+}. Sedimentary porewater diffuses out of anoxic sediments (Ben-Yaakov, 1973; Kremling et al., 1997), mixes with water above the substrate and may be inhaled by *A. islandica* (and other filter-feeding benthos). Dissolved manganese and other redox-sensitive elements can then reach the body fluids of the bivalves and eventually be incorporated into the shell. In case of Mn^{2+} this occurs swiftly after uptake from the water (Langlet et al., 2007). Mn^{2+} concentrations are highest near the sediment water interface and gradually decline with increasing distance from the seafloor as well as rising DO concentration in the free water column (Kremling and Petersen, 1978). The correlation between shell Mn/Ca values and DO measured in some distance from the sediment surface (e.g., approx. 5 m above the substrate in case of Mecklenburg Bight) indicates that the bioavailability of Mn^{2+} near the seafloor is proportional to DO concentrations in the free water column. This relationship was previously evoked to suggest that Mn/Ca_{shell} serves as a semiquantitative DO proxy in *Astarte* spp. and *A. islandica* (Schöne et al., 2021, 2022).

Due to the lack of direct measurements of DO concentration at the very sites at which the bivalves lived and inhaled water (i.e., the fluffy layer), or even better, the DO content of the coelomic fluid, we can only provide the average DO value that prevailed 5 m above the sediment surface when the disturbance lines were formed (below approx. 5 mL/L ≡ 516 µmol/L at 2.43 atm and 7.5 °C). The water inhaled by the bivalves at the seafloor, however, most certainly contained much less oxygen than indicated by the instrumental DO data, because of sedimentary porewater efflux. Presumably, DO concentration was less than 45 µmol/L (≡ 5 kPa, 0.43 mL/L ≡ 1.62 mg/L), i.e., the threshold at which the metabolic rate depression of *A. islandica* starts (Strahl et al., 2011). Controlled rearing experiments in future studies would be very useful to constrain and quantify the relationship between the prominence of disturbance lines and actual DO levels close to the seafloor where the bivalves live.

5.4.2 Microstructural characteristics of disturbance lines

Disturbance lines were associated with a strong reduction in shell growth rate (Fig. 5.4) and a concomitant formation of FCCL microstructure (Fig. 5.4+5.5). FCCL BMUs became increasingly smaller, more elongated and less convoluted (= lower surface roughness, higher

solidity) as DO levels dropped. The correlation between BMU size and DO fits well to the observation that *A. islandica* strongly reduces the metabolic rate under low-oxygen conditions (Theede et al., 1969; Taylor and Brand, 1975; Strahl et al., 2011). As a consequence, much less energy would be available to transport Ca^{2+} and HCO_3^- toward the site of biomineralization and H^+ ions away from it as well as to enzymatically convert metabolic CO_2 into bicarbonate ions. This would inevitably lead to a reduction of the BMU size, because an active ion transport is crucial to form abundant $CaCO_3$ (Wilbur and Saleuddin, 1983; Carré et al., 2006). Furthermore, based on the observation that low-DO induced stress changes the expression of certain genes (Philipp et al., 2012), it is speculated here that low-DO-induced physiological stress also influenced the synthesis of proteins responsible for the formation of a specific BMU habit. A change in the type and composition of shell-forming proteins may have been responsible for the production of increasingly smooth biominerals as DO supply dropped. If that hypothesis holds true, there may be scope to detect oxygen deficiency in the past solely by detailed BMU morphometry or even to quantify the DO depletion based on BMU habit. Future work should thus further explore the diagnostic potential of the morphological properties of the BMUs. As shown here, the relationship between DO and BMU size or elongation was statistically significant, but the explained variability too small and the error too large to be used to reconstruct DO concentration from morphometric data of the BMUs (Fig. 5.9). Perhaps, the surface roughness, size and shape or other parameters reveal a closer relationship with DO concentration if studied in three dimensions (e.g., Howes et al., 2021; Mehra et al., 2022).

5.4.3 Anaerobiosis and shell stability

As demonstrated by many controlled laboratory experiments (Oeschger, 1990), under the persistent absence of oxygen (anoxia) or the presence of H_2S (euxinia), *A. islandica* closes its valves for extended periods of time, ceases biomineralization and switches to an anaerobic metabolism once all entrapped oxygen is consumed (Crenshaw and Neff, 1969). Acidic metabolites generated by this type of adenosine triphosphate production (i.e., anaerobic glycolysis) are neutralized by the dissolution of inner shell surfaces (Crenshaw and Neff, 1969; Crenshaw, 1972; Oeschger, 1990). This process can readily explain the thinness (ca. 1 mm-tick; Fig. S5.1) of ocean quahog shells from the western Baltic Sea as formerly hypothesized by Weigelt (cited as personal communication in Oeschger, 1990).

The shells from the Baltic Sea were not only very thin, but also overall enriched in organic matrix compared to specimens inhabiting permanently normal marine, well-oxygenated settings (Fig. 5.4+5.5) (see also Li et al., 2015). Presumably, this is attributed to their lower

BMU coverage values (Fig. 5.7A) and to the fact that smaller BMUs come with a proportionally larger surface area (Fig. 5.7C) which is occupied by organic matrix (Fig. 5.7). The surplus of organics demonstrably increases the elastic properties of shells (cf. Li et al., 2015) which results in higher toughness and strength (Chen et al., 2008; Meyers et al., 2008). Given that the shells were very thin, this may have served as an effective strategy to withstand predatory attacks. Toward the outer shell surface, the organic content increased as indicated by broader inter-crystalline organic sheets (Fig. 5.5J) and the gradual broadening of the organic-rich annual growth bands (Fig. 5.5J). This organic enrichment at the shell periphery may have further contributed to the toughness of the shell and could also have provided a better protection against shell dissolution. However, porewaters of anoxic sediments are demonstrably buffered and the pH value rarely drops below 7 (Ben-Yaakov, 1973; Bonaglia et al., 2019). An alternative explanation for higher organic content in shell portions closer to the periostracum is improved resistance against microbial attack. While increased amounts of organics can attract microorganisms resulting in even stronger bioerosion of the shell, in dys/anoxic sediments – which exist at Mecklenburg Bight – the rate of microbial decomposition of organic compounds is strongly reduced relative to a setting where the upper few centimeters of the sediment are well-oxygenated (cf. Hedges and Keil, 1995; Hartnett et al., 1998; Jessen et al., 2017) like at the study site at NE Iceland, so that an organic-rich outer rim may still have fulfilled its task as an efficient physical barrier against predation.

The larger proportion of organic matrix relative to $CaCO_3$ in ocean quahogs from the Baltic Sea can be explained by generally smaller BMUs resulting from overall slower shell growth rates and lower metabolic rates (Strahl et al., 2011). *A. islandica* from localities outside the Baltic Sea not only grew considerably faster (Fig. S5.6, Table S5.1), but also produced larger BMUs, specifically in warmer, food-rich water (Höche et al., 2021, 2022a). In the Baltic Sea, however, the positive correlation between BMU size and temperature or food supply seems to have been offset by the negative effects of persistently reduced salinity (and episodically recurring severe oxygen depletion) on shell growth rate. For the stenohaline *A. islandica*, lowered salinity (in particular below 15) exerts physiological stress that demonstrably leads to slower shell growth (Hiebenthal et al., 2012). While salinity at the study site (approx. 15 to 25) remained within the physiological tolerance of that species (Oeschger and Storey, 1993; Cargnelli, 1999), the osmotic stress may have triggered the rerouting of energy to maintain cellular homeostasis (e.g., osmoregulation; Hiebenthal et al., 2012) instead of supporting shell formation. Alternatively or in addition to that, low salinity demonstrably limits calcification due to increasing energetic requirements (Sanders et al., 2018) for the uptake and transport of

calcium and bicarbonate ions across mantle epithelia toward the site of biomineralization, proton removal from the biomineralization front as well as the catalytic conversion of metabolic CO_2 into HCO_3^- by means of carbonic anhydrase (Marin et al., 2012; Sanders et al., 2018). Furthermore, with declining salinity, HCO_3^- and more importantly, the Ca^{2+} concentration decreases which can impede calcification. For *Mytilus* spp., a lower salinity threshold of 11 has been reported for calcification (Sanders et al., 2021). Assuming that the production of organic matrices proceeded at nearly similar rates, the reduced production of the mineral phase led to smaller BMUs and a higher proportion of organics vs $CaCO_3$ in *A. islandica*.

5.5 Summary and conclusions

Manganese-rich disturbance lines in shells of *A. islandica* can serve as a proxy to track past deoxygenation events. Based on their distinctive microstructure (fine complex crossed-lamellae instead of irregular simple prisms), these growth patterns can be confidently distinguished from periodic annually growth lines. While the regular occurrence during times of seasonal oxygen depletion and eventually hypoxia in bottom waters and the concomitant increase in Mn/Ca_{shell} values suggest a causal link between disturbed shell growth and limited oxygen availability, it currently remains unknown if strong oxygen depletion leads to microstructurally distinct disturbance lines that differ from those caused by other environmental stressors. At least in the studied specimens, neither extremely low temperature, salinity close to the lower physiological tolerance nor food scarcity caused the formation of disturbance lines.

With increasing oxygen deficiency, the disturbance lines became more prominent, contained more manganese and consisted of increasingly smaller and more elongated individual biomineral units with a larger perimeter-to-area ratio. Although the relationship between DO and BMU size or elongation was statistically significant, the explained variability (< 1.5 %) was too small and the error too large to reconstruct absolute DO values. BMU parameters may reveal a closer relationship with DO concentration if studied in three dimensions, something that future work should address. For a quantitative reconstruction of dissolved oxygen, it will also be necessary to measure the DO content directly at the sediment-water interface, i.e., the very position at which the bivalves lived and inhaled water. In the present study, we compared BMU parameters to DO measurements completed 5 m above the substrate assuming that disturbance lines started to form as soon as the lower DO threshold was reached at which the metabolic rate (as well as the biomineralization rate) of *A. islandica* decreases sharply, i.e., below 45 µmol/L (≡ 5 kPa, 0.43 mL/L or 1.62 mg/L; Strahl et al., 2011). Under anoxic and

euxinic conditions (Oeschger, 1990), the bivalves demonstrably cease shell formation, close their valves and switch to an anaerobic metabolism (Crenshaw and Neff, 1969) that eventually results in the dissolution of inner shell surfaces (Crenshaw and Neff, 1969; Crenshaw, 1972; Oeschger, 1990) and extremely thin shells (Schöne, 2013). Baltic Sea bivalves still have tough and resistant shells, because they contain a much larger proportion of organics than specimens from normal marine and well-oxygenated sites. This surplus of organics increases the elastic modulus and presumably relates at large to limited access to Ca^{2+} in the hyposaline environment (Sanders et al., 2021). Future studies should further explore the potential of BMU analyses to obtain quantitative data on DO or other environmental parameters.

5.6 Supplements material

The Supplementary Data for this article can be found online at: https://www.frontiersin.org/articles/10.3389/fmars.2023.1219716/full#supplementary-material

References

Andrén, E., Andrén, T., Kunzendorf, H., 2000. Holocene history of the Baltic Sea as a background for assessing records of human impact in the sediments of the Gotland Basin. Holocene 10, 687–702.

Arntz, W., E., Weber, W., 1970. Cyprina islandica L. (Mollusca, Bivalvia) als Nahrung von Dorsch und Kliesche in der Kieler Bucht. Ber. Dt. Wiss. Komm. Meeresforsch. 21, 193–209.

Ballesta-Artero, I., Zhao, L., Milano, S., Mertz-Kraus, R., Schöne, B. R., van der Meer, J., et al. 2018. Environmental and biological factors influencing trace elemental and microstructural properties of *Arctica islandica* shells. Sci. Total Environ. 645, 913–923.

Balzer, W., 1982. On the distribution of iron and manganese at the sediment/water interface: thermodynamic versus kinetic control. Geochim. Cosmochim. Acta 46, 1153–1161.

Belding, D. L., 1910. A report upon the scallop fishery of Massachusetts: Including the habits, life history of *Pecten irradians*, its rate of growth, and other facts of economic value. Wright & Potter, Boston, MA, USA, 155 pp.

Ben-Yaakov, S., 1973. pH buffering of pore water of recent anoxic marine sediments. Limnol. Oceanogr. 18, 86–94.

Berg, S., Kutra, D., Kroeger, T., Straehle, C. N., Kausler, B. X., Haubold, C., et al. 2019. ilastik: interactive machine learning for (bio)image analysis. Nat. Meth. 16, 1226–1232.

Bevelander, G., Nakahara, H., 1980. "Compartment and envelope formation in the process of biological mineralization," in *The mechanisms of biomineralization in animals and plants*. Eds. M. Ōmori and N. Watabe (Kanagawa, Japan: Tokai University Press), p. 19–27.

Böhm, C. F., Demmert, B., Harris, J., Fey, T., Marin, F., Wolf, S. E., 2016. Structural commonalities and deviations in the hierarchical organization of crossed-lamellar shells: a case study on the shell of the bivalve *Glycymeris glycymeris*. J. Mater. Res. 31, 536–546.

Bonaglia, S., Marzocchi, U., Ekeroth, N., Brüchert, V., Blomqvist, S., Hall, P. O., 2019. Sulfide oxidation in deep Baltic Sea sediments upon oxygenation and colonization by macrofauna. Mar. Biol. 166, 1–12.

Butler, P. G., Wanamaker, A. D., Scourse, J. D., Richardson, C. A., Reynolds, D. J., 2013. Variability of marine climate on the North Icelandic Shelf in a 1357-year proxy archive based on growth increments in the bivalve *Arctica islandica*. Palaeogeogr. Palaeoclimatol. Palaeoecol. 373, 141–151.

Caballero-Alfonso, A. M., Carstensen, J., Conley, D. J., 2015. Biogeochemical and

environmental drivers of coastal hypoxia. J. Mar. Syst. 141, 190–199.

Cardoso, J. F. M. F., Nieuwland, G., Witbaard, R., van der Veer, H. W., Machado, J. P., 2013. Growth increment periodicity in the shell of the razor clam *Ensis directus* using stable isotopes as a method to validate age. Biogeosciences 10, 4741–4750.

Cargnelli, L. M., 1999. Essential fish habitat source document. Ocean quahog, *Arctica islandica*, life history and habitat characteristics. NOAA Techn. Memorandum NMFS-NE-148, 20 pp.

Carré, M., Bentaleb, I., Bruguier, O., Ordinola, E., Barrett, N. T., Fontugne, M., 2006. Calcification rate influence on trace element concentrations in aragonitic bivalve shells: evidences and mechanisms. Geochim. Cosmochim. Acta 70, 4906–4920.

Carstensen, J., Conley, D. J., 2019. Baltic Sea hypoxia takes many shapes and sizes. Limnol. Oceanogr. Bull. 28, 125–129.

Carstensen, J., Andersen, J. H., Gustafsson, B. G., Conley, D. J., 2014a. Deoxygenation of the Baltic Sea during the last century. Proc. Natl. Acad. Sci. 111, 5628–5633.

Carstensen, J., Conley, D. J., Bonsdorff, E., Gustafsson, B. G., Hietanen, S., Janas, et al. 2014b. Hypoxia in the Baltic Sea: biogeochemical cycles, benthic fauna, and management. Ambio 43, 26–36.

Checa, A. G., 2018. Physical and biological determinants of the fabrication of molluscan shell microstructures. Front. Mar. Sci. 5, 353.

Chen, P.-Y., Lin, A. Y. M., Lin, Y.-S., Seki, Y., Stokes, A. G., Peyras, J., et al. 2008. Structure and mechanical properties of selected biological materials. J. Mech. Behav. Biomed. Mater. 1, 208–226.

Clark, G. R., 1974. Growth lines in invertebrate skeletons. Annu. Rev. Earth Planet. Sci. 2, 77–99.

Conley, D. J., Carstensen, J., Ærtebjerg, G., Christensen, P. B., Dalsgaard, T., Hansen, J. L., et al. 2007. Long-term changes and impacts of hypoxia in Danish coastal waters. Ecol. Appl. 17, S165–S184.

Conley, D. J., Björck, S., Bonsdorff, E., Carstensen, J., Destouni, G., Gustafsson, B. G., et al. 2009. Hypoxia-related processes in the Baltic Sea. Environ. Sci. Technol. 43, 3412–3420.

Crenshaw, M. A., 1972. The inorganic composition of molluscan extrapallial fluid. Biol. Bull. 143, 506–512.

Crenshaw, M. A., 1980. “Mechanisms of shell formation and dissolution,” in *Skeletal growth of aquatic organisms*. Eds. D. C. Rhoads and R. A. Lutz (New York + London: Plenum Press), 115–132.

Crenshaw, M. A., Neff, J. M., 1969. Decalcification at the mantle-shell interface in molluscs. Am. Zool. 9, 881–885.

Crippa, G., 2013. The shell ultrastructure of the genus *Glycymeris* DA COSTA, 1778: A comparison between fossil and recent specimens. Riv. Ital. Paleontol. E Stratigr. 119, 387–399.

Darr, A., Gogina, M., Zettler, M. L., 2014. Detecting hot-spots of bivalve biomass in the south-western Baltic Sea. J. Mar. Syst. 134, 69–80.

Dries, R. R., Theede, H., 1974. Resistance to oxygen deficiency in marine bottom invertebrates of western Baltic Sea. Mar. Biol. 25, 327–333.

Dunca, E., Mutvei, H., Goransson, P., Morth, C.-M., Schöne, B. R., Whitehouse, M. J., et al. 2009. Using ocean quahog (*Arctica islandica*) shells to reconstruct palaeoenvironment in Öresund, Kattegat and Skagerrak, Sweden. Int. J. Earth Sci. 98, 3–17.

Edge, D. C., Reynolds, D. J., Wanamaker, A. D., Griffin, D., Bureau, D., Outridge, C., et al. 2021. A multicentennial proxy record of Northeast Pacific Sea surface temperatures from the annual growth increments of *Panopea generosa*. Paleoceanogr. Paleoclimatology 36, e2021PA004291.

Epstein, S., Lowenstam, H. A., 1953. Temperature-shell-growth relations of recent and interglacial Pleistocene shoal-water biota from Bermuda. J. Geol. 61, 424–438.

Fennel, K., Testa, J. M., 2019. Biogeochemical controls on coastal hypoxia. Annu. Rev. Mar. Sci. 11, 105–130.

Filipsson, H. L., Nordberg, K., 2004. A 200-year environmental record of a low-oxygen fjord, Sweden, elucidated by benthic foraminifera, sediment characteristics and hydrographic data. J. Foraminifer. Res. 34, 277–293.

Gaillard, F., Reynaud, T., Thierry, V., Kolodziejczyk, N., von Schuckmann, K., 2016. In situ–based reanalysis of the global ocean temperature and salinity with ISAS: variability of the heat content and steric height. J. Clim. 29, 1305–1323.

Gaspar, M. B., Richardson, C. A., Monteiro, C. C., 1994. The effects of dredging on shell formation in the razor clam *Ensis siliqua* from Barrinha, southern Portugal. J. Mar. Biol. Assoc. U. K. 74, 927–938.

Hanna, E., Jónsson, T., Ólafsson, J., Valdimarsson, H., 2006. Icelandic coastal sea surface temperature records constructed: putting the pulse on air–sea–climate interactions in the northern North Atlantic. Part I: comparison with HadISST1 open-ocean surface temperatures and preliminary analysis of long-term patterns and anomalies of SSTs around Iceland. J. Clim. 19, 5652–5666.

Hartnett, H., E., Keil, R., G., Hedges, J., I., Devol, A., H., 1998. Influence of oxygen exposure time on organic carbon preservation in continental margin sediments. Nature 391, 572–575.

Hedges, J., I., Keil, R., G., 1995. Sedimentary organic matter preservation: an assessment and speculative synthesis. Mar. Chem. 49, 81–115.

Hem, J. D., 1963. Chemical equilibria and rates of manganese oxidation. US Geol. Surv. Water Supply Pap. 1667-A, 1–64.

Herreid, C., F., II 1980. Hypoxia in invertebrates. Comp. Biochem. Physiol. A Physiol. 67, 311–320.

Hiebenthal, C., Philipp, E. E. R., Eisenhauer, A., Wahl, M., 2012. Interactive effects of temperature and salinity on shell formation and general condition in Baltic Sea *Mytilus edulis* and *Arctica islandica*. Aquat. Biol. 14, 289–298.

Höche, N., Peharda, M., Walliser, E. O., Schöne, B. R., 2020. Morphological variations of crossed-lamellar ultrastructures of *Glycymeris bimaculata* (Bivalvia) serve as a marine temperature proxy. Estuar. Coast. Shelf Sci. 237, 106658.

Höche, N., Walliser, E. O., Winter, N. J. de, Witbaard, R., Schöne, B. R., 2021. Temperature-induced microstructural changes in shells of laboratory-grown *Arctica islandica* (Bivalvia). PLOS ONE 16, e0247968.

Höche, N., Walliser, E. O., Schöne, B. R., 2022a. Microstructural mapping of *Arctica islandica* shells reveals environmental and physiological controls on biomineral size. Front. Earth Sci. 9, 781305.

Höche, N., Zettler, M., L., Huang, X., Schöne, B., R., 2022b. Data for "Shell microstructures (disturbance lines) of *Arctica islandica* – A potential proxy for severe oxygen depletion."

Howes, B., Mehra, A., Maloof, A., 2021. Three-dimensional morphometry of ooids in oolites: a new tool for more accurate and precise paleoenvironmental interpretation. J. Geophys. Res. Earth Surf. 126, e2020JF005601.

Jessen, G. L., Lichtschlag, A., Ramette, A., Pantoja, S., Rossel, P. E., Schubert, C. J., et al. 2017. Hypoxia causes preservation of labile organic matter and changes seafloor microbial community composition (Black Sea). Sci. Adv. 3, e1601897.

Jilbert, T., Slomp, C. P., 2013. Rapid high-amplitude variability in Baltic Sea hypoxia during the Holocene. Geology 41, 1183–1186.

Jones, D. S., 1980. Annual cycle of shell growth increment formation in two continental shelf bivalves and its paleoecologic significance. Paleobiology 6, 331–340.

Jones, D. S., Arthur, M. A., Allard, D. J., 1989. Sclerochronological records of temperature and

growth from shells of *Mercenaria mercenaria* from Narragansett Bay, Rhode Island. Mar. Biol. 102, 225–234.

Karlson, K., Rosenberg, R., Bonsdorff, E., 2002. Temporal and spatial large-scale effects of eutrophication and oxygen deficiency on benthic fauna in Scandinavian and Baltic waters: a review. Oceanogr. Mar. Biol. Annu. Rev. 40, 427–489.

Kennish, M. J., Olsson, R. K., 1975. Effects of thermal discharges on the microstructural growth of *Mercenaria mercenaria*. Environ. Geol. 1, 44–64.

Kennish, M. J., an Loveland, R. E., 1980. Growth models of the northern quahog, *Mercenaria mercenaria* (Linné). Proc. Natl. Shellfish. Assoc. 70, 230–239.

Kremling, K., Petersen, H., 1978. The distribution of Mn, Fe, Zn, Cd and Cu in Baltic seawater; a study on the basis of one anchor station. Mar. Chem. 6, 155–170.

Kremling, K., Tokos, J. J. S., Brügmann, L., Hansen, H.-P., 1997. Variability of dissolved and particulate trace metals in the Kiel and Mecklenburg bights of the Baltic Sea, 1990–1992. Mar. Pollut. Bull. 34, 112–122.

Langlet, D., Alleman, L. Y., Plisnier, P.-D., Hughes, H., André, L., 2007. Manganese content records seasonal upwelling in Lake Tanganyika mussels. Biogeosciences 4, 195–203.

Leibnitz-Institut für Ostseeforschung Warnemünde 2021. ODIN 2. Available at: https://odin2.io-warnemuende.de/ [Accessed October 18, 2022].

Li, L., Weaver, J. C., Ortiz, C., 2015. Hierarchical structural design for fracture resistance in the shell of the pteropod *Clio pyramidata*. Nat. Commun. 6, 6216.

Limburg, K. E., Olson, C., Walther, Y., Dale, D., Slomp, C. P., Høie, H., 2011. Tracking Baltic hypoxia and cod migration over millennia with natural tags. Proc. Natl. Acad. Sci. 108, E177–E182.

Lohmann, G., Schöne, B. R., 2013. Climate signatures on decadal to interdecadal time scales as obtained from mollusk shells (*Arctica islandica*) from Iceland. Palaeogeogr. Palaeoclimatol. Palaeoecol. 373, 152–162.

Marali, S., Schöne, B. R., 2015. Oceanographic control on shell growth of *Arctica islandica* (Bivalvia) in surface waters of Northeast Iceland — Implications for paleoclimate reconstructions. Palaeogeogr. Palaeoclimatol. Palaeoecol. 420, 138–149.

Marin, F., Le Roy, N., Marie, B., 2012. The formation and mineralization of mollusk shell. Front. Biosci. S4, 1099–1125.

Mehra, A., Howes, B., Manzuk, R., Spatzier, A., Samuels, B. M., Maloof, A. C., 2022. A novel technique for producing three-dimensional data using serial sectioning and semi-automatic image classification. Microsc. Microanal., 1–16.

Merril, A. S., Chamberlin, J. L., Ropes, J. W., 1969. “Ocean quahog fishery,” in *The encyclopedia of marine resources*. Ed. F. E. Firth (New York, USA: Van Nostrand Reinhold Co.), 125–129.

Meyers, M. A., Lin, A. Y.-M., Chen, P.-Y., Muyco, J., 2008. Mechanical strength of abalone nacre: role of the soft organic layer. J. Mech. Behav. Biomed. Mater. 1, 76–85.

Milano, S., Schöne, B. R., Witbaard, R., 2017. Changes of shell microstructural characteristics of *Cerastoderma edule* (Bivalvia) — A novel proxy for water temperature. Palaeogeogr. Palaeoclimatol. Palaeoecol. 465, 395–406.

Oeschger, R., 1990. Long-term anaerobiosis in sublittoral marine invertebrates from the Western Baltic Sea: *Halicryptus spinulosus* (Priapulida), *Astarte borealis* and *Arctica islandica* (Bivalvia). Mar. Ecol. Prog. Ser. 59, 133–143.

Oeschger, R., Storey, K. B., 1993. Impact of anoxia and hydrogen sulphide on the metabolism of *Arctica islandica* L. (Bivalvia). J. Exp. Mar. Biol. Ecol. 170, 213–226.

Österblom, H., Hansson, S., Larsson, U., Hjerne, O., Wulff, F., Elmgren, R., et al., 2007. Human-induced trophic cascades and ecological regime shifts in the Baltic Sea. Ecosystems 10, 877–889.

Osterman, L. E., Poore, R. Z., Swarzenski, P. W., Turner, R. E., 2005. Reconstructing a 180 yr record of natural and anthropogenic induced low-oxygen conditions from Louisiana continental shelf sediments. Geology 33, 329–332.

Pannella, G., MacClintock, C., 1968. Biological and environmental rhythms reflected in molluscan shell growth. Mem. Paleontol. Soc. 2, 64–80.

Philipp, E. E. R., Wessels, W., Gruber, H., Strahl, J., Wagner, A. E., Ernst, I. M. A., et al. 2012. Gene expression and physiological changes of different populations of the long-lived bivalve Arctica islandica under low oxygen conditions. PLOS ONE 7, e44621.

Ramsay, K., Richardson, C. A., Kaiser, M. J., 2001. Causes of shell scarring in dog cockles *Glycymeris glycymeris* L. J. Sea Res. 45, 131–139.

Reynolds, D. J., Hall, I. R., Slater, S. M., Scourse, J. D., Halloran, P. R., Sayer, M. D. J., 2017. Reconstructing past seasonal to multicentennial-scale variability in the NE Atlantic Ocean using the long-lived marine bivalve mollusk *Glycymeris glycymeris*. Paleoceanogr. 32, 1153–1173.

Rue, E. L., Smith, G. J., Cutter, G. A., Bruland, K. W., 1997. The response of trace element redox couples to suboxic conditions in the water column. Deep-Sea Res. 44, 113–134.

Rueden, C. T., Schindelin, J., Hiner, M. C., DeZonia, B. E., Walter, A. E., Arena, E. T., et al. 2017. ImageJ2: ImageJ for the next generation of scientific image data. BMC

Bioinformatics 18, 529.

Rumohr, H., Krost, P., 1991. Experimental evidence of damage to benthos by bottom trawling with special reference to *Arctica islandica*. Meeresforschung 33, 340–345.

Sanders, T., Schmittmann, L., Nascimento-Schulze, J. C., Melzner, F., 2018. High calcification costs limit mussel growth at low salinity. Front. Mar. Sci. 5.

Sanders, T., Thomsen, J., Müller, J. D., Rehder, G., Melzner, F., 2021. Decoupling salinity and carbonate chemistry: low calcium ion concentration rather than salinity limits calcification in Baltic Sea mussels. Biogeosci. 18, 2573–2590.

Schindelin, J., Rueden, C. T., Hiner, M. C., Eliceiri, K. W., 2015. The ImageJ ecosystem: An open platform for biomedical image analysis. Mol. Reprod. Dev. 82, 518–529

Schneider, C. A., Rasband, W. S., Eliceiri, K. W., 2012. NIH Image to ImageJ: 25 years of image analysis. Nat. Methods 9, 671–675.

Schöne, B. R., 2013. *Arctica islandica* (Bivalvia): A unique paleoenvironmental archive of the northern North Atlantic Ocean. Glob. Planet. Change 111, 199–225.

Schöne, B. R., Dunca, E., Fiebig, J., Pfeiffer, M., 2005a. Mutvei's solution: An ideal agent for resolving microgrowth structures of biogenic carbonates. Palaeogeogr. Palaeoclimatol. Palaeoecol. 228, 149–166.

Schöne, B. R., Fiebig, J., Pfeiffer, M., Gleβ, R., Hickson, J., Johnson, A. L. A., et al. 2005b. Climate records from a bivalved Methuselah (Arctica islandica, Mollusca; Iceland). Palaeogeogr. Palaeoclimatol. Palaeoecol. 228, 130–148.

Schöne, B. R., Huang, X., Zettler, M. L., Zhao, L., Mertz-Kraus, R., Jochum, K. P., et al. 2021. Mn/Ca in shells of *Arctica islandica* (Baltic Sea) – A potential proxy for ocean hypoxia? Estuar. Coast. Shelf Sci. 251, 107257.

Schöne, B. R., Huang, X., Jantschke, A., Mertz-Kraus, R., Zettler, M. L., 2022. High-resolution reconstruction of dissolved oxygen levels in the Baltic Sea with bivalves–a multi-species comparison (*Arctica islandica, Astarte borealis, Astarte elliptica*). Front. Mar. Sci. 442, 820731.

Sohlenius, G., Emeis, K.-C., Andrén, E., Andrén, T., Kohly, A., 2001. Development of anoxia during the Holocene fresh–brackish water transition in the Baltic Sea. Mar. Geol. 177, 221–242.

Strahl, J., Dringen, R., Schmidt, M. M., Hardenberg, S., Abele, D., 2011. Metabolic and physiological responses in tissues of the long-lived bivalve *Arctica islandica* to oxygen deficiency. Comp. Biochem. Physiol. A. Mol. Integr. Physiol. 158, 513–519.

Taylor, A. C., Brand, A. R., 1975. Effects of hypoxia and body size on the oxygen consumption

of the bivalve *Arctica islandica* (L.). J. Exp. Mar. Biol. Ecol. 19, 187–196.

Theede, H., Ponat, A., Hiroki, K., Schlieper, C., 1969. Studies on the resistance of marine bottom invertebrates to oxygen-deficiency and hydrogen sulphide. Mar. Biol. 2, 325–337.

Vaquer-Sunyer, R., Duarte, C. M., 2008. Thresholds of hypoxia for marine biodiversity. Proc. Natl. Acad. Sci. 105, 15452–15457.

Vihtakari, M., Renaud, P. E., Clarke, L. J., Whitehouse, M. J., Hop, H., Carroll, M. L., et al. 2016. Decoding the oxygen isotope signal for seasonal growth patterns in Arctic bivalves. Palaeogeogr. Palaeoclimatol. Palaeoecol. 446, 263–283.

von Oertzen, J. A., Schulz, S., 1973. Beitrag zur geographischen Verbreitung und ökologischen Existenz von Bivalviern in der Ostsee. Beitr Meereskd. 32, 75–88.

Wanamaker Jr, A. D., Heinemeier, J., Scourse, J. D., Richardson, C. A., Butler, P. G., Eiríksson, J., et al. 2008. Very long-lived mollusks confirm 17th century AD tephra-based radiocarbon reservoir ages for North Icelandic shelf waters. Radiocarbon 50, 399–412.

Wanamaker Jr, A. D., Butler, P. G., Scourse, J. D., Heinemeier, J., Eiríksson, J., Knudsen, K. L., et al. 2012. Surface changes in the North Atlantic meridional overturning circulation during the last millennium. Nat. Commun. 3, 1–7.

Weidman, C., Jones, G., Lohmann, K. C., 1994. The long-lived mollusk *Arctica islandica*: a new paleoceanographic tool for the reconstruction of bottom temperatures for the continental shelves of the northern-North Atlantic Ocean. J. Geophys. Res. 99, 18305–18314.

Westman, P., Sohlenius, G., 1999. Diatom stratigraphy in five offshore sediment cores from the northwestern Baltic proper implying large scale circulation changes during the last 8500 years. J. Paleolimnol. 22, 53–69.

Wilbur, K. M., Saleuddin, A. S. M., 1983. “Shell Formation,” in *The Mollusca*. Eds. A. S. M. Saleuddin and K. M. Wilbur (Toronto, Canada: Academic Press), 235–287.

Winter, J. E., 1970. Filter feeding and food utilization in *Arctica islandica* L. and *Modiolus modiolus* L. at different food concentrations. Mar. Food Chains, 196–206.

Witbaard, R., Duineveld, G. C. A., De Wilde, P., 1997. A long-term growth record derived from *Arctica islandica* (Mollusca, Bivalvia) from the Fladen Ground (northern North Sea). J. Mar. Biol. Assoc. U. K. 77, 801–816.

Witbaard, R., Franken, R., Visser, B., 1998. Growth of juvenile *Arctica islandica* under experimental conditions. Helgoländer Meeresunters. 51, 417–431.

Zettler, M. L., Schiedek, D., Bobertz, B., 2007. Benthic biodiversity indices versus salinity gradient in the southern Baltic Sea. Mar. Pollut. Bull. 55, 258–270.

Zettler, M. L., Friedland, R., Gogina, M., Darr, A., 2017. Variation in benthic long-term data of transitional waters: Is interpretation more than speculation? PLOS ONE 12, e0175746.

Zhao, L., Walliser, E. O., Mertz-Kraus, R., Schöne, B. R., 2017. Unionid shells (*Hyriopsis cumingii*) record manganese cycling at the sediment-water interface in a shallow eutrophic lake in China (Lake Taihu). Palaeogeogr. Palaeoclimatol. Palaeoecol. 484, 97–108.

Zillén, L., Conley, D. J., Andrén, T., Andrén, E., Björck, S., 2008. Past occurrences of hypoxia in the Baltic Sea and the role of climate variability, environmental change and human impact. Earth-Sci. Rev. 91, 77–92.

6 High-resolution history of oxygen depletion in the SW Baltic Sea since the mid-19th century as revealed by bivalve shells

Xizhi Huang[1], Liqiang Zhao[2], Michael L. Zettler[3], Regina Mertz-Kraus[1], Klaus Peter Jochum[4], Bernd R. Schöne[1]

[1] Institute of Geosciences, University of Mainz, Mainz, Germany
[2] College of Fisheries, Guangdong Ocean University, Zhanjiang, China
[3] Leibniz Institute for Baltic Sea Research Warnemünde, Rostock, Germany
[4] Climate Geochemistry Department, Max Planck Institute for Chemistry, Mainz, Germany

Huang, X., Zhao, L., Zettler, M. L., Mertz-Kraus, R., Jochum, K. P., and Schöne, B.R. (2023). High-resolution history of oxygen depletion in the SW Baltic Sea since the mid-19th century as revealed by bivalve shells. Science of The Total Environment, 888, 164011.

This manuscript was published in the journal "*Science of the Total Environment*". I contributed to the measurement design, data curation, methodology, formal analysis, investigation, visualization, writing-original draft preparation and writing-review and editing. This work was supported by the DFG grant to BRS [SCHO793/22]

Authors' contributions:

XZH: Data curation, Methodology, Formal analysis, Investigation, Visualization, Writing-original draft preparation; Writing-review and editing.

LQZ: Conceptualization, Methodology, Writing-original draft preparation.

MLZ: Resources, Writing-review and editing.

RMK: Resources, Validation, Writing-review and editing.

KPJ: Resources, Validation.

BRS: Conceptualization, Data curation, Formal analysis, Funding acquisition, Investigation, Methodology, Project administration, Supervision, Validation, Visualization, Writing-original draft Preparation; Writing-review and editing.

Abstract

The Baltic Sea serves as a model region to study processes leading to oxygen depletion. Reconstructing past low-oxygen occurrences, specifically hypoxia, is crucial to understand current ecological disturbances and developing future mitigation strategies. The history of dissolved oxygen (DO) concentration in some Baltic Sea basins has been investigated in previous studies, but temporally well-constrained, inter-annual and better resolved DO reconstructions are still scarce. Here, we present precisely dated, high-resolution DO record since the mid-19th century reconstructed from Mn/Ca$_{shell}$ values of *Arctica islandica* (Bivalvia) collected in the Mecklenburg Bight. According to the data, this area experienced similar low oxygenation during the second half of the 19th century and the late 20th century, but DO variability increased: A 12–15-yr oscillation prevailed in the 19th century, but a 4–6-year period dominated in the late 20th century. Shortly after the onset of the Industrial Revolution around 1850, Mn/Ca$_{shell}$ values increased, indicating a DO decrease, probably caused by strong anthropogenic nutrient input. More recently, phosphate levels and inflows of oxygen-rich North Sea water have been identified as major factors controlling the bottom water oxygenation. For example, the increase in DO in the mid-1990s was linked to the decrease in phosphate content and several Major Baltic Inflows. The strong Ba/Ca$_{shell}$ rise between the 1860s and the turn of the century most likely reflects changes in diatom community structure rather than a bloom of mass phytoplankton. This is supported by largely unchanged Mn/Ca$_{shell}$ and shell growth. Decadal and multi-decadal cycles of shell growth rate correlated strongly with the Atlantic Multidecadal Variability, likely reflecting changes in atmospheric circulation patterns, precipitation rate and riverine nutrient supply. To further improve the management and protection of ecosystems in the Baltic Sea, a larger number of such high-resolution retrospective studies covering long periods of time and large regions are needed.

6.1 Introduction

Deoxygenation is a growing issue in global open oceans and coastal waters leading to hypoxia (Breitburg et al., 2018). Hypoxia is defined as a decrease in dissolved oxygen (DO) concentration below approx. 2.3 mg/L (Vaquer-Sunyer and Duarte, 2008; ≙ 1.6 mL/L or 72 µmol/L). Prolonged low-oxygen levels, can have substantial impacts on the ecosystem functioning and living resources by altering primary production, biodiversity and biogeochemical cycles (Diaz and Rosenberg, 2008). Hypoxia can also affect the survival of marine organisms through physiological impacts, such as metabolism and cellular performance (Leung and Cheung, 2018). Since hypoxia spreads rapidly worldwide at an unprecedented rate (Conley et al., 2011), it is imperative to broaden our understanding of its long-term development (Zhang et al., 2010; Carstensen et al., 2014). However, respective efforts have been impeded by the limited knowledge about changes of the oxygenation on time-scales of seasons and years, in particular prior to the instrumental era (Zillén and Conley, 2010; Jilbert and Slomp, 2013), thereby raising uncertainties in the prediction of future hypoxia conditions (Oschlies et al., 2018).

The Baltic Sea serves as a “time machine” for studying the consequences and potential mitigation of future coastal hypoxia as it is one of the largest oxygen-deficient settings in the world (Reusch et al., 2018). Over the past 20 years, the hypoxic area in the Baltic Sea has varied between 50,000 and 80,000 km2 (Kõuts et al., 2021). Up to ca. 115 coastal sites in the Baltic Sea have experienced hypoxia, representing 20 % of all known sites worldwide (Conley et al., 2011). The present spread of hypoxia in the Baltic Sea has increased mainly due to eutrophication induced by anthropogenic nutrient inputs (specifically, nitrogen and phosphorus) and stratification enhanced by climate change (Conley et al., 2007; Kabel et al., 2012; Caballero-Alfonso et al., 2015). Understanding patterns of environmental change at various spatial and temporal scales in the past can help to decipher the baseline conditions and provide data for numerical simulations, leading to better predictions of the effects of human activities on ecosystems and the development of remediation strategies (Carstensen et al., 2014; Caballero-Alfonso et al, 2015). Up to now, reconstructions of the history of Baltic hypoxia relied almost exclusively on proxies preserved in sedimentary archives (Jonsson et al., 1990; Emeis et al., 2003), i.e., foraminifera (Nordberg et al., 2000; Filipsson and Nordberg, 2004), diatom assemblages (Westman and Sohlenius, 1999; Witkowski and Pempkowiak, 1995) and redox-sensitive elements (Jilbert and Slomp, 2013).

Although sediment cores can provide information on millennial-scale variations in

oxygenation, poor temporal resolution and dating control constrain the ability to resolve seasonal to inter-annual DO changes. A highly promising archive that can overcome such limitations has recently been explored, i.e., bivalve shells (Zhao et al., 2017; Schöne et al., 2021, 2022). Periodic shell formation results in regular growth patterns consisting of growth lines and increments (reflecting periods of slow and fast growth, respectively) that serve as a calendar to place proxy records in an accurate temporal context (e.g., Schöne, 2013; Moss et al., 2021). Based on similar growth patterns, annual growth increment chronologies of specimens with overlapping lifespan can be crossdated to form time-series covering centuries to millennia (Witbaard et al., 1997; Butler et al., 2009, 2013; Black et al., 2016, 2019; Wanamaker et al., 2012; Holland et al., 2014; Reynolds et al., 2016; He et al., 2023), which can provide information on long-term climate and ecosystem variability. In the Baltic Sea, bivalves with long lifespan (i.e., several decades), such as *Arctica islandica* and *Astarte* spp., are not only particularly abundant and widely distributed (Zettler, 2001, 2002), but also highly tolerant to severe oxygen depletion (Theede et al., 1969; Taylor, 1976; Oeschger, 1990; Oeschger and Storey, 1993; Strahl et al., 2011). Based on these physiological and ecological characteristics, their shells hold great potential as archives to retrospectively monitor oxygen conditions in the Baltic Sea.

As recently demonstrated, DO concentrations can be inferred from Mn/Ca_{shell} data (Zhao et al., 2017; Schöne et al., 2022, 2022). Manganese (Mn) is a redox-sensitive element that occurs in particulate form when oxygen is present and in dissolved form under reducing conditions (Slomp et al., 1997). As the oxygen concentration in pore waters declines, Mn oxides and/or hydroxides are reduced to Mn^{2+} (Middelburg et al., 1987). The subsequent diffusion of Mn^{2+} into the overlying water body results in elevated Mn^{2+} content in hypoxic waters (Groeneveld et al., 2018). These manganese ions can be rapidly incorporated into the carbonate skeleton of calcifying organisms living under such oxygen-deficient conditions, e.g., into bivalve shells in less than one day (Langlet et al., 2006). Schöne et al. (2021, 2022) extracted monthly resolved Mn/Ca_{shell} time-series from bivalves from the Mecklenburg Bight and Fehmarn Belt that lived during the late 20^{th} and early 21^{st} century. In the present paper, Mn/Ca_{shell} chronologies were constructed from live-collected *A. islandica* specimens that cover the second half of the 19^{th} century as well as the late 20^{th} century to test the hypothesis that oxygen depletion occurred in the SW Baltic Sea since the mid-19^{th} century. Specifically, we have studied if the Mn/Ca_{shell} values of historical shells were significantly different from those of modern times. Persistent hypoxia can also reduce the thickness of shells (Kirby and Miller, 2005) through direct dissolution of inner shell surfaces by acidic metabolites (e.g., succinate,

Crenshaw et al., 1969; Burnett et al., 1988; Schöne, 2013; Schöne et al., 2022) that form during anaerobic metabolism. Similar shell thickness in historical and modern specimens suggested that the historical bivalves have been forced by critically low oxygen levels in the ambient water very much like modern specimens. In addition to molar Mn/Ca_{shell} ratios, Ba/Ca_{shell} values and annual shell growth rate were determined. The latter two proxies can provide information on primary production and phytoplankton dynamics in marine settings, i.e., shell growth rate increases when primary production increases, while Ba/Ca_{shell} peaks are indicative of blooms of certain diatom species which serve as food items for the bivalves (Stecher et al., 1996; Vander Putten et al., 2000; Bonitz et al., 2018; Poitevin et al., 2019; Fröhlich et al., 2022a, b). Ba/Ca_{shell} values and annual increment width can be used to identify the possible causes of oxygen depletion in the Baltic Sea during different time intervals, specifically eutrophication. Results of this study demonstrate the potential of bivalve shells in ecological research.

6.2 Material and methods

Ten specimens of *A. islandica* were collected alive from three localities (O4, MB2 and St12) and water depths of 23.5 to 25 m in the Mecklenburg Bight, SW Baltic Sea, Germany (Fig. 6.1; Table 6.1). All specimens – including two from a museum collection (locality O4), hereafter referred to as 'historical' shells – were preserved in 70 vol% ethyl alcohol with soft tissues. All specimens were still articulated and both valves present. Specimens from St12 were already used in a previous study (Schöne et al., 2021).

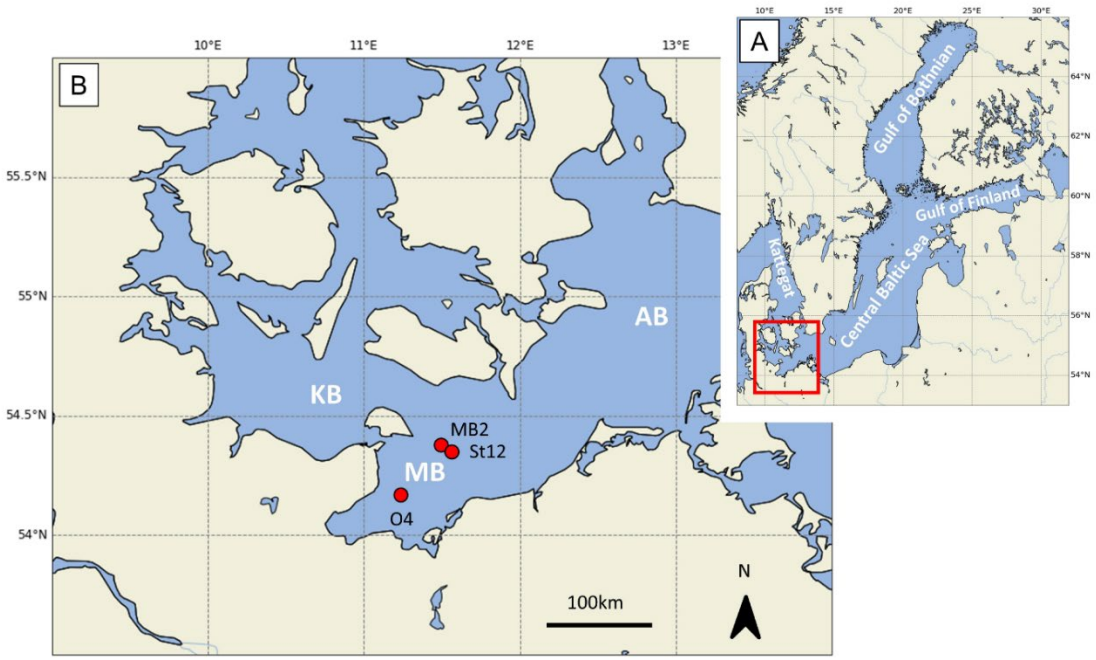

Figure 6.1 Map showing sampling localities (23.5 to 25 m water depth) of the bivalve *Arctica islandica* in the SW Baltic Sea. (A) Overview of the Baltic Sea. (B) Magnified map of the sample region (MB: Mecklenburg Bight) with the localities MB2, St12 and O4. KB: Kiel Bay; AB: Arkona Basin.

Table 6.1 Shells of *Arctica islandica* used in the present study for in-situ element chemical analysis (LA-ICP-MS). All specimens were collected alive from Mecklenburg Bight, Baltic Sea. The last character of the specimen ID denotes left (L) or right (R) valve. Wd = water depth. Position: ventral margin (vm) or hinge (h); #spots = number of LA-ICP-MS spots. Sample collection dates: MB2 = 22 June 1996; St12 = 25 Oct. 2001; O4 = Nov. 1904.

Locality	Specimen ID	Wd (m)	Latitude, longitude	Age (yr)	LA-ICP-MS: position, #spots; sampled time interval, sampled years of life
MB2	HR-MB2-96-A1L	24	54°19′55.75”N, 011°29′52.95” E	12	h, 38; 1987-1995, 3-11
St12	HR-MB2-96-A3L	24	54°19′55.75”N, 011°29′52.95” E	15	h, 49; 1984-1995, 3-14
	HR-MB2-96-A4L	24	54°19′55.75”N, 011°29′52.95” E	20	h, 56; 1979-1995, 3-19
	MLZ-St12-A4R	25	54°18′59.50”N, 011°33′E	19	vm, 329; 1987-2001, 5-19
	MLZ-St12-A5R	25	54°18′59.50”N, 011°33′E	15	vm, 326; 1991-2001, 5-15
	MLZ-St12-A6R	25	54°18′59.50”N, 011°33′E	14	vm, 373; 1991-2001, 4-14
	MLZ-St12-A7L	25	54°18′59.50”N, 011°33′E	7	vm, 183; 1997-2001, 3-7
	MLZ-St12-A9L	25	54°18′59.50”N, 011°33′E	8	vm, 151; 1998-2001, 5-8
O4	MOL 8215_04.XI.O4-A1L	23.5	54°10′N, 011°16′E	65	vm, 406; 1845-1904, 6-65
	MOL 8215_04.XI.O4-A2L	23.5	54°10′N, 011°16′E	59	vm, 354; 1856-1904, 11-59

6.2.1 Shell preparation

Shells were processed in the laboratory using sclerochronological techniques described, for instance, in Schöne et al. (2021). In brief, one valve of each specimen was wrapped in a protective layer of metal epoxy resin (WIKO EpoFix 05) and cut along the maximum growth axis (umbo to the ventral margin) perpendicular to the annual growth lines (Supplements). For this purpose, a low-speed precision saw (Buehler IsoMet 1000) was used equipped with a 0.4 mm thick diamond-coated saw blade (Buehler 15LC 11-4255) and operated at 175 to 225 rpm. From the above cutting axis, two ca. 3 mm-thick sections were obtained (Supplements) and mounted on glass slides using metal epoxy resin with the mirroring sides facing upward. Then, the cross-sectioned shell slabs were ground on glass plates using suspensions of 800 and 1200 grit SiC powder and polished with 1 µm Al_2O_3 suspension on a Buehler MasterTex cloth. Between each grinding and polishing step, the samples were ultrasonically cleaned with tap water. One cross-section was selected for growth pattern analysis and the other used for in-situ chemical analysis.

6.2.2 Growth pattern analysis

One polished section of each specimen was immersed in Mutvei's solution under constant stirring at 37 to 40 °C for ca. 18 min (Schöne et al., 2005). This treatment simultaneously etched the carbonate phase of the shell, preserved the organic matrix in three dimensions and stained acidic mucopolysaccharides and glycosaminoglycans (acidic mucosubstances and acetic mucins) blue. As the growth lines are rich in organics, they were stained darker blue than the carbonate-dominated portions between adjacent growth lines and could thus be more easily identified under the reflected-light microscope. Etched and dyed thick-sections were viewed under a binocular microscope (Olympus SZX16) equipped with sectoral (= one-quarter) dark-field ring-light illumination (Schott VisiLED MC1000) and photographed with a digital camera (Canon EOS 600D). The annual shell growth patterns provided a framework by which chemical data were placed in accurate temporal context. Furthermore, using standard sclerochronological methods (Butler et al., 2013; Cook and Peters, 1997; Helama et al., 2006; Schöne, 2013), a stacked annual growth increment width chronology was computed. For this purpose, heteroscedasticity (the correlation between local mean and variance) was removed from each series by means of adaptive power transformation. Then, the inherent age trends were estimated by stiff cubic spline functions and subsequently removed from the data. Finally, detrended chronologies were standardized and arithmetically averaged to form a stacked chronology for comparison with environmental variables.

6.2.3 In-situ chemical analysis

The concentrations of manganese (measured as ^{55}Mn) and barium (measured as ^{137}Ba) were determined with by laser ablation-inductively coupled plasma-mass spectrometry (LA-ICP-MS) in spot mode. Three specimens were analyzed at the Max Planck Institute for Chemistry (MPIC) at Mainz, the remaining samples at the Institute of Geosciences, Johannes Gutenberg University of Mainz (JGU) (Table S6.1). At the MPIC, a 213 nm Nd:YAG laser (UP-213 NewWave) coupled to a Thermo Fisher Element2 single collector sector-field ICP-MS (run at low-mass resolution mode) was used. Spots with a diameter of 55 µm and a spacing of 80 µm (measured between the midpoints of the LA spots) were placed along the axis of maximum growth in the hinge plate of the shells. Laser repetition rate and laser energy density on the samples were 10 Hz and ca. 16 J/cm^2, respectively. Background intensities were measured for 12 s. Times for ablation and washout equaled 60 s and 30 s, respectively. The system at JGU consisted of a 193

nm ArF Excimer laser (ESI NWR193) equipped with a TwoVol2 sample cell that was coupled to an Agilent 7500ce quadrupole ICP-MS. Spots with a diameter of 65 µm and a midpoint spacing of 85 µm were placed along the ventral margin of the shells (inner portion of the outer shell layer) as well as the axes of maximum growth in the hinge plate of the remaining specimens. Laser repetition rate was 10 Hz and the laser energy density on the samples ca. 3 J/cm^2. Each analysis consisted of 15 s of background, 30 s of ablation and 20 s of washout time.

Accuracy and precision of all LA-ICP-MS analyses were assessed by measuring different reference materials as quality control materials (QCMs). At both institutions, USGS MACS-3 was used, at JGU also USGS BCR-2G. For data measured at the MPIC, the synthetic glass, NIST SRM 612, was employed to calibrate the element concentrations of the shell samples and the remaining reference materials using the preferred values available at the GeoReM database (http://georem.mpch-mainz.gwdg.de/, application version 33, last access: 20 December 2022; Jochum et al., 2005, 2011). Signals of the measurements were monitored in time-resolved mode and processed using an in-house Excel spreadsheet (Jochum et al., 2007; Mischel et al., 2017). For the measurements performed at JGU, NIST SRM 610 and 612 were used as calibration material. The time-resolved signals were processed using LAtools (Branson et al., 2019). For both data reduction strategies, ^{43}Ca served as the internal standard. Element concentrations determined for the QCMs are given in Table S6.1. To compute molar element-to-calcium ratios (µmol/mol), a Ca content of 380,000 µg/g was assumed for the shells (Marali et al., 2017).

6.2.4 Seasonal temporal alignment and resampling of the chemical data

The rate of shell formation is not constant, but varies through seasons and lifetime of the bivalves controlled by internal physiological processes and external environmental changes (Clark, 1975; Hall, 1975; Kennish and Olsson, 1975; Jones and Quitmyer, 1996; Schöne, 2008). Therefore, samples taken from different shell portions represent different amounts of time. For direct comparison of the chemical data, mathematical resampling is required to adjust their temporal resolution (Hallmann et al., 2011). In a first step, the growth record was placed in accurate temporal context using the seasonal shell growth model for *A. islandica* in surface waters of the Baltic Sea (Schöne et al., 2021). Once the date of each LA sample (= the center of each LA spot) was determined, missing data between samples were computed by linear imputation. This approach provided an uninterrupted, artificial time-series with daily resolution from which monthly averages were computed (= resampling technique). Arithmetic averages

of resampled monthly element/Ca data provided weighted annual means.

6.2.5 Detrending of Mn/Ca_{shell} data

Mn/Ca_{shell} chronologies exhibited ontogenetic trends (Fig. S6.1), which were removed prior to comparison with environmental data or shell growth data following the method described in Schöne et al. (2021). Briefly, monthly Mn/Ca_{shell} data of each specimen were plotted against ontogenetic age and the declining trend of the average curve estimated with an exponential function (= regional curve normalization; Supplements). Instead of generating dimensionless Mn/Ca_{shell} values (which would be obtained by diving measured by predicted data), the level at the beginning of the time-series was set as an anchor point, and monthly Mn/Ca_{shell} values later in life were increased by the difference (offset) between this anchor point and the predicted Mn/Ca_{shell} value for each life stage. In the following sections, detrended Mn/Ca_{shell} data are reported.

6.2.6 Environmental data

Instrumental DO concentration, phosphate and temperature data were obtained from the website of the Leibniz Institute for Baltic Sea Research Warnemünde, IOW (https://odin2.io-warnemuende.de/; last access: 25 January 2023) for the closest station next to the locality where the bivalves lived, i.e., TF0012 (54°18′54.00″ N, 011°33′00.00″ E; 20–25 m water depth; Fig. 6.1). Since the data were taken at irregular time intervals and are incomplete, linear imputation was applied to compute an artificial, uninterrupted time-series with daily resolution from which monthly and annual averages were computed (Supplements). Mean daily river discharge data (station Bad Suelze 1), obtained from the website of the Federal Institute of Hydrology (https://portal.grdc.bafg.de; last access: 25 January 2023), provided the basis to compute growing season averages (Oct-Sep). Reconstructions of Major Baltic Inflows (MBIs) (barotropic inflows from the North Sea into the Baltic Sea) came from Mohrholz (2018) and the online repository of this paper (https://dx.doi.org/10.12754/data-2018-0004; last access: 25 January 2023). With these data, the total volumes of water and salt reaching the Baltic Sea were computed for each growing season. The time-series of the Atlantic Multidecadal Variability index (Enfield et al., 2001) was obtained from the NOAA Physical Sciences Laboratory from their website at https://psl.noaa.gov/data/timeseries/AMO/ (last access: 25 January 2023).

6.2.7 Statistical and spectral analyses

The Kruskal-Wallis test was applied to compare the chemical data of different time intervals. A p-value below 0.05 was referred to as a statistically significant difference. Continuous wavelet analysis (Morlet wavenumber 6) was conducted using the software PAST ver. 3.20 (https://www.nhm.uio.no/english/research/resources/past/) to determine periodic oscillations in the time-series and their temporal developed.

6.3 Results

Studied modern specimens of *A. islandica* from Mecklenburg Bight attained a lifespan of merely 20 years, whereas historical specimens from the same region grew three times older (Table 6.1; Fig. 6.2). Monthly element/Ca chronologies covered the time intervals 1845–1904 (locality O4), 1980–1995 (MB2), and 1987–2001 (St12) (Fig. 6.1–6.3; Table 6.1). 'Annual' (= growing season, Oct-Sep) average chronologies were available for 1846-1904 and 1981–2001 (given year stands for end of growing season; Fig. 6.4–6.6).

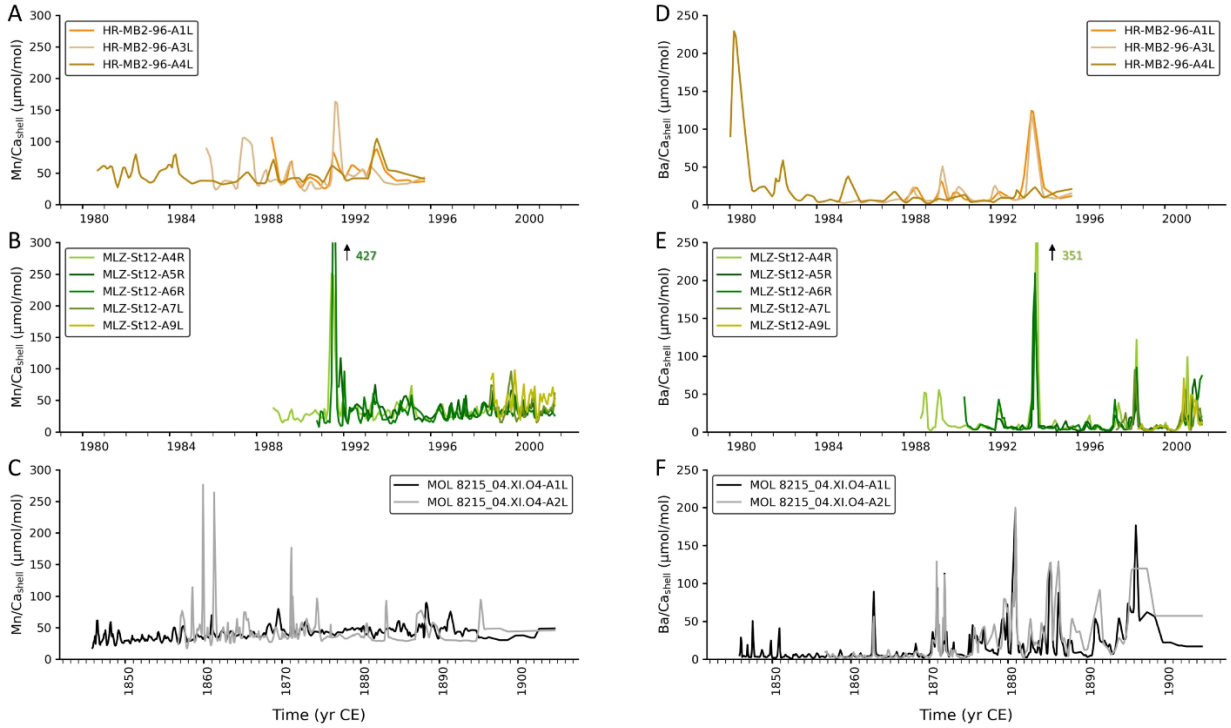

Figure 6.2 Mn/Ca_{shell} (detrended) and Ba/Cashell chronologies (monthly resolution) of ten specimens of *Arctica islandica* collected from three different sites in the Mecklenburg Bight. (A, D) MB2, (B, E) St12, (C, F) O4 (Fig. 6.1; Table 6.1). Numbers in boxes refer to specimen IDs.

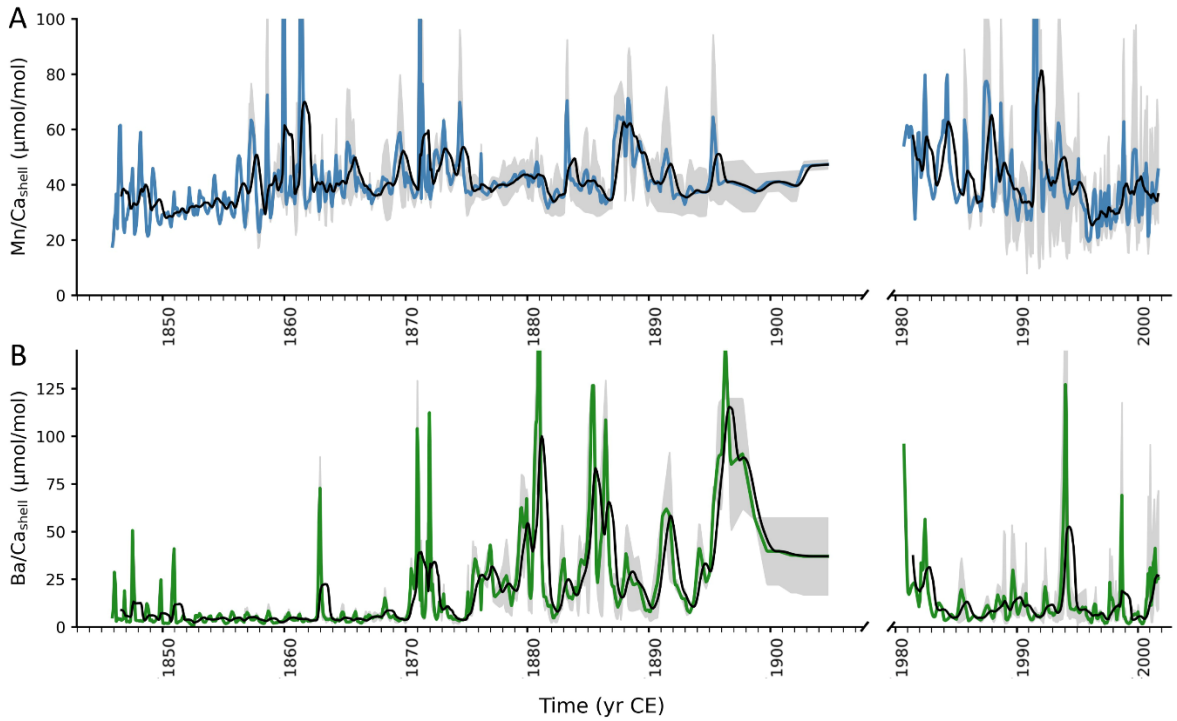

Figure 6.3 Monthly Mn/Ca$_{shell}$ (A) and Ba/Ca$_{shell}$ (B) time-series of *Arctica islandica* from Mecklenburg Bight (Fig. 6.1; Table 6.1). The historical portion of the chronology (19th century) was constructed from two contemporaneous specimens, the late 20th century record from eight specimens (arithmetic monthly means; see Table 6.1 and Fig. 6.2). Blue = manganese, green = barium. Gray shading indicates the maximum and minimum. For better identification of trends, a running average (10 months) was computed (black line).

6.3.1 Mn/Ca$_{shell}$ time-series

Monthly Mn/Ca$_{shell}$ curves exhibited a strong visual synchronicity (Fig. 6.2). In particular, peaks occurred at nearly the same time. This did not only apply to specimens from the same site (Fig. 6.2), but also to contemporaneous specimens of different localities (Fig. 6.2A+B). However, the peak heights differed by up to 165 % between modern specimens from the same site (locality MB2, 1991: 62 vs 163 µmol/mol) and by almost 600 % between specimens belonging to different sites (1991: St12 = 427 µmol/mol) (Fig. 6.2). In the historical specimens, peak heights differed by up to 644 % (1859: 37 vs 277 µmol/mol). With 184 µmol/mol, the average range of monthly Mn/Ca$_{shell}$ values (= difference between average minimum and maximum, i.e., 14 and 198 µmol/mol, respectively) was 84 % larger at locality St12 than at MB2 (average range = 100 µmol/mol; 25 to 125 µmol/mol). This result remained the same if the difference between the most extreme values within one individual were considered: 141 µmol/mol were attained at locality MB2 (specimen HR-MB2-96-A3L: 22 and 163 µmol/mol), but 419 µmol/mol at St12 (specimen MLZ-St12-A6R: 8 and 427 µmol/mol). In contrast, the lowest amplitudes were similar at both sites and equaled 80 µmol/mol (specimens HR-MB2-96-A1L and MLZ-St12-

A9L). Extreme values of historical shells fell between these figures (average range = 166 µmol/mol, i.e., 17 to 183 µmol/mol; largest amplitude = 260 µmol/mol; smallest amplitude = 72 µmol/mol) (Fig. 6.2). Typically, a distinct seasonal oscillation was developed with higher Mn/Ca_{shell} values occurring in the warm season and lower values in the cold season. However, a few Mn/Ca_{shell} peaks fell into winter (e.g., early 1860, early 1991). Note, above given comparisons were only provided for shell portions offering sufficient temporal resolution, i.e., where it was possible to compute monthly averages (Fig. 6.2+3A). The summary plot (Fig. 6.3) illustrates visually that no notable difference exists between monthly Mn/Ca_{shell} data of historical and modern shells (Fig. 6.3A). In the following, Mn/Ca_{shell} patterns are described on the basis of annually resolved chronologies (growing season averages, Oct–Sep), which provided a better insight into inherent trends, cycles and level shifts.

As shown in Figure 6.4, annual Mn/Ca_{shell} data varied on decadal time-scales during the time interval covered by the historical shells (1846 to 1904, 59 years; years denote end of growing season). Consistently strong and significant ($p < 0.05$) spectral power was found at periods of 12 to 15 years (Fig. 6.5A). In addition, shorter-term variability of 4 years was intermittently strong and significant. The stacked record of the late 20th century (combined chronologies of localities MB2 and St12) comprised only 21 years (1981–2001; Fig. 6.4) which was too short to identify decadal variability with statistical confidence. The chronology was dominated by strong variability on short time-scales (period length of ca. 2 to 4 years), particularly before 1993 (Fig. 6.5A). The low-frequency components were more easily inspected after applying a 5-yr running average to the data (Fig. 6.6A).

While no apparent monotonous long-term trends existed in the site-specific chronologies, several level shifts were detected. For example, during the late 20th century, Mn/Ca_{shell} values dropped from an average of 47 to 35 µmol/mol around 1993 (Fig. 6.4). Furthermore, between 1846 and 1855, average Mn/Ca_{shell} values were markedly lower (on average, 33 µmol/mol) than after this interval (average of 43 µmol/mol for 1856–1904) and no apparent long-term increase or decrease was found. This finding is corroborated by a non-parametric Kruskal Wallis test ($p = 0.0015$) for which the first 10 years were compared to the last 10 years (42 µmol/mol) of the historical part of the stacked chronology (1895-1904). The same result was obtained if slightly larger time intervals were chosen (13 years) that considered the decadal variability described above (see also Supplements for a stepwise, windowed assessment).

The reservation must be made that specimen MOL 8215-04.XI.O4-A2L showed much larger monthly Mn/Ca_{shell} peaks than specimen MOL 8215-04.XI.O4-A1L, especially at the

beginning of the chronology (Fig. 6.2). By combining the data of both specimens, these peaks were responsible for the abrupt Mn/Ca_{shell} level increase of the stacked annual chronology (Fig. 6.4). However, even if only specimen MOL 8215-04.XI.O4-A1L was studied, Mn/Ca_{shell} values during 1846–1855 were still significantly lower than during subsequent time intervals (Fig. 6.2). Instead of a stepwise change during the mid-1850s, Mn/Ca_{shell} of this specimen increased non-linearly between 1846 and the early 1890s, with a steeper rise in the beginning (approx. 1 µmol/mol) and a gradual shallowing of the slope between 1868 and 1894, followed by a slight decline during the turn of the century (Fig. 6.2). The first 10 years of this chronology (1846–1855) differed significantly ($p < 0.05$) from any of the following decades (1856–1865, 1866–1875, 1876–1885, 1886–1895) including 1895–1904.

Mn/Ca_{shell} values measured near the umbo or ventral margin of the two historical shells (= representing the first or last 21 years of the historical part of the stacked chronology, respectively) were statistically indistinguishable ($p > 0.05$) from those measured on average in the eight studied specimens from the late 20th century (MB2 and St12 combined: 21-year stacked record) (Fig. 6.4). It should be noted that bivalves from locality MB2 contained approx. 30 % more manganese in their shells than those from St12 (on average, 48 vs 37 µmol/mol, respectively; Fig. 6.2A+B). Therefore, a site-specific approach revealed slightly different results than such outlined above, i.e., Mn/Ca_{shell} values of late 19th century shells remained below ratios measured in modern specimens from MB2 ($p < 0.05$), but exceeded such from St12 ($p = 0.0012$). Values from the mid-19th century were smaller than such from MB2, but statistically indifferent from St12.

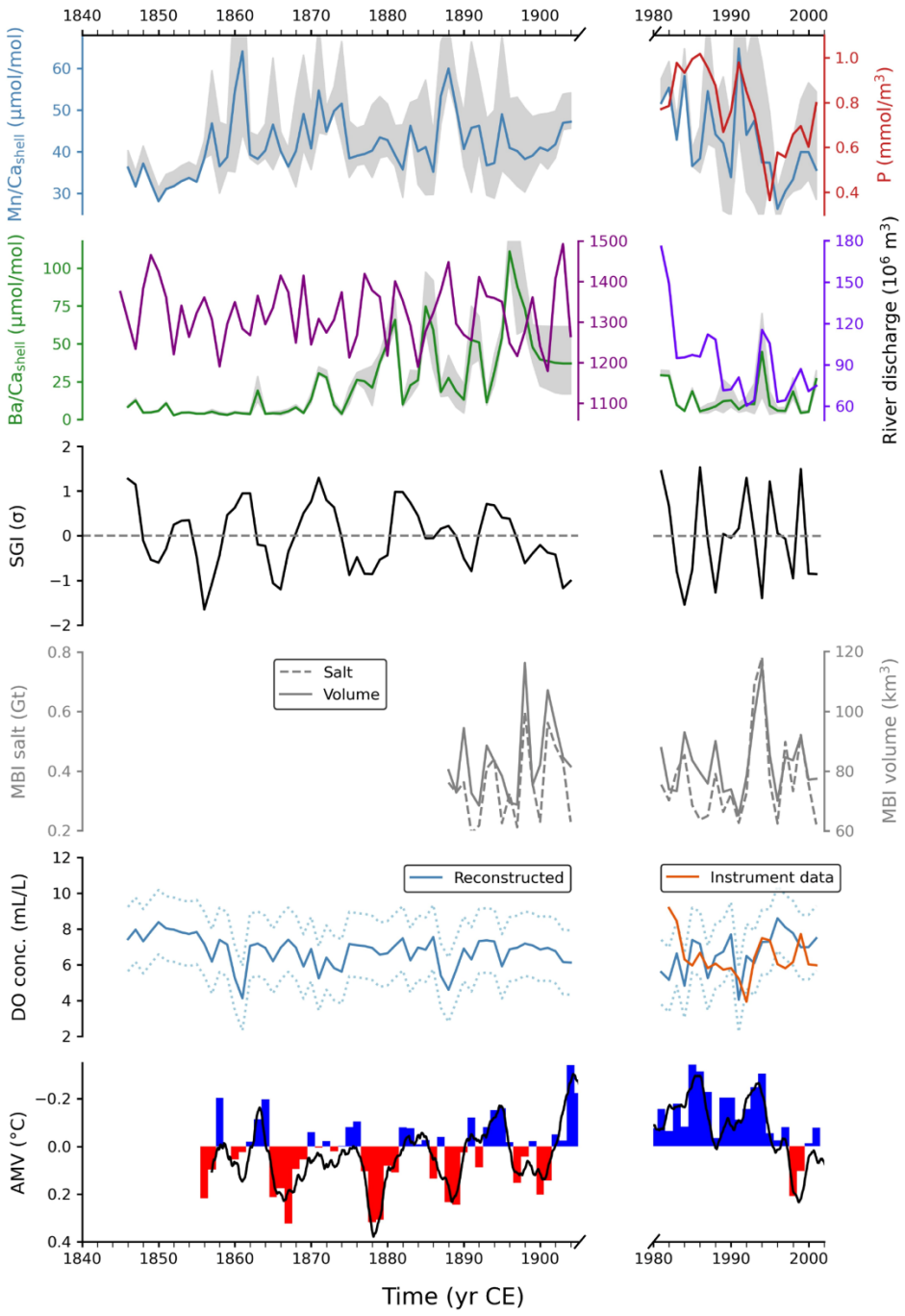

Figure 6.4 Annual Mn/Ca$_{shell}$ (blue) and Ba/Ca$_{shell}$ (green) time-series of *Arctica islandica* from Mecklenburg Bight in comparison to detrended annual shell growth (SGI), environmental variables (phosphate, river discharge, Major Baltic Inflow volume and salt) and the Atlantic Multidecadal Variability (AMV) (for details on data sources see section 2.6). The historical portion of the element/Ca chronology was computed from two, the modern part from eight contemporaneous specimens (arithmetic annual means). Gray shading represents the maximum and minimum values. Also shown is the reconstructed and instrumental DO concentration, the former comes with the 1σ prediction error (dotted lines) as illustrated in Figure 5.7. River discharge data (SW Baltic Sea) for the 19th century were taken from Hansson et al. (2011). Instrumental river runoff data are for just one river (station Bad Sülze 1).

6.3.2 Ba/Ca_{shell} time-series

The monthly resolved Ba/Ca_{shell} profiles of contemporaneous specimens exhibited a striking running similarity within and between sites (Fig. 6.2). Ba/Ca_{shell} peak heights of different specimens from the same site were largely similar (except for specimen HR-MB2-96-A4L during 1994; Fig. 6.2). However, similar to manganese, the height of Ba/Ca_{shell} peaks differed notably between contemporaneous specimens from different localities (i.e., by up to 197 %, and 1,430 % if specimen HR-MB2-96-A4L was included) (Fig. 6.2). The highest observed monthly Ba/Ca_{shell} peak (1994) attained only 124 µmol/mol at MB2, but 351 µmol/mol at St12. Average Ba/Ca_{shell} ranges of the three study sites and time intervals were in close agreement with each other (199, 155 and 182 µmol/mol at O4, MB2 and St12, respectively).

Annual Ba/Ca_{shell} showed a gradual, steady increase of the average from approx. 5 to 45 µmol/mol (Fig. 6.4). Likewise, the baseline and extremes increased steadily during the second part of the 19th century. During this time interval, extreme values ranged between approx. 2 and 103 µmol/mol. With an average of merely 14 µmol/mol and a range of 40 µmol/mol (extremes: 5 and 45 µmol; highest values occurred in 1994), Ba/Ca_{shell} values of the late 20th century remained significantly below such prevailing 100 years earlier ($p < 0.0001$) (Fig. 6.4). However, compared with the mid-19th century, modern specimens contained significantly larger amounts of barium ($p < 0.0001$). In contrast to manganese, the Ba/Ca_{shell} content in the shells from the two modern sites (MB2: on average, 15 µmol/mol, St12: 14 µmol/mol) was statistically indistinguishable ($p = 0.2689$). The long-term Ba/Ca_{shell} increase during the second half of the 19th century was superimposed by similar decadal variability as manganese, with period lengths of ca. 12–15 and 4–6 years (Fig. 6.5B). These signals became stronger toward the end of the 19th century, i.e., the variance increased. As in manganese, a four-year oscillation dominated in the late 20th century, but it was much less pronounced as in Mn/Ca_{shell}, while lower-frequency oscillations could not be detected owing to the shortness of the chronology (Fig. 6.5B). Low-pass filtering further enhanced the long-term upward trend during the 19th century, but the decadal variability was less strongly expressed as in the case of Mn/Ca_{shell} (Fig. 6.6B).

6.3.3 Shell growth increment width time-series

Similar to Mn/Ca_{shell} values, the annual shell growth rate fluctuated on decadal time-scales (ca. 10–15 years) during the 19th century, but on strong ca. 4–6-yr cycles in more recent times (Fig. 6.4, 6.5C). Furthermore, annual increments widths were governed by a multi-decadal oscillation, which could not be properly investigated due to the shortness of the chronology. Shell growth

increased gradually until ca. 1880 and then declined until the turn of the century (Fig. 6.4). Both the decadal and multidecadal oscillations were better seen after low-pass filtering with a 5-yr running average (Fig. 6.6C)

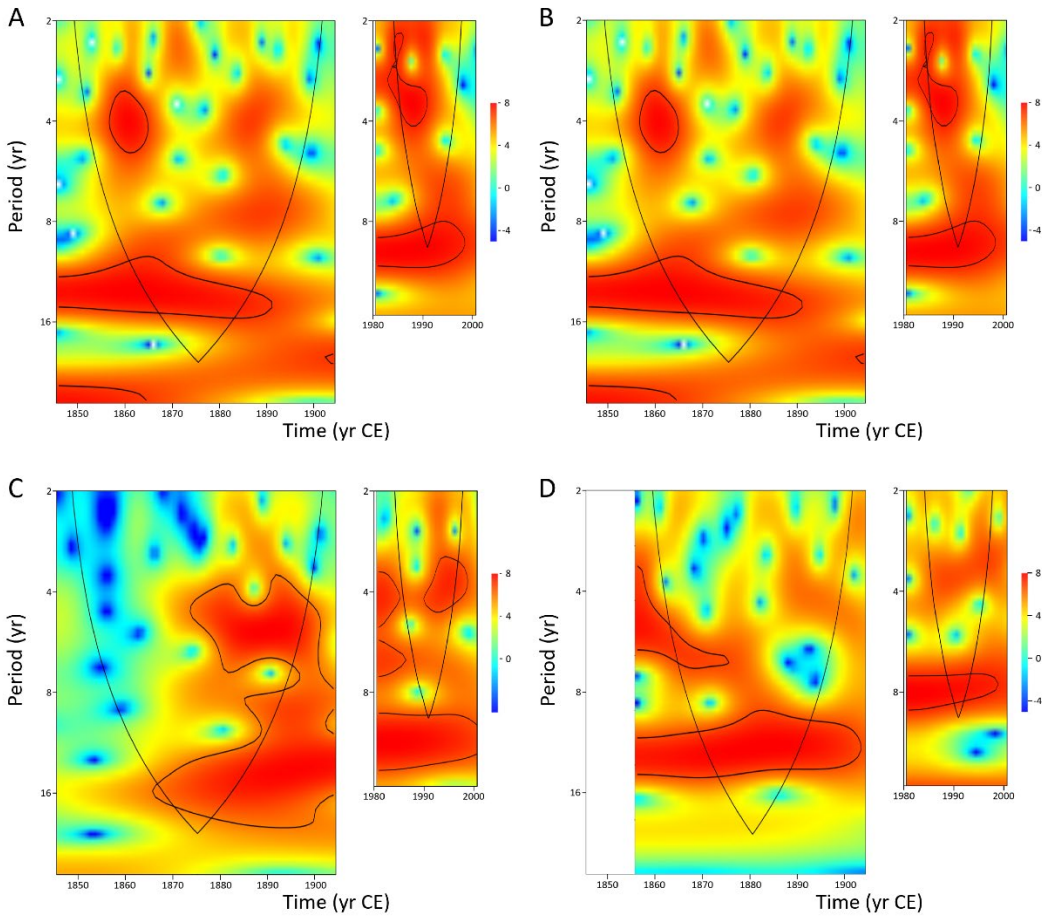

Figure 6.5 Continuous wavelet spectra (Morlet wavenumber 6) of annual Mn/Ca_{shell} (A), Ba/Ca_{shell} (B) and shell growth increment width (SGI, C) chronologies of *Arctica islandica* as well as the Atlantic Multidecadal Variability (AMV; arithmetic average of Dec.-March, D) revealing inter-annual and decadal variability (enhanced by the a 2-yr running average of monthly data, solid line). Data below the cone of influence refer to portions of the chronology where zero padding has reduced the variance. Spectral power increases from blue to red. Significant ($p < 0.05$) spectral power is encircled with solid black curves.

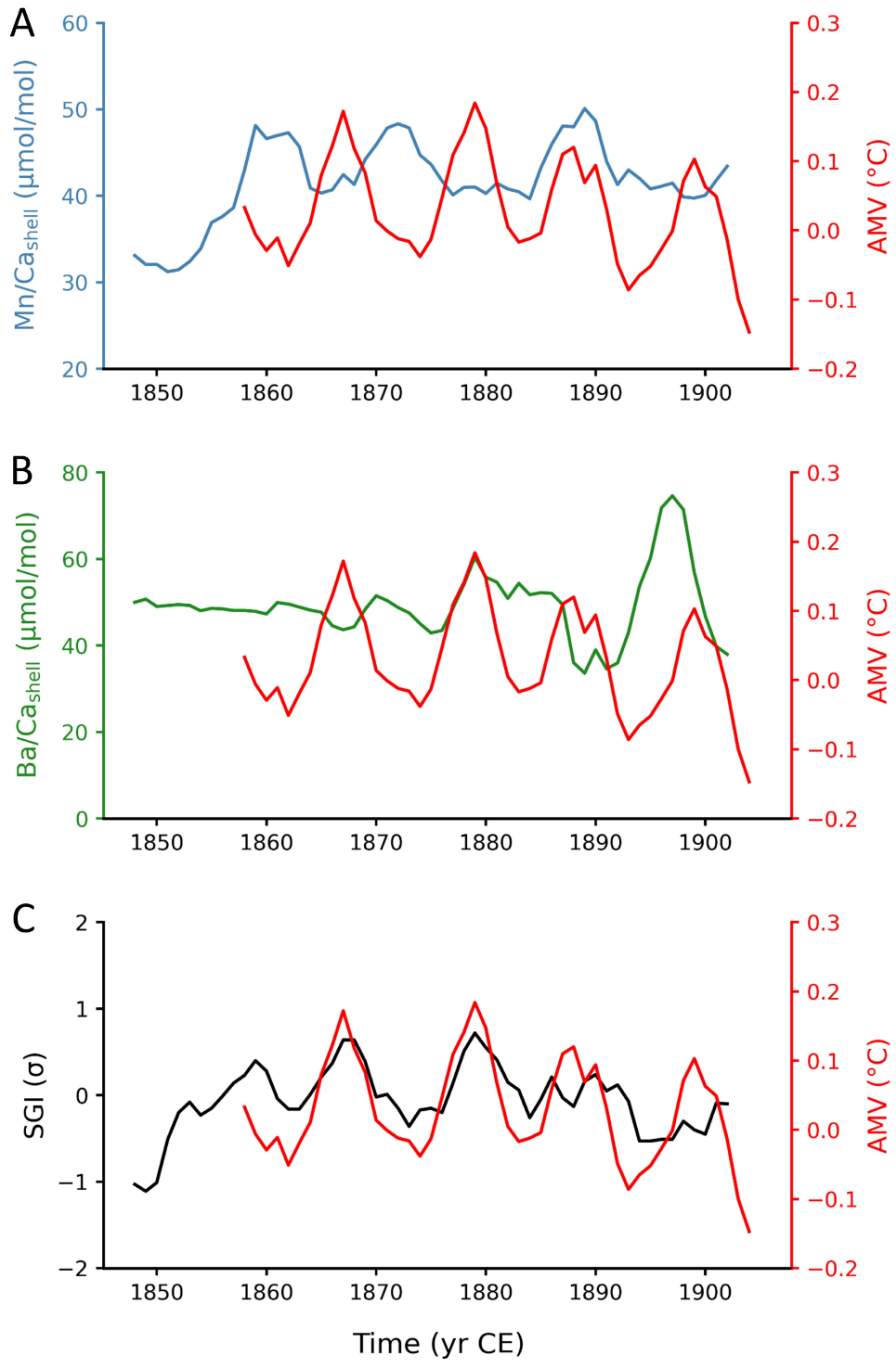

Figure 6.6 Low-pass filtered (5-yr running average) annual Mn/Ca$_{shell}$ (A), Ba/Ca$_{shell}$ (B) and shell growth increment width (SGI, C) chronologies of *Arctica islandica* in comparison to the low-frequency component (5-yr running moving average) of the Atlantic Multidecadal Variability (AMV, Dec.-March average). Note strong correspondence between SGI and AMV on decadal and multidecadal time-scales. In contrast, the correlation between AMV and Mn/Ca$_{shell}$ is non-stationary, and barely no agreement occurs between AMV and Ba/Ca$_{shell}$.

6.4 Discussion

According to the Mn/Ca_{shell} data of studied *A. islandica* specimens, bottom waters at Mecklenburg Bight experienced overall similar low-oxygen conditions including occasional summertime hypoxia during the second half of the 19th century as during the late 20th century (Fig. 6.3+6.4). The Mn/Ca_{shell} average and range of both time intervals was statistically indistinguishable. Besides distinct decadal and inter-annual variations, Mn/Ca_{shell} data also revealed conspicuous level shifts (Fig. 6.4). For example, during the 1850s, the DO concentration decreased gradually or stepwise (depending on whether only one of the two available historical shells were assessed or the average of both) and reached a steady level around 1860 that largely persisted until the turn of the century. During the 1980s, Mn/Ca_{shell} values fluctuated around a similar mean as such prevailing 100 years earlier, but a distinct drop to lower Mn/Ca_{shell} values and hence higher DO concentration occurred in the early 1990s (Fig. 6.4).

6.4.1. Ecological history of the SW Baltic Sea since the mid-19th century told by bivalve shells

The inferred bottom water oxygen depletion during the second half of the 19th century including the deoxygenation event in the mid-19th century (Fig. 6.4) agrees well with historical accounts of increased human-induced environmental perturbations (Zillén et al., 2008) and changes in sedimentary archives in deeper waters of the Baltic Sea at that time (e.g., Zillén and Conley, 2010; Kabel et al., 2012; Jokinen et al., 2018). Mn/Ca_{shell} values increased shortly after the start of the Industrial Revolution in NW Europe (around 1850), which was associated, amongst others, with major land-use changes (cropland expansion on deforested land), accelerating population growth and a significantly increased flux of nutrients into the Baltic Sea (Zillen et al., 2008; Andrén, 1999). The latter is evidenced by a marked $\delta^{15}N$ increase in sediment cores, e.g., from the Arkona Basin during the 1850s (Voß & Struck, 1997; see also Norbäck Ivarsson et al., 2019). The nutrient surplus propelled primary production in surface waters (Andrén, 1999; Andrén et al., 1999) and increased the export of organic substances to the seafloor, which – along with seasonal stratification preventing ventilation of deeper waters – led to a notable decline of the oxygen content below the halocline. A direct comparison of the shell data with nearby sediment cores is extremely challenging or virtually impossible, because sediments of the Mecklenburg Bight are often heavily perturbed by natural (bioturbation, hydroturbation)

and anthropogenic processes (bottom trawling etc.) (Bunke et al., 2019) and thus strongly time-averaged. However, the onset of dark laminated sediments with high organic carbon content, for instance, in cores from the Gotland Basin and the Gulf of Finland suggest large areas of the Baltic Sea were affected by severe oxygen depletion since approx. the mid-19th century (Jonsson et al., 1990; Zillén and Conley, 2010; Kabel et al., 2012; Jokinen et al., 2018).

Eutrophication is also considered as the main reason for the significant change in diatom assemblages in the SW Baltic Sea that started in the 1850s or 1860s and led to a dominance of planktonic taxa (Andrén, 1999; Andrén et al., 1999; Norbäck Ivarsson et al., 2019). Interestingly, the strong increase in Ba/Ca_{shell} values between the 1860s and 1900 (Fig. 6.4) occurred contemporaneously with this gradual shift in diatom community structure suggesting a causal link. Likewise, the strongly reduced Ba/Ca values in shells from the late 20th century (Fig. 6.4) may result from a continued change in diatom community structure which has been described for the SW Baltic Sea (Wasmund et al., 2008; Wasmund & Zettler 2023). As demonstrated for pectinids, the digestion of Ba-rich phytoplankton, in particular certain diatom species, after major blooms results in sharp Ba/Ca_{shell} peaks (Vander Putten et al., 2000; Lazareth et al., 2003; Thébault et al., 2009; Fröhlich et al., 2022a, b). Although such a link has not been explored in other bivalves, it seems highly likely that the same principle applies to *A. islandica*. Hence, future studies should assess which Ba-rich phytoplankton species are on the menu of ocean quahogs.

Higher Ba/Ca_{shell} peaks may not only reflect an increased proportion of edible Ba-enriched species in the phytoplankton community, but also indicate that larger amounts of such cells were present as the result of elevated nutrient availability. Higher nutrient levels can result from increased river runoff (while nutrient concentrations in the river water remain unchanged) or increased nutrient loads (at unchanged freshwater discharge volumes). The first hypothesis can be precluded, because no major changes in riverine freshwater discharge have occurred during the second half of the 19th century (Hansson et al., 2011) (Fig. 6.4). On the other hand, a gradual increase of nutrients arriving in the Baltic Sea is well documented by stable nitrogen isotope profiles of sediment cores (Voß and Struck, 1997; Norbäck Ivarsson et al., 2019) suggesting higher nutrient concentrations in terrestrial runoff. Eutrophication, however, does not selectively stimulate the proliferation of Ba-rich phytoplankton, but also increases the abundance of other edible and nutritive primary producers which will not be recorded by Ba/Ca_{shell} (Thébault et al., 2009; Fröhlich et al., 2022a). This in turn, should have resulted in increasingly faster shell growth rates and lower oxygen levels, which were both not observed (Fig. 6.4). Modulated by decadal fluctuations, annual increments widths of *A. islandica*

increased gradually until ca. 1880, but then declined until the turn of the century although Ba/Ca_{shell} values continued to rise (Fig. 6.4, 6.6A+C). Likewise, Mn/Ca_{shell} values did not reveal a long-term upward trend that would indicate a continued deterioration of oxygen depletion (Fig. 6.4, 6.6B). These findings suggest that observed Ba/Ca_{shell} changes were most likely coupled to an increased proportion of Ba-rich cells in the diet of *A. islandica*, caused by changes in the phytoplankton community structure as reported by Andrén et al. (1999).

Interestingly, shell growth of *A. islandica* is significantly positively correlated to the Atlantic Multidecadal Variation (or Oscillation, AMV, December–March average) index (Fig. 6.4, 6.6C). The AMV describes decadal-scale sea surface temperature (SST) variations in the North Atlantic Ocean (Schlesinger and Ramankutty, 1994) with major periods of ca. 50 to 70 years (Delworth and Mann, 2000; Keenlyside et al., 2008; Mann et al., 2021), but also variations in the 12–15-year band (Fig. 6.5D, 6.6). While the studied stacked shell increment width chronology was not long enough to statistically verify the coupling with the multidecadal component of the AMV, the general increase of the shell growth rate toward the 1880 and decline afterward corresponded well to the low-frequency change of the AMV index chronology (Fig. 6.6C). More importantly, the 12–15-year oscillations of both chronologies were strongly synchronous (Fig. 6.6C). The link between shell growth and this climate index may be explained by AMV-modulated precipitation patterns in the Baltic Sea sector and associated effects on riverine discharge (Börgel et al., 2018), and thus changes in nutrient supply. A visual comparison of reconstructed river discharge data of the southern Baltic Sea (Hansson et al., 2011) and the SGI chronology reveals some agreement on decadal time-scales (Fig. 6.4). However, a much more detailed analysis is required in subsequent studies using longer shell growth increment chronologies constructed from a larger number of bivalve shells covering more recent time intervals for which instrumental river runoff data are available.

Decadal variability with similar period lengths as described above for the AMV and shell growth was also observed in the Mn/Ca_{shell} chronology of the 19th century indicating that DO concentration likewise fluctuated on ca. 12 to 15-year cycles (Fig. 6.6A). In contrast to the AMV, only a weak positive correlation ($R^2 = 0.16$, $p = 0.0015$) was found with shell growth rate if the low frequency domains were targeted. Faster growth of. *A. islandica* with increasing oxygen depletion could indicate that the competition for food decreased, because other benthic organisms were less tolerant against low-DO than ocean quahogs and thus slowed down their metabolic rate. In addition, the low-pass filtered Mn/Ca_{shell} time-series was negatively, but not significantly correlated to the MBI and total salt volume chronologies. The replenishment of bottom water with saline, oxygenated North Sea water apparently resulted in lower amounts of

dissolved Mn and hence lower Mn/Ca_{shell} values. Furthermore, Mn/Ca_{shell} was non-stationarily correlated to the AMV if the low frequency components were compared, i.e., a significant inverse coupling existed between 1846 and 1880 ($R^2 = 0.58$, $p < 0.0001$), but opposite for the remaining 24 years ($R^2 = 0.18$, $p = 0.0396$) (Fig. 6.6A). The reason for this remains unresolved.

In more recent times, the mechanisms driving Mn/Ca_{shell} and Ba/Ca_{shell} values could be compared to a much larger number of instrumental environmental datasets. For example, Mn/Ca_{shell} and phosphate were distinctly positively correlated (Fig. 6.4; $R^2 = 0.23$, $p = 0.0165$) supporting the assumption that oxygen depletion is coupled with high nutrient loads. Furthermore, Ba/Ca_{shell} values were positively tied to river discharge volumes (Fig. 6.4; $R^2 = 0.24$, $p = 0.0138$) which can be explained by the influx of nutrients and subsequent growth of (Ba-rich) phytoplankton. The conspicuous negative shift of Mn/Ca_{shell} during the early 1990s appears to have been caused by a combination of reduced nutrient loads and better oxygenation of bottom waters (Fig. 6.4), a phenomenon that has been observed in the wider Baltic Sea (Conley et al., 2009). Phosphate levels dropped by ca. 1/3 (average of 0.89 mmol/m^3 in the 1980s to 0.57 mmol/m^3 in the late 1990s) (Fig. 6.4), predominantly as a result of urban sewage treatment (Andersen et al., 2017), and a series of strong barotropic inflows occurred during that time (Fig. 6.4), specifically between October 1993 and June 1994 (Mohrholz, 2018) (Supplements) which renewed bottom water DO levels. Actually, the total volume of salt transported to the Baltic Sea by MBIs during the growing seasons (Oct.–Sep.) of 1992/3 and 1993/4 were among the largest recorded between 1887 and 2018 (Mohrholz, 2018) (Supplements). A similar result is obtained if the average volume of salt is considered (Fig. 6.4). Phosphate levels remained low in subsequent years which likely helped to maintain improved oxygen conditions in bottom waters in following years, despite stronger river discharge pulses in 1994 and 1995 (Fig. 6.4). These runoff events were accompanied by Ba/Ca_{shell} peaks indicating blooms of Ba-rich diatoms (Fig. 6.4). The ecosystem improvement in the late 1990s has also been reported from many other regions in the Baltic Sea and is associated with distinctly reduced eutrophication (Andersen et al., 2017).

6.4.2 Faithfulness of Mn/Ca_{shell}-based DO reconstructions

As recently demonstrated, with declining amounts of oxygen in ambient water, the concentration of manganese relative to calcium in the shell carbonate of *A. islandica* increases (Schöne et al., 2021, 2022). This finding was corroborated in the present study by a more

extensive dataset. By combining data from Mecklenburg Bight and Fehmarn Belt, it also became clear that the slope and intercept of the negative linear relationship between Mn/Ca_{shell} and DO concentration was very similar between different regions (Fig. 6.7). Despite that, Mn/Ca_{shell} remains a qualitative DO indicator until a rigorous calibration is available. So far, the calibration is based on DO measurements completed approximately 1 m above the sediment surface, but not on the oxygen concentration of the water inhaled by the bivalves or the porewater that engulfs the mantle tissue while the animal is feeding. The latter is relevant because manganese could have reached the body fluids by diffusion through the mantle epithelia. It would be useful if future studies addressed the question if DO in the free water column is linearly correlated to the oxygen concentration closer to the seabed where the bivalves filter-feed. Furthermore, it needs to be quantified how much Mn in the shell comes from direct contact of the soft tissues with sedimentary porewater.

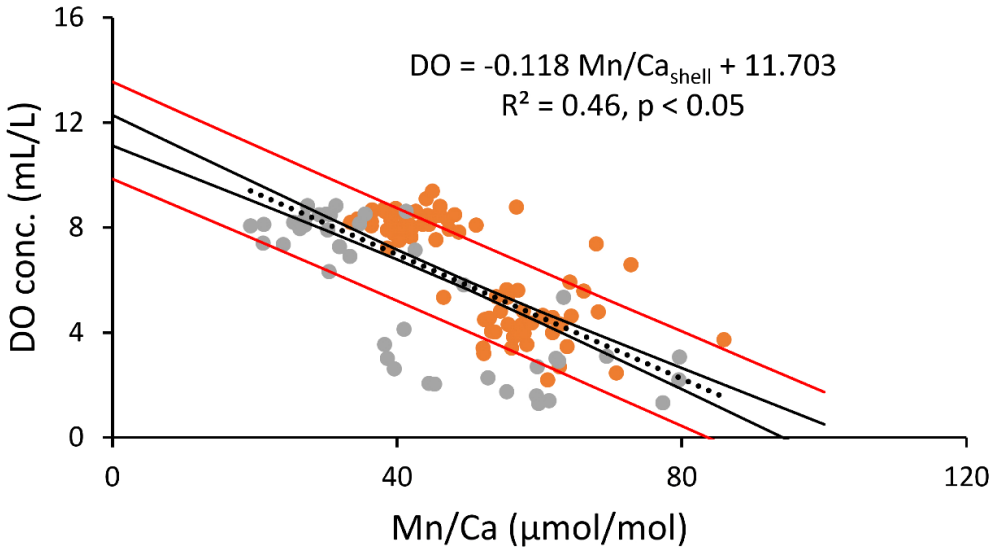

Figure 6.7 Updated tentative linear model to predict DO concentrations (some decimeters above the seafloor) using Mn/Ca_{shell} values of *Arctica islandica*. In this plot, seasonal extremes of the current study (localities MB2 and St12; gray; one winter outlier omitted that resulted from the ingestion of particulate Mn) were combined with published data of *A. islandica* shells from Fehmarn Belt (orange; Schöne et al., 2022). Black curves = 95% confidence intervals of the regression lines; red curves = 1σ prediction intervals. The precision error equals 1.8 mL/L.

6.5 Conclusions

Climate change has major impacts on ecosystem health, especially in the Baltic Sea, which suffers from biodiversity reduction and ecosystem degradation from multiple stressors, such as temperature rise, acidification and hypoxia. In order to improve ecosystem management and conservation, it is necessary to obtain past environmental data (e.g., hypoxia) on long-time scales in the Baltic Sea. Geochemical data in bivalve shells *A. islandica* from the Baltic Sea can provide long-term and high-resolution environmental information, where Mn/Ca_{shell} ratios were linked to DO concentrations in the water column (Schöne et al., 2021, 2022) and shell Ba/Ca profiles may be associated with blooms of digestible diatoms. Here, this multiproxy approach was utilized to reconstruct the DO history in Mecklenburg Bight since the mid-19th century. The data revealed that seasonal deoxygenation in the western Baltic Sea was already present in the mid-19th century indicating that the trophic state of the SW Baltic Sea was affected by human activity since the onset of the Industrial Revolution. Notably, in the last decade of the 20th century, better oxygen conditions were observed in the SW Baltic Sea due to increased baroclinic inflows and the mitigation of eutrophication. The geochemical profiles in shells can be used as temporally well-constrained proxies to track the history and mechanisms of hypoxia.

The present study also demonstrated the potential of bivalves in ecological research. Bivalve shells can complement sedimentary records by providing a precise and highly-resolved temporal framework of ecological changes in the past. This applies in particular to settings where laminae in sediments are weakly developed or entirely absent, such as in the central Mecklenburg Bight. Although it would be possible to construct longer shell chronologies covering many generations of bivalves by combining growth increment records of live-collected and fossil specimens with overlapping lifespan (e.g., Witbaard et al., 1997; Marchitto et al., 2000; Black et al., 2016, 2019), it will remain extremely challenging and time-consuming to match the temporal coverage of sediment cores. This applies specifically to the Baltic Sea where hostile environmental conditions limit the lifespan of marine bivalves (Schöne et al., 2022) Overall, future research should broaden the spatial and temporal scales for retrospective monitoring of the Baltic deoxygenation. Furthermore, emphasis should be placed on improved calibration of the manganese and barium-to-calcium ratios in bivalve shells.

6.6 Supplementary data

Table S6.1 During chemical analysis, the average concentration and standard deviation (1σ) of manganese (Mn) and barium (Ba) in reference materials USGS MACS-3 and USGS BCR-2G were determined. Three *Arctica islandica* specimens (HR-MB2-96-A1L, A3L, A4L) were measured at the Max Planck Institute for Chemistry, Mainz (MPIC) and the other specimens at the Institute of Geosciences, Johannes Gutenberg University of Mainz (JGU). Reference values were taken from the GeoReM database (preferred complied values, http://georem.mpch-mainz.gwdg.de/, application version 33; Jochum et al. 2005, 2011).

Reference material	USGS MACS-3		USGS BCR-2G	
Element (µg/g)	Mn	Ba	Mn	Ba
Ref. values	512 ± 25	59.6 ± 1.4	1550 ± 70	683 ± 7
MOL8215_04.XI.O4-A1L	512 ± 11	59.4 ± 19.6	1552 ± 20	697 ± 11
MOL8215_04.XI.O4-A2L	518 ± 10	62.3 ± 3.5	1554 ± 18	684 ± 10
HR-MB2-96-A1L	454 ± 18	54.3 ± 1.7		
HR-MB2-96-A3L	454 ± 18	54.3 ± 1.7		
HR-MB2-96-A4L	453 ± 14	53.7 ± 1.7		
MLZ-St12-A4R	522 ± 11	61.1 ± 5.2	1570 ± 22	711 ± 24
MLZ-St12-A5R	516 ± 10	60.4 ± 2.3	1551 ± 18	713 ± 17
MLZ-St12-A6R	513 ± 11	60.0 ± 9.0	1549 ± 24	703 ± 23
MLZ-St12-A7L	527 ± 11	63.0 ± 2.7	1582 ± 23	718 ± 16
MLZ-St12-A9L	517 ± 10	61.8 ± 5.7	1549 ± 28	704 ± 15
HR-Nr4-Hol3-77-A1R	519 ± 8	59.3 ± 1.4	1552 ± 16	700 ± 11
HR-Stat20-80-A1R	523 ± 12	60.2 ± 1.6	1564 ± 16	718 ± 9

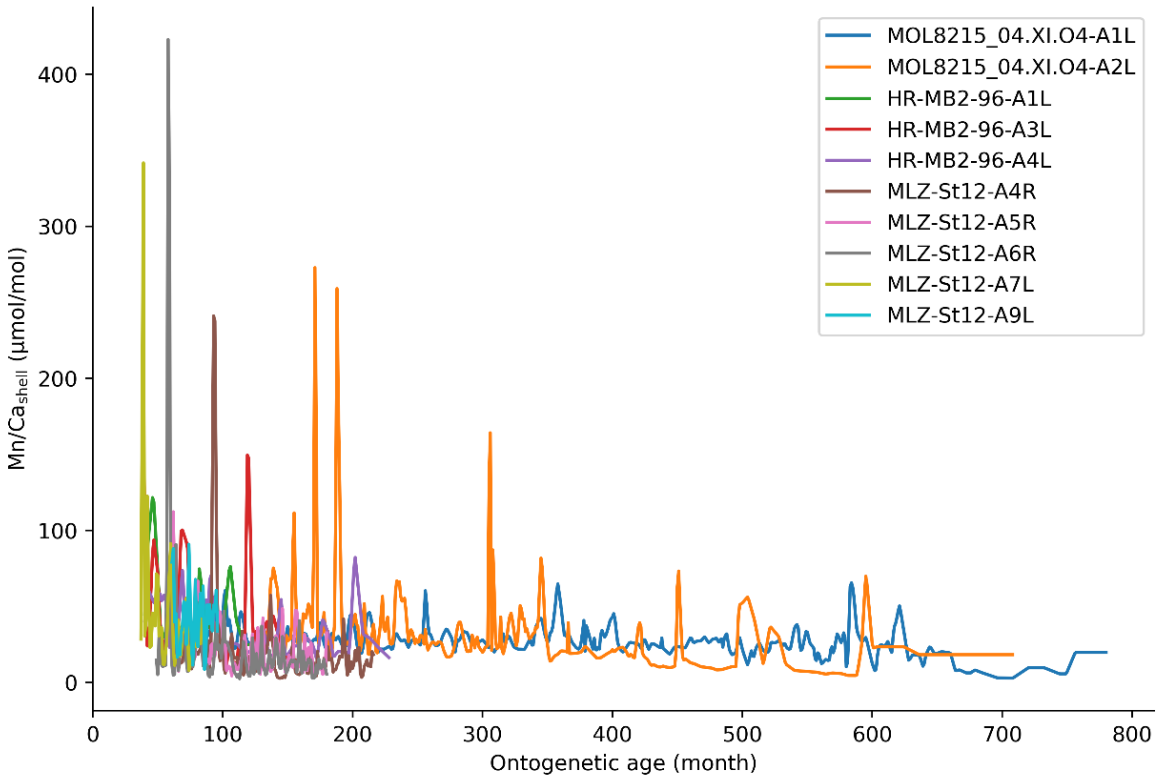

Fig. S6.1. Mn/Cashell chronologies (monthly resolution) of *Arctica islandica* reveal ontogenetic trends.

References

Andersen, J.H., Carstensen, J., Conley, D.J., Dromph, K., Fleming-Lehtinen, V., Gustafsson, B.G., Josefson, A.B., Norkko, A., Villnas, A., Murray, C., 2017. Long-term temporal and spatial trends in eutrophication status of the Baltic Sea. Biol. Rev. 92, 135–149.

Andrén, E., 1999. Changes in the composition of the diatom flora during the last century indicate increased eutrophication of the Oder estuary, south-western Baltic Sea. Estuar. Coastal Shelf Sci. 48, 665–676.

Andrén, E., Shimmield, G., Brand, T., 1999. Environmental changes of the last three centuries indicated by siliceous microfossil records from the southwestern Baltic Sea. Holocene 9, 25–38.

Black, B.A., Griffin, D., van der Sleen, P., Wanamaker, J.R., Speer, J.H., Frank, D.C., Stahle, D.W., Pederson, N., Copenheaver, C.A., Trouet, V., Griffin, S., Gillanders, B.M., 2016. The value of crossdating to retain high-frequency variability, climate signals, and extreme events in environmental proxies. Global Change Biol. 22, 2582–2595.

Black, B.A., Andersson, C., Butler, P.G., Carroll, M., DeLong, K.L., Reynolds, D.J., Schöne, B.R., Scourse, J., van der Sleen, P., Wanamaker, A.D., Witbaard, R. 2019. The revolution in marine paleoecology and paleoclimatology. Biol. Lett. 15, 20180665.

Börgel, F., Frauen, C., Neumann, T., Schimanke, S., Meier, H.E.M., 2018 Impact of the Atlantic multidecadal oscillation on Baltic Sea variability. Geophys. Res. Lett. 45, 9880-9888.

Bonitz, F.G.W., Andersson, C., Trofimova, T., Hátún, H., 2018. Links between phytoplankton dynamics and shell growth of *Arctica islandica* on the Faroe Shelf. J. Mar. Syst. 179, 72–87.

Branson, O., Fehrenbacher, J.S., Vetter, L., Sadekov, A.Y., Eggins, S.M., Spero, H.J., 2019. LAtools: A data analysis package for the reproducible reduction of LA-ICP-MS data. Chem. Geol. 504, 83–95.

Breitburg, D., Levin, L.A., Oschlies, A., Grégoire, M., Chavez, F.P., Conley, D.J., Garçon, V., Gilbert, D., Gutiérrez, D., Isensee, K., Jacinto, G.S., Limburg, K.E., Montes, I., Naqvi, S.W.A., Pitcher, G.C., Rabalais, N.N., Roman, M.R., Rose, K.A., Seibel, B.A., Telszewski, M., Yasuhara, M., Zhang, J., 2018. Declining oxygen in the global ocean and coastal waters. Science 359. Eaam7240.

Burnett, L.E., 1988. Physiological responses to air exposure: acid-base balance and the role of branchial water stores. Amer. Zool. 28, 125–135.

Bunke, D., Leipe, T,, Moros, M., Morys, C., Tauber, F., Virtasalo, J.J., Forster, S., Arz, H.W.,

2019. Natural and anthropogenic sediment mixing processes in the south-western Baltic Sea. Front. Mar. Sci. 6, 677.

Butler, P.G., Scourse, J.D., Richardson, C.A., Wanamaker Jr, A.D., Bryant, C.L., Bennell, J.D., 2009. Continuous marine radiocarbon reservoir calibration and the 13C Suess effect in the Irish Sea: Results from the first multi-centennial shell-based marine master chronology. Earth Planet. Sci. Lett. 279, 230–241.

Butler, P.G., Wanamaker Jr, A.D., Scourse, J.D., Richardson, C.A., Reynolds, D.J., 2013. Variability of marine climate on the North Icelandic Shelf in a 1357-year proxy archive based on growth increments in the bivalve *Arctica islandica*. Palaeogeogr. Palaeoclimatol. Palaeoecol. 373, 141–151.

Caballero-Alfonso, A.M., Carstensen, J., Conley, D.J., 2015. Biogeochemical and environmental drivers of coastal hypoxia. J. Mar. Syst. 141, 190–199.

Carstensen, J., Conley, D.J., Bonsdorff, E., Gustafsson, B.G., Hietanen, S., Janas, U., Jilbert, T., Maximov, A., Norkko, A., Norkko, J., Reed, D.C., Slomp, C.P., Timmermann, K., Voss, M., 2014. Hypoxia in the Baltic Sea: Biogeochemical cycles, benthic fauna, and management. Ambio 43, 26–36.

Crenshaw, M.A., Neff, J.M., 1969. Decalcification at the mantle-shell interface in molluscs. Amer. Zool. 9, 881–885.

Clark, G.R., 1975. Periodic growth and biological rhythms in experimentally grown bivalves. In: Rosenberg G.D., Runcorn S.K., (Eds.), Growth Rhythms and the History of the Earth's Rotation. Wiley, London, pp 103–117.

Cook, E.R., Peters, K., 1997. Calculating unbiased tree-ring indices for the study of climatic and environmental change. Holocene, 7, 361–370.

Conley, D.J., Carstensen, J., Ærtebjerg, G., Christensen, P.B., Dalsgaard, T., Hansen, J.L.S., Josefson, A.B., 2007. Long-term changes and impacts of hypoxia in Danish Coastal waters. Ecol. Appl. 17, S165–S184.

Conley, D.J., Bjorck, S., Bonsdorff, E., Carstensen, J., Destouni, G., Gustafsson, B.G., Hietanen, S., Kortekaas, M., Kuosa, H., Meier, H.E., Muller-Karulis, B., Nordberg, K., Norkko, A., Nurnberg, G., Pitkanen, H., Rabalais, N.N., Rosenberg, R., Savchuk, O.P., Slomp, C.P., Voss, M., Wulff, F., Zillen, L., 2009. Hypoxia-related processes in the Baltic Sea. Environ. Sci. Technol. 43, 3412–3420.

Conley, D.J., Carstensen, J., Aigars, J., Axe, P., Bonsdorff, E., Eremina, T., Haahti, B.M., Humborg, C., Jonsson, P., Kotta, J., Lännegren, C., Larsson, U., Maximov, A., Medina, M.R., Lysiak-Pastuszak, E., Remeikaitė-Nikienė, N., Walve, J., Wilhelms, S., Zillén, L.,

2011. Hypoxia is increasing in the coastal zone of the Baltic Sea. Environ. Sci. Technol. 45, 6777–6783.

Delworth, T. L., Mann, M.E., 2000. Observed and simulated multidecadal variability in the Northern Hemisphere. Clim. Dyn. 16, 661–676.

Diaz, R.J., Rosenberg, R., 2008. Spreading dead zones and consequences for marine ecosystems. Science 321, 926–929.

Emeis, K.-C., Struck, U., Blanz, T., Kohly, A., Voβ, M., 2003. Salinity changes in the central Baltic Sea (NW Europe) over the last 10000 years. Holocene 13, 411–421.

Enfield, D.B., Mestas-Nuñez, A.M., Trimble, P.J., 2001. The Atlantic Multidecadal Oscillation and its relationship to rainfall and river flows in the continental U.S.. Geophys. Res. Lett. 28, 2077–2080.

Filipsson, H.L., Nordberg, K., 2004. A 200-year environmental record of a low-oxygen fjord, Sweden, elucidated by benthic foraminifera, sediment characteristics and hydrographic data. J. Foramin. Res. 34, 277–293.

Fröhlich, L., Siebert, V., Huang, Q., Thébault, J., Jochum, K.P., Schöne, B.R., 2022a. Deciphering the potential of Ba/Ca, Mo/Ca and Li/Ca profiles in the bivalve shell *Pecten maximus* as proxies for the reconstruction of phytoplankton dynamics. Ecol. Indic. 141, 109121.

Fröhlich, L., Siebert, V., Walliser, E.O., Thébault, J., Jochum, K.P., Chauvaud, L., Schöne, B.R., 2022b. Ba/Ca profiles in shells of *Pecten maximus* – A proxy for specific primary producers rather than bulk phytoplankton. Chem. Geol. 593, 127743.

Groeneveld, J., Filipsson, H.L., Austin, W.E.N., Darling, K., McCarthy, D., Quintana Krupinski, N.B., Bird, C., Schweizer, M., 2018. Assessing proxy signatures of temperature, salinity, and hypoxia in the Baltic Sea through foraminifera-based geochemistry and faunal assemblages. J. Micropalaeontol. 37, 403–429.

Hall Jr, C.A., 1975. Latitudinal variation in shell growth patterns of bivalve molluscs: implications and problems. In Rosenberg, G.D., Runcorn, S.K., (Eds.), Growth Rhythms and the History of the Earth's Rotation. Wiley, London, 163–174.

Hallmann, N., Schone, B.R., Irvine, G.V., Burchell, M., Cokelet, E.D., Hilton, M.R., 2011. An improved understanding of the Alaska Coastal current: The application of a bivalve growth-temperature model to reconstruct freshwater-influenced paleoenvironments. Palaios 26, 346–363.

Hansson, D., Eriksson, C., Omstedt, A., Chen, D., 2011. Reconstruction of river runoff to the Baltic Sea, AD 1500–1995. Int. J. Climatol. 31, 696–703.

He, G., Xiong, X., Peng, Y., Yang, C., Xu, Y., Liu, X., Liang, J., Masanja, F., Yang, K., Xu, X., Zheng, Z., Deng, Y., Leung, J. Y. S., Zhao, L., 2023. Transcriptomic responses reveal impaired physiological performance of the pearl oyster following repeated exposure to marine heatwaves. Sci. Total Environ. Res. 854, 158726.

Helama, S., Schöne, B.R., Black, B.A., Dunca, E., 2006. Constructing long-term proxy series for aquatic environments with absolute dating control using a sclerochronological approach: introduction and advanced applications. Mar. Freshw. Res. 57, 591–599.

Holland, H.A., Schöne, B.R., Marali, S., Jochum, K.P., 2014. History of bioavailable lead and iron in the Greater North Sea and Iceland during the last millennium - a bivalve sclerochronological reconstruction. Mar. Pollut. Bull. 87, 104–116.

Jilbert, T., Slomp, C.P., 2013. Rapid high-amplitude variability in Baltic Sea hypoxia during the Holocene. Geology 41, 1183–1186.

Jochum, K.P., Nohl, U., Herwig, K., Lammel, E., Stoll, B., Hofmann, A.W., 2005. GeoReM: A new geochemical database for reference materials and isotopic standards. Geostand. Geoanalyt. Res. 29, 333–338.

Jochum, K.P., Stoll, B., Herwig, K., Willbold, M., 2007. Validation of LA-ICP-MS trace element analysis of geological glasses using a new solid-state 193 nm Nd:YAG laser and matrix-matched calibration. J. Anal. At. Spectrom. 22, 112–121.

Jochum, K.P., Weis, U., Stoll, B., Kuzmin, D., Yang, Q., Raczek, I., Jacob, D.E., Stracke, A., Birbaum, K., Frick, D.A., Günther, D., Enzweiler, J., 2011. Determination of reference values for NIST SRM 610-617 glasses following ISO guidelines. Geostand. Geoanalytical Res. 35, 397–429.

Jokinen, S.A., Virtasalo, J.J., Jilbert, T., Kaiser, J., Dellwig, O., Arz, H.W., Hänninen, J., Arppe, L., Collander, M., Saarinen, T., 2018. A 1500-year multiproxy record of coastal hypoxia from the northern Baltic Sea indicates unprecedented deoxygenation over the 20th century. Biogeosci. 15, 3975–4001.

Jones, D.S., Quitmyer, I.R., 1996. Marking time with bivalve shells: oxygen isotopes and season of annual increment formation. Palaios, 340–346.

Jonsson, P., Carman, R., Wulff, F., 1990. Laminated sediments in the Baltic – A tool for evaluating nutrient mass balances. Ambio 152–158.

Kabel, K., Moros, M., Porsche, C., Neumann, T., Adolphi, F., Andersen, T.J., Siegel, H., Gerth, M., Leipe, T., Jansen, E., Sinninghe Damsté, J.S., 2012. Impact of climate change on the Baltic Sea ecosystem over the past 1,000 years. Nature Clim. Change 2, 871–874.

Keenlyside, N.S., Latif, M., Jungclaus, J., Roeckner, E., 2008. Advancing decadal-scale climate

prediction in the North Atlantic sector. Nature, 453, 84-88.

Kennish, M.J., Olsson, R.K., 1975. Effects of thermal discharges on the microstructural growth of *Mercenaria mercenaria*. Environ. Geol. (Springer) 1, 41–64.

Kõuts, M., Maljutenko, I., Elken, J., Liu, Y., Hansson, M., Viktorsson, L., Raudsepp, U., 2021. Recent regime of persistent hypoxia in the Baltic Sea. Environ. Res. Commun 3, 075004.

Kirby, M.K., Miller, H.M., 2005. Response of a benthic suspension feeder (*Crassostrea virginica* Gmelin) to three centuries of anthropogenic eutrophication in Chesapeake Bay. Estuarine, coastal and shelf science, Coast. Shelf Sci. 62, 679-689.

Langlet, D., Alunno-Bruscia, M., Rafélis, M., Renard, M., Roux, M., Schein, E., Buestel, D., 2006. Experimental and natural cathodoluminescence in the shell of *Crassostrea gigas* from Thau lagoon (France): ecological and environmental implications. Mar. Ecol. Prog. Ser. 317, 143–156.

Lazareth, C.E., Vander Putten, E., André L, Dehairs, F., 2003. High-resolution trace element profiles in shells of the mangrove bivalve *Isognomon ephippium*: a record of environmental spatio-temporal variations? Estuar. Coast. Shelf Sci. 57, 1103–1114.

Leung, J.Y.S., Cheung, N.K.M., 2018. Effects of hypoxia and non-lethal shell damage on shell mechanical and geochemical properties of a calcifying polychaete. Biogeosciences, 15, 3267-3276.

Mann, M.E., Steinman, B.A., Brouillette, D.J., Miller, S., 2021. Multidecadal climate oscillations during the past millennium driven by volcanic forcing. Science 371, 1014–1019.

Marali, S., Schöne, B.R., Mertz-Kraus, R., Griffin, S.M., Wanamaker, A.D., Matras, U., Butler, P.G., 2017. Ba/Ca ratios in shells of *Arctica islandica* —Potential environmental proxy and crossdating tool. Palaeogeogr. Palaeoclimatol. Palaeoecol. 465, 347–361.

Marchitto Jr., T.M., Jones, G.A., Goodfriend, G.A., Weidman, C.R., 2000. Precise temporal correlation of holocene mollusk shells using sclerochronology. Quat. Res. 53, 236–246.

Middelburg, J.J., De Lange, G.J., van Der Weijden, C.H., 1987. Manganese solubility control in marine pore waters. Geochim. Cosmochim. Ac. 51, 759–763.

Mischel, S.A., Mertz-Kraus, R., Jochum, K.P., Scholz, D., 2017. TERMITE: An R script for fast reduction of laser ablation inductively coupled plasma mass spectrometry data and its application to trace element measurements. Rapid Commun. Mass Spectrom. 31, 1079–1087.

Mohrholz, V., 2018. Major Baltic Inflow statistics – Revised. Front. Mar. Sci. 5, 384.

Moss, D.K., Surge, D., Zettler, M.L., Orland, I., Burnette, A., Fancher, A. 2021: Age and growth

of *Astarte borealis* (Bivalvia) from the southwestern Baltic Sea using secondary ion mass spectrometry. Mar. Biol. 168, 1-11.

Norbäck Ivarsson, L.N., Andrén, T., Moros, M., Andersen, T.J., Lönn, M., Andrén, E., 2019. Baltic Sea coastal eutrophication in a thousand year perspective. Front. Environ. Sci 7, 88.

Nordberg, K., Gustafsson, M., Krantz, A.-L., 2000. Decreasing oxygen concentrations in the Gullmar Fjord, Sweden, as confirmed by benthic foraminifera, and the possible association with NAO. J. Mar. Syst. 23, 303–316.

Oeschger, R., 1990. Long-term anaerobiosis in sublittoral marine invertebrates from the Western Baltic Sea: *Halicryptus spinulosus* (Priapulida), *Astarte borealis* and *Arctica islandica* (Bivalvia). Mar. Ecol. Prog. Ser. 59, 133–143.

Oeschger, R., Storey, K.B., 1993. Impact of anoxia and hydrogen sulphide on the metabolism of *Arctica islandica* L. (Bivalvia). J. Exp. Mar. Biol. Ecol. 170, 213–226.

Oschlies, A., Brandt, P., Stramma, L., Schmidtko, S., 2018. Drivers and mechanisms of ocean deoxygenation. Nature Geosci. 11, 467–473.

Poitevin, P., Thébault, J., Siebert, V., Donnet, S., Archambault, P., Doré, J., Chauvaud, L., Lazure, P., 2019. Growth response of *Arctica islandica* to North Atlantic oceanographic conditions since 1850. Front. Mar. Sci. 6, 483.

Reusch, T.B.H., Dierking, J., Andersson, H.C., Bonsdorff, E., Carstensen, J., Casini, M., Czajkowski, M., Hasler, B., Hinsby, K., Hyytiäinen, K., Johannesson, K., Jomaa, S., Jormalainen, V., Kuosa, H., Kurland, S., Laikre, L., MacKenzie, B.R., Margonski, P., Melzner, F., Oesterwind, D., Ojaveer, H., Refsgaard, J.C., Sandström, A., Schwarz, G., Tonderski, K., Winder, M., Zandersen, M., 2018. The Baltic Sea as a time machine for the future coastal ocean. Sci. Adv. 4, eaar8195.

Reynolds, D.J., Scourse, J.D., Halloran, P.R., Nederbragt, A.J., Wanamaker, A.D., Butler, P.G., Richardson, C.A., Heinemeier, J., Eiríksson, J., Knudsen, K.L., Hall, I.R., 2016. Annually resolved North Atlantic marine climate over the last millennium. Nature Commun. 7, 13502.

Schlesinger, M.E., Ramankutty, N., 1994. An oscillation in the global climate system of period 65–70 years. Nature, 367, 723–726.

Schöne, B.R., 2008. The curse of physiology—challenges and opportunities in the interpretation of geochemical data from mollusk shells. Geo-Mar. Lett. 28, 269–285.

Schöne, B.R., 2013. *Arctica islandica* (Bivalvia): A unique paleoenvironmental archive of the northern North Atlantic Ocean. Glob. Planet. Change 111, 199–225.

Schöne, B.R., Dunca, E., Fiebig, J., Pfeiffer, M., 2005. Mutvei's solution: An ideal agent for resolving microgrowth structures of biogenic carbonates. Palaeogeogr. Palaeoclimatol. Palaeoecol. 228, 149–166.

Schöne, B.R., Huang, X., Zettler, M.L., Zhao, L., Mertz-Kraus, R., Jochum, K.P., Walliser, E.O., 2021. Mn/Ca in shells of *Arctica islandica* (Baltic Sea) – A potential proxy for ocean hypoxia? Estuar. Coast. Shelf Sci. 251, 107257.

Schöne, B.R., Huang, X., Jantschke, A., Mertz-Kraus, R., Zettler, M.L., 2022. High-resolution reconstruction of dissolved oxygen levels in the Baltic Sea with bivalves – a multi-species comparison (*Arctica islandica*, *Astarte borealis*, *Astarte elliptica*). Front. Mar. Sci. 9, 820731.

Slomp, C.P., Malschaert, J.F.P., Lohse, L., Van Raaphorst, W., 1997. Iron and manganese cycling in different sedimentary environments on the North Sea continental margin. Cont. Shelf Res. 17, 1083–1117.

Stecher, H.A., Krantz, D.E., Lord, C.J., Luther, G.W., Bock, K.W., 1996. Profiles of strontium and barium in *Mercenaria mercenaria* and *Spisula solidissima* shells. Geochem. Cosmochim. Acta 60, 3445–3456.

Strahl, J., Brey, T., Philipp, E.E., Thorarinsdóttir, G., Fischer, N., Wessels, W., Abele, D., 2011. Physiological responses to self-induced burrowing and metabolic rate depression in the ocean quahog *Arctica islandica*. J. Exp. Biol. 214, 4223–33.

Taylor, A.C., 1976. Burrowing behaviour and anaerobiosis in the bivalve *Arctica islandica* (L.). J. Mar. Biol. Assoc. U.K. 56, 95–109.

Theede, H., Ponat, A., Hiroki, K., Schlieper, C., 1969. Studies on the resistance of marine bottom invertebrates to oxygen-deficiency and hydrogen sulphide. Mar. Biol. 2, 325–337.

Thébault, J., Chauvaud, L., L'Helguen, S., Clavier, J., Barats, A., Jacquet, S., Pécheyran, C., Amouroux, D., 2009. Barium and molybdenum records in bivalve shells: Geochemical proxies for phytoplankton dynamics in coastal environments? Limnol. Oceanogr. 54, 1002–1014.

Vander Putten, E., Dehairs, F., Keppens, E., Baeyens, W., 2000. High resolution distribution of trace elements in the calcite shell layer of modern *Mytilus edulis*: environmental and biological controls. Geochim. Cosmochim. Acta 64, 997-1011.

Vaquer-Sunyer, R., Duarte, C.M., 2008. Thresholds of hypoxia for marine biodiversity. Proc. Natl. Acad. Sci. U.S.A. 105, 15,452–15,457.

Voß, M., Struck, U., 1997. Stable nitrogen and carbon isotopes as indicator of eutrophication of the Oder river (Baltic sea). Mar. Chem. 59, 35–49.

Wanamaker, A.D., Butler, P.G., Scourse, J.D., Heinemeier, J., Eiríksson, J., Knudsen, K.L., Richardson, C.A., 2012. Surface changes in the North Atlantic meridional overturning circulation during the last millennium. Nature Commun. 3, 899.

Wasmund, N., Göbel, J., von Bodungen, B., 2008. 100-years-changes in the phytoplankton community of Kiel Bight (Baltic Sea). J. Mar. Syst. 73, 300–322.

Wasmund, N., Zettler, M.L., 2023. Long-term trends of the offshore ecosystems. In: Schubert, H., Müller, F., (Eds.), Southern Baltic coastal systems analysis. Ecological Studies. Springer, Cham., pp. 163-174.

Westman, P., Sohlenius, G., 1999. Diatom stratigraphy in five offshore sediment cores from the northwestern Baltic proper implying large scale circulation changes during the last 8500 years. J. Paleolimnol. 22, 53–69.

Witbaard, R., Duineveld, G.C.A., deWilde, P.A.W.J., 1997. A long-term growth record derived from *Arctica islandica* (Mollusca, Bivalvia) from the Fladen Ground (northern North Sea). J. Mar. Biol. Ass. U.K. 77, 801–816.

Witkowski, A., Pempkowiak, J., 1995. Reconstructing the development of human impact from diatoms and ^{210}Pb sediment dating (the Gulf of Gdansk - southern Baltic Sea). Geogr. Pol. 65, 63–78.

Zettler, M.L., 2001. Distribution, abundance and some population characteristics of the ocean quahog, *Arctica islandica* (Linnaeus, 1767), in the Mecklenburg Bight (Baltic Sea). J. Shellfish Res. 20, 161–169.

Zettler, M.L., 2002. Ecological and morphological features of the bivalve *Astarte borealis* (Schumacher, 1817) in the Baltic Sea near its geographical range. J. Shellfish Res. 21, 33–40.

Zhang, J., Gilbert, D., Gooday, A.J., Levin, L., Naqvi, S.W.A., Middelburg, J.J., Scranton, M., Ekau, W., Peña, A., Dewitte, B., Oguz, T., Monteiro, P.M.S., Urban, E., Rabalais, N.N., Ittekkot, V., Kemp, W.M., Ulloa, O., Elmgren, R., Escobar-Briones, E., Van der Plas, A.K., 2010. Natural and human-induced hypoxia and consequences for coastal areas: synthesis and future development. Biogeosci. 7, 1443–1467.

Zhao, L., Walliser, E.O., Mertz-Kraus, R., Schöne, B.R., 2017. Unionid shells (*Hyriopsis cumingii*) record manganese cycling at the sediment-water interface in a shallow eutrophic lake in China (Lake Taihu). Palaeogeogr. Palaeoclimatol. Palaeoecol. 484, 97–108.

Zillén, L., Conley, D.J., 2010. Hypoxia and cyanobacteria blooms - are they really natural features of the late Holocene history of the Baltic Sea? Biogeosci. 7, 2567–2580.

Zillén, L., Conley, D.J., Andrén, T., Andrén, E., Björck, S., 2008. Past occurrences of hypoxia in the Baltic Sea and the role of climate variability, environmental change and human impact. Earth Sci. Rev. 91, 77–92.

7 Summary and outlook

Reconstructing the history of dissolved oxygen and hypoxia in coastal waters has relied almost exclusively on proxies archived in sediment cores, with major drawbacks including low temporal resolution and poor dating control. As demonstrated here, bivalve shells have the potential to complement the sedimentary record by providing a precise and highly resolved timeframe of ecological changes in the past. So far, only one research demonstrated a link between Mn/Ca_{shell} values of the freshwater mussel, *Hyriopsis cumingii* and DO changes in pore water of shallow lakes (Zhao et al., 2017), without further quantifying or calibrating the relationship. Furthermore, the applicability of the Mn/Ca_{shell}-based DO proxy to coastal areas such as the Baltic Sea needed to be further explored. Thus, this thesis aimed to calibrate and develop the shell Mn/Ca ratio as a quantitative DO indicator and apply this technique to infer the DO-history in the Baltic Sea over the past centuries with unprecedented temporal resolution.

As shown in Chapter 3, the concentration of manganese relative to calcium in the shell carbonate of *A. islandica* varied seasonally and exhibited a statistically significant negative correlation with the amount of dissolved oxygen in the ambient water of the Mecklenburg Bight, Baltic Sea. This study firstly highlighted the great potential of shell Mn/Ca values, particularly for the ocean quahog *A. islandica,* as a DO recorder in the Baltic Sea. To further prove the reliability and generalizability of Mn/Ca_{shell}-based DO reconstructions, Chapter 4 assembled an extensive dataset of three different bivalve species (*A. islandica*, *Astarte borealis, A. elliptica*) from Fehmarn Belt. The precision by which DO could be reconstructed varied between ± 1.6 mL/L (*A. islandica*, *A. borealis*) and ± 1.5 mL/L (*A. elliptica*). In other words, *Astarte* spp. records DO in a similar way as *A. islandica* and can thus serve as alternative DO archive. Considering the difference in the biogeographic distributions of the three species in the Baltic Sea (Zettler et al., 2001; Darr et al., 2014), these findings are very useful for retrospective monitoring of DO and hypoxia over a wide range of spatial and temporal scales. All three studied species (*A. islandica*, *A. borealis* and *A. elliptica*) can be used for high-resolution DO reconstructions, though species-specific limitations exist including differences in DO tolerance, lifespan and temporal resolution. For instance, *Astarte spp.* is slightly more resistant to oxygen depletion than *A. islandica* and may thus provide more comprehensive DO data, but has a shorter lifespan. In turn, *A. islandica* grows faster resulting in less time-averaged data. If more than a single species is available for DO reconstructions, these differences may complement each other and thereby improve the robustness of he DO reconstructed from Mn/Ca_{shell} values.

The strong covariations between Mn/Ca_{shell} values and DO concentration found in Chapters 3 to 6 demonstrated that manganese in the shells is mainly derived from the dissolved Mn in the surrounding waters. Effects of other environmental factors on the shell Mn/Ca_{shell} data were identified (Chapter 3), for instance, extreme Mn/Ca_{shell} peaks can originate from the ingestion of Mn-rich organic particles that can be resuspended after MBIs and/or occasional strong riverine influxes. Controlled laboratory experiments in future studies would certainly be useful to shed light on the relative importance of the different Mn sources.

Aside from chemical analyses, Chapter 5 further demonstrated that the shell ultrastructure, specifically the prominence of disturbance lines, may serve as a qualitative indicator of low-DO severity in the Baltic Sea. Based on their distinctive ultrastructure (fine complex crossed-lamellae instead of irregular simple/spherulitic prisms), these growth structures can be confidently distinguished from periodic annually growth lines. However, disturbance lines should only be used as a complementary proxy to Mn/Ca_{shell} values, because other environmental stressors (i.e., oxygen depletion, low temperature, a lack of food availability or predator attack) may result in similar ultrastructure features. Future studies should further explore the potential of shell morphology analyses to obtain quantitative data on DO or other environmental parameters.

Based on previous studies, Chapter 6 applied this geochemical proxy to identify DO changes in the Baltic Sea prior to the instrumental era. All studied specimens of *A. islandica* lived at nearly the same locality and water depth (ca. 25 m) in the Mecklenburg Bight. The Mn/Ca_{shell} values of historical specimens (second half of the 19th century) were not significantly different from those of modern specimens (20th century). This led to the conclusion that the SW Baltic Sea already experienced seasonal deoxygenation in the mid-19th century. These findings are in agreement with DO data of sedimentary archives (e.g., Zillén and Conley, 2010; Kabel et al. 2012; Jokinen et al. 2018; Wasmund et al.,2008; Wasmund and Zettler, 2023). The low DO content in historical times may have been caused by strong anthropogenic nutrient input after the onset of the Industrial Revolution around 1850, which is particularly evident from a gradual rise of Ba/Ca_{shell} reflecting a massive change in diatom community structure. Since bivalve shells can be accurately aligned chronologically, they can thus provide a more detailed understanding of historical DO trends than sediment records. Following the Mn/Ca_{shell} data, the DO levels in the 19th century varied with a period of 12 to 15 years, while a higher frequency of 4 to 6 years prevailed in the late 20th century. In more recent times, the bottom water oxygenation was synergistically affected by phosphate levels and saline oxygen-rich water inflows from the North Sea. Oxygen conditions improved in the mid-1990s, which was linked

to a reduction in phosphate content and several baroclinic inflows.

In summary, in the present thesis, a new multiproxy approach was developed and applied to retrospective track the DO history and assess mechanisms of hypoxia in the Baltic Sea. To further constrain the use of Mn/Ca_{shell} as a proxy for DO, laboratory experiments should be conducted. So far, the calibration was based on DO measurements completed approximately 1 m above the sediment surface, but not in the water inhaled by the bivalves or the porewater that engulfs the mantle tissue while the animals were feeding. It would be useful if future studies addressed the question if DO in the free water column is linearly correlated to the oxygen concentration closer to the seabed where the bivalves filter-fed. Furthermore, it needs to be quantified how much Mn in the shell comes from direct contact of the soft tissues with sedimentary porewater. Future studies should continue the work started here and use (independently dated) fossil shells to reconstruct the DO history of the more distant past and across a larger region. Such data could help to improve ecosystem management and conservation in the Baltic Sea.

References

Darr, A., Gogina, M, Zetler, M. L., 2014. Detecting hot-spots of bivalve biomass in the south-western Baltic Sea. J. Mar. Syst. 134, 69–80.

Jokinen, S.A., Virtasalo, J.J., Jilbert, T., Kaiser, J., Dellwig, O., Arz, H.W., Hänninen, J., Arppe, L., Collander, M., Saarinen, T., 2018. A 1500-year multiproxy record of coastal hypoxia from the northern Baltic Sea indicates unprecedented deoxygenation over the 20th century. Biogeoscience 15, 3975–4001.

Wasmund, N., Göbel, J., von Bodungen, B., 2008. 100-years-changes in the phytoplankton community of Kiel Bight (Baltic Sea). J. Mar. Syst. 73, 300–322.

Wasmund, N., Zettler, M.L., 2023. Long-term trends of the offshore ecosystems. In: Schubert, H., Müller, F., (Eds.), Southern Baltic coastal systems analysis. Ecol. Res. Springer, Cham., 163–174 pp.

Kabel, K., Moros, M., Porsche, C., Neumann, T., Adolphi, F., Andersen, T.J., Siegel, H., Gerth, M., Leipe, T., Jansen, E., Sinninghe Damsté, J.S., 2012. Impact of climate change on the Baltic Sea ecosystem over the past 1,000 years. Nat. Clim. Change 2, 871–874.

Zhao, L., Walliser, E.O., Mertz-Kraus, R., Schöne, B.R., 2017. Unionid shells (*Hyriopsis cumingii*) record manganese cycling at the sediment-water interface in a shallow eutrophic lake in China (Lake Taihu). Palaeogeogr. Palaeoclimatol. Palaeoecol. 484, 97–108.

Zettler, M.L., Bönsch, R., Gosselck, F., 2001. Distribution, abundance, and some population characteristics of the ocean quahog, *Arctica islandica* (Linnaeus, 1767) in the Mecklenburg Bight (Baltic Sea). J. Shellfish Res. 20, 161–169

Zillén, L., Conley, D.J., 2010. Hypoxia and cyanobacteria blooms - are they really natural features of the late Holocene history of the Baltic Sea? Biogeoscience 7, 2567–2580.